COMPUTATIONAL CHARACTERIZATION OF DISORDERED METAL-ORGANIC FRAMEWORKS

A Dissertation
Presented to
The Academic Faculty

by

Rebecca Han

In Partial Fulfillment
of the Requirements for the Degree
Doctor of Philosophy in the
School of Chemical & Biomolecular Engineering

Georgia Institute of Technology
May 2019

COMPUTATIONAL CHARACTERIZATION OF DISORDERED METAL-ORGANIC FRAMEWORKS

Approved by:

Dr. David S. Sholl, Advisor
School of Chemical & Biomolecular Engineering
Georgia Institute of Technology

Dr. Krista S. Walton
School of Chemical & Biomolecular Engineering
Georgia Institute of Technology

Dr. Sankar Nair
School of Chemical & Biomolecular Engineering
Georgia Institute of Technology

Dr. Angus P. Wilkinson
School of Chemistry & Biochemistry
Georgia Institute of Technology

Dr. Ryan P. Lively
School of Chemical & Biomolecular Engineering
Georgia Institute of Technology

Date Approved: February 20, 2019

For my parents and grandparents, who made it possible for me to have the opportunities they never had.

ACKNOWLEDGEMENTS

First and foremost, I am sincerely grateful to my thesis advisor Dr. David Sholl. His dedication to practical insight, application, and communication has made our computational work significant to a broad audience. I feel fortunate to have an advisor who supported all my endeavors, and I can't imagine a better Ph.D. experience than the one I have had in his group.

I would also like to express my appreciation to my committee members Dr. Ryan Lively, Dr. Sankar Nair, Dr. Krista Walton, and Dr. Angus Wilkinson. In particular, I want to thank Dr. Nair for his experimental collaboration; his unique perspective was valuable in shaping my research projects.

Special thanks to the Department of Energy for funding my research. It was a privilege to meet and work with such a diverse network of colleagues in the UNCAGE-ME Energy Frontier Research Center. I especially thank Dr. JR Schmidt at the University of Wisconsin-Madison, who has been an exceedingly patient and helpful collaborator, even hosting me at UW-M and teaching me advanced computational methods.

In addition to external collaborators, I received untold help and advice from many fruitful discussions with my fellow group members. I am fortunate to have met my good friends Charles Pueschel and Jack Findley; the camaraderie, thought-provoking conversations, and general fun times we shared will last well beyond our years together at Georgia Tech. I also worked closely with and learned from Dr. Joshua Howe, Dr. Souryadeep Bhattacharyya, Dr. Chu Han, Dr. Raghu Thyagarajan, Dr. Anny Liu, Mayank Agrawal, and Jongwoo Park. Thanks also to the undergraduate researchers who worked with me: Akshay Chiddarwar, Vik Gopal, and Dinushka Herath.

Outside of my Sholl group friends, I had the great pleasure of going to Costco (nearly) every Wednesday with Thomas Kwok, Jay Joshi, Julian Hungerford, Eli Carter, Carmen Chen, and Jason Lee – I will do my best to keep the tradition of our weekly pilgrimage next year. Many thanks also to my interesting, inspiring fellow officers in the PhD2Consulting Club. It was encouraging to know and befriend such exceptional students. Special thanks to Chris Tung, the best roommate I could have asked for these past four years.

I would be remiss without mentioning the prayers and care I received from the saints in Atlanta. My deepest appreciation goes to Amanda Thomas who has been a friend, a sister, and a true companion. I will miss the numerous other full-time serving ones and young families who lived near Tech; you will be in my thoughts and prayers, and I hope to see you all at the semi-annual trainings.

Finally, I save my greatest thanks for my family. I am indebted to my parents, Dr. Jung Han and Shingyu Tsao, without whose guidance and direction I would not have pursued this Ph.D. My brother Jasper has also been a tremendous source of spiritual inspiration. My journey these past five years, and my next steps to LA and Boston, are possible through my family's unwavering love and support.

Rebecca Han, Atlanta, February 2019

TABLE OF CONTENTS

LIST OF TABLES

LIST OF FIGURES

SUMMARY

Metal-organic frameworks (MOFs) are a class of crystalline nanoporous adsorbents with numerous applications due to their highly tunable physical and chemical properties. However, MOFs are limited by their susceptibility to degradation in humid and acid environments common to many industrial processes. We focus on zeolitic imidazolate frameworks (ZIFs), a MOF subclass with high thermal stability which can be synthesized in many topologies. In this thesis, we study disorder in ZIFs at local and superlattice length scales by building computational models of defects, simulating bulk properties of the defect material, and comparing our theoretical insights against experimental measurements. We first demonstrated that inherent extended defects such as stacking faults are favorable, suggesting that these defects will be introduced during synthesis and are therefore prevalent in real ZIF materials. Then we consider degradation induced by exposure to H_2O, CO_2, SO_2, and NO_2 on a broad set of ZIFs. While simulation alone cannot fully predict ZIF stability, it will be valuable in elucidating new degradation pathways of more complex attacking species. Following on this work, we investigated how local defects accumulate until the bulk structure degrades. The mechanism we proposed explains favorable defect propagation as a means to reduce or eliminate the strain energy. Finally, we performed meta-analysis on a fundamental question: how reproducible is MOF synthesis research? While our findings are not encouraging, we propose an "Olympic medal" hierarchy standard and suggest ways the research community can improve reproducibility.

CHAPTER 1. INTRODUCTION

1.1 Metal-Organic Frameworks: Appeal, Applications, and Limitations

Metal-organic frameworks (MOFs) are a class of crystalline, microporous adsorbents with promising properties for sensing[1], separations[2], catalysis[3], and gas storage[4] applications. Discovered in the late 1990's[5-6], they are still relatively new compared to traditional porous structures like activated carbon or zeolites, over which they have a few key advantages – greater pore size, surface area and volume; and extensive physical and chemical tunability. The latter, in particular, has generated two decades of excitement: roughly 230 zeolites[7] have been synthesized since the late 1940's, while more than 37,000 MOFs[8] have been reported in less than half that time. MOFs are constructed of metal nodes linked by organic ligands through coordination bonds[9]. This simple "molecular building block" model belies the highly application-tailored selectivity and specificity made possible by modifying choice of synthesis solvent[10], organic linker[11], metal center[12], and/or post-synthetic processing[13].

Unfortunately, the tendency of MOFs to degrade in humid or acidic environments[14] limits their practical implementation and widespread industrial adoption[15]. This lability relative to conventional porous materials has been attributed to the Lewis acid-base nature of metal-linker coordination bonds, where strong electron donors can act as a competing Lewis base to the organic ligand[14,16]. Donor-substituted bonds may result in undercoordinated defect sites that drive reactivity with adsorbents and increase kinetic degradation[17]. However, it has been found that introducing defects in a controlled manner can be yet another avenue through which to tune desirable crystal qualities[18-19]. Whether

defects are harmful or helpful, they are likely ubiquitous in a real material. Optimizing material performance requires thorough knowledge of defect structure, distribution, and impact on experimentally measured properties.

We focus on zeolitic imidazolate frameworks (ZIFs), a subclass of MOFs with exceptional chemical and thermal stability[20]. As the name suggests, ZIFs are topologically isomorphic with zeolites; the aluminosilicate Si-O-Si bond angle is similar to the bond angle between Zn^{2+} or Co^{2+} centers tetrahedrally linked by functionalized imidazolates. ZIFs are primarily distinguished by functionalization of the imidazole ligand and framework connectivity. A wide range of linker and topology choices are synthetically accessible. Designing a set of ZIFs with the same linker but different topology, or vice versa, allows for controlled investigation of specific structure-property relationships. As a result, ZIFs have been widely studied experimentally and computationally[21-24], particularly the structure known as ZIF-8, which has 2-methylimidazolate ligands and crystallizes in the sodalite (SOD) topology[20]. ZIF-8 is known for its robust stability at high temperatures, including immersion in boiling water and basic solvents[20], as well as its ability to form heterogeneous mixed-linker structures where a fraction of the 2-methylimidazolate ligands are replaced by alternative imidazole linkers that change the overall hydrophobicity or pore size without changing the framework topology[25].

1.2 Challenges of Defect Characterization

Defects in MOFs (or other crystals) can broadly fall under two categories[17]: point defects that disrupt a localized metal-linker site, or extended defects that disrupt long-range order of the crystal structure. Either kind of defect may form during synthesis, often associated with rapid crystallization that "locks" many imperfections into place[26], or

intentionally "engineered" by using an appropriate modulator[27]. Defects, point and extended, can also by induced after synthesis through solvent removal[28], particle bombardment, or exposure to extreme thermal/chemical conditions.

Characterizing defects in MOFs experimentally offers many challenges. Scanning probe and confocal fluorescence microscopy have been successfully used to image one- and two-dimensional dislocations[29-30] and extended pockets of correlated defects[31]. Although these techniques can detect long-range disorder, they do not always yield a detailed picture of defect density and morphology. Moreover, high-energy microscopy and scattering measurements typically lack the resolution to identify point defects[32] without destroying beam-sensitive organic ligands[33]. If a defect reaction is known, adsorbed product species may be identified as evidence of defect formation using Fourier-Transfer Infrared Spectroscopy (FTIR)[34-35]. Linker decoordination can also be inferred from increased N_2 uptake and Brunauer-Emmett-Teller (BET) surface area[36-37], but neither of these characterizations can determine where or how the point defects are distributed through the framework. For this reason, molecular models are a powerful and complementary tool for studying disorder in the bulk structure. Calculations often assume an ideal crystal, but recent literature has increasingly come to characterize ubiquity and importance of defects. Detailed knowledge of "real" MOFs will allow accurate prediction of changes in adsorption[38], diffusion[39], or catalytic processes[34,40] due to defects. In this work, we use quantum mechanical models to describe local defects, classical calculations to elucidate long-range disorder, and finally also predict physical properties of the defective crystal for comparison against experimental characterization.

1.3 Computational Theory

1.3.1 Density functional theory (DFT)

Density functional theory (DFT) is a quantum mechanical modelling method that approximates a solution to the time-independent many-body Schrödinger equation[41]. First developed for solid-state calculations in the 1970s, DFT was not accurate enough for quantum chemistry calculations until more refined approximations were introduced in the 1990s[42]. Compared to other electronic structure methods such as Hartree-Fock theory, coupled-cluster/configuration-interaction theory, or Møller–Plesset perturbation theory, DFT is less computationally costly and therefore suitable for larger systems.

To understand why DFT is such an elegant and versatile method, we must first define the problem it solves. The Schrödinger equation is to quantum mechanics what Newton's second law is to classical mechanics; solving the Schrödinger equation defines the state of a quantum system at every spatial position and time. We are interested in solutions to the many-body time-independent Schrödinger equation (TISE). This restriction implies that our solutions will be stationary states, or eigenvectors, of the total energy of the system. The latter quantity is also known as the Hamiltonian operator $\widehat{H}$, and therefore the simplest form of the TISE is

$$\widehat{H}\Psi = E\Psi \tag{1-1}$$

where Ψ is the wavefunction describing the state and E is the energy level of the state. For a many-body system, Ψ describes the spatial positions of all the atomic nuclei and electrons in three-dimensional space. Given M nuclei and N electrons, this wavefunction has 3(N+M) variables – finding the solution to such a system becomes exponentially difficult and costly with size.

A key simplification arises because each proton or neutron in the nucleus is more than 1800 times heavier than the electron[41]. Thus, the electronic movements are nearly instantaneous compared to changes in nuclear positions. The Born-Oppenheimer approximation allows motion of the nuclei and electrons to be separated:

$$\Psi_{\text{total}} = \psi_{electronic} \times \psi_{nuclear} \tag{1-2}$$

Assuming the nuclei positions are fixed, the many-electron TISE becomes:

$$\hat{H}\psi_e = \left[-\frac{\hbar^2}{2m}\sum_{i=1}^{N}\nabla_i^2 + \sum_{i=1}^{N}V(\vec{r}_i) + \sum_{i=1}^{N}\sum_{j<i}U(\vec{r}_i,\vec{r}_j)\right]\psi_e = E\psi_e \tag{1-3}$$

where the three terms in the Hamiltonian are, in order, kinetic energy of each electron, interaction energy between each electron and all the nuclei, and interaction energy between different electrons[41]. However, this is still a highly complicated problem because the electronic wavefunction is still 3N-dimensional function. For a simple molecule like CO_2, the wavefunction has 66 coordinates; for a cluster of 100 Pt atoms, ψ_e contains 23,000 variables[41].

In 1964, Hohenberg and Kohn proved two fundamental theorems that established a basis for DFT by allowing simplification of a 3N-dimensional equation to one with only 3 variables[43]. The first theorem states that the total energy is a unique functional of electron density, or in corollary, that the ground state electron density uniquely determines the total energy and therefore all other properties of the system. Because the electron density $n(\vec{r})$ is a three-dimensional function obtained by integrating the electronic wavefunction ψ_e over three-dimensional space[44], the system can alternatively be described by a new wavefunction $\psi[n(\vec{r})]$ that is a functional of electron density. Here a functional indicates a function that takes a function as input and returns a single number – definite integrals are

a functional of the function that is integrated. We can re-express the TISE using the density functional, with $\hat{T}$, $\hat{V}$, and $\hat{U}$ corresponding to the three bracketed terms in Equation 1-3:

$$\left(\hat{T} + \hat{V} + \hat{U}\right) \psi[n(\vec{r})] = E[n(\vec{r})]\, \psi[n(\vec{r})] \tag{1-4}$$

The second Hohenberg-Kohn theorem is a variational principle that tells us how to search for solutions or approximations to this new energy functional: the functional defining the ground state energy of the system only returns the lowest energy if the input density is the true ground state density.

Based on these two theorems, Kohn and Sham introduced a method to find the energy functional by expressing the electron density using a set of equations each involving a single electron[45]:

$$\left[-\frac{\hbar^2}{2m}\nabla^2 + V_{ext}(\vec{r}) + V_H(\vec{r}) + V_{XC}(\vec{r})\right] \phi_i(\vec{r}) = \varepsilon_i \phi_i(\vec{r}) \tag{1-5}$$

The single-electron orbital $\phi_i(\vec{r})$ is closely related to the electron density but also accounts for electron spin. The first three terms in brackets are analogous to the three bracketed terms in Equation 1-3: $-\frac{\hbar^2}{2m}\nabla^2$ is the kinetic energy, $V_{ext}(\vec{r})$ is the external potential, and $V_H(\vec{r})$ is the Hartree potential describing Coulombic repulsion between electrons. One small but important difference between the Hartree potential and the previous electron-electron interaction potential is that the definition of the Hartree potential

$$V_H(\vec{r}) = e^2 \int n(\vec{r}')/|\vec{r} - \vec{r}'|\ d^3\vec{r}' \tag{1-6}$$

includes the unphysical interaction of an electron with itself. The fourth term $V_{XC}(\vec{r})$ is a new term that captures the self-interaction correction, along with all the interactions not included in the previous three potentials, with form:

$$V_{XC}(\vec{r}) = \delta E_{XC}[n(\vec{r}')]/\delta n(\vec{r}')\ . \tag{1-7}$$

Finding an accurate form of the exchange-correlation functional $V_{XC}(\vec{r})$ is highly difficult for most interesting systems, although it can be derived exactly for the uniform electron gas. In this example, the electron density is a constant at each spatial position, and the exchange-correlation energy can be set to the exchange-correlation potential per electron of a uniform electron gas[45]:

$$E_{XC}[n(\vec{r})] = \int n(\vec{r})\, \epsilon_{XC}[n(\vec{r})]\, d\vec{r}\,. \tag{1-8}$$

This approximation is called the local density approximation (LDA) because it only uses the local electron density to define the electron-correlation functional. The generalized gradient approximation (GGA) in Equation 1-9 is a versatile and widely used functional which is more accurate for systems with strong electron-electron interactions because it captures inhomogeneity in electron density by applying gradient corrections; we primarily use the PBE-GGA functional developed by Perdew, Bruke, and Ernzerhof[46].

$$E_{XC}[n(\vec{r})] = \int n(\vec{r})\, \epsilon_{XC}(\vec{r})\, F[n(\vec{r}), \nabla n(\vec{r})]\, d\vec{r}\,. \tag{1-9}$$

Since much of the work in this thesis involves humid systems, describing hydrogen bonding and London dispersion becomes critical. The PBE-GGA functional does not accurately describe long-range forces[47] and requires dispersion corrections[48]. We use the Grimme DFT-D2 and D3 corrections which sum over pairwise atom pairs with sixth, or sixth and eighth order dispersion coefficients, respectively[49].

1.3.2 Molecular dynamics (MD)

Molecular dynamics (MD) is a classical simulation method that solves Newton's equations of motions for a many-particle system subject to a force field[50]. Each particle in the system has a position and velocity in three dimensions. By taking ensemble averages, we can also calculate system properties such as energy and temperature at any moment in

time. We calculate the force on each particle after small time steps and update the position, velocity, and other measurables. The simulation is finished when the system reaches equilibrium, where the average properties no longer change with additional time steps.

While the MD algorithm is simple, the challenge is efficient calculation of forces at each step. Force is the first derivative of the potential in a specific direction. The Lennard-Jones (LJ) potential is a mathematically simple model that approximates the interaction between a pair of neutral atoms or molecules[51]

$$V_{LJ}(r) = 4\varepsilon\left[\left(\frac{\sigma}{r}\right)^{12} - \left(\frac{\sigma}{r}\right)^{6}\right] \tag{1-10}$$

where ε is the depth of the potential well, σ is the distance at which the interparticle potential is zero, and r is the distance between the particles. The corresponding force for this potential in the x direction is then

$$f_x(r) = \frac{\partial V(r)}{\partial x} = \frac{48\varepsilon x}{r^2}\left[\left(\frac{\sigma}{r}\right)^{12} - \frac{1}{2}\left(\frac{\sigma}{r}\right)^{6}\right] \tag{1-11}$$

For a system with N particles, calculating the force on a particle due to all its neighbours is a $3N^2$ dimensional problem. Verlet integration is a numerical method that allows us to approximate solutions to Newton's equations of motions once the forces are known[52]:

$$r(t + \Delta t) \approx 2r(t) - r(t - \Delta t) + \frac{f(t)}{m}\Delta t^2 \, . \tag{1-12}$$

1.3.3 Diffraction theory

Crystalline structures such as MOFs can be defined by all atoms in a unit cell that are periodically translated through space by the lattice vectors $(\hat{x}, \hat{y}, \hat{z})$ of the unit cell. Knowing the positions and types of all the unit cell atoms and the lattice vectors allows us to calculate the ideal X-ray diffraction (XRD) pattern of the structure. Experimental XRD

spectra are collected by bombarding a crystalline sample with X-rays at a range of incident angles. When the incident X-rays are scattered by internal crystal planes, a detector measures the angles at which the reflected X-rays return. These are recorded as peaks in the diffraction spectra, and the angles and intensities at which they occur depend on the atomic structure of the material being investigated.

Since peaks occur as a result of constructive interference, calculating the crystal planes that give rise to such interference becomes a mathematically solvable problem. The lattice planes are defined as a family of planes orthogonal to each lattice vector. Notated by Miller indices $\langle hkl \rangle$, these planes are spaced a constant distance d_{hkl} apart, determined by the lattice vectors. For every lattice vector in real space, there is a reciprocal lattice vector obtained by taking the Fourier transform of the real vector. The reciprocal space is also known as momentum space, and the momentum difference between incident and diffracted X-rays is one reciprocal lattice vector. Therefore, given a set of real lattice vectors $(\hat{x}, \hat{y}, \hat{z})$ describing the unit cell, the reciprocal lattice vectors $(\hat{a}, \hat{b}, \hat{c})$ are calculated as shown:

$$\hat{a} = 2\pi\,(\hat{y} \times \hat{z}) / \big(\hat{x} \cdot (\hat{y} \times \hat{z})\big)\,. \tag{1-13}$$

$$\hat{b} = 2\pi\,(\hat{z} \times \hat{x}) / \big(\hat{y} \cdot (\hat{z} \times \hat{x})\big)\,. \tag{1-14}$$

$$\hat{c} = 2\pi\,(\hat{x} \times \hat{y}) / \big(\hat{z} \cdot (\hat{x} \times \hat{y})\big)\,. \tag{1-15}$$

The interplanar spacing for an arbitrary lattice plane can then be calculated from the reciprocal lattice vectors and the angles α, β, γ between the real lattice vectors:

$$\frac{1}{d_{hkl}}^2 = h^2\hat{a}^2 + k^2\hat{b}^2 + l^2\hat{c}^2 + 2hk\hat{a}\hat{b}\cos\gamma + 2hl\hat{a}\hat{c}\cos\beta + 2kl\hat{b}\hat{a}\cos\alpha \tag{1-16}$$

From this, we can find the diffraction peak position using the Bragg model of diffraction which relates the spacing between planes to the scattering angle θ for an incident particle of specified wavelength λ

$$\lambda = 2d_{hkl} \sin\theta \ . \tag{1-17}$$

The amplitude (intensity) and phase of the diffracted beams depend on the atomic coordinates and species through a quantity called the structure vector F_{hkl} which represents the vector sum of waves reflected from all atoms. For m atoms in the unit cell with atomic positions (x_j, y_j, k_j), fractional occupancy N_j, and scattering efficiency f_j, the structure factor is calculated as

$$F_{hkl} = \sum_{j=1}^{m} N_j f_j \exp(2\pi i\left(hx_j + ky_j + lz_j\right)) \ . \tag{1-18}$$

The structure factor considers electromagnetic interactions and depends on the size, vibration, and number of electrons around an atom. Because it is usually approximated, the simulated diffraction peaks will often not have the same relative intensities as experimentally measured peaks, but the peak positions should not differ.

1.4 Dissertation Scope

The topics addressed in this thesis advance the current understanding of inherent (native) and exposure induced disorder in ZIFs. Detailed mechanistic models are proposed to describe these defect systems and confirmed through comparison with experimental characterization. Finally, we also discuss the reproducibility of MOF synthesis and characterization in the literature, to give additional perspective into the challenges of studying these fascinating, versatile, and complicated materials.

Chapter 2 is motivated by the lack of knowledge regarding extended defects in ZIFs. **Stacking faults are well-known and prevalent in zeolites; do they exist in topologically isomorphic ZIFs? If so, what is their effect on experimental measurables?**

Chapter 3 presents a comprehensive study of humid and acid-gas degradation across a wide variety of ZIFs. **Computational predictors have been identified for MOF water stability; can we identify a set of calculated properties that predict ZIF stability?**

Chapter 4 proposes the first detailed analysis of defect propagation in ZIF-8. **Given a single bond-breaking event, where and how do subsequent defects form? At what threshold of defect propagation is the structure "amorphous"?**

Chapter 5 takes a birds-eye view of experimental reproducibility by combing the literature on MOF synthesis. **How often is a typical MOF synthesis repeated? If repeated, how quantitatively comparable are the results?**

1.5 REFERENCES

1. Kreno, L. E.; Leong, K.; Farha, O. K.; Allendorf, M.; Van Duyne, R. P.; Hupp, J. T., Metal–Organic Framework Materials as Chemical Sensors. *Chem Rev* **2011**, *112*, 1105-1125.

2. Li, J. R.; Kuppler, R. J.; Zhou, H. C., Selective Gas Adsorption and Separation in Metal-Organic Frameworks. *Chem Soc Rev* **2009**, *38*, 1477-504.

3. Lee, J.; Farha, O. K.; Roberts, J.; Scheidt, K. A.; Nguyen, S. T.; Hupp, J. T., Metal-Organic Framework Materials as Catalysts. *Chem Soc Rev* **2009**, *38*, 1450-9.

4. Keskin, S.; van Heest, T. M.; Sholl, D. S., Can Metal-Organic Framework Materials Play a Useful Role in Large-Scale Carbon Dioxide Separations? *Chem Sus Chem* **2010**, *3*, 879-91.

5. Yaghi, O. M.; Li, G.; Li, H., Selective Binding and Removal of Guests in a Microporous Metal-Organic Framework. *Nature* **1995**, *378*, 703-706.

6. Li, H.; Eddaoudi, M.; O'Keeffe, M.; Yaghi, O. M., Design and Synthesis of an Exceptionally Stable and Highly Porous Metal-Organic Framework. *Nature* **1999**, *402*, 276-279.

7. Baerlocher, C.; McCusker, L. B., Database of Zeolite Structures: http://www.iza-structure.org/databases/. *Structure Commission of the International Zeolite Association (IZA-SC)*, **1996**.

8. Groom, C. R.; Allen, F. H., The Cambridge Structural Database in Retrospect and Prospect. *Angew Chem Int Ed Engl* **2014**, *53*, 662-671.

9. Zhou, H.-C.; Long, J. R.; Yaghi, O. M., Introduction to Metal–Organic Frameworks. *Chem Rev* **2012**, *112*, 673-674.

10. Li, C. P.; Du, M., Role of Solvents in Coordination Supramolecular Systems. *Chem Commun* **2011**, *47*, 5958-72.

11. Lalonde, M. B.; Mondloch, J. E.; Deria, P.; Sarjeant, A. A.; Al-Juaid, S. S.; Osman, O. I.; Farha, O. K.; Hupp, J. T., Selective Solvent-Assisted Linker Exchange (SALE) in a Series of Zeolitic Imidazolate Frameworks. *Inorg Chem* **2015**, *54*, 7142-4.

12. Sun, D.; Sun, F.; Deng, X.; Li, Z., Mixed-Metal Strategy on Metal-Organic Frameworks (MOFs) for Functionalities Expansion: Co Substitution Induces Aerobic Oxidation of Cyclohexene over Inactive Ni-MOF-74. *Inorg Chem* **2015**, *54*, 8639-43.

13. Cohen, S. M., Postsynthetic Methods for the Functionalization of Metal-Organic Frameworks. *Chem Rev* **2012**, *112*, 970-1000.

14. Bosch, M.; Zhang, M.; Zhou, H.-C., Increasing the Stability of Metal-Organic Frameworks. *Adv Chem* **2014**, *2014*, 1-8.

15. Furukawa, H.; Müller, U.; Yaghi, O. M., "Heterogeneity Within Order" in Metal–Organic Frameworks. *Angew Chem Int Ed Engl* **2015**, *54*, 3417-3430.

16. Burtch, N. C.; Jasuja, H.; Walton, K. S., Water Stability and Adsorption in Metal-Organic Frameworks. *Chem Rev* **2014**, *114*, 10575-612.

17. Sholl, D. S.; Lively, R. P., Defects in Metal-Organic Frameworks: Challenge or Opportunity? *J Phys Chem Lett* **2015**, 3437-3444.

18. Shearer, G. C.; Chavan, S.; Ethiraj, J.; Vitillo, J. G.; Svelle, S.; Olsbye, U.; Lamberti, C.; Bordiga, S.; Lillerud, K. P., Tuned to Perfection: Ironing out the Defects in Metal–Organic Framework UiO-66. *Chem Mater* **2014**, *26*, 4068-4071.

19. Fang, Z., et al., Structural Complexity in Metal-Organic Frameworks: Simultaneous Modification of Open Metal Sites and Hierarchical Porosity by Systematic Doping with Defective Linkers. *J Am Chem Soc* **2014**, *136*, 9627-36.

20. Park, K. S.; Ni, Z.; Cote, A. P.; Choi, J. Y.; Huang, R.; Uribe-Romo, F. J.; Chae, H. K.; O'Keeffe, M.; Yaghi, O. M., Exceptional Chemical and Thermal Stability of Zeolitic Imidazolate Frameworks. *Proc Natl Acad Sci USA* **2006**, *103*, 10186-91.

21. Huang, X. C.; Lin, Y. Y.; Zhang, J. P.; Chen, X. M., Ligand-Directed Strategy for Zeolite-Type Metal–Organic Frameworks: Zinc (II) Imidazolates with Unusual Zeolitic Topologies. *Angew Chem Int Ed Engl* **2006**, *45*, 1557-1559.

22. Banerjee, R.; Phan, A.; Wang, B.; Knobler, C.; Furukawa, H.; O'Keeffe, M.; Yaghi, O. M., High-Throughput Synthesis of Zeolitic Imidazolate Frameworks and Application to CO_2 Capture. *Science* **2008**, *319*, 939-943.

23. Banerjee, R.; Furukawa, H.; Britt, D.; Knobler, C.; O'Keeffe, M.; Yaghi, O. M., Control of Pore Size and Functionality in Isoreticular Zeolitic Imidazolate Frameworks and Their Carbon Dioxide Selective Capture Properties. *J Am Chem Soc* **2009**, *131*, 3875-3877.

24. Chen, B.; Yang, Z.; Zhu, Y.; Xia, Y., Zeolitic Imidazolate Framework Materials: Recent Progress in Synthesis and Applications. *J Mater Chem A* **2014**, *2*, 16811-16831.

25. Thompson, J. A.; Brunelli, N. A.; Lively, R. P.; Johnson, J. R.; Jones, C. W.; Nair, S., Tunable CO_2 Adsorbents by Mixed-Linker Synthesis and Postsynthetic Modification of Zeolitic Imidazolate Frameworks. *J Phys Chem C* **2013**, *117*, 8198-8207.

26. Ravon, U.; Savonnet, M.; Aguado, S.; Domine, M. E.; Janneau, E.; Farrusseng, D., Engineering of Coordination Polymers for Shape Selective Alkylation of Large Aromatics and the Role of Defects. *Micropor Mesopor Mater* **2010**, *129*, 319-329.

27. Vermoortele, F.; Bueken, B.; Le Bars, G. l.; Van de Voorde, B.; Vandichel, M.; Houthoofd, K.; Vimont, A.; Daturi, M.; Waroquier, M.; Van Speybroeck, V., Synthesis Modulation as a Tool to Increase the Catalytic Activity of Metal–Organic Frameworks: The Unique Case of UiO-66 (Zr). *J Am Chem Soc* **2013**, *135*, 11465-11468.

28. Cai, W.; Lee, T.; Lee, M.; Cho, W.; Han, D.-Y.; Choi, N.; Yip, A. C.; Choi, J., Thermal Structural Transitions and Carbon Dioxide Adsorption Properties of Zeolitic Imidazolate Framework-7 (ZIF-7). *J Am Chem Soc* **2014**, *136*, 7961-7971.

29. Walker, A. M.; Slater, B., Comment Upon the Screw Dislocation Structure on HKUST-1 {111} Surfaces. *Cryst Eng Comm* **2008**, *10*, 790.

30. Ameloot, R.; Vermoortele, F.; Hofkens, J.; De Schryver, F. C.; De Vos, D. E.; Roeffaers, M. B., Three-Dimensional Visualization of Defects Formed During the Synthesis of Metal-Organic Frameworks: A Fluorescence Microscopy Study. *Angew Chem Int Ed Engl* **2013**, *52*, 401-5.

31. Cubillas, P.; Anderson, M. W.; Attfield, M. P., Crystal Growth Mechanisms and Morphological Control of the Prototypical Metal–Organic Framework MOF-5 Revealed by Atomic Force Microscopy. *Chem Eur J* **2012**, *18*, 15406-15415.

32. Fang, Z.; Bueken, B.; De Vos, D. E.; Fischer, R. A., Defect-Engineered Metal-Organic Frameworks. *Angew Chem Int Ed Engl* **2015**, *54*, 7234-54.

33. Kashtiban, R. J.; Sloan, J.; Marchbank, H. R.; Dunne, P. W.; Walton, R. I. In *Electron Microscopy Study of Metal-Organic Framework Materials*, European Microscopy Congress, Manchester Central, United Kingdom, September 16 2012; Manchester Central, United Kingdom, 2012.

34. Chizallet, C.; Lazare, S.; Bazer-Bachi, D.; Bonnier, F.; Lecocq, V.; Soyer, E.; Quoineaud, A.-A.; Bats, N., Catalysis of Transesterification by a Nonfunctionalized Metal-Organic Framework: Acido-Basicity at the External Surface of ZIF-8 Probed by FTIR and Ab Initio Calculations. *J Am Chem Soc* **2010**, *132*, 12365-12377.

35. Nguyen, L. T.; Le, K. K.; Truong, H. X.; Phan, N. T., Metal–Organic Frameworks for Catalysis: The Knoevenagel Reaction Using Zeolite Imidazolate Framework ZIF-9 as an Efficient Heterogeneous Catalyst. *Catal Sci Technol* **2012**, *2*, 521-528.

36. Wu, H.; Chua, Y. S.; Krungleviciute, V.; Tyagi, M.; Chen, P.; Yildirim, T.; Zhou, W., Unusual and Highly Tunable Missing-Linker Defects in Zirconium Metal-Organic Framework UiO-66 and Their Important Effects on Gas Adsorption. *J Am Chem Soc* **2013**, *135*, 10525-32.

37. Gadipelli, S.; Guo, Z., Postsynthesis Annealing of MOF-5 Remarkably Enhances the Framework Structural Stability and CO_2 Uptake. *Chem Mater* **2014**, *26*, 6333-6338.

38. Ghosh, P.; Colón, Y. J.; Snurr, R. Q., Water Adsorption in UiO-66: The Importance of Defects. *Chem Commun* **2014**, *50*, 11329-11331.

39. Walker, A. M.; Slater, B.; Gale, J. D.; Wright, K., Predicting the Structure of Screw Dislocations in Nanoporous Materials. *Nat Mater* **2004**, *3*, 715.

40. Feyand, M.; Mugnaioli, E.; Vermoortele, F.; Bueken, B.; Dieterich, J. M.; Reimer, T.; Kolb, U.; De Vos, D.; Stock, N., Automated Diffraction Tomography for the Structure Elucidation of Twinned, Sub-Micrometer Crystals of a Highly Porous, Catalytically Active Bismuth Metal–Organic Framework. *Angew Chem Int Ed Engl* **2012**, *124*, 10519-10522.

41. Sholl, D.; Steckel, J. A., *Density Functional Theory: A Practical Introduction*; John Wiley & Sons, 2011.

42. Eschrig, H., *The Fundamentals of Density Functional Theory*; Springer, 2003; Vol. 2.

43. Hohenberg, P.; Kohn, W., Inhomogeneous Electron Gas. *Phys Rev B* **1964**, *136*, B864.

44. Capelle, K., A Bird's-Eye View of Density-Functional Theory. *Braz J Phys* **2006**, *36*, 1318-1343.

45. Kohn, W.; Sham, L. J., Self-Consistent Equations Including Exchange and Correlation Effects. *Phys Rev* **1965**, *140*, A1133.

46. Perdew, J. P.; Burke, K.; Ernzerhof, M., Generalized Gradient Approximation Made Simple. *Phys Rev Lett* **1996**, *77*, 3865-3868.

47. Grimme, S., Density Functional Theory with London Dispersion Corrections. *Comput Mol Sci* **2011**, *1*, 211-228.

48. Thanthiriwatte, K. S.; Hohenstein, E. G.; Burns, L. A.; Sherrill, C. D., Assessment of the Performance of DFT and DFT-D Methods for Describing Distance Dependence of Hydrogen-Bonded Interactions. *J Chem Theor Comput* **2010**, *7*, 88-96.

49. Grimme, S.; Antony, J.; Ehrlich, S.; Krieg, H., A Consistent and Accurate Ab Initio Parametrization of Density Functional Dispersion Correction (DFT-D) for the 94 Elements H-Pu. *J Chem Phys* **2010**, *132*, 154104.

50. Frenkel, D.; Smit, B., *Understanding Molecular Simulation: From Algorithms to Applications*; Elsevier, 2001; Vol. 1.

51. Jones, J. E., On the Determination of Molecular Fields.—II. From the Equation of State of a Gas. *Proc R Soc Lond A* **1924**, *106*, 463-477.

52. Verlet, L., Computer "Experiments" on Classical Fluids. I. Thermodynamical Properties of Lennard-Jones Molecules. *Phys Rev* **1967**, *159*, 98.

CHAPTER 2. STACKING FAULTS IN ZIF-8 POLYMORPHS*

2.1 Introduction

Metal organic frameworks (MOFs) are crystalline porous materials self-assembled from metal centers connected by organic linkers. They have potential applications in catalysis[1], gas adsorption[2], separation[3-4], storage[5], sensing[6-7], and drug delivery[8] processes. MOFs are attractive because they can be tailored through choice of synthesis solvent[9], organic linkers[10], and metal centers[11]. Alternatively, various post-synthetic modifications and ligand mixing strategies can provide further functionality[12-13]. A potential weakness of MOFs is their susceptibility to degradation in aqueous or acid gas environments[14], which can limit application and lifetime. Improvements in MOF thermal and chemical stability are likely to play a key role in expanding the scope of these materials for industrial implementation[15]. Based in part on the well-known catalytic properties of point defects in zeolites[16], it has been hypothesized that MOF degradation is often driven by reactivity of adsorbents with defect sites on the MOF's external surface and in the bulk structure[17-18]. To discuss the defects that can exist in MOFs, it is useful to first consider defects in zeolites. The interchangeability of Al/P/Si centers in tetrahedral zeolite frameworks allows the existence of range of point defects such as local substitutions[19] or vacancies[20]. The large number of polymorphs of silica that exist also allow a wide range of extended defects in zeolites such as stacking faults[21]. MOFs also exhibit a variety of point defects. Linker vacancies or fragments have been found with FTIR and N_2 adsorption isotherms in

* Material in this chapter has been previously published as Han, R.; Sholl, D.S. "Computational Model and Characterization of Stacking Faults in ZIF-8 Polymorphs". *J Phys Chem C* **2016**, 120, 27380−27388.

HKUST-1[22], MOF-5[23-25], UiO-66[26], and MIL-140[27] among other MOFs. Metal cluster vacancies are not as widely reported but have been inferred with XPS and EXAFS in MOF-505[28]. In some cases, disorder in MOFs is intentionally induced in the form of point defects, such as the introduction of monocarboxylate modulators during UiO-66 synthesis to control the defect concentration by terminating an open metal site in lieu of a linker[29-30].

Extended defects in MOFs are more difficult to detect than in zeolites since organic linkers are often destroyed by traditional electron microscopy techniques for visualizing zeolite stacking faults[31]. By supplementing a coordinating molecule, however, Xiao *et al.* demonstrated that certain MOF structures can be sufficiently stabilized for high resolution electron microscopy[32]. Confocal microscopy (CFM) and AFM have been used to image plane dislocations[33], fractures[34], and dislocation growth spirals[35] in HKUST-1. Small-angle synchrotron X-ray scattering and CFM can also identify mesoscale cavities of correlated linker and metal vacancies in MOF-5[36]. Nonetheless there is not a systematic categorization of extended defects in MOFs analogous to intergrowth disorder in metals and aluminosilicates. Here we investigate one prototypical example of stacking faults in MOFs using computer simulation by suggesting defect structures and predicting their impact on chemical or physical properties that can be compared to experimental measurements.

A natural way to connect known extended defects in zeolites to MOFs is to consider zeolitic imidazolate frameworks (ZIFs), which, as their name indicates, share many structural features with zeolites. Since the Zn-Im-Zn bond angle is similar to the nominally 145° Si-O-Si zeolite bond angle, ZIFs are topologically isomorphic with zeolites. Although only a fraction of the 200+ recognized zeolite topologies[37] have been experimentally synthesized as ZIFs, theoretical studies of hypothetical ZIF polymorphs have investigated

the relationship between structure and stability. Lewis *et al.* performed DFT geometry optimization to calculate total energy of a series of experimentally observed and hypothetical ZIFs with the imidazole (Im) linker[38]. Lewis *et al.* used the observed trend between energy and framework density to suggest several hypothetical structures that should be experimentally accessible. Bouëssel du Bourg *et al.* further analyzed stability of the hypothetical ZIF polymorphs studied by Lewis *et al.* but at a range of temperatures and pressures using classical simulations[39]. More recent modeling work included correcting for free energy of solvation energy to further compare the relative thermodynamic stability of ZIF polymorphs under synthesis conditions[40]. Large libraries of ZIF polymorphs have been generated and analyzed in computer simulations by using similar libraries of hypothetical zeolites[41].

In this chapter, we focus on stacking faults in ZIFs. Stacking faults are known to exist in a number of zeolite topologies, and intergrowth disorder in particular provides a convenient one-dimensional model system where a bulk zeolite is built from a layered construction of the unit cell. A useful illustration of the information that can come from computer simulations of these defects comes from the work of Slawiński *et al*.[42] If a single layer is defined as type A, then a type B layer can be defined with an inversion symmetry to A, with or without an offset perpendicular to the stacking direction depending on the specific structure. The bulk structure is then specified by a single degree of a freedom, the stacking sequence, which dictates whether each layer is A or B type. A pair of zeolites that are built from the same unit cell with different stacking fault rate are known as an intergrowth pair (e.g. one structure is formed AAAA and its pair is formed ABAB). Using this definition, Slawiński *et al.* generated models of CHA zeolites with different faulting

densities and simulated their X-ray diffraction (XRD) patterns[42]. These calculations showed that XRD is sufficiently sensitive to detect approximately 1% defect levels in CHA. Comparisons of the calculated powder patterns to experimental spectra measured for a nominally "defect-free" zeolite showed that even this material had a low degree of faulting[42].

We adapt the methods of Slawiński *et al*. to examine the implications of stacking faults in ZIF polymorphs. By choosing several zeolite structures known to exhibit these kinds of defects, we assess the formation energy of stacking faults in the analogous ZIF-8 polymorphs. Our analysis allows us to consider a specific example of an experimentally reported ZIF, for which we find convincing evidence that the experimentally reported material includes a sizeable density of stacking faults.

2.2 Computational Methods

2.2.1 Molecular mechanics optimization

Due to system size constraints for electronic structure calculations, ZIF structures were energy minimized with force field (FF) methods. The calculations performed in this study used a fully flexible force field developed for ZIF-8 with atomic parameters taken from a generalized AMBER force field (GAFF[43]) modified to match experimental bond lengths and angles[44]. Because this FF is specific to the methylimidazolate linker used in ZIF-8, no FF-based calculations were performed for ZIFs made from linkers with other functional groups. All calculations used fully periodic simulation volumes. Ewald summation was used to calculate Coulombic interactions to a relative accuracy of 10^{-6}. Molecular Dynamics (MD) and energy minimization calculations were carried out with

LAMMPS[45]. Lattice constants and atoms were relaxed using a Polak-Ribiere version of the conjugate gradient algorithm.

2.2.2 Density functional theory (DFT) optimization

Selected structures containing fifteen hundred atoms or fewer were optimized with plane-wave density functional theory (DFT). Calculations were performed in the Vienna Ab-initio Simulation Package (VASP) with projector-augmented wave (PAW) method pseudopotentials[46] and the Perdew-Burke-Ernzerhof (PBE) generalized-gradient approximation (GGA) functional[47]. Atomic positions were first relaxed using a conjugate gradient algorithm with a cutoff energy of 480 eV until all forces were less than 0.05 eV/Å. Subsequently both atomic positions and lattice constants were optimized with the same cutoffs and tolerances. In all calculations, reciprocal space was sampled only at the Γ-point.

2.2.3 Pore diameter and surface area simulation

Pore limiting diameters[48] (PLD) and Brunauer-Emmett-Teller (BET) surface areas were calculated using the Zeo++ software[49]. All atomic radii were taken from the Cambridge Crystallography Data Center (CCDC). The pore dimension of interest was the diameter of the channel parallel to the stacking dimension (perpendicular to the fault interface). These PLD calculations were performed with a ten-sphere (S10) cluster approximation for the Voronoi decomposition[50], which graphs the void space and identifies accessible channel systems. Once the Voronoi network was established, the dimensionality of each channel could be calculated and the surface area could be integrated using Monte Carlo sampling to determine the BET surface area. The channel radius and probe molecule radius were both set as 1.8 Å, which is comparable to the size of a nitrogen gas molecule.

2.2.4 X-ray diffraction (XRD) simulation

Powder diffraction patterns were simulated in Mercury[51] with source wavelength λ = 1.54056 Å (corresponding to Cu Kα radiation). Lattices were composed of 1×1×50 unit cells with 50 stacking layers and 27600 atoms. Hydrogen atoms were assigned isotropic atomic displacements of 0.06 $Å^2$; all other atoms were assumed to have 0.05 $Å^2$ displacements. Peaks were assumed to be symmetric with pseudo-Voight shape and 0.05° full width half maximum.

2.3 Results and Discussion

2.3.1 Defining a stacking fault model

We identified five zeolite topologies known to form intergrowths: CHA, FAU, CDO, RTH, and TON. The defect free zeolite structures were obtained from the Database of Zeolite Structures[37]. Stacking layers of the defect free zeolite (type A layers) were defined such that the z axis contained the stacking fault. Faulted (type B) layers were related to the defect free layers through inversion symmetry. In order to analyze the stacking disorder in MOF materials, an isomorphic ZIF was initially constructed for each topology using the ZIF-8 2-methyl imidazolate (mIm) organic linker by (i) replacing each Si of the zeolite with a Zn ion, (ii) replacing the oxygen in the Si-O-Si bond with a mIm ligand, and (iii) scaling the unit cell dimensions such that all bond lengths are consistent with bonds in ZIF-8. We denote each material as STR-ZIF8, where STR is the three letter zeolite structure type.

It is important to note that the five polymorphs we have examined do not include the experimentally observed structure of ZIF, SOD-ZIF8[52]. **Table 2.1** compares energies

of the relaxed defect free polymorphs relative to the SOD-ZIF8 structure. The experimentally realized ZIF-8 material (SOD-ZIF8) is unsurprisingly predicted to be lower energy than the hypothetical polymorphs. These energy differences from our FF calculations are of similar scale to the relative energies between geometry optimized hypothetical $Zn(IM)_2$ polymorphs and SOD-$Zn(IM)_2$, reported by Lewis *et al.* using DFT methods.[38] In Section 2.3.6, we also compare our results to a ZIF based on linkers with a different functional group than ZIF-8 that has been experimentally observed in one of the structures we analyzed, namely CHA.

Table 2.1. ZIF polymorph energies relative to SOD-ZIF8.

Structure (STR-ZIF8)	Energy relative to SOD-ZIF8 (*kJ/mol/Zn*)
CHA topology ZIF-8 polymorph (CHA-ZIF8)	2.72
FAU topology ZIF-8 polymorph (FAU-ZIF8)	1.57
RTH topology ZIF-8 polymorph (RTH-ZIF8)	1.91
CDO topology ZIF-8 polymorph (CDO-ZIF8)	2.21
TON topology ZIF-8 polymorph (TON-ZIF8)	1.02

2.3.2 Energy differences between defective and defect-free structures

A 1×1×4 superlattice was constructed for each ZIF-8 polymorph. The defect structure contained a single substituted type B layer, as shown for the CHA-ZIF8 polymorph in **Figure 2.1 (**additional polymorphs in **Figure A.1** through **Figure A.4**), creating two stacking interfaces (AB) and (BA) each containing 16 interfacial Zn centers. At 2208 atoms (96 Zn) in the superlattice, CHA-ZIF8 was the smallest structure; FAU-ZIF8 was the largest with 17664 atoms (768 Zn). All structures were relaxed using force field methods. The formation energy of a defect is defined as follows, where the total energy is normalized by the number of metal (Zn) centers in the structure[38]:

$$\Delta E_{formation} = E_{defect\ structure} - E_{defect\ free\ structure} \quad (2\text{-}1)$$

This definition is not intended to imply that the defect formation energy is distributed evenly among all atoms (or bonds) in a structure, but it has the advantage that it allows comparison with previously computed energy differences between ZIF-8 polymorphs[38].

Table 2.2. Defect formation energy for ZIF-8 polymorphs, force field calculations.

Structure	$\Delta E_{formation}$ (*kJ/mol/Zn atom*)
CHA-ZIF8	-0.39
FAU-ZIF8	-0.12
RTH-ZIF8	-1.03
CDO-ZIF8	-0.85
TON-ZIF8	-2.36

Table 2.2 lists formation energies of introducing a stacking fault for each polymorph. The magnitude of formation energies, ranging from 0.1 to 1 kJ/mol/Zn, is generally smaller than the energy differences between the defect free polymorphs and SOD-ZIF8 (see **Table 2.1**). One unexpected exception is that the presence of stacking faults in TON-ZIF8 is predicted by our FF calculations to stabilize the structure such that it has a lower energy than SOD-ZIF8. A second interesting observation from these results is that all of the defect formation energies are negative. This suggests that materials with stacking faults are enthalpically favored relative to the defect-free structures, and stacking faults may offer stability. In contrast, there is an energy penalty associated with forming a fault interface in aluminosilicates such as the FAU/EMT intergrowth pair[53] or other magneso-silicates[54].

To determine whether the ZIF-8 force field used for the calculations above can appropriately describe ZIFs with the same mIm linker but different topologies, minimized energies were also calculated using DFT for the CHA-ZIF8 polymorph with and without a

stacking fault. Smaller 1×1×2 systems (AA) and (AB) were compared; these supercells each contain 1104 atoms. The resulting formation energy of a CHA-ZIF8 stacking fault was -1.07 kJ/mol/Zn atom calculated with DFT and -0.67 kJ/mol/Zn atom computed using force field methods. The two results are both negative and of similar order of magnitude, indicating good agreement between the two levels of theory. This provides a reasonable degree of confidence in the FF results presented in **Table 2.2**.

2.3.3 Comparing pore diameter and surface area of defect and defect-free structures

The effect of stacking faults on molecular diffusion in the polymorphs we have considered can be measured by the relevant pore limiting diameters (PLD) in the stacking direction, since changes in the PLD would result in different molecular hopping rates. These pore diameters are listed in **Table A.1**. In the CDO and TON polymorphs there are no pores normal to the plane of stacking faults, so the defects have no impact on diffusion. For the five topologies considered, introduction of a stacking fault has no significant impact on diffusion. The presence of a stacking fault does not change CHA-ZIF8 and FAU-ZIF8 pore diameters along the stacking direction, and increases the channel diameter in RTH-ZIF8 by 0.34 Å. Similarly, there was no significant surface area penalty associated with a stacking fault (data shown in **Table A.2**), an unsurprising result given that pore diameters were not significantly affected by disorder. An implication of these results is that agreement between experimentally observed and predicted surface areas for these or similar materials cannot be used to exclude (or demonstrate) the presence of stacking faults.

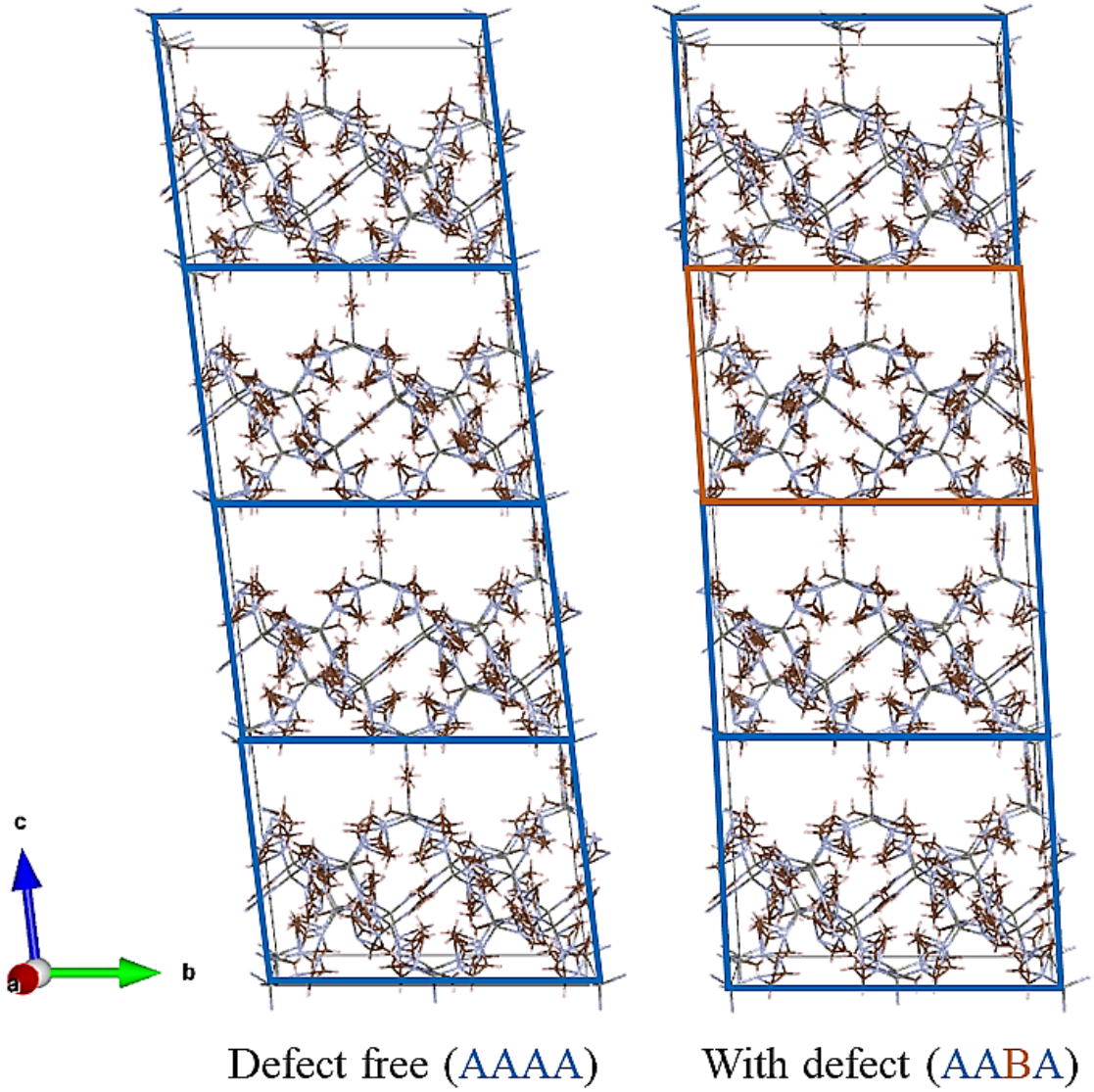

Figure 2.1. CHA-ZIF8 polymorph with and without a stacking fault. The defect free (type A) layer is shown in blue. The inverted layer (type B), which forms two fault interfaces, is shown in red.

2.3.4 X-ray diffraction (XRD) analysis of ideal and defective crystals

X-ray diffraction is an ideal tool for characterizing deviations from long-range order in crystalline materials. Here, we compare simulated spectra of ZIFs with and without stacking faults to correlate changes in XRD peaks to defect density. We focus on the CHA topology as a case study since an experimentally observed material exists that has the same topology as the hypothetical ZIF-8 CHA polymorph we have studied to a synthesized

hybrid of ZIF-8 and ZIF-76. IM-22[55] also known as ZIF-301[56], is the first known ZIF with the CHA topology, synthesized with equal parts 2-methylimidazolate (2-mIm) and 5-chlorobenzimidazolate (ClbIm) linkers. Because of the mixed linkers in IM-22, this material can be thought of as a hybrid of ZIF-8 and ZIF-76[57]. Its temperature stability and large pore volume have suggested its use for separation of C_6 paraffins[55]. Nguyen *et al.* also synthesized the isomorphs ZIF-300 and ZIF-302 which replace the ClbIm linkers with methylbenzimidazolate (mbIm) and bromobenzimidazolate (BrbIm), respectively.

The following discussion will first investigate how stacking faults can potentially be detected from changes to the characteristic peaks of CHA-ZIF8. By creating hypothetical structures with known stacking sequences and calculating the corresponding diffraction pattern, we identify correlations between stacking fault ratio (SFR) and XRD spectra. After identifying the XRD signatures of stacking faults, we will apply this knowledge to compare simulated and measured ZIF-301 powder patterns to test the hypothesis that we will find evidence for the presence of stacking faults in the experimental XRD spectra.

2.3.5 Estimating fault density from XRD

Stacking faults are parameterized by the density of defects as well as an order parameter describing the precise sequence of layers. The stacking fault ratio (SFR) is defined as

$$\mathrm{SFR} = \frac{\#\ \text{of defect interfaces}}{\#\ \text{of total layers}} \tag{2-2}$$

where defect interfaces are stacking transitions (A to B or vice versa) and the total number of layers is fixed for a periodic unit. Defining an order parameter is more complicated.

Short of specifying the complete stacking sequence, one convenient order parameter is the average ratio of consecutive A and B layers. For example, in a periodic 50 layer superlattice, the ratio A:B = 4:1 if the first 40 layers are type A and the next 10 layers are type B.

Figure 2.2 demonstrates the dependence of scattering on the layer order parameter for CHA-ZIF8 with SFR = 0.02. This 2% defect density is sufficient to induce noticeable changes from the spectra of the defect-free material, with several peaks broadening or splitting. For example, the main peak at 6.7° shows more peak splitting with increased number of faulting interfaces. The peak at 9.2° varies in relative intensity (the most peak in each pattern was used to normalize each spectrum) and width. While the peak at 8.3° shows some splitting, it remains fairly narrow whereas the peak 10.6° both splits and broadens.

The data above provides unambiguous evidence that stacking faults create noticeable effects in the XRD spectra of CHA-ZIF8. It may be challenging, however, to deduce the degree of stacking disorder from an experimental XRD measurement because of confounding effects such as finite crystal size effects and other complications. It is therefore useful to seek signatures within XRD spectra that are strongly correlated to the presence of stacking faults.

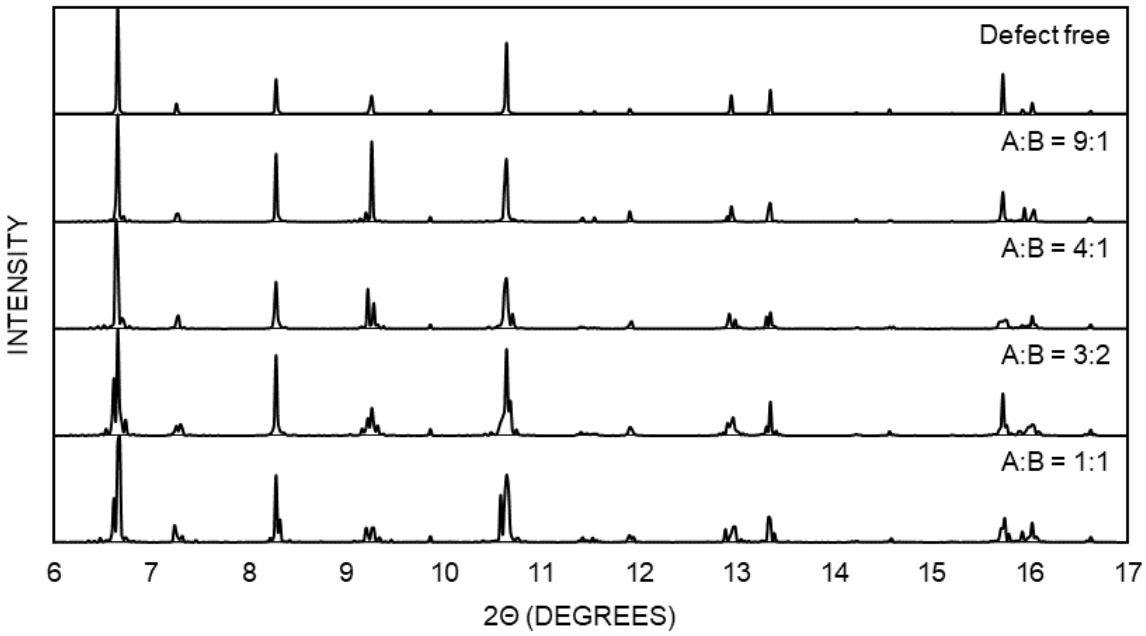

Figure 2.2. Simulated XRD spectra for CHA-ZIF8 as a function of the ratio of consecutive A to B layers for SFR = 0.02 (1 stacking interface in 50 layers).

To seek correlations of the type just discussed, we simulated the XRD spectra of a large number of CHA-ZIF8 samples. In each sample, the faulting probability was defined as the probability that the next (subsequent) stacking layer is not the same type as the current layer; in a superlattice with infinitely many layers, the SFR approaches the faulting probability. For each sample, we constructed a CHA-ZIF8 volume with 50 layers generated given a target faulting probability by inserting a stacking fault in each layer with the specified faulting probability. Then the actual SFR was then calculated for each structure by counting the fraction of defect interfaces in the 50 layer unit. For each of the simulated spectra, we scaled the maximum peak value to 100 and determined the peak intensities, positions, areas, and full-width half-maximum (FWHM). We defined signature peaks of the defect free CHA-ZIF8 structure as those with intensity greater than or equal to 5% of the maximum peak intensity. The corresponding 2θ position ±0.5° of each signature peak was considered the domain over which area was integrated for XRD patterns of defect

structures. Since stacking faults are exhibited as peak splitting and broadening in the diffraction patterns, we identified peak intensities of defect spectra as the maximum intensities on each peak domain. FWHM was determined by identifying the range of 2θ values for which spectral intensity was greater than or equal to half the peak intensity.

This procedure was repeated for ten simulated structures at a range of SFR values from 0 to 0.42. For each SFR, the XRD spectra and calculated peak properties were averaged. Various changes in peak intensity and area are evident as a function of SFR, shown in **Figure A.5**. In particular, the peaks at 6.66° and 10.64° show more splitting and broadening with increasing SFR, while the relative intensity of the peaks at 9.25° and 12.95° diminish with higher defect density.

To quantify the visual trends, principal component analysis (PCA) was employed to score peak intensities, positions, areas, and FWHM for the set of data with ten peaks for each of ten XRD spectra for each of nineteen SFR (not including SFR = 0, which has a unique structure). Peak position and FWHM did not vary significantly with SFR, but relative peak intensity and area each had primary and secondary principal components that respectively accounted for more than 80% and 7% of the variation. The strongest trends were selected from peaks with high correlation coefficients for the largest principal components. **Figure 2.3** shows how relative intensity of the peak at 10.64° decreases almost linearly with increasing SFR, while the relative intensity at 15.72° decreases dramatically for low SFR and then approaches a constant. Similarly, **Figure 2.4** shows how the area of the peaks at 9.26° and 10.64° decrease in linear relation to increasing SFR. The left correlation in **Figure 2.4** suggests that a peak 9.26° to 8.28° area ratio of 0.68 could correspond to SFR = 0 or SFR = 0.22-0.2; additional experimental analysis would be

necessary to determine whether a defect-free sample (i.e. SFR = 0) were realistic. Additional correlations as well as PCA coefficients and components are presented in the Appendix A (**Table A.3** and **Table A.4**; **Figure A.6** and **Figure A.7**).

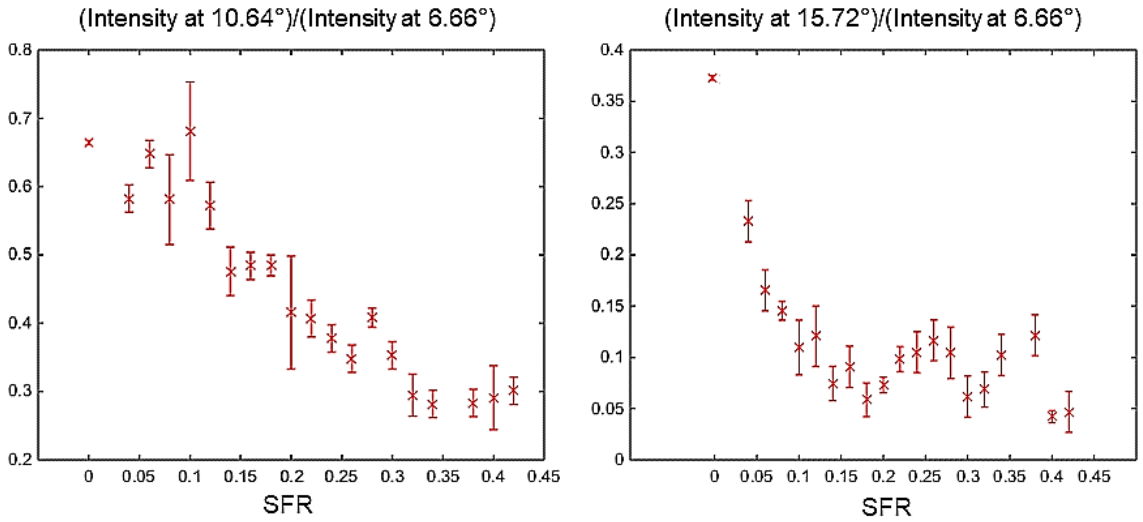

Figure 2.3. Strongest correlations of average peak intensity ratios to SFR.

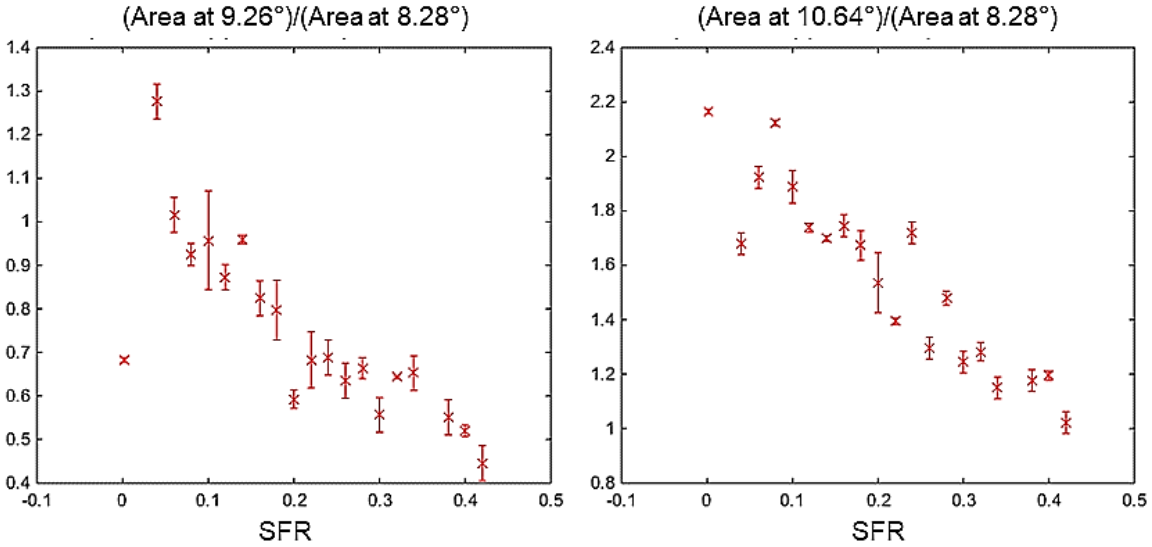

Figure 2.4. Strongest correlations of average peak area ratios to SFR.

The impact of SFR on XRD spectra visible in **Figure 2.2** and quantified in **Figures Figure 2.3** and **Figure 2.4** for the hypothetical CHA-ZIF8 polymorph are also evident when comparing experimental diffraction spectra of the CHA zeolite (chabazite). Li *et al.* investigated two different Si/Al ratio variants of chabazite, representing frameworks with intergrowth between the CHA and AEI topologies[58]. Their respective powder patterns exhibit significant peak broadening and splitting compared to the narrow peaks in high silica chabazite[59]. Prominent broadening and splitting of the peaks at 20.51° and 30.44° (in **Figure A.8**) correspond to structural changes at the $(3\bar{1}0)$ and $(42\bar{1})$ diffraction planes. These changes may be related to the CHA-ZIF8 peak intensity correlations shown in **Figure 2.3**, where the peak at 10.64° is a result of interference from the (310) plane and the peak at 15.72° is a result of interference from the $(4\bar{2}1)$ plane.

2.3.6 Predicting the presence of stacking faults in hybrid ZIFs with CHA topology

If an experimental XRD measurement were available for CHA-ZIF8, the peak intensities and areas could be calculated, scored, and compared to the reported trends in order to estimate the sample's SFR. While CHA-ZIF8 is a hypothetical structure, ZIF-30X (where X = 0 for mbIm, 1 = ClbIm, or 2 for BrbIm) is a synthesized ZIF with CHA topology. Unfortunately the compositional differences between ZIF-8 and ZIF-30X invalidate use of the FF developed for ZIF-8[43], which in turn currently precludes direct modeling and optimizing of extended defects in ZIF-30X.

To aid interpretation of the experimentally reported ZIF-30X XRD results, we first generated a unit cell of ZIF-301 according to experimental lattice constants and postulated linker distribution[56]. The ClbIm ligand in ZIF-301 is the smallest of the ZIF-30X linkers, and therefore the easiest to optimize; however, it is expected that for steric reasons, the

structures of ZIF-300, ZIF-301, and ZIF-302 will look similar in terms of linker distribution[56]. Of the 72 linker positions in the unit cell, Nguyen *et al*. identified 18 specifically occupied by mIm and 18 by ClbIm, as well as 36 nonspecific positions that could be occupied by either linker. We populated the nonspecific linker positions by staggering ClbIm, the bulkier ligand, around each ring to minimize steric hindrance and maximize symmetry. DFT optimization of defect-free ZIF-301 was performed to relax atomic positions for fixed lattice constants. We varied the occupation of the 36 nonspecific linker positions to obtain mIm:ClbIm ratios from 0.8 (16/20) to 1 (18/18). Simulated diffraction of the geometry optimized structures, shown in **Figure 2.5**, yield equivalent powder patterns with slight differences in peak intensity but not position or width. The CHA-ZIF8 powder pattern is shown for comparison. Since the peaks in the diffraction patterns for CHA-ZIF8 and ZIF-301 are not shared and represent scattering off different diffraction planes, we unfortunately cannot directly extend the SFR analysis in **Figure 2.3** and **Figure 2.4** to ZIF-30X.

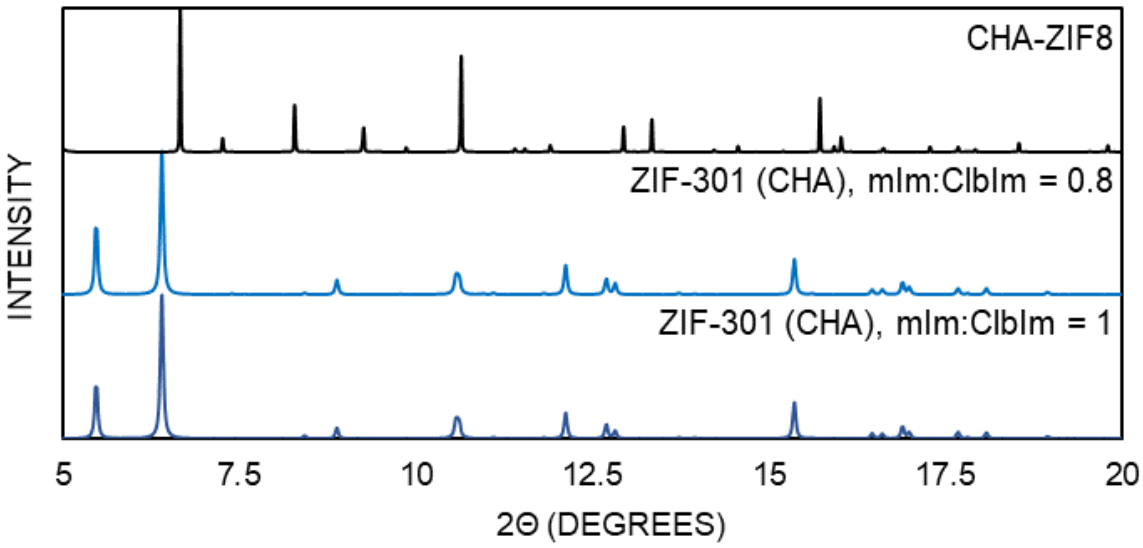

Figure 2.5. Simulated XRD spectra of relaxed CHA-ZIF8 and ZIF-301 with different linker ratios. The lack of shared peaks prevents extension of SFR analysis to the ZIF-301 structure. Linker distribution and composition (for mIm:ClbIm close to 1) have an effect on peak intensity, but not position or width.

Figure 2.6 compares XRD spectra simulated for the ZIF-301 DFT-minimized structure (yellow, labelled "mIm:ClbIm = 1") as well as experimental PXRD patterns of activated ZIF-300, ZIF-301, and ZIF-302 reproduced from Nguyen *et al.*[56] Peak splitting in the experimental data is visible in the peaks at 5.4°, 6.5°, 11.8°, and 12.9°, while broadening is also seen at 17.4°, 21.5°, and 23.6°. The similarity of key features is expected for structures with approximately equal lattice constants (PXRD measured lattice dimensions of the three ZIF-30X variants did not differ by more than 0.5 Å in any dimension[56]) and the same topology. The differences in which peaks split and how they split across the powder patterns could indicate structural deviations specific to the sample. The similarity between the experimental and simulated patterns, as well as reported crystal purity and lack of guest molecules detected in TGA[56], suggest the existence of stacking faults could explain the peak splitting and broadening observed experimentally. We

therefore conclude that the experimental data of Nguyen *et al*. provides indirect evidence for the presence of stacking faults in ZIF-30X crystals.

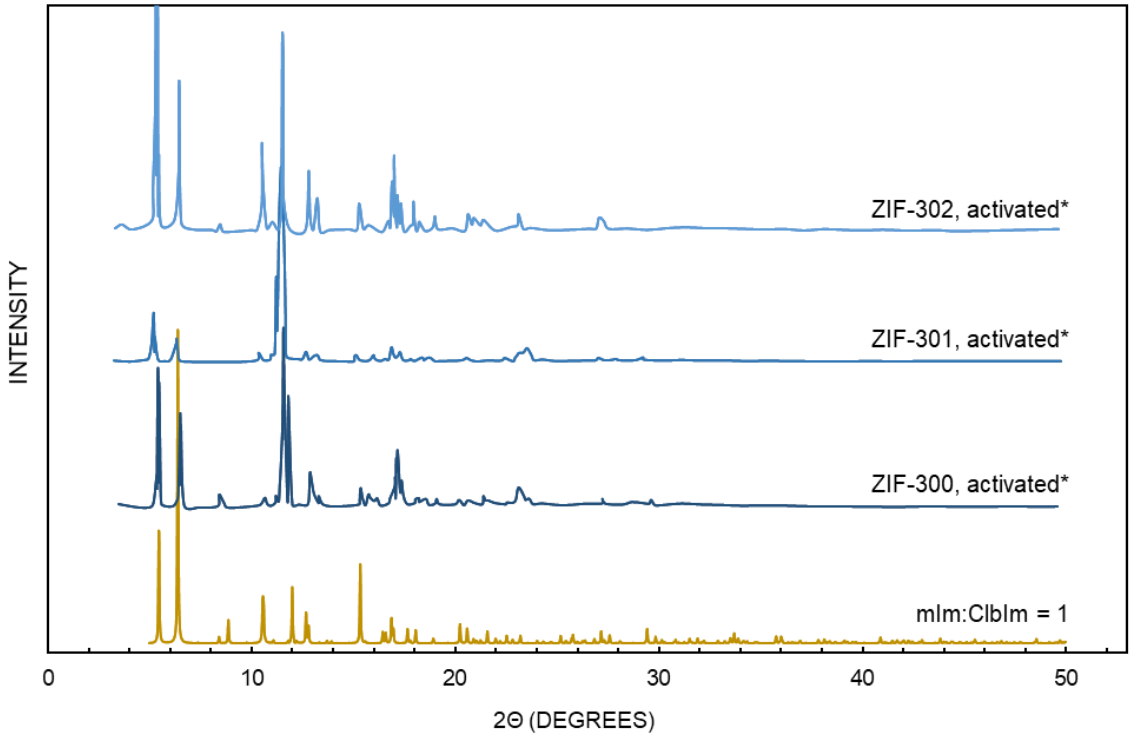

Figure 2.6. Comparison of simulated diffraction spectra for ZIF-301 and experimental PXRD patterns for activated samples of ZIF-300, ZIF-301, and ZIF-302, reproduced from Nguyen *et al*.[56] (indicated by *).

2.4 Conclusion

In summary, we demonstrated that stacking faults in ZIFs can be energetically accessible or even favorable by examining five ZIF-8 polymorphs where the topologically analogous zeolite is known to form intergrowth structures. We also assessed the impact of extended defects on material properties. There was no significant change in channel diameters of pores along the stacking direction for the five topologies considered. The cavity diameters were larger upon including a fault interface, which may imply lower

kinetic barriers to diffusion. There was no surface area penalty associated with stacking faults.

We simulated X-ray diffraction (XRD) patterns for a series of structures in the CHA topology with varying stacking fault ratios (SFR). The narrow diffraction peaks of a pristine structure were observed to split and broaden upon introducing stacking faults. We created a model associating trends in XRD features to defect density in the CHA-ZIF8 polymorph. Strong correlations were identified for variations in peak intensities and areas with increasing SFR.

Connecting our work to existing experimental literature, we found indications of defects based on reported powder patterns of ZIF-301, an experimental CHA topology ZIF with hybrid mIm/ClbIm linkers described by Nguyen *et al*.[56] Comparing measured and simulated XRD spectra for ZIF-301 indicated possible defect-induced peak broadening and splitting in the experimental patterns, consistent with stacking faults. We therefore conclude that stacking faults are likely to exist in real ZIFs.

APPENDIX A. SUPPORTING INFORMATION FOR CHAPTER 2

A.1 Additional ZIF-8 Polymorphs Emphasizing the Extended Defect

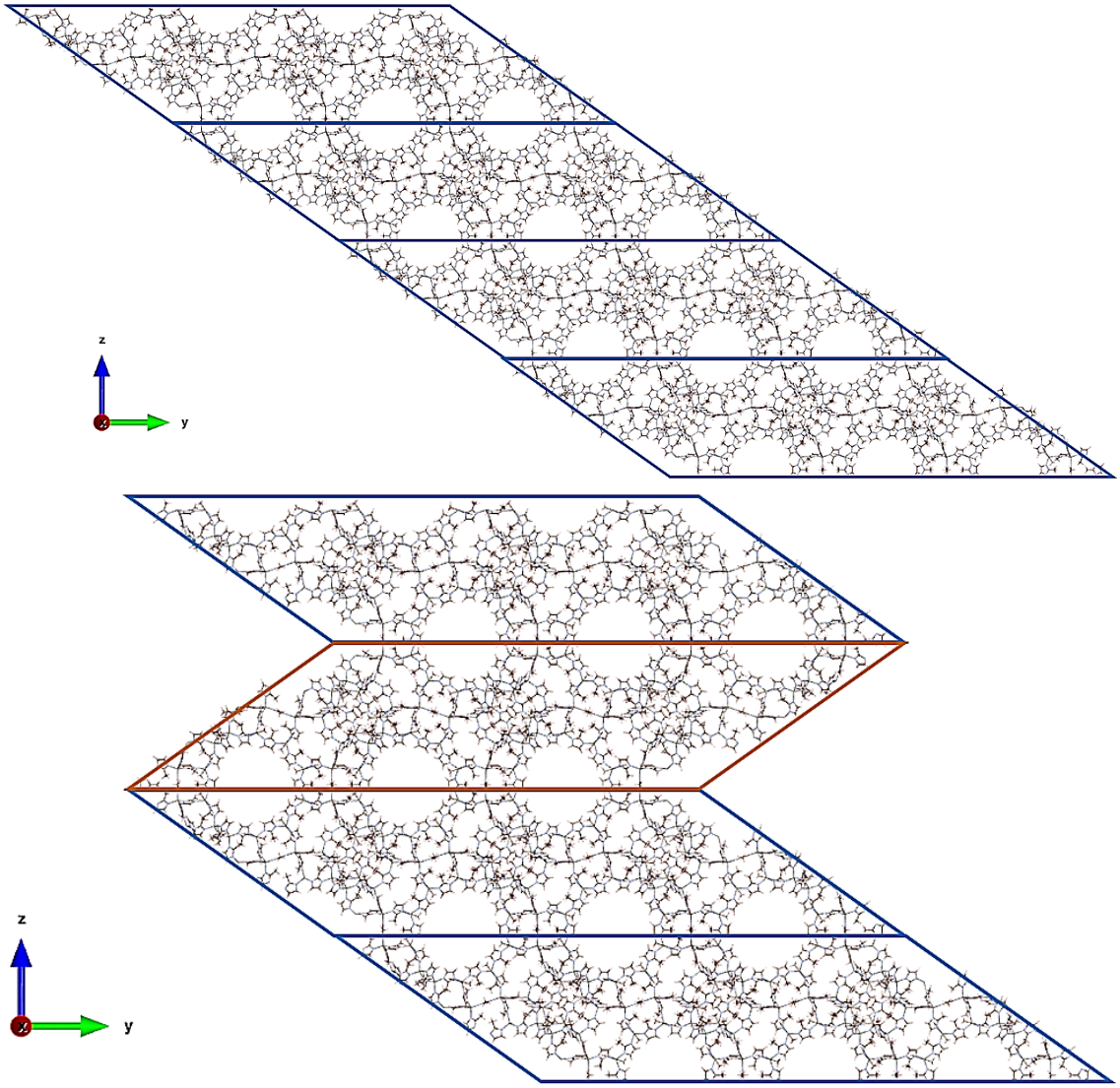

Figure A.1. FAU-ZIF8 without (top) and with (bottom) a stacking fault. The defect free (type A) layer is shown in blue. The inverted layer (type B), which forms two fault interfaces, is shown in red.

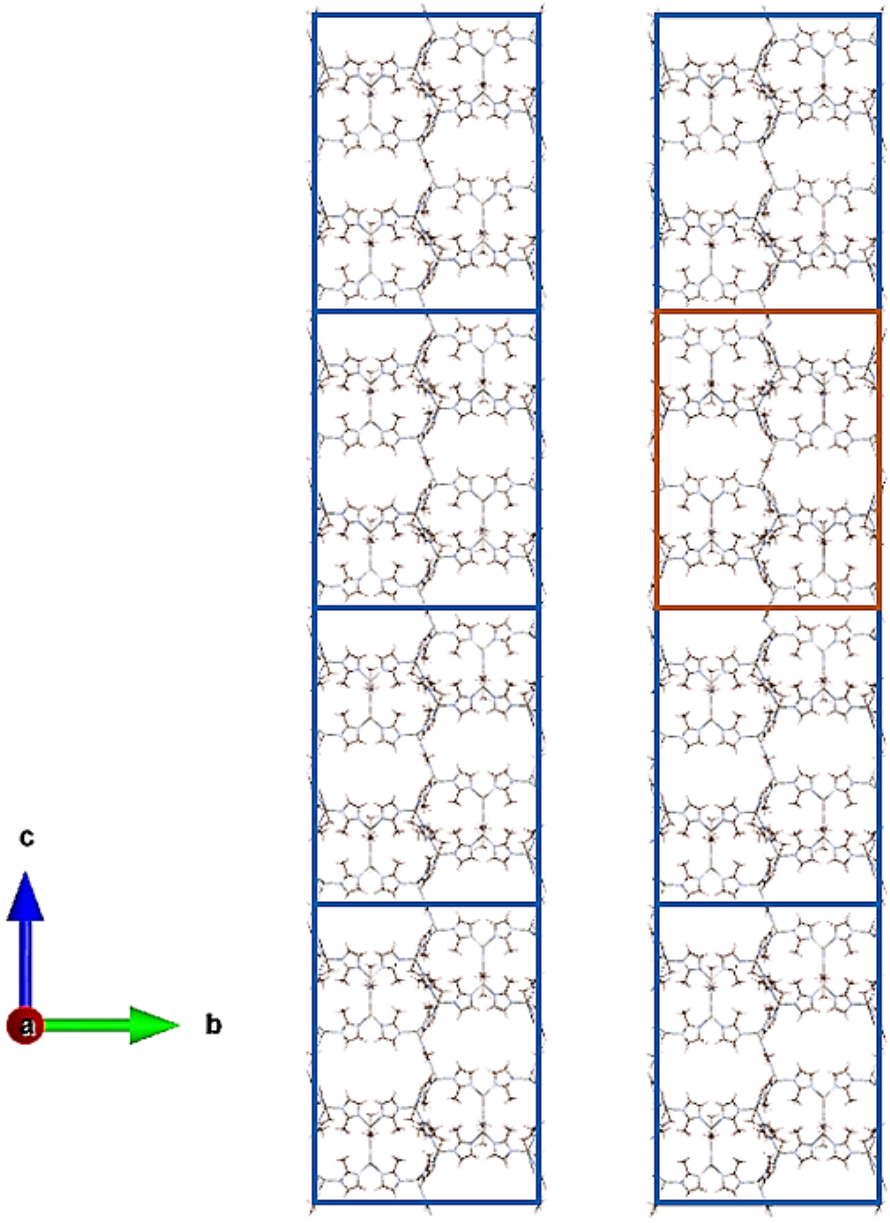

Figure A.2. CDO-ZIF8 without (left) and with (right) a stacking fault. The defect free (type A) layer is shown in blue. The inverted layer (type B), which forms two fault interfaces, is shown in red.

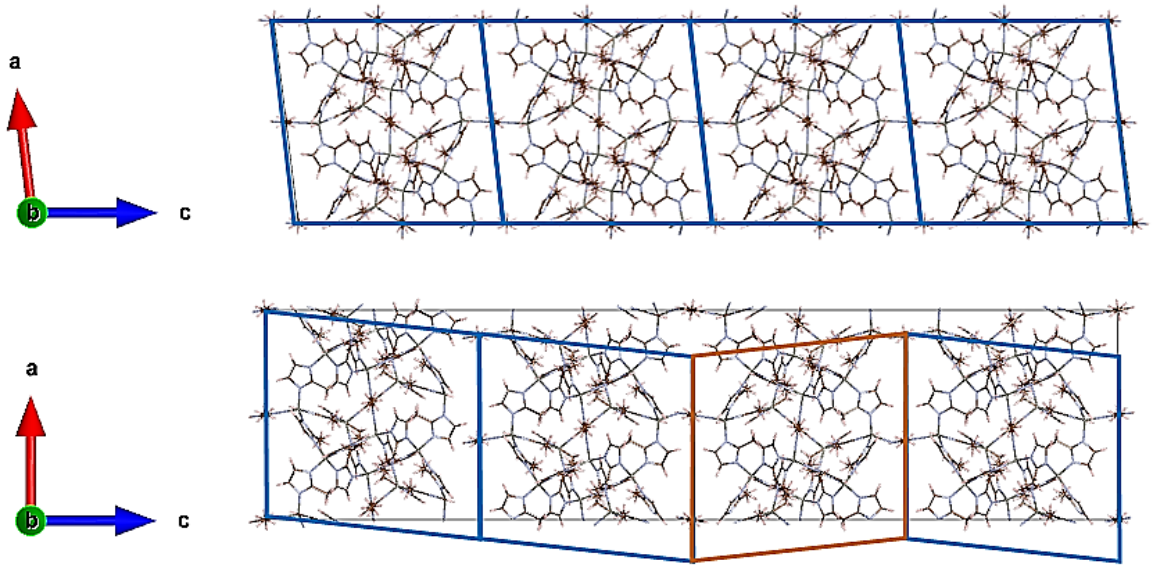

Figure A.3. RTH-ZIF8 without (top) and with (bottom) a stacking fault. The defect free (type A) layer is shown in blue. The inverted layer (type B), which forms two fault interfaces, is shown in red.

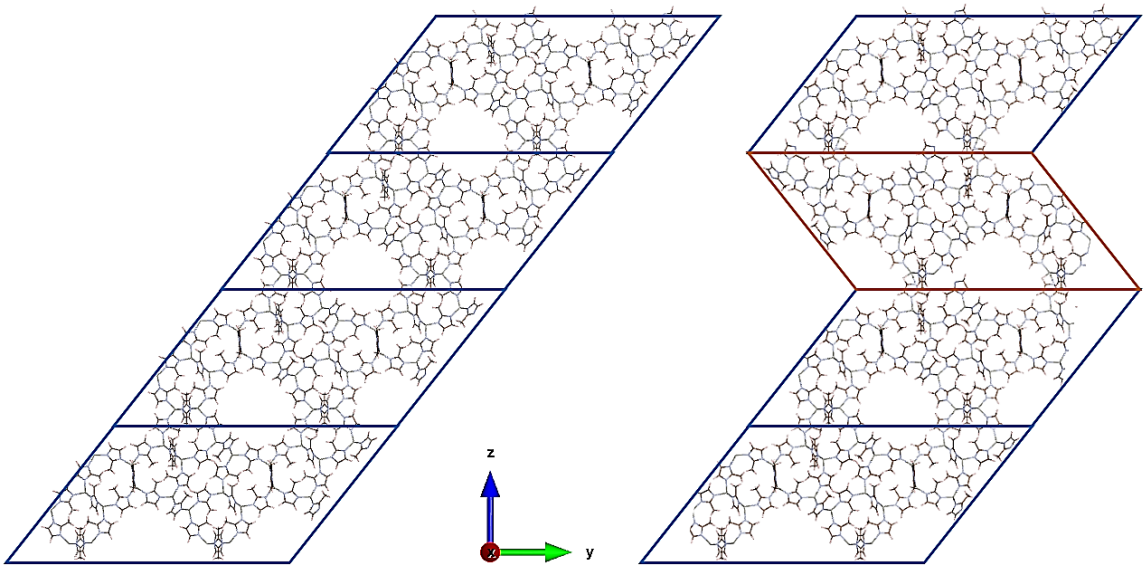

Figure A.4. TON-ZIF8 without (left) and with (right) a stacking fault. The defect free (type A) layer is shown in blue. The inverted layer (type B), which forms two fault interfaces, is shown in red.

A.2 Comparison of Simulated Pore Diameter and Surface Area for ZIF-8 Polymorphs With and Without a Stacking Fault

Table A.1. Pore limiting diameters in structures with and without a stacking fault.

	CHA-ZIF8	FAU-ZIF8	CDO-ZIF8	RTH-ZIF8	TON-ZIF8
Defect free (AAAA) structure					
Is there diffusion along the stacking direction?	Yes	Yes	No	Yes	No
If so, what is the relevant pore diameter for diffusion in that direction?	6.52 Å	13.77 Å		15.37 Å	
Structure with a single stacking fault (AABA)					
Is there diffusion along the stacking direction?	Yes	Yes	No	Yes	No
If so, what is the relevant pore diameter for diffusion in that direction?	6.52 Å	13.77 Å		15.71 Å	

Table A.2. Surface area penalty associated with a stacking fault.

Structure	Surface area [m^2/g]	% Difference
CHA-ZIF8	2019.3	
	2006.5	-0.6
FAU-ZIF8	1396.19	
	1396.68	0.1
RTH-ZIF8	1596.1	
	1546.2	-3.1
CDO-ZIF8	1680.6	
	1675.7	-0.3
TON-ZIF8	1506.0	
	1477.1	-1.9
ZIF-8[27]	1439.7	

A.3 Simulated CHA-ZIF8 XRD Pattern of Increasing Stacking Fault Ratio (SFR)

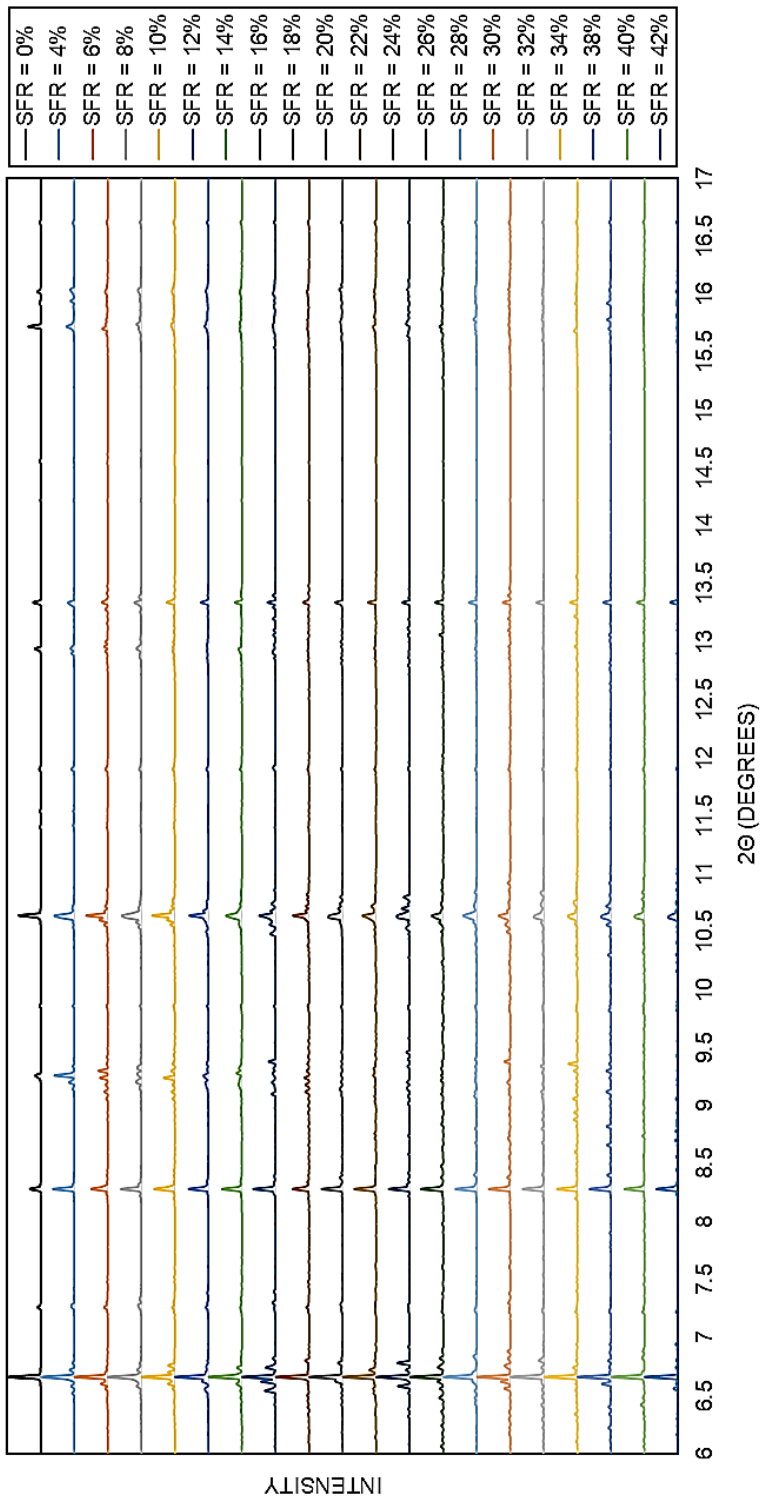

Figure A.5. XRD spectra averaged over ten structures for each SFR.

A.4 Principal Components and Additional Correlations

Coefficients of principal component analysis (PCA) for peak intensity and area are listed in **Table A.3** and **Table A.4**, representing the correlation of the original variables (i.e. signature peaks in the CHA-ZIF8 XRD spectrum) with the principal components determined by PCA. All principal components (PCs) were standardized to have mean at 0. Percent variance explains the percentage of total variance of the data explained by a particular principal component; PCs are listed in order of importance.

Principal components are interpreted by finding the most strongly correlated variables for each component. Strongly correlated variables have coefficients with large magnitudes (positive or negative). Correlations with magnitude greater than 0.5 were considered important, indicated in the table by the highlighted/boldfaced coefficients. The closer the coefficient is the 1, the more strongly the variable is correlated to the PC. Positive coefficients indicate that the variables (peak intensity or area) vary with the principal component, while negative coefficients imply an inverse variation.

Table A.3. Principal component coefficients for peak intensity.

	PC 1	PC 2	PC 3	PC 4	PC 5	PC 6	PC 7	PC 8	PC 9
peak at 6.66	0.00	0.00	0.00	0.00	0.00	0.00	0.00	0.00	**1**
peak at 7.26	0.07	-0.06	-0.11	0.06	0.07	0.37	**0.91**	0.04	0
peak at 8.28	-0.11	0.26	**0.86**	-0.18	0.03	0.15	0.09	-0.33	0
peak at 9.26	**0.67**	**0.68**	-0.15	-0.22	0.10	-0.03	-0.01	0.05	0
peak at 10.64	**0.69**	**-0.67**	0.24	-0.15	-0.01	0.00	-0.05	-0.06	0
peak at 12.94	0.09	0.01	0.18	**0.58**	**0.78**	-0.07	-0.06	0.13	0
peak at 13.34	-0.07	0.00	0.31	-0.23	-0.05	-0.24	0.12	**0.88**	0
peak at 15.72	0.21	0.13	0.19	**0.69**	**-0.59**	-0.24	0.11	0.02	0
peak at 16.04	0.06	0.04	0.04	0.18	-0.15	**0.85**	-0.36	0.31	0
% variance	*70.48*	*19.54*	*5.36*	*2.52*	*1.04*	*0.54*	*0.36*	*0.15*	*0*

Table A.4. Principal component coefficients for peak areas.

	PC 1	PC 2	PC 3	PC 4	PC 5	PC 6	PC 7	PC 8	PC 9
peak at 6.66	**0.60**	**-0.52**	-0.02	-0.59	0.09	0.03	-0.09	0.01	-0.03
peak at 7.26	0.10	0.01	-0.03	0.02	0.18	0.19	0.38	-0.24	**0.75**
peak at 8.28	**0.56**	**0.69**	-0.04	-0.08	-0.40	-0.02	-0.17	-0.05	0.08
peak at 9.26	-0.01	-0.16	**0.90**	0.04	-0.38	0.02	0.04	-0.11	0.06
peak at 10.64	0.36	-0.44	-0.25	**0.70**	-0.33	-0.08	-0.06	-0.06	0.04
peak at 12.94	0.21	0.09	0.02	0.12	0.13	0.49	**0.52**	-0.39	-0.51
peak at 13.34	0.14	0.03	0.01	-0.01	-0.12	-0.24	**0.67**	**0.68**	-0.04
peak at 15.72	0.08	0.02	0.11	0.18	0.13	**0.73**	-0.29	**0.56**	0.09
peak at 16.04	0.34	0.15	0.33	0.32	**0.70**	-0.36	-0.12	0.03	-0.05
% variance	*66.40*	*22.74*	*4.80*	*3.19*	*1.47*	*0.65*	*0.46*	*0.21*	*0.08*

Based on the variables identified by the first four principal components, which account for over 97% of the variance of both peak intensity and peak area with stacking fault rate (SFR), additional correlations of importance are shown in **Figure A.6** and **Figure A.7**.

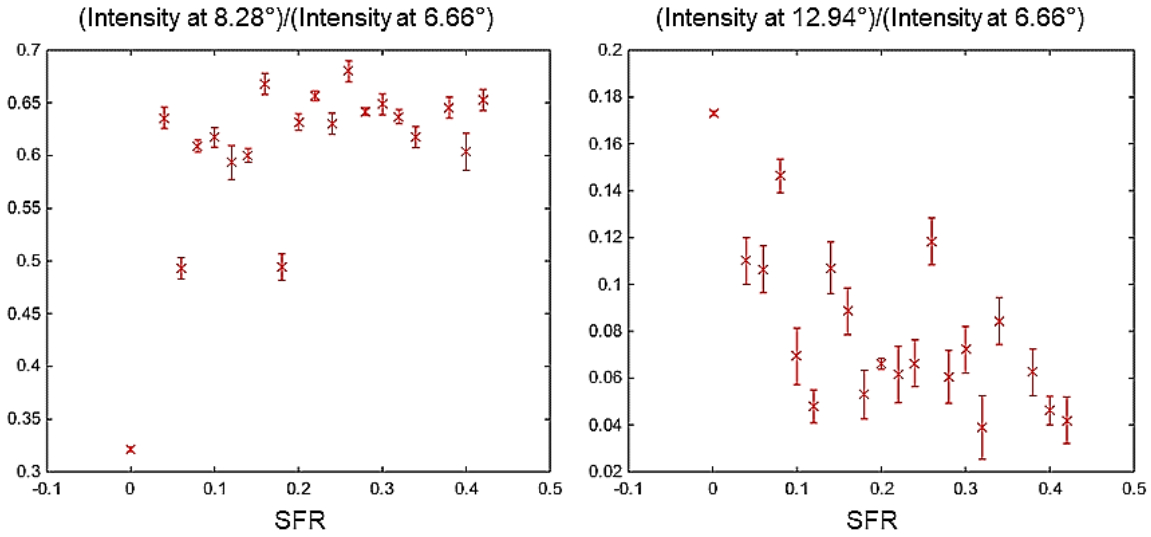

Figure A.6. Correlations of peak intensity to SFR, including standard deviation within each SFR.

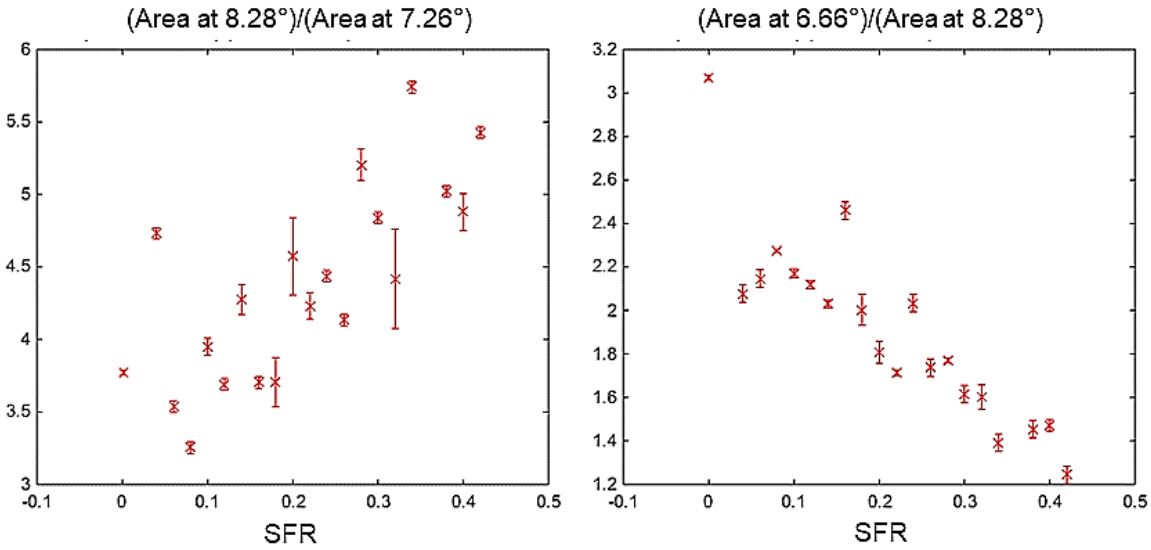

Figure A.7. Correlations of peak areas to SFR, including standard deviation within each SFR.

A.5 Stacking Fault Effect on XRD of Silica Chabazite (CHA)

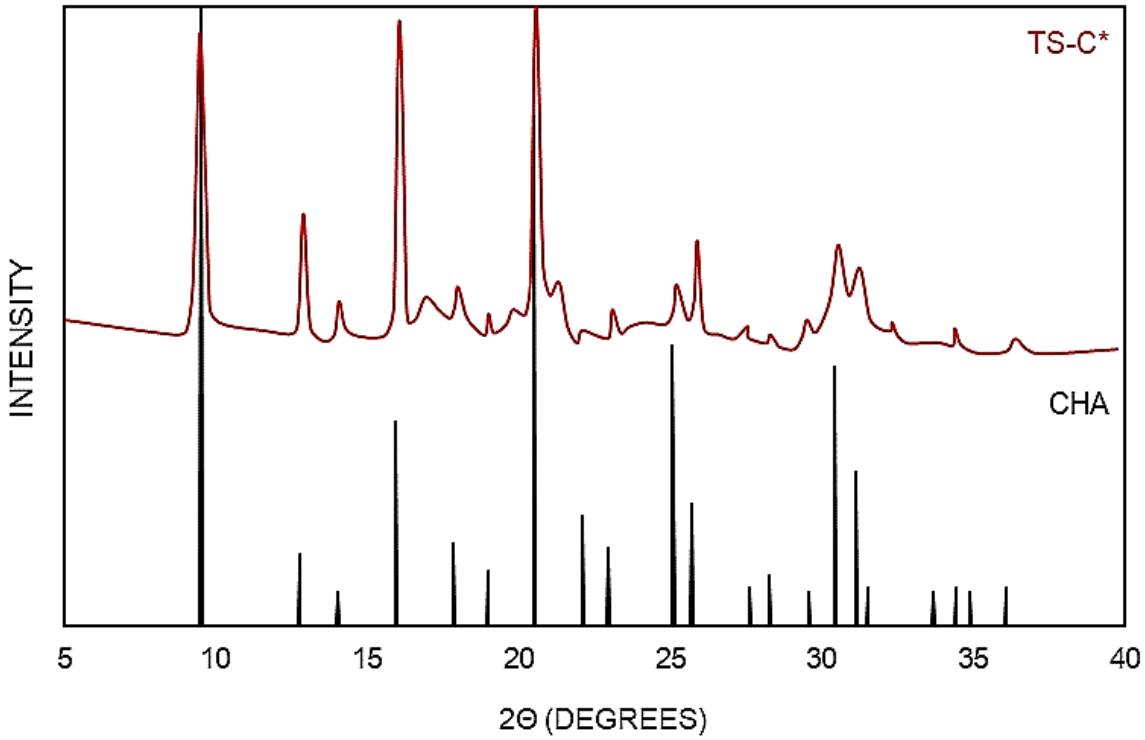

Figure A.8. Comparison of silica chabazite (CHA) powder pattern and the peak broadening/splitting evident in an intergrowth structure (TS-C, reproduced from Li *et al.*[51]).

A.6 REFERENCES

1. Lee, J.; Farha, O. K.; Roberts, J.; Scheidt, K. A.; Nguyen, S. T.; Hupp, J. T., Metal-Organic Framework Materials as Catalysts. *Chem Soc Rev* **2009**, *38*, 1450-9.

2. Bourrelly, S., *et al*., Explanation of the Adsorption of Polar Vapors in the Highly Flexible Metal Organic Framework MIL-53(Cr). *J Am Chem Soc* **2010**, *132*, 9488-9498.

3. Li, J. R.; Kuppler, R. J.; Zhou, H. C., Selective Gas Adsorption and Separation in Metal-Organic Frameworks. *Chem Soc Rev* **2009**, *38*, 1477-504.

4. Keskin, S.; van Heest, T. M.; Sholl, D. S., Can Metal-Organic Framework Materials Play a Useful Role in Large-Scale Carbon Dioxide Separations? *Chem Sus Chem* **2010**, *3*, 879-91.

5. Millward, A. R.; Yaghi, O. M., Metal-Organic Frameworks with Exceptionally High Capacity for Storage of Carbon Dioxide at Room Temperature. *J Am Chem Soc* **2005**, *127*, 17998-9.

6. Khoshaman, A. H.; Bahreyni, B., Application of Metal Organic Framework Crystals for Sensing of Volatile Organic Gases. *Sensor Actuat B Chem* **2012**, *162*, 114-119.

7. Achmann, S.; Hagen, G.; Kita, J.; Malkowsky, I. M.; Kiener, C.; Moos, R., Metal-Organic Frameworks for Sensing Applications in the Gas Phase. *Sensors (Basel)* **2009**, *9*, 1574-89.

8. Horcajada, P.; Serre, C.; Maurin, G.; Ramsahye, N. A.; Balas, F.; Vallet-Regi, M.; Sebban, M.; Taulelle, F.; Ferey, G., Flexible Porous Metal-Organic Frameworks for a Controlled Drug Delivery. *J Am Chem Soc* **2008**, *130*, 6774-6780.

9. Li, C. P.; Du, M., Role of Solvents in Coordination Supramolecular Systems. *Chem Commun* **2011**, *47*, 5958-72.

10. Lalonde, M. B.; Mondloch, J. E.; Deria, P.; Sarjeant, A. A.; Al-Juaid, S. S.; Osman, O. I.; Farha, O. K.; Hupp, J. T., Selective Solvent-Assisted Linker Exchange (SALE) in a Series of Zeolitic Imidazolate Frameworks. *Inorg Chem* **2015**, *54*, 7142-4.

11. Sun, D.; Sun, F.; Deng, X.; Li, Z., Mixed-Metal Strategy on Metal-Organic Frameworks (MOFs) for Functionalities Expansion: Co Substitution Induces Aerobic Oxidation of Cyclohexene over Inactive Ni-MOF-74. *Inorg Chem* **2015**, *54*, 8639-43.

12. Cohen, S. M., Postsynthetic Methods for the Functionalization of Metal-Organic Frameworks. *Chem Rev* **2012**, *112*, 970-1000.

13. Eum, K., *et al*., Highly Tunable Molecular Sieving and Adsorption Properties of Mixed-Linker Zeolitic Imidazolate Frameworks. *J Am Chem Soc* **2015**, *137*, 4191-7.

14. Bosch, M.; Zhang, M.; Zhou, H.-C., Increasing the Stability of Metal-Organic Frameworks. *Adv Chem* **2014**, *2014*, 1-8.

15. Burtch, N. C.; Jasuja, H.; Walton, K. S., Water Stability and Adsorption in Metal-Organic Frameworks. *Chem Rev* **2014**, *114*, 10575-612.

16. Yuan, S.; Si, H.; Fu, A.; Chu, T.; Tian, F.; Duan, Y. B.; Wang, J., Location of Si Vacancies and [Ti(OSi)$_4$] and [Ti(OSi)$_3$OH] Sites in the MFI Framework: A Large Cluster and Full Ab Initio Study. *J Phys Chem A* **2011**, *115*, 940-7.

17. Sholl, D. S.; Lively, R. P., Defects in Metal-Organic Frameworks: Challenge or Opportunity? *J Phys Chem Lett* **2015**, 3437-3444.

18. Fang, Z.; Bueken, B.; De Vos, D. E.; Fischer, R. A., Defect-Engineered Metal-Organic Frameworks. *Angew Chem Int Ed Engl* **2015**, *54*, 7234-54.

19. Yang, J.; Li, L.; Li, W.; Wang, J.; Chen, Z.; Yin, D.; Lu, J.; Zhang, Y.; Guo, H., Tuning Aluminum Spatial Distribution in ZSM-5 Membranes: A New Strategy to Fabricate High Performance and Stable Zeolite Membranes for Dehydration of Acetic Acid. *Chem Commun (Camb)* **2014**, *50*, 14654-7.

20. Baerlocher, C.; Xie, D.; McCusker, L. B.; Hwang, S. J.; Chan, I. Y.; Ong, K.; Burton, A. W.; Zones, S. I., Ordered Silicon Vacancies in the Framework Structure of the Zeolite Catalyst SSZ-74. *Nat Mater* **2008**, *7*, 631-5.

21. Willhammar, T.; Sun, J.; Wan, W.; Oleynikov, P.; Zhang, D.; Zou, X.; Moliner, M.; Gonzalez, J.; Martinez, C.; Rey, F.; Corma, A., Structure and Catalytic Properties of the Most Complex Intergrown Zeolite ITQ-39 Determined by Electron Crystallography. *Nat Chem* **2012**, *4*, 188-94.

22. Položij, M.; Rubeš, M.; Čejka, J.; Nachtigall, P., Catalysis by Dynamically Formed Defects in a Metal-Organic Framework Structure: Knoevenagel Reaction Catalyzed by Copper Benzene-1,3,5-Tricarboxylate. *Chem Cat Chem* **2014**, *6*, 2821-2824.

23. Ravon, U.; Savonnet, M.; Aguado, S.; Domine, M. E.; Janneau, E.; Farrusseng, D., Engineering of Coordination Polymers for Shape Selective Alkylation of Large Aromatics and the Role of Defects. *Micropor Mesopor Mater* **2010**, *129*, 319-329.

24. Huang, B. L.; Ni, Z.; Millward, A.; McGaughey, A. J. H.; Uher, C.; Kaviany, M.; Yaghi, O., Thermal Conductivity of a Metal-Organic Framework (MOF-5): Part II. Measurement. *Int J Heat Mass Transf* **2007**, *50*, 405-411.

25. Gadipelli, S.; Guo, Z., Postsynthesis Annealing of MOF-5 Remarkably Enhances the Framework Structural Stability and CO_2 Uptake. *Chem Mater* **2014**, *26*, 6333-6338.

26. Shearer, G. C.; Chavan, S.; Ethiraj, J.; Vitillo, J. G.; Svelle, S.; Olsbye, U.; Lamberti, C.; Bordiga, S.; Lillerud, K. P., Tuned to Perfection: Ironing out the Defects in Metal–Organic Framework UiO-66. *Chem Mater* **2014**, *26*, 4068-4071.

27. Guillerm, V., Ragon, F.; Dan-Hardi, M.; Devic, T.; Vishnuvarthan, M.; Campo, B.; Vimont, A.; Clet, G.; Yang, Q.; Maurin, G.; Férey, G.; Vittadini, A.; Gross, S.; Serre, C., A Series of Isoreticular, Highly Stable, Porous Zirconium Oxide Based Metal-Organic Frameworks. *Angew Chem Int Ed Engl* **2012**, *51*, 9267-71.

28. Shen, L., Yang, S. W.; Xiang, S.; Liu, T.; Zhao, B.; Ng, M. F.; Göettlicher, J.; Yi, J.; Li, S.; Wang, L.; Ding, J.; Chen, B.; Wei, S. H.; Feng, Y. P., Origin of Long-Range Ferromagnetic Ordering in Metal-Organic Frameworks with Antiferromagnetic Dimeric-Cu(II) Building Units. *J Am Chem Soc* **2012**, *134*, 17286-90.

29. Schaate, A.; Roy, P.; Godt, A.; Lippke, J.; Waltz, F.; Wiebcke, M.; Behrens, P., Modulated Synthesis of Zr-Based Metal-Organic Frameworks: From Nano to Single Crystals. *Chemistry* **2011**, *17*, 6643-51.

30. Fang, Z., Dürholt, J. P.; Kauer, M.; Zhang, W.; Lochenie, C.; Jee, B.; Albada, B.; Metzler-Nolte, N.; Pöppl, A.; Weber, B.; Muhler, M.; Wang, Y.; Schmid, R.; Fischer, R. A., Structural Complexity in Metal-Organic Frameworks: Simultaneous Modification of Open Metal Sites and Hierarchical Porosity by Systematic Doping with Defective Linkers. *J Am Chem Soc* **2014**, *136*, 9627-36.

31. Kashtiban, R. J.; Sloan, J.; Marchbank, H. R.; Dunne, P. W.; Walton, R. I. In *Electron Microscopy Study of Metal-Organic Framework Materials*, European Microscopy Congress, Manchester Central, United Kingdom, September 16 2012; Manchester Central, United Kingdom, 2012.

32. Xiao, B., *et al*., Chemically Blockable Transformation and Ultraselective Low-Pressure Gas Adsorption in a Non-Porous Metal Organic Framework. *Nat Chem* **2009**, *1*, 289-294.

33. Ameloot, R.; Vermoortele, F.; Hofkens, J.; De Schryver, F. C.; De Vos, D. E.; Roeffaers, M. B., Three-Dimensional Visualization of Defects Formed During the Synthesis of Metal-Organic Frameworks: A Fluorescence Microscopy Study. *Angew Chem Int Ed Engl* **2013**, *52*, 401-5.

34. Shöâeè, M.; Agger, J. R.; Anderson, M. W.; Attfield, M. P., Crystal Form, Defects and Growth of the Metal Organic Framework HKUST-1 Revealed by Atomic Force Microscopy. *Cryst Eng Comm* **2008**, *10*, 646.

35. Walker, A. M.; Slater, B., Comment Upon the Screw Dislocation Structure on HKUST-1 {111} Surfaces. *Cryst Eng Comm* **2008**, *10*, 790.

36. Choi, K. M.; Jeon, H. J.; Kang, J. K.; Yaghi, O. M., Heterogeneity within Order in Crystals of a Porous Metal-Organic Framework. *J Am Chem Soc* **2011**, *133*, 11920-3.

37. Baerlocher, C.; McCusker, L. B., Database of Zeolite Structures: http://www.iza-structure.org/databases/. *Structure Commission of the International Zeolite Association (IZA-SC)*, **1996.**

38. Lewis, D. W.; Ruiz-Salvador, A. R.; Gómez, A.; Rodriguez-Albelo, L. M.; Coudert, F.-X.; Slater, B.; Cheetham, A. K.; Mellot-Draznieks, C., Zeolitic Imidazole Frameworks: Structural and Energetics Trends Compared with Their Zeolite Analogues. *Cryst Eng Comm* **2009**, *11*, 2272.

39. Bouëssel du Bourg, L.; Ortiz, A. U.; Boutin, A.; Coudert, F.-X., Thermal and Mechanical Stability of Zeolitic Imidazolate Frameworks Polymorphs. *APL Mater* **2014**, *2*, 124110.

40. Gee, J. A.; Sholl, D. S., Characterization of the Thermodynamic Stability of Solvated Metal–Organic Framework Polymorphs Using Molecular Simulations. *J Phys Chem C* **2013**, *117*, 20636-20642.

41. Simon, C. M., *et al*., The Materials Genome in Action: Identifying the Performance Limits for Methane Storage. *Energy Environ Sci* **2015**, *8*, 1190-1199.

42. Sławiński, W. A.; Wragg, D. S.; Akporiaye, D.; Fjellvåg, H., Intergrowth Structure Modelling in Silicoaluminophosphate SAPO-18/34 Family. *Micropor Mesopor Mater* **2014**, *195*, 311-318.

43. Zhang, L.; Hu, Z.; Jiang, J., Sorption-Induced Structural Transition of Zeolitic Imidazolate Framework-8: A Hybrid Molecular Simulation Study. *J Am Chem Soc* **2013**, *135*, 3722-8.

44. Gee, J. A.; Chung, J.; Nair, S.; Sholl, D. S., Adsorption and Diffusion of Small Alcohols in Zeolitic Imidazolate Frameworks ZIF-8 and ZIF-90. *J Phys Chem C* **2013**, *117*, 3169-3176.

45. Plimpton, S., Fast Parallel Algorithms for Short–Range Molecular Dynamics. *J Comput Phys* **1995**, *117*, 1-19.

46. Blöchl, P. E., Projector Augmented-Wave Method. *Phys Rev B* **1994**, *50*, 17953-17979.

47. Perdew, J. P.; Burke, K.; Ernzerhof, M., Generalized Gradient Approximation Made Simple. *Phys Rev Lett* **1996**, *77*, 3865-3868.

48. Haldoupis, E.; Watanabe, T.; Nair, S.; Sholl, D. S., Quantifying Large Effects of Framework Flexibility on Diffusion in MOFs: CH_4 and CO_2 in ZIF-8. *Chem Phys Chem* **2012**, *13*, 3449-52.

49. Haranczyk, M.; Rycroft, C. H.; Willems, T. F.; Martin, R. L. *Zeo ++*, http://www.maciejharanczyk.info/Zeopp/download.html.

50. Martin, R. L.; Smit, B.; Haranczyk, M., Addressing Challenges of Identifying Geometrically Diverse Sets of Crystalline Porous Materials. *J Chem Inf Model* **2012**, *52*, 308-18.

51. Macrae, C. F.; Bruno, I. J.; Chisholm, J. A.; Edgington, P. R.; McCabe, P.; Pidcock, E.; Rodriguez-Monge, L.; Taylor, R.; van de Streek, J.; Wood, P. A., Mercury CSD 2.0– New Features for the Visualization and Investigation of Crystal Structures. *J Appl Crystallogr* **2008**, *41*, 466-470.

52. Pimentel, B. R.; Parulkar, A.; Zhou, E. K.; Brunelli, N. A.; Lively, R. P., Zeolitic Imidazolate Frameworks: Next-Generation Materials for Energy-Efficient Gas Separations. *Chem Sus Chem* **2014**, *7*, 3202-40.

53. Treacy, M. M. J.; Vaughan, D. E. W.; Strohmaier, K. G.; Newsam, J. M., Intergrowth Segregation in FAU-EMT Framework Materials. *Proc R Soc Lond A* **1996**, *452*, 813-840.

54. Jahn, S.; Martoňák, R., Plastic Deformation of Orthoenstatite and the Ortho- to High-Pressure Clinoenstatite Transition: A Metadynamics Simulation Study. *Phys Chem Miner* **2007**, *35*, 17-23.

55. Peralta, D.; Chaplais, G.; Simon-Masseron, A.; Barthelet, K.; Pirngruber, G. D., Separation of C_6 Paraffins Using Zeolitic Imidazolate Frameworks: Comparison with Zeolite 5A. *Ind Eng Chem Res* **2012**, *51*, 4692-4702.

56. Nguyen, N. T.; Furukawa, H.; Gandara, F.; Nguyen, H. T.; Cordova, K. E.; Yaghi, O. M., Selective Capture of Carbon Dioxide under Humid Conditions by Hydrophobic Chabazite-Type Zeolitic Imidazolate Frameworks. *Angew Chem Int Ed Engl* **2014**, *53*, 10645-8.

57. Jayachandrababu, K. C.; Verploegh, R. J.; Leisen, J.; Nieuwendaal, R. C.; Sholl, D. S.; Nair, S., Structure Elucidation of Mixed-Linker Zeolitic Imidazolate Frameworks by Solid-State ^{1}H CRAMPS NMR Spectroscopy and Computational Modeling. *J Am Chem Soc* **2016**.

58. Li, Y.; Huang, Y. G.; Guo, J.; Zhang, M.; Wang, D.; Wei, F.; Wang, Y., Hierarchical SAPO-34/18 Zeolite with Low Acid Site Density for Converting Methanol to Olefins. *Catal Today* **2014**, *233*, 2-7.

59. Eilertsen, E. A.; Arstad, B.; Svelle, S.; Lillerud, K. P., Single Parameter Synthesis of High Silica CHA Zeolites from Fluoride Media. *Micropor Mesopor Mater* **2012**, *153*, 94-99.

CHAPTER 3. ZIF DEGRADATION BY ACID GASES*

3.1 Introduction

Acid gases (SO_2, NO_x, CO_2, etc.) are harmful to human health, atmospheric conditions, and climate change.[1-3] Humid flue gas exit streams generated from the combustion of fossil fuel sources are rich in CO_2 (13-15% by volume) and are estimated to account for 87% of SO_2 and 67% of NO_x emissions in the United States.[1] There have been numerous efforts to capture acid gas emissions at generation sources through processes such as wet flue gas desulfurization for SO_2, selective catalytic reduction for NO_x and liquid amine based absorption for CO_2.[1-2] However, the many challenges associated with these industrial processes – high capital and operating costs, high temperature requirements, large water consumption, catalyst deactivation, energy intensive adsorbent regeneration – motivate a need for cost-effective alternatives.[2,4-5] Metal-organic frameworks (MOFs) are crystalline microporous adsorbents that have shown promise for acid gas capture, especially a subclass with high thermal stability known as zeolitic imidazolate frameworks (ZIFs).[6-8] ZIFs consist of Zn^{2+} or Co^{2+} metal centers tetrahedrally coordinated to imidazole-derived organic linkers. The similarity in size of their pore apertures to many industrially useful molecules make them promising candidates for adsorptive and membrane-based separations.[9-10]

* Material in this chapter has been previously published as Bhattacharyya, S.; Han, R.; Kim, W.G.; Chiang, Y.; Jayachandrababu, K.C.; Hungerford, J.T.; Dutzer, M.R.; Ma, C.; Walton, K.S.; Sholl, D.S., Nair, S. "Acid Gas Stability of Zeolitic Imidazolate Frameworks: Generalized Kinetic and Thermodynamic Characteristics". *Chem Mater* **2018**, 30, 4089-4101; and as Bhattacharyya, S.; Han, R.; Joshi, J.N.; Zhu, G.; Lively, R.P.; Walton, K.S.; Sholl, D.S.; Nair, S. "Stability of Zeolitic Imidazolate Frameworks in NO_2" in *J Phys Chem C* **2019**.

To realize practical applications of ZIFs, it is critical to understand not only adsorbent selectivity and capacity, but also chemical stability towards the adsorbent of interest. Recently, several authors have studied the acid gas (humid SO_2, NO_x, CO_2) stability of ZIF-8, one of the most widely-reported ZIF materials in the literature.[11-16] The deleterious effects of humidity, SO_2 and NO_2 on the gas adsorption properties of ZIF-8 were first reported by Han *et al*.[17] Mottillo *et al.* linked changes in ZIF-8 PXRD after exposure to humid CO_2 to formation of a complex carbonate species.[11] Based on existing defects suggested by theoretical investigations[15-16], Battacharyya *et al.* proposed mechanisms for ZIF-8 degradation in humid CO_2 and SO_2.[14, 18] Surprisingly, ZIF-8 was stable (as seen in retained pore volume and bulk crystallinity) to mild aqueous SO_2 exposure, although the crystal surface was seen to etch away preferentially along the (110) facet.[19]

Despite the experimental work summarized above, there is still a lack of generalized understanding for ZIF stability. ZIFs display a large variety of framework topologies and imidazole functional group sizes (impacting pore size and steric environment), polarities (impacting hydrophobicity/hydrophilicity), or electron-withdrawing properties (impacting intrinsic strength of the Zn-N coordination bonds).[20] These factors necessarily affect bulk acid gas stability. In this chapter our goal was to identify computed properties that correlate with and predict experimental stability for a broad set of ZIF adsorbents and acidic adsorbates. Previous attempts to computationally predict MOF stability have investigated ligand pK_a[21], bond order, metal coordination number[22], formation enthalpies and activation energies of hydrolysis and ligand displacement reactions[23], and molecular dynamics of adsorption loading[24-25].

Ten ZIF species were selected for investigation, encompassing three different topologies (SOD, RHO, ANA) and five functionalized imidazole ligands (2-methyl imidazole, 2-ethyl imidazole, benzimidazole, imidazole-2-carboxaldehyde, 4,5-dichloroimidazole, 2-nitroimidazole), and including two hybrid mixed-linker species. The framework and linker combinations give rise to a broad range of pore window and cage sizes (see **Table 3.1**). Using such a comprehensive set of structures enables us to elucidate

Table 3.1. Characteristics of the 10 ZIFs investigated in this work.

Adsorbent	Linker	Topology	Pore Size (Å)	Cage Size (Å)
ZIF-8	2-methyl imidazole	SOD	3.4	11.6
ZIF-14	2-ethyl imidazole	ANA	2.2	2.2
ZIF-8_{15}-14_{85}	hybrid	SOD	3.4	8.5
ZIF-7	benzimidazole	SOD	2.9	4.31
ZIF-11	benzimidazole	RHO	3.0	14.6
ZIF-90	2-carboxaldehyde	SOD	3.5	11.2
ZIF-8_{50}-90_{50}	hybrid	SOD	3.4	11.2
ZIF-71	4,5-dichloroimidazole	RHO	4.2	16.5
ZIF-71	4,5-dichloroimidazole	SOD	3.2	8.6
ZIF-65	2-nitroimidazole	SOD	3.4	10.4

the effect of framework versus functional group by keeping one fixed and comparing the other's contribution to stability upon exposure to CO_2, SO_2, and NO_2 in dry and humid environments. We first describe experimental stability of the ZIF materials under acid gas exposure (dry, humid, aqueous), as characterized by powder X-ray diffraction (PXRD) and nitrogen physisorption (NP). We then detail the considerations necessary in building computational models that accurately resolve differences among the synthesized synthesized materials. Once we have established realistic models, we calculate several

well-known stability indicators used in MOF literature. By comparing our results against experimental stability, we examine the possibility of stability correlations from our data and assess the validity of these previously reported stability indicators.

3.2 Experimental Methods[†]

3.2.1 Material synthesis and characterization

ZIFs materials were synthesized based upon procedures reported in several previous works[10, 26-29] and complete details are reported by Bhattacharyya *et al*[30]. Activated ZIF samples before and after exposure to acid gases were characterized with PXRD, NP at 77 K or CO_2 physisorption at 273 K, energy-dispersive X-ray spectroscopy (EDX), and Fourier-transform infrared spectroscopy (FTIR). PXRD measurements were conducted on an X'Pert Pro PANalytical x-ray diffractometer (Bragg-Brentano geometry, CuKα anode at 45 kV and 40 mA, X'celerator detector). PXRD patterns were collected with a step size of 0.02° 2θ and scan time of 10 s/step over 4-50° 2θ. The peak intensities were normalized with respect to the highest-intensity peak for each ZIF. Textural analyses were conducted by NP at 77 K using a BET surface area analyzer (Tristar, Micromeritics).

BET surface areas were calculated in individually determined pressure ranges[31]. EDX measurements were carried out with the LEO 1550 scanning electron microscope (Zeiss Electron Microscopy) and EDX analysis was done at 15 kV. Spectrometer gain and beam current were optimized with a Si wafer standard before sample measurements and the library calibration files of the Inca software (Oxford Instruments) were used to calculate

[†] All experimental work reported in this chapter was led by Dr. Souryadeep Bhattacharyya from Dr. Sankar Nair's research group at the Georgia Institute of Technology, Atlanta, GA. The proposed mechanisms in Table 3.3 were also developed by Dr. Bhattacharyya.

elemental quantities. Areas of 100 μm × 100 μm were selected for each EDX measurement and at least 10 independent areas were measured and averaged for each sample.

FTIR spectroscopy was recorded by a Thermo Scientific Nicolet iS50 FT-IR equipped with an iS50 ATR module. Samples were analyzed in powder form from 550-4000 cm^{-1} with 96 scans with a resolution of 2 cm^{-1}. Additional *in situ* Diffuse Reflectance Infrared Fourier Transform Spectroscopy (DRIFTS) experiments were performed on a FTIR spectrometer (Thermo, Nicolet iS50) equipped with a liquid nitrogen cooled MCT/A detector, a diffuse reflectance accessory (Praying Mantis, Harrick), and a high temperature reaction chamber (HVC, Harrick). The chamber used in NO_2 exposure experiments was coated with SilcoNert. KBr was loaded into the chamber before each sample and measured as IR background. Pre-activated ZIF samples were loaded into the sample chamber and reactivated *in situ* at 383 K under 20 cc min^{-1} He flow for 3 hours. After cooling to 298 K, the He gas was switched to 20 cc min^{-1} 1000 ppm NO_2 with balancing N_2. IR spectra was recorded at pre-programmed intervals with 32 scans and 4 cm^{-1} resolution for the duration of exposure.

Water adsorption measurements were conducted with the IGAsorp DVS moisture sorption analyzer at 308 K. Each experiment was preceded by in situ activation under a high-purity nitrogen stream at 383 up to 12 hours. Adsorption data was collected at adsorbate relative humidities (P/P_0, where P_0 is the saturation vapor pressure of water) ranging from 0.05 to 0.95. Each data point was collected with sufficient time (1-6 hours) for equilibration.

3.2.2 Acid gas and aqueous acid exposure

Humid acid gas exposures were maintained at 85% relative humidity with SO_2 concentration of 20-40 ppm (humid SO_2) or 12% CO_2 concentration (humid CO_2). Dry sulfur dioxide (Airgas, anhydrous, 99.98% purity) adsorption isotherms were measured at 298 K for pressures ranging from 0 to approximately 2.5 bar using a lab-built volumetric system. Each sample (30-50 mg) was outgassed under dynamic vacuum at 453 K for 5 hours. SO_2 adsorption loading was determined by measuring the pressure drop in the sample cell and converting to moles using the Peng-Robinson equation of state. For humid SO_2 exposure, activated samples were exposed to varying concentrations (ppm) of SO_2 in air with relative humidity of 85% for different time intervals at room temperature (298 K). The acid gas mixture was prepared according to previous literature reports[32], with slight modifications. Sulfur dioxide gas was generated from a 400 mL aqueous solution of 0.5 mg/mL $NaHSO_3$ at a pH of 3.7 at 318 K. The temperature of the solution was maintained with a water bath (VWR). Air at 60 cc/min was bubbled through the solution and carried humid SO_2 gas stream to the exposure unit (Secador mini-desiccator). Gas concentration inside the transparent exposure unit was continuously monitored with the portable PAC 7000 SO_2 detector (Dräger). Data from the detector was transferred to a computer after the exposure run was finished. A second SO_2 sensor was kept running outside the exposure unit for leak detection. Steady state levels of SO_2 and relative humidity were achieved within a few hours. The $NaHSO_3$ solution was refilled to maintain SO_2 level after every 2 days. The water bath, acid gas generator unit and exposure unit were all placed inside a fume hood with a high exhaust rate and handled with caution at all times. For humid CO_2 exposure, activated samples were exposed to a 12% CO_2/12% N_2/76% He stream

humidified at a relative humidity of 90% for 3 days at 298 K. The dry gas mixture was bubbled at 60 cc/min through deionized water and the humid stream generated entered the exposure chamber (a Secador mini-desiccator). In all experiments, the relative humidity in the chamber was continuously monitored by a commercially available humidity sensor (Ambient Weather). All samples were re-activated at 453 K in vacuum for 24 hours after exposure and prior to characterization.

For aqueous SO_2 exposures, dilute aqueous solutions of SO_2 were prepared by diluting a stock solution of aqueous SO_2 (6.2%, Sigma Aldrich). The SO_2 concentration of 2.5×10^{-5} mol/kg was determined based on the concentration in equilibrium with 20 ppm SO_2 in the vapor phase, according to Henry's law ($K_{H,\,SO2}$ = 1.25 mol/kg·bar[33]). A solution at the desired concentration was introduced into a 60 mL glass vial with approximately 200 mg of ZIF-8 and sealed. The vials were briefly sonicated to ensure good dispersions of the particles within the solutions. After 5 days at room temperature, the resulting solids were centrifuged and washed with DI water and methanol. All samples were re-activated at 453 K in vacuum for 24 hours after exposure experiments prior to characterization.

Dry NO_2 exposures used a packed bed built by adding 100 mg powder samples to a fritted 6 mm × 4 mm × 4.5 in. (O.D. × I.D. × L) quartz glass thermal desorption tube (Supelco) that was placed in a custom-made fixed-bed gas exposure setup. To ensure safe hazardous gas testing, the entire fixed-bed system was housed in a well-ventilated chemical hood with real-time gas sensors for safety. An upstream pressure gauge was utilized to confirm the absence of detectable pressure drop during gas exposure. Additionally, outlet lines were fed to a 1N NaOH solution to scrub eluted acid gas streams. Packed samples were flushed with ultra-high purity nitrogen (Airgas) at 75 cc min^{-1} and activated *in situ*

for 2 hours at 453 K. After cooling to ambient conditions, 1000 ppm NO_2 gas in balance N_2, (Airgas), was passed through the fixed-bed at a flow rate of 75 cc min^{-1} for about 2 hours and 25 min (100 ppm-days of NO_2 gas exposure). Upon completion of the exposure, the bed was flushed with N_2 for 30 min and the sample removed for further characterization.

Humid NO_2 exposure was achieved by exposing activated ZIF to ~20 ppm of NO_2 in air at 75% relative humidity (R.H.) for 5 days (~100 ppm-days) at 298 K. The NO_2 gas was generated from a 400 cc aqueous solution of 0.5 mg/mL $NaNO_2$ at a pH of 4.0 at 318 K in accordance with reported literature[32]. Air at 40 cc min^{-1} was bubbled through the solution and carried humid NO_2 gas stream into the exposure unit (Secador mini-desiccator), where the portable PAC 7000 NO_2 detector (Dräger) measured NO_2 concentrations at regular intervals. Relative humidity was monitored inside the transparent exposure unit using a humidity sensor (Ambient Weather). The $NaNO_2$ solution was refilled every 24 hours and the custom-made unit was placed inside a fume hood for safe operation. Following exposure, samples were re-activated at 453 K for 24 hours in vacuum.

3.3 Computational Methods

3.3.1 Density functional theory (DFT) optimization

The experimentally reported structures of ZIF-7, ZIF-8, ZIF-11, ZIF-71 RHO, and ZIF-90 were optimized using plane-wave density functional theory (DFT).[9, 34-36] Theoretical SOD structures were generated for ZIF-14 SOD, ZIF-71 SOD, and ZIF-65 by replacing all methylimidazole linkers in the ZIF-8 framework with the corresponding functionalized imidazole linker, and then re-optimizing using DFT. Converged atomic

coordinates and lattice parameters are listed in Appendix B.1. Calculations were performed in the Vienna Ab-initio Simulation Package (VASP) with projector-augmented wave (PAW) method pseudopotentials[37] and the Perdew-Burke-Ernzerhof (PBE) generalized-gradient approximation (GGA) functional[38]. Atomic positions were first relaxed using a conjugate gradient algorithm with a cutoff energy of 480 eV until all forces were less than 0.05 eV/Å. Subsequently both atomic positions and lattice constants were optimized with the same cutoffs and tolerances. In all calculations, reciprocal space was sampled only at the Γ-point.

3.3.2 Linker fragment pKa and atomic charge calculations

pK_a values were calculated for the conjugated acids of the functionalized imidazolate linkers. Gaussian 09 was used to geometry-optimize the neutral and anionic linker fragments for each ZIF considered. Gas phase optimization was performed at the B3LYP/(6-311++G(d,p)) level of theory using DFT. The free energy was a sum of the entropy, zero-point energy (ZPE), and thermal correction term. Aqueous solvation Gibbs energies were calculated using SMD.[39] Because the reference states of the gas (1 atm) and aqueous phase (1 M) were different, they are interconverted as follows:

$$\Delta G_{gas}(1\ M) = \Delta G_{gas}(1\ atm) + RT\ln(24.46) \quad (3\text{-}1)$$

Experimental values for the proton free energies $G_{gas}(H^+)$ and $\Delta G_{solv}(H^+)$ were used: -6.28 kcal/mol[21] and -265.9 kcal/mol[40] respectively. A Born-Haber thermodynamic cycle was used to convert between the gas and aqueous phase free energies.[41]

$$pK_a = \left[G_{gas}(A^-) - G_{gas}(HA) + \Delta G_{solv}(A^-) - \Delta G_{solv}(HA) - 270.28\right]/1.364 \quad (3\text{-}2)$$

Density Derived Electrostatic and Chemical (DDEC) net atomic charges were calculated using the Chargemol software developed by Manz and Limas.[42-43]

3.3.3 Pore window and cage size calculations

Pore window and cage diameters were calculated using the Zeo++ software[44]. All atomic radii were taken from the Cambridge Crystallography Data Center (CCDC). The dimensions reported in **Table 3.1** are the maximum pore and cage diameters along any diffusion direction. These calculations were performed with a ten-sphere (S10) cluster approximation for the Voronoi decomposition[45], which graphs the void space and identifies accessible channel systems. Once the Voronoi network was established, the dimensionality of each channel was calculated and the surface area was integrated using Monte Carlo sampling to determine the BET surface area. The channel radius and probe molecule radius were both set as 1.8 Å, which is comparable to the size of a nitrogen gas molecule.

3.4 Results and Discussion

3.4.1 ZIFs exhibit varied stability when exposed to H_2O, SO_2, and CO_2

Experimental results for H_2O, SO_2, and CO_2 exposure are shown as a stability chart in **Table 3.2**, where stability was determined by a combination of PXRD and pore volume measurements. Exposure conditions are listed (left to right) from dry acid gas conditions to humid air, liquid water and aqueous SO_2, and finally humid acid gas conditions. A ZIF was considered stable (colored green) under a particular exposure condition if it maintained its crystal structure and at least 90% of its pore volume. There were two forms of ZIF instability noted. Amorphous degradation (**Table 3.2**, colored red) was characterized by decreasing pore volume, surface area, and PXRD peak intensities. A different type of phase

Table 3.2. Bulk stability of ZIF materials upon exposure to different H_2O, SO_2, and CO_2 conditions at 298 K. Stability is color-coded – green: stable, yellow: phase change instability, red: degradation instability.

Adsorbent	Topology	Linker pK_a	Dry SO_2	Dry CO_2	Humid Air	Liq. Water	Aq. SO_2	Humid SO_2	Humid CO_2
ZIF-8	SOD	20.12							
ZIF-14	ANA	19.56							
ZIF-$8_{15}14_{85}$	SOD	*19.56*							
ZIF-7	SOD	14.86							
ZIF-11	RHO	14.86							
ZIF-90	SOD	13.58							
ZIF-$8_{50}90_{50}$	SOD	*13.58*							
ZIF-71	RHO	11.01							
ZIF-71	SOD	11.01							
ZIF-65	SOD	10.22							

change instability was seen for several materials (**Table 3.2**, colored yellow), where the original structure transformed into a dense and non-porous phase upon exposure to any humidity. Though the resulting structure is crystalline, it has severely reduced pore volume and limited capacity for adsorption or diffusion. Metal-linker bonds must be broken and rearranged in order for this kind of phase transition to occur, so this form of instability mechanistically requires similar initial steps to the amorphous degradation instability. Therefore, we observe that all 10 ZIFs are stable to dry acid gas, all excepting ZIF-65 and the SOD polymorph of ZIF-71 are stable in humid air, only ZIF-8 and ZIF-90 are stable in liquid water, and only the RHO polymorph of ZIF-71 is stable to humid acid gases.

3.4.2 Traditional stability indicators do not correlate well with ZIF exposure

A number of stability indicators for ZIFs/MOFs have been discussed in literature, often in the context of water induced MOF degradation.[22] Higher coordination number and high oxidation state of the metal center have been correlated with greater MOF stability[23], but since all ZIFs have the same Zn^{2+} metal center and tetrahedral coordination, this factor cannot explain differences between ZIF species. The strength of the metal-linker coordination bond is also considered a key factor in determining MOF/ZIF stability. Linker pK_a (*i.e.*, its relative ease of protonation) has been used as an indicator for the strength of the Zn-N coordination bond, where a higher value correlates with higher thermodynamic stability[21]. According to Lewis acid-base theory, the basicity of the conjugated base (*i.e.*, ability of the nitrogen atom to donate electrons and form a Zn-N coordination bond) of a weaker acid (*i.e.*, low K_a of the protonated ZIF linker) is stronger than that of the conjugated base of a stronger acid.

The ZIFs in **Table 3.2** are arranged by decreasing linker p*K*a value. Contrary to previous expectations, it is clear that pK_a does not correlate strongly with the experimental observations of ZIF stability under water or acid gases. While ZIF-8 with the highest ligand pK_a (20.12) is stable in water, ZIF-14 and ZIF-8_{15}-14_{85} with pK_a values (19.56) close to ZIF-8 are unstable. Low pK_a values correlate with phase transitions in aqueous solutions for both ZIF-71 (11.01) and ZIF-65 (10.22) but not in ZIF-7 (14.86), which changes phase yet has a higher pK_a than materials stable against phase transitions in aqueous solution such as ZIF-90 (13.58). Likewise, for humid acid gas exposure there is no obvious relationship between high pK_a and stability, with the most stable ZIF-71 RHO (11.01) having one of the lowest pK_a values.

We also calculated DDEC charges (**Table B.1**) for each atomic species in the DFT-optimized linker fragments to determine whether there is a significant difference in the charge distributions. Higher electron densities (more negative charge) on the coordinating atom of MOF linkers have been correlated with higher stability of the coordination bond[21]. However, there were negligible variations (on the order of 0.01*e*) between the atomic charges on the imidazole nitrogens, indicating that charge distribution also cannot explain stability differences in ZIFs.

3.4.3 Formation energy as a predictor of thermodynamic stability

Since degradation proceeds through a series of bond-breaking reactions, the enthalpy required to form a water or acid-induced defect often serves as a good predictor of the thermodynamic stability of the material in that environment[23]. We define a defect as a single hydrolysis event where an attacking species inserts into the Zn-N bond and protonates the dangling linker, with formation energy

$$\Delta E = E_{\text{defect ZIF}} - E_{\text{pristine ZIF}} - E_{\text{isolated attacking molecule}}. \quad (3\text{-}3)$$

Calculating each of these three energies requires accurate models describing the adsorbent, adsorbate, and the final defect state. We restrict our density functional theory (DFT) calculations to SOD topology ZIFs and gas-phase reactions. Sodalite ZIFs have roughly 500 atoms per unit cell compared to RHO (more than 800 atoms) and ANA (more than 1000 atoms), both of which were too computationally expensive to simulate.

Dry acid gas and humid air exposure were considered pure-component conditions, where we assume the water or acid gas molecule is the only species present. Each Zn-N bond is protonated by a single attacking molecule. However, under humid acid gas conditions, the actual identity of the attacking species is more ambiguous. For instance, when considering humid SO_2, it is not clear whether H_2O and SO_2 will first react in the vapor phase to form a hydrated acidic complex that attacks the Zn-N bond, or whether H_2O and SO_2 react separately with the Zn-N in a multi-step mechanism. Although many complicated reactions have been suggested[47], we propose three simplified possibilities for the adsorbate in **Figure 3.1**. Analogous models can be constructed for humid CO_2. For each degradation event, we chose the attacking species that yielded the lowest formation energy – H_2SO_4 and H_2CO_3 were strongly favored over the other adsorbate models.

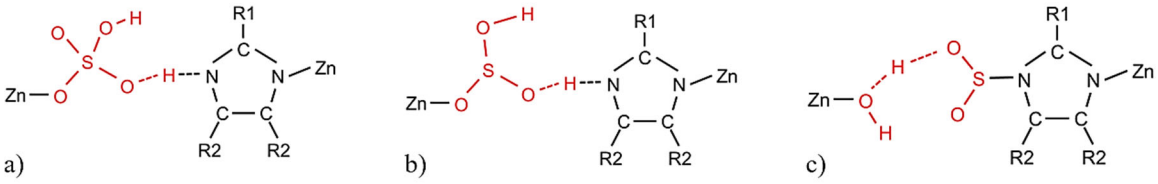

Figure 3.1. Three possible models for the humid SO_2 adsorbate which cleaves the Zn-N bond: a) SO_2 oxidizes to H_2SO_4, b) H_2O and SO_2 pre-react to form H_2SO_3, or c) H_2O first inserts into Zn-N bond followed by SO_2 adsorbing to N.

When considering the local metal-linker geometry, we had to draw a distinction between isomorphic structures. Topology describes framework connectivity without specifying the symmetry; various crystals can have sodalite connectivity while belonging to different space groups. Although ZIF-8, ZIF-7, ZIF-90, and ZIF-65 crystallize in unique structures, Schweinefuss *et al*. synthesized multiple isomorphs of ZIF-71 SOD[28]. These variations arise because there are multiple ways to orient linkers in the SOD 6-member (6M) rings with respect to the plane of the window. Since ZIF-71 has dichloroimidazole linkers, rotation of the imidazole about the Zn-Zn axis causes profound changes on the cage shape to avoid steric interference between chlorine atoms on neighboring linkers. We geometry optimized the three known stable isomorphs of ZIF-71 SOD[48-49], each having significantly different energy per Zn linker (relative energies in **Table 3.3**), and simulated the XRD patterns of the defect free structures (**Figure 3.2**). The SOD III isomorph is the most stable, with the lowest energy per Zn atom, but based on the powder diffraction patterns we can see that the simulated SOD III spectra has many peaks that do not appear in the experimental spectra, indicating that the experimental material is likely not SOD III. The experimental pattern has peaks that are present in SOD I and SOD II but does not match either exactly, indicating that the synthesized material is likely a combination of SOD I and SOD II.

Table 3.3. DFT optimized energies of three stable ZIF-71 isomorphs, normalized by the number of Zn atoms.

ZIF-71 Isomorph	Energy of Pristine Structure (eV/Zn)
SOD I	0.14
SOD II	0.26
SOD III	0.00

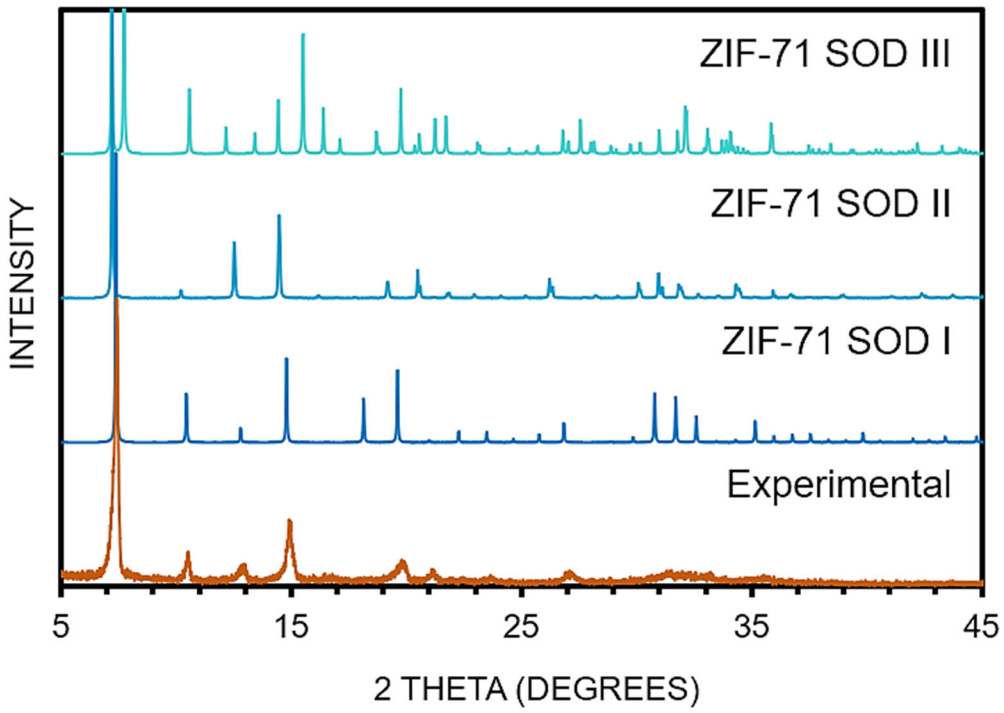

Figure 3.2. Simulated diffraction pattern for three stable ZIF-71 SOD isomorphs (blue) shown in comparison to experimental PXRD of synthesized ZIF-71 SOD (orange). The experimental spectra shares peaks with both SOD I and SOD II, but does not match either perfectly, while the simulated SOD III spectra has many peaks not in the experimental diffraction pattern.

Finally, we considered the conformation and termination of the defect product state. This involved finding multiple local minima to best determine the global minimum energy state. Once a Zn-N bond is cleaved, the linker is only anchored to the framework by the remaining Zn-N bond. It may remain in the original Zn-Im-Zn plane, or it may rotate out

of plane and into an adjacent pore volume. The attacking species may also either protonate imidazole while the deprotonated molecule then adsorbs to the open Zn site, or the attacking species may adsorb to the open Zn site leaving the imidazole nitrogen with its lone pair. As the size and complexity of the attacking species increases, there are more conformations to explore. We found that formation energy varies on the order of 0.1 eV depending on how the heavy (non-hydrogen) atoms were placed, with preference given to structures that maintained ideal tetrahedral bonding angles. Once the heavy atoms were placed, different conformations involving hydrogen atoms only resulted in energy variation on the order of 0.01 eV, an order of magnitude lower. Exploring the conformation space allowed us to define an upper bound on instability. For each degradation event we chose the defect state with the lowest formation energy.

Table 3.4. DFT calculated formation energies (all in eV) for degradation on SOD topology ZIFs shown with experimental stability color coding.

Adsorbent	Topology	Linker pK_a	Humid Air	Humid SO_2	Humid CO_2
ZIF-8	SOD	20.12	0.61	-0.59	-0.57
ZIF-14	SOD	*19.56*	0.72	-0.20	0.20
ZIF-7	SOD	14.86	0.27	-0.80	-0.32
ZIF-90	SOD	13.58	0.25	-0.02	0.25
ZIF-71	SOD	11.01	-0.04	-0.53	-0.04
ZIF-65	SOD	10.22	0.74	-0.47	-0.31

Table 3.4 shows the formation energies for dangling linker defects in comparison with experimental stability observations. A negative formation energy indicates lower stability and a more thermodynamically favorable degradation reaction. We expect to see all stable (green) experiments with positive energy value and all unstable (red and yellow)

experiments with a negative energetic value. While many of the formation energies correlate well with stability, there are a few exceptions such as the humid CO_2 induced defect formation in ZIF-14 and ZIF-90, and ZIF-65 defect formation in humid air. Therefore, we must conclude that thermodynamic stability trends reasonably well with experimental observation but cannot be used as the sole predictor of material stability.

3.4.4 Explaining the high stability of ZIF-71 RHO

Of all the ZIFs surveyed, ZIF-71 RHO was the only material stable in humid acid gas environments, and therefore the most interesting candidate for potential application. Thus far, all the traditional stability predictors that correlate well with MOF degradation are unable to explain the high stability of ZIF-71 RHO, particularly with respect to the low stability of ZIF-71 SOD. Topology is apparently the only distinction between these two polymorphs, yet other pairs of RHO and SOD polymorphs with the same linker have similar stability, such as ZIF-14 RHO and the majority ZIF-14 hybrid SOD structure, or ZIF-7 and ZIF-11. Unlike the previously examined stability indicators describing local bond strength and chemistry, topology influences long range bulk properties, particularly the pore and cage dimensions (seen in **Table 3.1**). Quantifying the impact of topology on stability is challenging, since degradation reactions are localized events that only depend on the metal-linker geometry and the two ZIF-71 polymorphs have nearly identical bond angles and lengths.

Although we previously we only calculated formation energies of SOD structures for expediency and efficiency, we now extended our calculations to investigate H_2SO_4 induced defect formation in the ZIF-71 RHO topology as well four other hypothetical ZIF-71 topologies (CRB, DFT, CAG, and GIS) with fewer than 500 atoms per unit cell. The

hypothetical polymorphs were constructed from the analogous zeolite frameworks with lattice constants and fractional atomic positions scaled accordingly, Si replaced by Zn, and oxygen atoms replaced by dichloroimidazole. Formation energies and incremental formation energies are given in **Table 3.5**, where the latter is defined as:

$$\Delta\Delta E_{H2SO4,polymorph} = \Delta E_{H2SO4,polymorph} - \Delta E_{H2SO4,SOD} \quad (3\text{-}4)$$

The incremental formation energy for a polymorph predicts the thermodynamic stability in H_2SO_4 of the ZIF-71 polymorph compared to ZIF-71 SOD. A negative value implies the polymorph is more stable while a positive value implies SOD is more stable. The magnitude of incremental formation energy varies from 0.02-0.26 eV among the different polymorphs; $\Delta\Delta E_{H2SO4,RHO}$ is -0.09 eV, indicating that ZIF-71 RHO is more stable than ZIF-71 SOD, but within the variance among other polymorphs.

Table 3.5. Formation energies and incremental formation energies for H_2SO_4 induced defects in ZIF-71 polymorphs. Pore size and cage size are listed for the pristine polymorphs, and atomic coordinates are available in Appendix B.1.

ZIF-71	ΔE_{H2SO4} (eV)	$\Delta\Delta E_{H2SO4}$ (eV)	Pore Size (Å)	Cage Size (Å)
SOD	-0.53	0	3.4	11.6
RHO	-0.62	-0.09	4.2	16.5
CRB	-0.55	-0.02	2.5	3.4
DFT	-0.76	-0.26	4.8	6.2
CAG	-0.46	0.07	1.5	3.7
GIS	-0.42	0.11	3.8	6.9

We can compare the formation energy variation due to topology against the formation energy variation due to linker functionalization since our earlier formation energy calculations involved ZIFs with different linker chemistry but the same SOD topology. Considering the formation energies calculated in **Table 3.4**, an incremental energy of 0.09 eV would be enough to change the predicted stability of ZIF-90 in humid

SO_2, and ZIF-71 SOD in air or humid CO_2. An incremental formation energy of 0.26 eV, the difference between the ZIF-71 SOD and DFT polymorphs, would be enough to change the predicted stability of ZIF-14 in humid SO_2 or humid CO_2, and ZIF-90 in humid air or humid CO_2. This agrees with previous work finding that the range of $\Delta\Delta E_{H2O}$ among different ZIF-8 polymorphs ranges between 0.06-0.30 eV and overlaps with the range from 0.22-0.60 eV of $\Delta E_{H2O}50$. The impact of topology on defect formation is on the same energy scale as the impact of linker functionalization, and we would not anticipate the exceptional stability of ZIF-71 RHO *a priori* based on thermodynamic stability alone.

Kinetically stable MOFs have been categorized as materials that degrade in aqueous conditions but not under humid exposure, even at 90% relative humidity[22]. Since this definition seems to fit the observed stability of ZIF-71 RHO, we also investigated kinetic stability as a predictor. One way to quantify kinetic stability is through hydrophobicity, which is often associated with kinetic stability in the context of water exposure. It is hypothesized that a hydrophobic linker prevents water, or any hydrophilic attacking species formed in humid acid gas conditions, from reaching the vicinity of the MOF metal center[22]. Materials that absorb < 1 mmol/g water at 85% relative humidity are considered hydrophobic. From the experimental water adsorption isotherms (**Figure B.1**), we can see that ZIF-71 RHO is the most hydrophobic structure with an uptake of only 0.19 mmol/g at 85% RH. However, according to the above definition, ZIF-8, ZIF-8_{15}-14_{85}, ZIF-7, and ZIF-11 are also hydrophobic materials yet they are all unstable under humid acid gas exposure.

This discussion above leads us to conclude that there is no single or simple explanation for the exceptional stability of ZIF-71 RHO; rather, it is likely a synergistic combination of multiple factors, from high hydrophobicity, to topology, to steric effects.

This unique robustness makes ZIF-71 RHO an attractive candidate for industrial separations and warrants further investigation of its performance.

3.4.5 ZIFs previously stable to SO_2 and CO_2 are unstable upon NO_2 exposure

In Sections 3.4.1 through 3.4.4 we presented a detailed mechanistic model of ZIF interaction with dry and humid SO_2 and CO_2, alongside corresponding experimental stability observations. Upon exposing ZIFs to NO_2, we find remarkably different degradation behavior. We chose to study ZIF-8, ZIF-90, and ZIF-71 RHO as representative ZIFs out of the list of 10 ZIFs investigated earlier because they comprehensively span the range of SO_2 stability. ZIF-71 RHO showed no measurable degradation to humid SO_2, and while ZIF-8 and ZIF-90 both degraded in humid SO_2, they had the highest and lowest degradation rates[30], respectively.

Degradation was characterized by increase in amorphous background and loss of peak intensity in the PXRD patterns (**Figure B.2**), as well as loss of surface area and porosity measured by nitrogen adsorption isotherms (**Figure B.4** and **Table B.12**). These observations indicate that ZIFs are significantly unstable to dry NO_2. Whereas all 10 ZIFs in **Figure B.2** were stable to dry SO_2 and CO_2, all three ZIFs here degrade in dry NO_2. In the hydrophobic ZIF-8, the presence of humidity slows the degradation process in relation to dry NO_2, a surprising finding also reported for the hydrophobic MOF UiO-66[51]. In the hydrophilic ZIF-90, humidity accelerates framework degradation. In the hydrophobic ZIF-71, humid NO_2 drives a phase change to nonporous ZIF-72[28] while prolonged exposure to dry NO_2 results in slow amorphous degradation. To understand this behavior, we considered possible mechanisms for nitrogen degradation.

It is well known that NO_2 is a strong oxidizing agent that reacts strongly with unsaturated bonds via hydrogen abstraction and radical dimerization mechanisms[52-54]. As a dry gas, NO_2 (~1000 ppm) will react with unsaturated organics at ambient temperature to form nitrates or nitrites through hydrogen abstraction[55-57]. Formation of nitro, nitramine groups, and nitrous acid (HONO) have also been reported during gas-phase reactive adsorption of NO_2 on carbonaceous materials at ambient temperature[58-61]. The presence of imidazoles in ZIFs creates the strong possibility of similar mechanisms. We propose an H-abstraction degradation pathway by nitrous acid in **Figure 3.3** and identify the presence of nitro, nitrite, or nitrate species with FTIR (see **Figure B.5**) that are consistent with this mechanism. ZIF-8, ZIF-90, and ZIF-71 all exhibit strong decrease in aromatic and aliphatic C-H stretching and bending vibrations upon dry NO_2 exposure, and a new 1700 cm^{-1} stretch corresponding to adsorbed HONO produced through free radical H-abstraction.

The scheme in **Figure 3.3** proceeds with NO_2 abstracting hydrogen from the imidazole linker to form nitrous acid (HONO), followed by additional NO_2 free radicals reacting with the newly formed imidazole radical, and finally forming nitro, organic nitrite or nitrate species[52,62-63,67-68]. Decreased crystallinity of the ZIFs after dry NO_2 exposure, and the presence of inorganic nitrites and nitrates, are consistent with Zn-N bond cleavage.

There are two alternative reactions that can lead to Zn-N bond-breaking. One pathway supposes that nitrous acid produced by H-abstraction attacks the Zn-N bond (**Figure 3.3 A**), protonating the imidazole N and forming an inorganic nitrite, which is then oxidized[64] by NO_2 to form an inorganic nitrate. The protonated imidazole can react with nitric or nitrous acid to form nitramines and nitrosamines[65-68]. A second possibility occurs

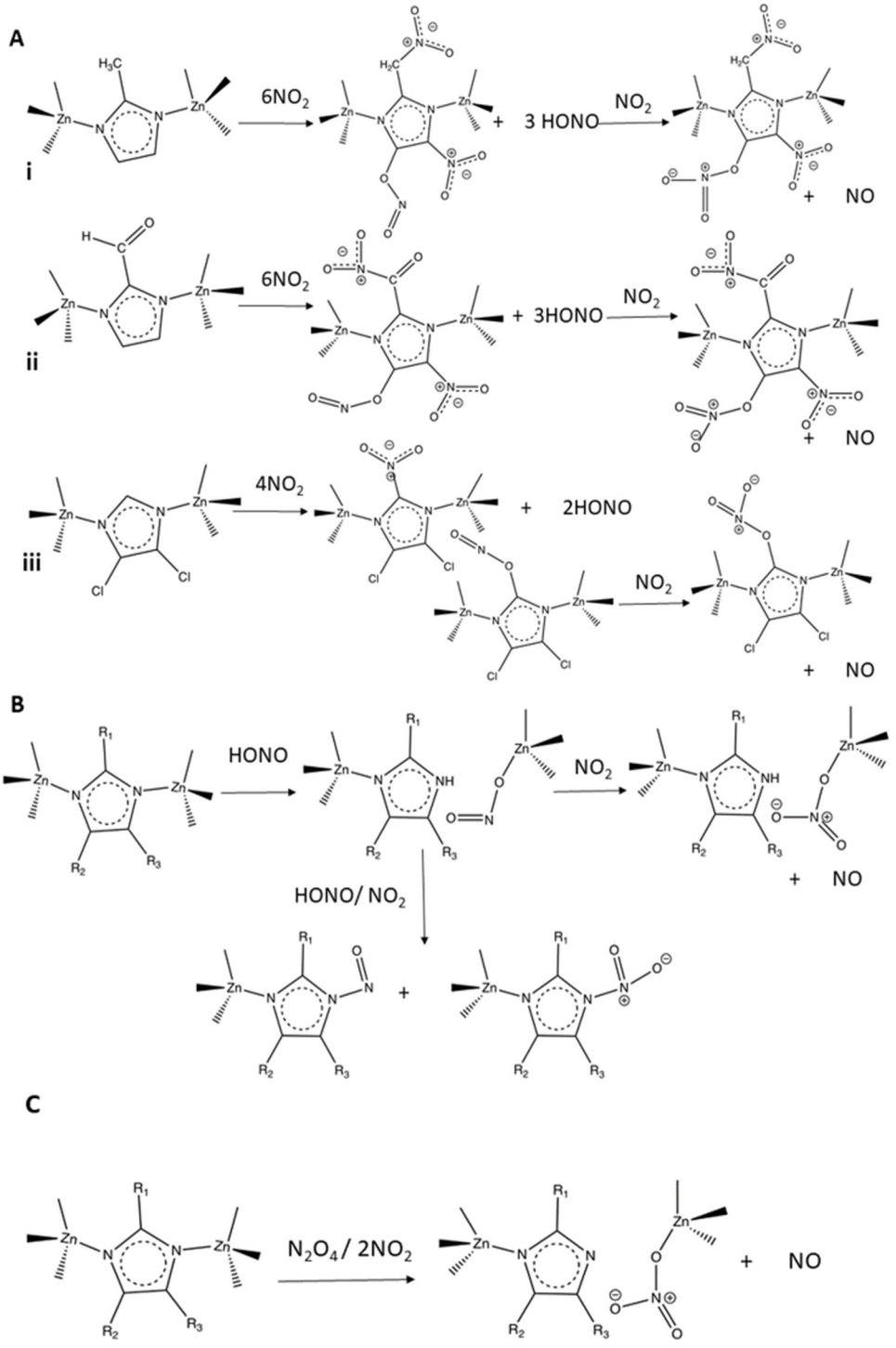

Figure 3.3. Reactants and product species generated during degradation of ZIFs under dry NO_2 exposure: (A) Stoichiometrically balanced reactions of ZIF-8 (i), ZIF-90 (ii) and ZIF-71 (iii) are individually shown, while (B) and (C) are valid for any of the ZIF linkers (having general functional groups R_1, R_2 and R_3 at the 2, 4, and 5-positions).

because NO_2 has been observed to oxidize ionic salts at ppm concentrations to form inorganic nitrites, which can be further oxidized to NO and other nitrate species[64,69-70]. Reactive adsorption of NO_2 on metals (including Zn) and metal oxides can also proceed at ambient temperature *via* disproportionation of two NO_2 molecules or the N_2O_4 dimer to form a surface nitrate and evolve NO[71-73], leading to Zn-N bond cleavage (**Figure 3.3 C**).

In summary, the free radical H-abstraction mechanism explains the formation of organic N-containing groups (observed in the FTIR spectra) leading to functionalized imidazole linkers (rather than degradation of the ZIF *per se*); whereas the observed formation of nitrosamines, nitramines and inorganic nitrites/nitrates (produced by secondary reactions with HONO or by reaction with the Zn metal centers) is responsible for Zn-N bond cleavages and degradation of the ZIF structure.

To determine the most dominant mechanism in **Figure 3.3**, we computed defect formation energies for six reactions of ZIF-8 with NO_2 by subtracting the total energy of the products from the reactants (listed in **Table 3.6**). Negative defect formation energies imply a thermodynamically favorable degradation reaction. Reactions 1-3, which represent hydrogen abstraction by dry NO_2 in ZIF-8 forming nitro or nitrite groups along with HONO, are all very favorable, strongly indicating that the H-abstraction mechanism (**Figure 3.3 A**) is dominant. Nitrous or nitric acid species attacking ZIF-8 and forming inorganic nitrites/nitrates is also favorable (**Table 3.6,** Reactions 4-5), albeit with considerably less negative formation energies. This conclusion may explain why ZIF-71 is the most stable of the three ZIFs to dry NO_2 exposure, degrading after ~1000 ppm-days of exposure instead of 100 ppm-days. The dichloroimidazole linker only has a single (aromatic) C-H bond, unlike ZIF-8 or ZIF-90 linkers which have multiple aromatic bonds

(two each) and aliphatic (three and one, respectively) C-H bonds. Fewer aromatic C-H bonds most strongly affects rate of H-abstraction from the linkers. Therefore, while direct attack on Zn sites by reactive dry NO_2 adsorption cannot be ruled out, the observed speciation patterns and reactivity difference of the three ZIFs suggest that it plays a minor role at best.

Table 3.6. DFT calculated defect formation energies (eV) of ZIF-8 reactions

#	Reaction Scheme	ΔE (eV)
1	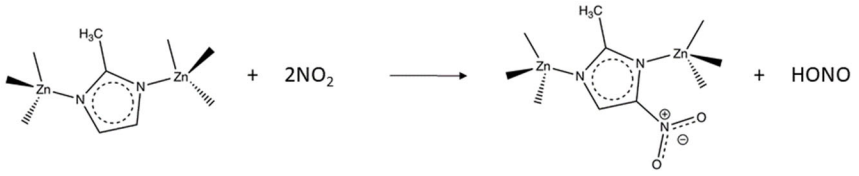	-1.95
2	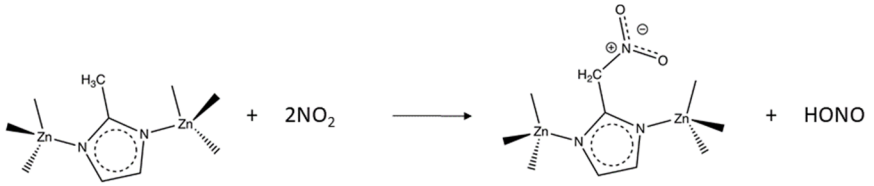	-1.73
3	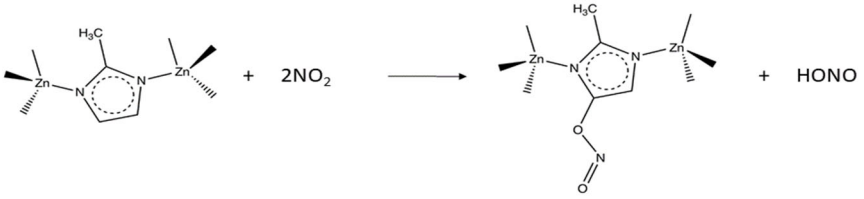	-1.69
4	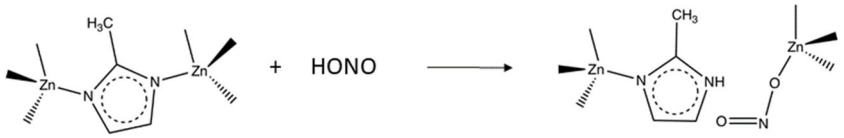	-0.10
5	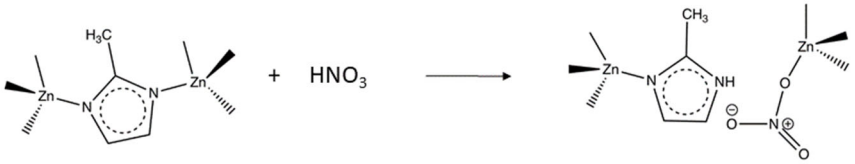	-0.29
6	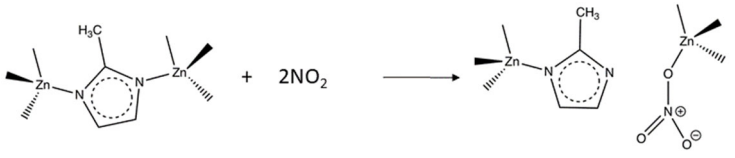	1.07

3.5 Conclusion

We have conducted a systematic investigation of the phenomenological and mechanistic aspects of structural changes occurring in ten ZIF materials upon exposure to the acid gases CO_2 and SO_2, and three of those materials under NO_2 exposure. All ZIFs investigated under dry CO_2 and SO_2 were observed to be stable under such exposure conditions, while only ZIF-71 RHO was stable under humid SO_2 and CO_2 conditions. Various conventional indicators of thermodynamic and kinetic stability were evaluated to explain the observed humid acid gas stability, but none were able to satisfactorily explain the observations. This analysis indicates that new stability indicators are necessary to predict ZIF degradation behavior. Indeed, it is likely that combination of predictors will be necessary to understand the exceptional stability of ZIF-71 RHO.

Further exposure under dry and humid NO_2 revealed that the simpler degradation pathways describing humid SO_2 and CO_2 degradation do not translate well to nitrous and nitric acid gases. None of the ZIFs investigated were stable under prolonged dry or humid NO_2 exposures, in stark contrast with the high stability towards dry SO_2 and CO_2. The much higher reactivity of dry NO_2 over dry SO_2 can be attributed to its free radical nature, and we proposed a free radical hydrogen abstraction mechanism that results in formation of various nitro-, nitrites, nitrates, nitrosamines and nitramines. This picture of degradation was supported by DFT calculations and FTIR measurements. We envision similar mechanisms of NO_2 attack on other MOFs, which make NO_2 a much more potent hindrance to widespread use of MOFs in acid gas-related applications and would require new approaches to stabilize ZIF/MOF materials.

APPENDIX B. SUPPORTING INFORMATION FOR CHAPTER 3

Table B.1. Calculated DDEC charges on the coordinating nitrogen atom of the imidazole linker for different ZIFs investigated in this work.

Adsorbent	Linker	Average Charge on Nitrogen (Hartree atomic units)
ZIF-8	2-methyl imidazole	-0.36
ZIF-14	2-ethyl imidazole	-0.35
ZIF-7	benzimidazole	-0.36
ZIF-90	imidazole-2-carboxaldehyde	-0.30
ZIF-71	4,5-dichloroimidazole	-0.35
ZIF-65	2-nitroimidazole	-0.06

B.1 Atomic coordinates of all geometry-optimized pristine ZIF structures

Table B.2. Cartesian atomic coordinates and lattice vectors for ZIF-8 (SOD)

Atom Type	x	y	z
Lattice vectors	17.18492	0	0
	-0.00025	17.2169	0
	0.018165	-0.00611	17.20257
C	6.494682	0.152004	10.71184
C	6.35803	15.48655	11.81712
C	6.976436	1.477868	10.22366
C	0.161716	10.71628	6.493652
C	15.46345	10.84783	5.38985
C	1.489212	10.23689	6.979651
C	10.71406	17.05648	10.71626
C	10.86699	1.710527	11.83901
C	10.22064	15.73406	10.23094
C	17.03618	6.491642	6.487409
C	1.731538	6.355622	5.379486
C	15.71158	6.981425	6.970339

C	6.491519	17.05835	6.493208
C	6.345095	1.714857	5.373096
C	6.973912	15.73314	6.982637
C	17.04006	10.71281	10.70972
C	1.72998	10.85238	11.82777
C	15.71343	10.23395	10.22087
C	10.71093	0.153878	6.486314
C	10.86269	15.49926	5.364106
C	10.21775	1.47636	6.971699
C	0.166305	6.488132	10.71264
C	15.47099	6.350093	11.82067
C	1.490806	6.979257	10.2308
C	10.69891	6.494232	0.155522
C	11.83759	6.347122	15.48451
C	10.20852	6.975596	1.480777
C	6.50226	6.48973	17.04593
C	6.341016	5.389321	1.724045
C	6.9936	6.970666	15.72091
C	6.487054	10.72447	0.156087
C	5.395773	10.85936	15.47909
C	6.977194	10.23922	1.479916
C	10.71721	10.71614	17.04805
C	10.84468	11.82915	1.72596
C	10.22491	10.23456	15.72361
C	11.82193	10.86264	1.717766
C	10.85914	5.381682	15.47724
C	5.363648	6.35589	1.716825
C	6.360991	11.83797	15.4852
C	15.46584	11.82335	6.358412
C	15.46993	5.381164	10.84564
C	5.371811	1.714545	6.343662
C	1.733909	11.82236	10.85375
C	11.83093	15.4975	6.339751
C	1.732954	5.385517	6.353373
C	5.377572	15.4934	10.85379
C	11.8348	1.712615	10.86288
C	15.07749	8.763065	2.113155
C	14.93608	6.88097	3.217853
C	15.56811	10.08823	1.632102
C	8.764202	2.103045	15.09635
C	6.890421	2.242939	13.9764
C	10.09042	1.623693	15.58621
C	2.107172	8.450671	2.109036

C	2.258767	10.32236	3.230837
C	1.616303	7.125798	1.626703
C	8.453062	15.09651	15.09323
C	10.33299	14.95749	13.98483
C	7.127485	15.58662	15.57333
C	15.09205	8.446803	15.08717
C	14.93801	10.31813	13.96515
C	15.58665	7.124623	15.57223
C	8.439862	2.114602	2.108884
C	10.3222	2.249071	3.214102
C	7.113829	1.632484	1.621982
C	2.127409	8.759114	15.08932
C	2.26192	6.876234	13.98476
C	1.644926	10.08365	15.58012
C	8.750513	15.10314	2.112678
C	6.878765	14.96342	3.235924
C	10.0737	15.58448	1.61718
C	2.11669	15.09915	8.757228
C	3.222529	14.96859	6.874999
C	1.628065	15.57973	10.08344
C	15.08762	15.09876	8.445624
C	14.94486	13.99248	10.32654
C	15.5783	15.58067	7.120694
C	15.0873	2.108898	8.756351
C	13.96263	2.258147	6.885842
C	15.58002	1.624728	10.07963
C	2.116301	2.110634	8.445353
C	2.261401	3.22984	10.31915
C	1.625763	1.626701	7.121157
C	3.225653	2.250267	10.32498
C	2.25139	13.99572	6.874141
C	13.96651	14.95801	10.31881
C	14.93418	3.230437	6.884512
C	6.885641	3.212815	14.9505
C	6.87173	13.99404	2.26137
C	13.97011	10.31915	14.94111
C	10.32132	3.220853	2.24188
C	3.245864	6.884823	14.94453
C	10.33624	13.99238	14.96368
C	13.95766	6.888965	2.252463
C	3.226656	10.32456	2.254874
H	6.61933	14.72462	12.54355
H	14.7027	10.58681	4.662066

H	10.62086	2.460647	12.5832
H	9.193701	15.81528	9.844715
H	10.19916	14.98659	11.03695
H	10.85807	15.35602	9.423622
H	2.490295	6.613058	4.648127
H	15.79219	8.008037	7.357816
H	14.96497	7.003459	6.16367
H	15.33415	6.34305	7.77715
H	6.594833	2.465834	4.631317
H	2.480358	10.60155	12.56975
H	10.61624	14.74886	4.62034
H	9.191136	1.395212	7.358859
H	10.19557	2.223814	6.165678
H	10.85586	1.854356	7.778499
H	14.71222	6.606547	12.55237
H	1.409749	8.006234	9.844322
H	2.236952	7.000997	11.03796
H	1.869016	6.342015	9.423489
H	12.58211	6.59619	14.73601
H	6.598926	4.661739	2.486276
H	8.021185	7.356311	15.79839
H	7.012797	6.162866	14.97528
H	6.355009	7.77708	15.34273
H	4.666122	10.60116	14.71913
H	10.58757	12.55687	2.488265
H	9.197629	9.848259	15.80195
H	10.20516	11.04209	14.97771
H	10.86374	9.428414	15.34505
H	12.56732	10.613	2.465237
H	10.60022	4.654654	14.71481
H	9.181008	7.361432	1.403796
H	10.18959	6.168033	2.226692
H	10.84761	7.781825	1.858684
H	4.619287	6.605303	2.465374
H	6.60953	12.58124	14.73513
H	8.00436	9.852381	1.401524
H	6.997421	11.04523	2.22733
H	6.337587	9.432669	1.856148
H	14.70722	12.55497	6.615501
H	1.415164	9.849907	8.007057
H	2.233528	11.04575	6.998047
H	1.866367	9.430808	6.340185
H	14.71086	4.651341	10.58527

H	4.629522	2.46589	6.591307
H	7.361196	15.80834	8.009778
H	6.16607	14.98756	7.001736
H	7.77983	15.35574	6.343052
H	2.493985	12.55284	10.59777
H	15.78794	9.847868	9.193249
H	14.96975	11.04353	10.2028
H	15.33481	9.427923	10.85956
H	12.57197	14.74602	6.590457
H	2.492561	4.656047	6.613151
H	4.634452	14.7431	10.60543
H	7.362438	1.402367	9.195958
H	6.16878	2.223495	10.20499
H	7.783619	1.854735	10.86197
H	12.57575	2.464214	10.6124
H	15.19511	6.117986	3.944214
H	16.59497	10.01033	1.244824
H	15.58868	10.8341	2.439595
H	14.92962	10.46639	0.825647
H	6.140788	1.992254	13.23362
H	2.012313	11.07269	3.974605
H	0.588148	7.201491	1.242017
H	1.59841	6.380296	2.434688
H	2.255022	6.747625	0.820334
H	11.09088	15.21228	13.2516
H	7.206435	16.61409	15.95917
H	6.382453	15.60713	14.76515
H	6.74903	14.94929	16.38048
H	15.18363	11.06867	13.22123
H	16.61404	7.206067	15.95741
H	15.60763	6.37721	14.76611
H	14.94875	6.746094	16.37909
H	11.08155	1.990478	3.944284
H	1.998559	6.113226	13.26021
H	6.130773	15.21407	3.980406
H	3.952199	15.22903	6.115795
H	15.20342	13.2655	11.08912
H	16.60566	15.96691	7.19795
H	15.59739	14.77359	6.374276
H	14.939	16.38698	6.743335
H	13.21795	2.010477	6.136985
H	2.013824	3.973385	11.06924
H	0.598541	1.239894	7.199261

H	1.605633	2.433328	6.374348
H	2.265089	0.820236	6.744386
H	3.95486	1.990971	11.08504
H	1.992018	13.26763	6.112903
H	0.600617	15.96611	10.00652
H	1.608785	14.77225	10.82927
H	2.267141	16.3862	10.46065
H	13.22169	15.20716	11.067
H	15.18125	3.972911	6.133159
H	16.60739	1.238581	10.00148
H	15.59955	2.431644	10.82626
H	14.94087	0.818535	10.45743
H	6.125409	3.943351	15.2059
H	10.01585	1.238191	16.61414
H	10.83437	2.433081	15.60388
H	10.46906	0.818123	14.94679
H	6.110913	13.2637	2.006862
H	9.991737	15.96995	0.589905
H	10.81934	14.77671	1.595342
H	10.45417	16.39068	2.254639
H	13.22855	11.07002	15.1919
H	11.08127	3.950043	1.9819
H	7.1906	1.24512	0.594988
H	6.367616	2.439572	1.602342
H	6.737623	0.82572	2.261225
H	3.991238	6.135916	15.19063
H	1.259525	10.00451	16.60774
H	2.451956	10.82992	15.6005
H	0.837392	10.46143	14.94286
H	11.09739	13.26582	15.22683
H	13.21337	6.140499	2.002561
H	3.967157	11.07651	2.004317
N	7.059317	16.67512	11.72833
N	16.65503	10.15194	5.474993
N	10.16381	0.52397	11.7469
N	0.539252	7.049538	5.462937
N	7.049277	0.528628	5.468116
N	0.540489	10.15389	11.73572
N	10.15967	16.68604	5.45612
N	16.66315	7.044429	11.7379
N	11.74687	7.043226	16.67588
N	7.0435	5.475747	0.536859
N	5.486175	10.15642	16.66684

N	10.14064	11.74241	0.539667
N	11.72879	10.16646	0.52674
N	10.15655	5.468843	16.6643
N	5.455041	7.052067	0.525592
N	7.057774	11.74901	16.6751
N	16.65843	11.74108	7.051741
N	16.6616	5.467911	10.15006
N	5.464281	0.528424	7.047467
N	0.546217	11.73561	10.15191
N	11.73478	16.68351	7.044538
N	0.541095	5.470874	7.04882
N	5.464013	16.68487	10.15903
N	11.73825	0.526868	10.15762
N	15.63814	8.068528	3.131798
N	8.079808	1.544324	14.06951
N	1.555466	9.136088	3.138856
N	9.139901	15.65069	14.06583
N	15.64201	9.132095	14.057
N	9.129801	1.55394	3.13026
N	1.56011	8.064328	14.07492
N	8.069009	15.66068	3.141339
N	3.137662	15.66181	8.068412
N	15.64786	14.07937	9.139658
N	14.05994	1.55305	8.07173
N	1.564581	3.14167	9.129135
N	3.134673	1.547697	9.137154
N	1.557759	14.07673	8.066476
N	14.05768	15.65393	9.12743
N	15.64026	3.136798	8.069036
N	8.072635	3.125924	15.65347
N	8.058141	14.0806	1.557301
N	14.06746	9.133123	15.64585
N	9.129	3.137299	1.548407
N	3.160469	8.076985	15.6386
N	9.145088	14.07962	15.65978
N	14.04808	8.081027	1.557686
N	3.130553	9.139031	1.549358
Zn	8.606447	17.20474	12.90326
Zn	17.18597	8.602651	4.300232
Zn	8.602136	0.002207	4.301042
Zn	0.01395	8.596587	12.90069
Zn	12.90701	8.602846	17.20153
Zn	8.608011	4.298689	17.20096

Zn	4.315175	8.607374	17.19781
Zn	8.594473	12.91417	0.007644
Zn	0.01014	12.90734	8.604003
Zn	17.19361	4.298735	8.598108
Zn	4.305554	-0.0019	8.603283
Zn	12.89712	17.21309	8.599746

Table B.3. Cartesian atomic coordinates and lattice vectors for ZIF-14 (SOD)

Atom Type	x	y	z
	16.83217	0	0
Lattice vectors	0.001541	17.79956	0
	-0.30369	0.35816	17.11496
C	0.160511	11.12948	6.489052
C	-0.03886	6.888374	10.72042
C	0.795786	7.07043	0.933039
C	0.686025	1.19758	6.589705
C	1.444467	10.53374	6.988038
C	1.175069	7.480972	10.0662
C	1.421241	15.44801	11.17677
C	1.796526	7.27341	2.075086
C	1.632878	2.380454	6.82637
C	1.41394	16.39026	9.970817
C	1.202327	10.73975	15.51668
C	1.572905	11.01431	11.59205
C	1.583286	6.848059	5.648519
C	1.483523	5.896374	6.630284
C	1.719939	12.01299	10.66144
C	2.141064	8.707595	2.328696
C	1.979851	2.616746	8.264814
C	1.943605	15.86008	8.670285
C	1.77219	9.425838	15.07244
C	2.086604	14.78656	6.765595
C	2.052394	10.74892	3.118175
C	1.974391	3.427614	10.29896
C	1.870011	7.451238	14.12041
C	2.693681	11.41664	6.95451
C	2.525523	7.319827	10.77531
C	2.01775	12.01205	15.25984
C	2.915994	15.87777	6.705368
C	2.887291	2.401791	10.24709
C	3.017509	10.70499	2.140534
C	2.865917	7.52676	15.0619

C	5.287929	6.428892	1.685481
C	5.33317	1.91259	6.214664
C	5.084701	16.43628	10.70228
C	5.255827	11.17474	15.42905
C	6.704906	9.690026	2.379852
C	6.504014	16.13042	15.23524
C	6.205986	5.413379	1.589638
C	6.340324	1.79061	5.290114
C	6.061426	16.48397	11.66501
C	6.078662	12.27232	15.38163
C	6.303024	11.20086	0.337353
C	6.169188	17.6896	6.365687
C	6.142402	0.549307	10.52038
C	6.06188	7.012821	16.90874
C	6.679704	14.55238	2.199906
C	6.700435	15.51818	3.17527
C	6.48725	3.458629	14.84047
C	6.467121	2.412488	13.95215
C	6.357672	16.29133	6.884493
C	6.546456	1.850943	9.882828
C	6.602092	11.10352	1.805491
C	6.616304	7.674595	15.68329
C	6.667531	6.859114	14.38985
C	6.752384	1.845799	1.598332
C	6.627716	0.666199	0.620794
C	7.733184	15.65836	6.699104
C	7.497735	2.768875	10.6428
C	8.159376	2.180326	1.993106
C	7.925118	15.81064	14.91322
C	8.556333	15.66794	2.015988
C	8.365708	2.349579	15.04913
C	9.821403	16.24048	1.447891
C	9.606606	1.746642	15.64393
C	9.894442	6.418419	2.648027
C	9.802559	7.25214	1.365722
C	9.948433	1.732847	6.583697
C	9.609379	16.40415	10.34326
C	9.726286	11.40353	15.43663
C	10.1681	3.05468	1.984788
C	10.13244	2.067693	2.938177
C	9.915665	15.85494	14.00712
C	9.909439	14.88777	14.98119
C	10.41733	6.679968	0.123638

C	10.51322	0.37385	6.280831
C	10.38254	17.61417	10.78901
C	10.03917	11.51211	16.90128
C	10.28721	11.92758	1.838198
C	10.36996	5.918018	15.37326
C	10.81348	16.30205	5.178131
C	10.81336	1.627198	11.94691
C	10.10056	2.26321	8.004461
C	10.3033	15.40541	9.423994
C	11.05468	15.33067	1.435757
C	9.745169	10.00291	14.82955
C	10.87478	2.599813	15.70356
C	11.1494	10.86036	1.804636
C	11.71324	16.34205	6.212902
C	11.77281	1.493436	10.97567
C	11.31959	6.908123	15.41339
C	13.56038	11.87851	14.06014
C	13.72756	7.177894	2.110617
C	13.55395	2.366148	6.996698
C	13.72082	15.56455	10.24534
C	13.09327	11.29528	15.23341
C	14.43419	3.41858	7.025503
C	14.72166	7.197677	3.058495
C	14.40362	11.00513	13.38267
C	14.66844	14.57247	10.21741
C	14.50802	9.221842	2.250446
C	14.76639	2.199785	8.815659
C	14.78962	15.68696	8.334215
C	14.36563	9.35435	15.02118
C	14.12407	6.843241	7.762473
C	14.48981	9.693001	10.05376
C	15.02802	11.22157	5.519917
C	15.11055	12.24692	6.427814
C	14.97666	5.682517	10.9633
C	14.94446	6.698688	11.88162
C	14.76039	10.66647	1.947426
C	15.32576	16.3149	7.081212
C	15.43802	1.548395	9.99043
C	14.99436	8.205679	15.76659
C	15.3894	15.48527	5.797059
C	15.49936	2.326653	11.30748
C	15.08028	6.808224	15.15619
C	14.95693	7.376973	6.603739

C	15.10106	11.08894	10.00642
C	15.90592	10.90034	0.953115
C	16.36506	6.873337	6.431186
C	16.50499	11.23707	10.5236
H	16.70298	7.62421	1.126113
H	16.55381	1.36005	7.083659
H	0.496329	1.066624	5.51521
H	0.540736	6.006511	0.832523
H	0.91748	7.765217	17.09547
H	1.124343	0.268227	6.969777
H	0.375172	16.71961	9.796278
H	0.221609	10.84205	15.032
H	0.789932	14.5675	11.0132
H	1.026979	15.97098	12.0587
H	1.0069	10.66469	16.59699
H	0.981443	8.554961	9.919009
H	1.274316	10.20507	8.027601
H	1.385419	6.844885	2.999585
H	1.1802	3.295604	6.421636
H	1.625882	9.617513	6.410733
H	1.243461	7.041195	9.06321
H	1.872141	14.02859	6.021334
H	1.587414	6.638029	13.46206
H	1.70455	11.57612	3.727792
H	1.677452	4.062843	11.12645
H	2.562089	7.873611	11.7205
H	2.588346	12.30159	7.593326
H	2.711233	6.711965	1.844873
H	2.56181	2.212792	6.260344
H	1.98129	17.30225	10.20551
H	1.425351	12.88862	15.55671
H	2.286488	10.59805	12.29481
H	2.435808	7.151534	5.050197
H	2.234921	5.232165	7.041916
H	2.5817	12.62602	10.42135
H	2.433735	15.09944	11.41951
H	2.922619	11.7543	5.93439
H	2.749805	6.264928	10.98585
H	2.272378	12.12515	14.19761
H	3.326241	7.710122	10.13158
H	3.559604	10.84814	7.321164
H	2.94807	12.02372	15.8382
H	3.536399	16.24512	5.895898

H	3.528909	1.988466	11.01849
H	3.655534	11.48863	1.74778
H	3.595941	6.787852	15.37346
H	4.606381	6.669364	2.492691
H	4.71212	2.766101	6.464098
H	4.368891	15.65784	10.46357
H	4.700583	10.67733	14.64135
H	5.725039	9.202436	2.446669
H	6.339456	16.10057	16.32055
H	5.80417	15.41237	14.77998
H	5.66861	6.521169	14.08183
H	7.356168	9.052591	1.769225
H	5.917666	13.82338	1.952321
H	5.739363	4.215252	15.04713
H	5.962324	15.77274	3.927952
H	5.704331	2.102084	13.24628
H	5.594501	15.62951	6.441215
H	5.620717	2.398707	9.643818
H	5.570847	0.485864	0.380568
H	6.041719	8.594114	15.51712
H	6.29466	2.73404	1.141071
H	6.245563	17.13253	14.87264
H	7.119882	9.729913	3.396173
H	6.747364	2.516441	4.594374
H	6.444534	4.622296	2.291368
H	6.381927	12.88722	14.54044
H	6.347896	15.75218	12.41151
H	6.171747	1.62225	2.50652
H	5.847316	11.66199	2.384268
H	6.113551	16.32107	7.957635
H	6.987592	1.608843	8.900019
H	7.075235	7.480376	13.58033
H	6.849119	1.230396	16.79618
H	7.314762	5.979119	14.4833
H	7.087098	3.091077	11.60706
H	7.964187	15.47058	5.643521
H	7.037947	17.54676	1.05524
H	7.55063	11.63159	1.972499
H	7.639657	8.006404	15.9235
H	7.763261	14.6888	7.214264
H	7.689141	3.669363	10.04352
H	8.466082	2.291411	10.82867
H	8.53203	16.28585	7.111489

H	8.739291	7.444301	1.152059
H	8.879289	1.694697	6.328256
H	8.679406	16.75632	9.863848
H	8.728475	11.84044	15.29554
H	9.347433	5.47298	2.558841
H	9.453685	6.979474	3.483887
H	9.611299	16.55534	0.412094
H	9.358347	1.431594	16.67158
H	10.38272	2.459786	5.8737
H	9.273155	15.88562	11.25523
H	10.41369	12.0455	14.86138
H	10.04541	17.16054	2.00423
H	9.811006	0.820183	15.08889
H	9.991036	12.56697	2.663139
H	10.16504	5.174581	14.61185
H	10.6305	15.53318	4.436489
H	10.67726	2.39608	12.69855
H	9.62842	14.56087	9.230046
H	9.309885	10.03089	13.82165
H	9.575264	3.223265	8.09719
H	10.90209	14.44376	0.810582
H	10.74106	3.489187	16.32882
H	10.25805	8.236411	1.533706
H	10.97791	3.71106	1.686371
H	10.90672	1.70001	3.602579
H	9.675187	1.572754	8.742253
H	10.71668	16.18714	13.35598
H	10.70935	14.23602	15.3138
H	9.168733	9.290061	15.43129
H	10.55238	15.84734	8.453507
H	10.9368	6.189053	2.908225
H	11.19761	2.932144	14.70819
H	11.32188	14.9882	2.444205
H	11.91532	15.87858	1.028301
H	11.69379	2.010912	16.13896
H	11.22453	15.00389	9.862085
H	11.14854	2.438764	8.274809
H	10.76253	9.607537	14.72972
H	11.72731	10.39541	2.596322
H	12.45167	15.61542	6.531702
H	12.61205	2.131746	10.72646
H	12.06879	7.186641	14.68145
H	13.11632	6.359883	1.745041

H	12.81131	2.091676	6.256579
H	13.01686	15.83783	11.02291
H	12.47805	11.8401	15.95614
H	13.14981	7.350676	7.771184
H	13.52877	9.692545	9.522421
H	14.49946	2.569381	11.69087
H	14.40225	15.11276	5.493371
H	14.09484	6.408129	14.88759
H	14.20881	10.92262	4.87571
H	14.38005	12.99801	6.70434
H	14.25134	4.905182	10.75355
H	14.17931	6.954069	12.60339
H	13.83359	11.10906	1.554843
H	14.73092	17.22066	6.900376
H	14.93406	0.58513	10.15258
H	14.49348	8.139829	16.73831
H	14.41277	7.216242	5.658668
H	14.43003	11.79611	10.52181
H	14.29515	9.34987	11.07655
H	13.92986	5.767379	7.686585
H	14.59871	4.211533	6.304244
H	14.7573	11.22178	12.37718
H	15.13545	6.394161	3.658596
H	14.92654	13.84542	10.97904
H	14.98915	11.19636	2.882844
H	15.11676	11.42931	8.962985
H	15.03263	8.473432	6.694192
H	14.60057	7.027579	8.728972
H	15.14447	8.954059	9.57772
H	15.77369	16.11179	4.980094
H	16.00885	1.720912	12.0694
H	15.51492	6.130725	15.90324
H	16.05985	3.262065	11.20333
H	15.72816	6.77315	14.27543
H	16.06231	14.62642	5.895454
H	16.34296	16.66827	7.306086
H	16.46991	1.303615	9.686759
H	16.01969	8.542521	15.98106
H	15.39194	10.78168	17.1052
H	16.04449	11.97491	0.771097
H	0.01688	10.49816	1.341351
N	0.351586	7.453952	5.519027
N	0.277706	10.52877	11.51364

N	0.184403	5.903761	7.117633
N	0.52027	12.15614	9.995667
N	1.503015	9.48687	3.235018
N	1.483152	14.76782	8.009099
N	1.1891	8.654377	14.11678
N	1.405208	3.561822	9.047721
N	3.077358	9.413344	1.648907
N	2.892183	1.896789	8.959682
N	2.835118	16.54421	7.912092
N	2.805583	8.771902	15.66029
N	5.379719	7.205068	0.547011
N	5.132339	17.61599	9.989866
N	5.222402	0.713131	6.885793
N	5.193363	10.73402	16.73965
N	6.880683	5.549732	0.391625
N	6.862984	0.510504	5.380413
N	6.544252	12.51346	16.65885
N	6.727115	17.69407	11.5546
N	7.853849	14.64199	1.477603
N	7.887338	16.21417	3.060155
N	7.689243	3.428781	15.52187
N	7.657868	1.725409	14.07558
N	8.920473	3.132653	1.397539
N	8.861193	1.525189	2.947949
N	8.658743	16.43345	13.96423
N	8.648717	14.8583	15.54879
N	9.786101	12.11033	0.565889
N	9.619612	5.99082	16.53095
N	10.06094	17.45536	5.22364
N	9.94055	0.566217	11.83027
N	11.1908	10.37821	0.505987
N	11.52515	17.5236	6.911226
N	11.50146	0.349162	10.24536
N	11.16099	7.608026	16.59263
N	13.59191	8.458027	1.60653
N	13.79078	16.25653	9.052154
N	13.75804	1.6061	8.131044
N	13.34651	10.00364	15.62923
N	15.20619	8.489104	3.150265
N	15.18799	3.323267	8.17989
N	14.93265	9.840492	13.89675
N	15.33738	14.64285	9.008579
N	16.22232	10.52788	5.54891

N	16.35627	12.1997	7.025845
N	16.1462	5.797555	10.23944
N	16.09773	7.447839	11.74396
Zn	0.056597	13.4564	8.521231
Zn	16.53627	9.085368	12.81762
Zn	3.983434	0.310763	8.412961
Zn	4.280077	8.853445	0.139367
Zn	8.056794	13.76622	17.10675
Zn	8.388718	17.79481	4.167219
Zn	8.237381	18.05648	12.8426
Zn	8.127854	4.722845	16.99848
Zn	12.6032	17.81012	8.593336
Zn	12.4514	8.903062	0.01477
Zn	16.73301	9.011705	4.345591
Zn	16.59878	4.662807	8.651903

Table B.4. Cartesian atomic coordinates and lattice vectors for ZIF-7 (SOD)

Atom Type	x	y	z
	22.989	0	0
Lattice vectors	-11.4945	19.90906	0
	0	0	15.763
C	15.76294	0.592265	2.771551
C	-4.26844	19.31679	12.99145
C	14.59461	13.35498	2.77155
C	-3.10011	6.55408	12.99145
C	4.125945	5.961818	2.771553
C	7.368554	13.94724	12.99145
C	4.268443	7.228617	8.025884
C	18.72056	6.044088	2.482782
C	14.59461	0.082273	8.025883
C	8.394388	13.19043	2.482783
C	15.62045	12.59817	8.025887
C	7.368555	0.674537	2.482779
C	-7.22606	13.86497	13.28022
C	7.226057	12.68044	7.737116
C	3.100114	6.718626	13.28022
C	-3.10011	19.82678	7.737116
C	4.125946	19.23452	13.28022
C	-4.12594	7.310887	7.737113
C	3.114184	18.83867	3.558367
C	8.380316	1.070386	12.20463
C	-6.37736	13.18669	3.558365

C	17.87186	6.722374	12.20464
C	3.263178	7.792762	3.558369
C	8.231322	12.1163	12.20463
C	3.114183	5.565966	8.8127
C	-3.11418	7.706739	1.695966
C	5.117141	19.82304	8.812698
C	6.377359	13.35873	1.695969
C	-8.23132	14.42911	8.812703
C	-3.26318	18.75265	1.695964
C	14.60868	12.20232	14.06703
C	8.380317	14.34309	6.950299
C	5.117142	6.550332	14.06703
C	6.377359	0.08602	6.950301
C	14.75768	1.156408	14.06704
C	19.72582	5.479944	6.950297
C	2.338254	17.94239	4.301675
C	9.156247	1.966673	11.46132
C	-5.21319	12.96285	4.301673
C	16.70769	6.946207	11.46133
C	2.874936	8.912881	4.301676
C	8.619564	10.99618	11.46132
C	2.338253	4.66968	9.556009
C	-2.33825	8.603026	0.952658
C	6.281314	19.5992	9.556006
C	5.213187	13.58256	0.95266
C	-8.61956	15.54923	9.556009
C	-2.87494	17.63253	0.952657
C	13.83275	11.30603	14.81034
C	9.156248	15.23938	6.20699
C	6.281313	6.326499	14.81034
C	5.213187	0.309854	6.206993
C	14.36944	2.276528	14.81034
C	20.11407	4.359824	6.206989
C	13.52719	4.523439	1.869881
C	-2.03269	15.38562	13.89312
C	12.30799	9.453173	1.869881
C	-0.81349	10.45589	13.89312
C	8.648318	5.932447	1.869882
C	2.846182	13.97661	13.89312
C	2.03269	11.15979	7.124215
C	20.95631	2.112914	3.384452
C	0.813493	16.08952	7.124215
C	10.68101	17.09224	3.384452

C	-2.84618	12.5688	7.124215
C	2.846183	0.703906	3.384452
C	-9.46181	17.79614	12.37855
C	9.461809	8.749266	8.638785
C	0.813492	2.816819	12.37855
C	10.68101	3.819533	8.638785
C	8.648317	19.20515	12.37855
C	14.34068	7.340258	8.638784
C	2.104858	16.69145	3.735544
C	9.389643	3.217607	12.02746
C	-4.01315	13.38619	3.735543
C	15.50765	6.522867	12.02746
C	1.908294	9.740474	3.735544
C	9.586207	10.16858	12.02746
C	2.104857	3.418746	8.989877
C	-2.10486	9.85396	1.51879
C	18.97585	0.113486	8.989876
C	4.013149	13.15922	1.518791
C	13.40279	16.37683	8.989878
C	-1.90829	16.80494	1.518788
C	13.59936	10.0551	14.24421
C	9.389644	16.49031	6.773123
C	7.481351	6.749839	14.24421
C	-7.48135	19.79557	6.773123
C	13.40279	3.104122	14.24421
C	-1.90829	3.532231	6.773122
C	14.22985	5.744218	1.783102
C	-2.73535	14.16484	13.9799
C	10.89944	9.451302	1.783104
C	0.595062	10.45776	13.9799
C	9.354214	4.713537	1.783103
C	2.140286	15.19552	13.9799
C	2.735348	12.38057	7.037437
C	20.25365	0.892134	3.471231
C	-0.59506	16.08766	7.037438
C	12.08956	17.09411	3.471229
C	-2.14029	11.34989	7.037437
C	2.140286	1.922816	3.47123
C	-8.75915	19.01692	12.29177
C	8.759151	7.528487	8.725563
C	-0.59506	2.81495	12.29177
C	12.08956	3.821403	8.725562
C	9.354213	17.98624	12.29177

C	13.63479	8.559167	8.725562
C	2.612483	16.34025	2.468167
C	8.882016	3.568807	13.29483
C	-3.96281	14.00141	2.468165
C	15.45731	5.907649	13.29483
C	1.350332	9.476456	2.468167
C	10.14417	10.4326	13.29483
C	2.612484	3.067546	7.722501
C	-2.61248	10.20516	2.786166
C	19.02619	0.728705	7.722499
C	3.962814	12.544	2.786167
C	12.84483	16.11281	7.7225
C	-1.35033	17.06896	2.786167
C	14.10698	9.703899	12.97683
C	8.882017	16.84151	8.040499
C	7.531686	7.365057	12.97683
C	-7.53169	19.18035	8.0405
C	12.84483	2.840103	12.97683
C	-1.35033	3.796249	8.040499
C	14.82218	3.902107	3.773033
C	-3.32768	16.00695	11.98997
C	12.19859	10.88534	3.773033
C	-0.70409	9.023721	11.98997
C	7.462731	5.121611	3.773033
C	4.031768	14.78745	11.98997
C	3.327684	10.53846	9.027366
C	19.66132	2.734246	1.4813
C	0.704086	17.52169	9.027366
C	10.79041	15.66007	1.481301
C	-4.03177	11.75796	9.027366
C	4.03177	1.514741	1.481301
C	-8.16681	17.17481	14.2817
C	8.166817	9.370598	6.735634
C	0.704087	4.248986	14.2817
C	10.79041	2.387367	6.735634
C	7.46273	18.39432	14.2817
C	15.52627	8.151093	6.735634
C	3.644607	18.47773	2.290721
C	7.849892	1.431325	13.47228
C	-6.32999	13.82651	2.290719
C	17.82449	6.082545	13.47228
C	2.685385	7.513872	2.290723
C	8.809116	12.39519	13.47228

C	3.644607	5.205028	7.545054
C	-3.64461	8.067678	2.963612
C	16.65901	0.553808	7.545052
C	6.329988	12.7189	2.963615
C	14.17988	14.15022	7.545056
C	-2.68538	19.03154	2.96361
C	15.13911	11.84138	12.79939
C	7.849894	14.70403	8.217945
C	5.164511	7.190161	12.79939
C	-5.16451	19.35525	8.217947
C	14.17988	0.877518	12.79939
C	-2.68538	5.758834	8.217943
C	3.388181	17.22426	1.723823
C	8.106319	2.6848	14.03918
C	-5.11623	14.23118	1.723822
C	16.61073	5.677879	14.03918
C	1.728056	8.362679	1.723824
C	9.766443	11.54638	14.03918
C	3.38818	3.951553	6.978157
C	-3.38818	9.321153	3.53051
C	17.87277	0.958474	6.978155
C	5.116235	12.31423	3.530511
C	13.22256	14.99903	6.978158
C	-1.72806	18.18273	3.530509
C	14.88268	10.58791	12.23249
C	8.10632	15.9575	8.784842
C	6.378265	7.594828	12.23249
C	-6.37826	18.95058	8.784843
C	13.22256	1.726326	12.23249
C	-1.72806	4.910026	8.784841
C	13.81403	3.582364	2.854533
C	-2.31953	16.3267	12.90847
C	12.97957	10.17212	2.854532
C	-1.48507	9.736942	12.90847
C	7.689905	6.154576	2.854534
C	3.804594	13.75448	12.90846
C	2.319526	10.21872	8.108867
C	20.66947	3.053989	2.3998
C	1.48507	16.80847	8.108867
C	10.00943	16.37329	2.399801
C	-3.8046	12.79093	8.108869
C	3.804596	0.481777	2.399799
C	-9.17497	16.85507	13.3632

C	9.174974	9.690341	7.654133
C	1.48507	3.535765	13.3632
C	10.00943	3.100588	7.654134
C	7.689904	19.42728	13.3632
C	15.2991	7.118128	7.654132
C	16.28105	3.99181	5.38146
C	-4.78655	15.91725	10.38154
C	11.39147	12.1039	5.38146
C	0.103032	7.805156	10.38154
C	6.810983	3.813342	5.38146
C	4.683517	16.09572	10.38154
C	4.786554	10.62816	10.63579
C	18.20245	2.644543	15.63587
C	-0.10303	18.74026	10.63579
C	11.59753	14.44151	15.63587
C	-4.68352	10.4497	10.63579
C	4.683518	2.82301	15.63587
C	-6.70795	17.26452	0.127127
C	6.707947	9.280895	5.127206
C	-0.10303	5.467551	0.127127
C	11.59753	1.168802	5.127205
C	6.810983	17.08605	0.127127
C	16.17802	9.459362	5.127207
C	15.51862	5.134448	3.696341
C	-4.02412	14.77461	12.06666
C	10.78313	10.8723	3.69634
C	0.71137	9.036761	12.06666
C	8.181752	3.90231	3.69634
C	3.312748	16.00675	12.06666
C	4.024119	11.7708	8.950674
C	18.96488	1.501904	1.557993
C	-0.71137	17.50865	8.950674
C	12.20587	15.67311	1.557993
C	-3.31275	10.53866	8.950673
C	3.312749	2.734043	1.557993
C	-7.47038	18.40715	14.20501
C	7.470381	8.138257	6.812325
C	-0.71137	4.235946	14.20501
C	12.20587	2.400407	6.812326
C	8.181751	17.17502	14.20501
C	14.80725	9.370394	6.812326
C	15.23303	6.070208	2.692388
C	-3.73853	13.83885	13.07061

C	10.11553	10.15709	2.692389
C	1.378967	9.751971	13.07061
C	9.13494	3.681762	2.692388
C	2.35956	16.2273	13.07061
C	3.738528	12.70656	7.946721
C	19.25047	0.566145	2.561945
C	-1.37897	16.79344	7.946723
C	12.87347	16.38832	2.561944
C	-2.35956	10.31812	7.946721
C	2.359561	2.954591	2.561946
C	-7.75597	19.34291	13.20105
C	7.755972	7.202497	7.816278
C	-1.37897	3.520736	13.20106
C	12.87347	3.115617	7.816277
C	9.134939	16.95447	13.20105
C	13.85406	9.590942	7.816279
H	16.86923	3.714977	6.253957
H	-5.37473	16.19408	9.509041
H	11.33712	12.75169	6.25396
H	0.157376	7.157367	9.509039
H	6.277153	3.442388	6.253959
H	5.217348	16.46667	9.50904
H	5.374726	10.35133	11.50829
H	17.61427	2.921375	14.76337
H	-0.15738	19.38804	11.50829
H	11.65188	13.79372	14.76337
H	-5.21735	10.07874	11.50829
H	5.217348	3.193965	14.76337
H	-6.11977	16.98768	0.999625
H	6.119774	9.557728	4.254708
H	-0.15738	6.115339	0.999626
H	11.65188	0.521014	4.254707
H	6.277152	16.71509	0.999627
H	16.71185	9.830317	4.254706
H	15.77552	7.013694	2.62877
H	-4.28102	12.89536	13.13423
H	9.027207	10.15515	2.628773
H	2.467293	9.753907	13.13423
H	9.68078	2.740212	2.628771
H	1.81372	17.16885	13.13423
H	4.281015	13.65005	7.883105
H	7.213485	19.53172	2.625562
H	-2.46729	16.7915	7.883107

H	-9.02721	16.39026	2.62556
H	-1.81372	9.376566	7.883105
H	1.813721	3.896141	2.625563
H	4.281016	0.377341	13.13744
H	7.213485	6.259012	7.879895
H	20.52171	3.518799	13.13744
H	13.96179	3.117554	7.879893
H	9.680779	16.01292	13.13744
H	13.30822	10.53249	7.879895
H	2.40408	15.34913	2.068732
H	9.090421	4.559933	13.69427
H	-3.00027	14.31649	2.068732
H	14.49477	5.592568	13.69427
H	0.596192	10.1525	2.068732
H	10.89831	9.756557	13.69427
H	2.404079	2.07642	7.323065
H	-2.40408	11.19629	3.185601
H	19.98873	1.043785	7.323065
H	3.000271	12.22892	3.185601
H	12.09069	16.78885	7.323066
H	-0.59619	16.39291	3.185601
H	13.89858	8.712773	12.5774
H	9.09042	17.83264	8.439934
H	8.494229	7.680138	12.5774
H	-8.49423	18.86527	8.439934
H	12.09069	3.516149	12.5774
H	-0.59619	3.120204	8.439933
H	3.770744	16.95335	0.738415
H	7.723758	2.955711	15.02458
H	-5.0729	14.69794	0.738414
H	16.5674	5.211114	15.02459
H	1.302159	8.166825	0.738416
H	10.19234	11.74223	15.02458
H	3.770743	3.680642	5.992749
H	-3.77074	9.592064	4.515919
H	17.9161	1.425239	5.992748
H	5.0729	11.84747	4.515919
H	12.79666	14.80318	5.99275
H	-1.30216	18.37859	4.515917
H	15.26524	10.31699	11.24708
H	7.723757	16.22842	9.770251
H	6.421601	8.061592	11.24708
H	-6.4216	18.48382	9.770251

H	12.79666	1.530472	11.24708
H	-1.30216	5.10588	9.77025
H	13.27356	2.637457	2.910171
H	-1.77906	17.2716	12.85283
H	14.06812	10.17651	2.910171
H	-2.57362	9.732545	12.85283
H	7.141824	7.095086	2.910173
H	4.352676	12.81397	12.85283
H	1.779061	9.273809	8.164504
H	-1.77906	3.998896	2.344162
H	2.573617	16.81287	8.164504
H	8.920884	16.3689	2.344163
H	-4.35268	13.73144	8.164506
H	-7.14182	19.45033	2.344161
H	13.27356	15.91016	13.41884
H	9.715441	10.63525	7.598496
H	2.573617	3.54016	13.41884
H	8.920883	3.096192	7.598496
H	18.63632	0.458734	13.41884
H	15.84718	6.177618	7.598494
H	1.507151	15.96398	4.283778
H	9.987349	3.945076	11.47922
H	-3.08429	13.2323	4.283777
H	14.57879	6.676762	11.47922
H	1.577139	10.62184	4.283778
H	9.91736	9.287221	11.47922
H	1.507151	2.691276	9.538112
H	-1.50715	10.58143	0.970555
H	8.410212	19.86865	9.538111
H	3.084288	13.31311	0.970556
H	-9.91736	17.25819	9.538111
H	-1.57714	15.92357	0.970556
H	13.00165	9.32763	14.79244
H	9.987349	17.21778	6.224888
H	8.410213	6.595945	14.79244
H	3.084288	0.040409	6.224889
H	13.07164	3.985485	14.79244
H	21.41186	2.650867	6.224888
H	13.97952	6.448098	0.988157
H	-2.48502	13.46096	14.77484
H	10.41502	8.882573	0.988159
H	1.079478	11.02648	14.77484
H	10.08895	4.578387	0.988158

H	1.405545	15.33067	14.77484
H	2.485022	13.08445	6.242491
H	20.50398	0.188255	4.266176
H	-1.07948	15.51893	6.242493
H	12.57398	17.66284	4.266174
H	-1.40554	11.21474	6.242492
H	1.405545	2.057966	4.266175
H	-9.00948	19.7208	11.49682
H	9.009478	6.824607	9.520508
H	-1.07948	2.24622	11.49683
H	12.57398	4.390132	9.520506
H	10.08896	17.85109	11.49682
H	12.90005	8.694318	9.520507
H	1.93953	18.20579	5.282594
H	9.554971	1.703264	10.48041
H	-5.24194	12.48584	5.282592
H	16.73645	7.423215	10.48041
H	3.302415	9.126481	5.282594
H	8.192085	10.78258	10.48041
H	1.93953	4.933088	10.53693
H	-1.93953	8.339618	15.73474
H	6.252556	19.1222	10.53693
H	5.241945	14.05957	15.73474
H	-8.19209	15.76283	10.53693
H	-3.30241	17.41893	15.73474
H	13.43403	11.56944	0.02826
H	9.554971	14.97597	5.226072
H	6.252555	5.849491	0.028259
H	5.241944	0.786863	5.226074
H	14.79691	2.490128	0.028261
H	19.68659	4.146224	5.226071
H	16.23673	1.566969	2.691834
H	-4.74223	18.34209	13.07117
H	13.5136	13.27793	2.691833
H	-2.0191	6.631124	13.07117
H	4.733172	5.064155	2.691835
H	6.761328	14.8449	13.07116
H	4.742227	8.203322	7.946167
H	18.24677	5.069383	2.5625
H	13.5136	0.005229	7.946167
H	9.475399	13.26748	2.5625
H	16.22767	11.70051	7.946169
H	6.761329	1.572197	2.562498

H	-6.75227	14.83967	13.2005
H	6.752272	11.70574	7.816833
H	2.019101	6.641583	13.2005
H	-2.0191	19.90383	7.816833
H	4.733172	18.33686	13.2005
H	-4.73317	8.20855	7.816831
H	12.7351	4.309718	1.153056
H	-1.2406	15.59934	14.60994
H	12.88912	8.874062	1.153057
H	-1.39462	11.035	14.60994
H	8.859275	6.725277	1.153058
H	2.635225	13.18378	14.60994
H	1.240601	10.94607	6.407389
H	-1.2406	2.326634	4.101277
H	1.394625	15.51042	6.40739
H	10.09988	17.67135	4.101276
H	-2.63523	13.36163	6.407391
H	-8.85927	19.82013	4.101275
H	12.7351	17.58242	11.66172
H	10.2539	8.962987	9.355611
H	1.394624	2.237709	11.66172
H	10.09988	4.398643	9.35561
H	20.35377	0.088925	11.66172
H	14.12973	6.547427	9.355608
N	15.0169	0.228454	3.828737
N	-3.5224	19.68061	11.93426
N	15.28271	12.89079	3.828735
N	-3.78821	7.018264	11.93426
N	4.183896	6.789813	3.82874
N	7.310605	13.11925	11.93426
N	3.522402	6.864806	9.083069
N	-3.5224	6.4079	1.425598
N	3.788205	19.52715	9.083068
N	7.706296	13.65462	1.425599
N	-7.31061	13.42617	9.083073
N	-4.18389	19.7556	1.425593
N	15.0169	13.50116	14.3374
N	7.972098	13.04425	6.679931
N	3.788205	6.254443	14.3374
N	7.706294	0.381909	6.679931
N	15.6784	0.15346	14.33741
N	18.80511	6.482891	6.679927
N	15.33299	3.1935	4.854453

N	-3.83849	16.71556	10.90855
N	12.55686	11.68201	4.854454
N	-1.06236	8.227045	10.90855
N	6.593656	5.033543	4.854453
N	4.900844	14.87552	10.90855
N	3.838492	9.829854	10.10879
N	19.15051	3.442852	0.39988
N	1.062355	18.31837	10.10879
N	10.43215	14.8634	0.39988
N	-4.90084	11.66989	10.10879
N	4.900845	1.60281	0.39988
N	-7.65601	16.46621	15.36312
N	7.656008	10.0792	5.654213
N	1.062355	5.045661	15.36312
N	10.43214	1.590692	5.654213
N	6.593656	18.30625	15.36312
N	16.39535	8.239162	5.654213
N	4.38127	19.55505	1.822817
N	7.11323	0.354014	13.94018
N	-7.6313	13.92583	1.822814
N	19.1258	5.983233	13.94019
N	3.250033	6.337249	1.822818
N	8.244466	13.57181	13.94018
N	4.38127	6.28234	7.07715
N	18.60773	6.990366	3.431516
N	15.3577	0.65312	7.077147
N	7.631301	12.61959	3.431519
N	14.74453	12.9736	7.07715
N	8.244468	0.299103	3.431515
N	-7.11323	12.91869	12.33148
N	7.11323	13.62672	8.68585
N	3.863201	7.289472	12.33148
N	-3.8632	19.25594	8.685851
N	3.250033	19.60996	12.33148
N	-3.25003	6.935456	8.685849
N	16.44183	5.161106	4.734761
N	-4.94733	14.74795	11.02824
N	10.29844	11.65849	4.734761
N	1.196061	8.250564	11.02824
N	7.743232	3.089457	4.73476
N	3.751267	16.8196	11.02824
N	4.947331	11.79746	9.989095
N	18.04167	1.475247	0.519572

N	-1.19606	18.29485	9.989095
N	12.69056	14.88692	0.519572
N	-3.75127	9.725809	9.989094
N	3.751269	3.546897	0.519573
N	-6.54717	18.43381	15.24343
N	6.547168	8.1116	5.773905
N	-1.19606	5.022143	15.24343
N	12.69056	1.61421	5.773905
N	7.743231	16.36216	15.24343
N	15.24577	10.18325	5.773905
Zn	14.64281	1.395303	5.387265
Zn	-3.14831	18.51376	10.37573
Zn	14.45923	11.98341	5.387267
Zn	-2.96473	7.925648	10.37573
Zn	5.381465	6.530351	5.387268
Zn	6.113035	13.37871	10.37573
Zn	3.148309	8.031656	10.6416
Zn	19.84069	5.24105	15.63007
Zn	2.964732	18.61976	10.6416
Zn	8.529768	14.562	15.63007
Zn	-6.11303	13.1667	10.6416
Zn	6.113035	0.106002	15.63006
Zn	-8.34619	14.66801	0.132931
Zn	8.346191	11.8774	5.121401
Zn	2.964732	5.347058	0.132933
Zn	8.529768	1.289295	5.1214
Zn	5.381465	19.80306	0.132935
Zn	17.60754	6.742354	5.121398

Table B.5. Cartesian atomic coordinates and lattice vectors for ZIF-11 (RHO)

Atom Type	x	y	z
	17.14313	0	0
Lattice vectors	0.005087	17.16192	0
	0.003801	0.004397	17.0516
C	15.06955	8.751062	2.207815
C	6.380263	0.165795	10.60525
C	15.04238	8.38434	14.96899
C	6.380981	16.9929	6.335988
C	14.98258	2.148153	8.647967
C	6.49414	10.68153	0.172267
C	14.96072	15.055	8.35218
C	6.480578	6.426849	16.85805

C	2.178555	8.747108	14.99263
C	10.6648	0.149327	6.319614
C	2.158082	8.430663	2.18852
C	10.72421	17.00668	10.58452
C	2.080189	2.173256	8.372893
C	10.74425	10.66724	16.8675
C	2.126309	15.02609	8.728791
C	10.73072	6.40012	0.1978
C	8.739257	14.98107	2.068349
C	0.15002	6.452667	10.7155
C	8.749673	2.081005	14.83691
C	0.168089	10.78053	6.468779
C	8.438815	15.01618	14.87385
C	16.98425	6.44473	6.449475
C	8.370584	2.106971	2.07903
C	16.98077	10.74702	10.73181
C	14.89276	6.943792	3.401042
C	6.230256	15.48263	11.74214
C	14.8684	10.22751	13.83238
C	6.196239	1.647754	5.159884
C	14.81391	3.345912	6.845102
C	6.268932	11.86799	15.41847
C	14.76141	13.9279	10.19838
C	6.284043	5.221343	1.601498
C	2.349259	6.914801	13.83379
C	10.84494	15.47462	5.172099
C	2.368057	10.25707	3.350648
C	10.8707	1.678664	11.73656
C	2.31574	3.368096	10.16907
C	10.92527	11.86344	1.612857
C	2.270598	13.8663	6.901678
C	10.95283	5.238309	15.4324
C	6.879109	14.80821	3.181249
C	15.475	6.282111	11.8905
C	6.925957	2.276949	13.67254
C	15.48198	10.92701	5.308499
C	6.958058	3.285704	14.63035
C	15.48122	11.93001	6.273705
C	6.936533	13.78889	2.236302
C	15.47124	5.287651	10.91782
C	10.25555	14.83068	13.69256
C	1.688116	6.275978	5.317892
C	10.19239	2.264618	3.252142

C	1.673529	10.92024	11.88083
C	10.19131	3.264428	2.283389
C	1.666447	11.90454	10.89803
C	10.24462	13.83246	14.66031
C	1.672047	5.290799	6.301315
C	3.262043	14.84347	6.888716
C	11.93874	6.219513	15.45539
C	3.285595	2.37039	10.16711
C	11.9045	10.87543	1.634844
C	3.35718	6.938729	14.79231
C	11.82428	15.47954	6.15989
C	3.375608	10.21461	2.393508
C	11.87033	1.674853	10.7675
C	13.77893	14.91221	10.16599
C	5.305785	6.210469	1.621271
C	13.82577	2.367667	6.822451
C	5.28481	10.88442	15.43721
C	13.89238	6.943277	2.434245
C	5.238724	15.49343	10.76534
C	13.85761	10.19001	14.78906
C	5.201854	1.64686	6.132393
C	15.57372	10.01971	1.709755
C	6.872676	1.454732	10.1485
C	15.55841	7.109977	15.4421
C	6.846623	15.71207	6.837926
C	15.43084	1.64438	9.932578
C	7.004099	10.22134	1.450038
C	15.46301	15.48855	7.060196
C	6.938529	6.92986	15.57689
C	1.666685	10.02493	15.45857
C	10.17939	1.440525	6.7731
C	1.637901	7.157607	1.722176
C	10.25954	15.72126	10.09217
C	1.567124	1.689637	7.103998
C	10.29295	10.16619	15.58293
C	1.674474	15.52312	10.01728
C	10.22697	6.852848	1.480673
C	10.02316	15.4957	1.623299
C	1.433201	6.912246	10.21481
C	10.01869	1.565556	15.3217
C	1.450183	10.31613	6.970491
C	7.163844	15.52389	15.34905
C	15.69269	6.940517	6.895336

C	7.095921	1.604182	1.592186
C	15.69024	10.26299	10.27461
Zn	0.079414	8.627293	4.36721
Zn	8.580402	17.09131	12.68413
Zn	0.071229	8.577016	12.83321
Zn	8.51016	17.0924	4.216153
Zn	17.0606	4.307597	8.5971
Zn	8.635347	12.84438	16.96688
Zn	17.08884	12.9138	8.642972
Zn	8.584066	4.241007	16.9531
Zn	4.226555	0.069019	8.464267
Zn	12.90783	8.51955	0.093321
Zn	4.323714	8.574972	0.088701
Zn	12.8293	0.049014	8.4005
H	15.12254	6.204003	4.160544
H	6.478213	14.72109	12.47422
H	15.10344	10.99337	13.10018
H	6.42473	2.389719	4.401663
H	15.0349	4.126156	6.125798
H	6.469788	12.63848	14.68318
H	14.97514	13.18186	10.95492
H	6.493801	4.437978	2.321074
H	2.124243	6.172038	13.07661
H	10.61021	14.71989	4.429428
H	2.161361	11.00003	4.1125
H	10.62818	2.429304	12.48225
H	2.111789	4.133711	10.90973
H	10.71179	12.64745	2.330703
H	2.027525	13.1178	6.154319
H	10.74716	4.475375	14.69067
H	6.115095	15.03632	3.916293
H	14.73411	6.514149	12.64859
H	6.17039	2.052944	12.92672
H	14.73444	10.68138	4.560679
H	6.239117	4.069056	14.84071
H	14.72459	12.67399	6.497996
H	6.206749	13.02203	1.999844
H	14.73216	4.524436	10.70461
H	10.98664	15.04531	12.92161
H	2.451332	6.516116	4.585019
H	10.93942	2.026105	4.002299
H	2.428692	10.68363	12.62266
H	10.94496	4.012055	2.058773

H	2.402014	12.66928	10.6758
H	10.97282	13.05784	14.87044
H	2.418817	4.541539	6.543609
H	3.99721	15.0746	6.125192
H	12.72299	6.433099	14.73796
H	4.066603	2.1601	10.88896
H	12.66571	10.66625	2.377348
H	4.117423	6.198191	15.01679
H	12.58623	14.74265	6.387597
H	4.165823	10.92549	2.1828
H	12.6136	2.430029	10.53554
H	13.0185	15.15446	10.901
H	4.54219	6.421071	2.361005
H	13.06433	2.164075	6.078895
H	4.496774	10.67605	14.72226
H	13.12081	6.209727	2.230749
H	4.490681	14.74314	10.53106
H	13.09745	10.92822	15.02229
H	4.434529	2.382168	6.343827
H	16.48753	10.39133	2.230881
H	7.778602	1.822494	10.68461
H	16.48196	6.76175	14.92252
H	7.922209	10.74874	1.799514
H	16.37686	14.95171	6.713011
H	0.743385	10.36865	14.93362
H	9.284226	1.819701	6.226824
H	0.711347	6.817694	2.242632
H	9.301547	6.334181	1.824453
H	10.35303	16.42638	2.143423
H	10.37328	0.642557	14.80593
H	1.831283	10.86886	7.86024
H	1.804004	6.368251	9.315097
H	6.806259	16.43883	14.81919
H	15.32658	7.839636	6.346544
H	6.728094	0.691862	2.118934
H	15.31468	9.359549	10.80919
H	2.21962	16.42302	10.38634
H	0.665889	2.226235	6.727935
H	10.81726	9.245089	15.2356
H	10.81262	15.3318	9.206672
H	6.417016	7.851477	15.22755
H	14.88926	0.738712	10.29243
H	6.30686	15.34315	7.741301

O	15.05797	10.65759	0.790777
O	6.350241	2.112523	9.246964
O	15.04151	6.445894	16.34141
O	6.480991	9.330789	2.125235
O	14.93913	16.37001	6.376192
O	2.182418	10.70007	16.34998
O	10.69804	2.091618	7.682297
O	2.154809	6.479771	0.832124
O	2.073639	0.7624	6.467434
O	10.76178	7.730075	2.164073
O	10.71751	14.97213	0.750899
O	10.67434	2.084413	16.22694
O	2.087469	9.387512	6.470317
O	2.086572	7.823722	10.72678
O	6.502908	15.01198	16.25405
O	15.03018	6.427698	7.798569
O	6.45103	2.117993	0.6779
O	15.03689	10.79181	9.372546
O	0.766752	15.00874	10.67328
O	9.412887	10.69816	14.90138
O	9.330565	15.08818	10.5975
O	7.822666	6.39797	14.89977
O	16.33011	2.160596	10.60082
O	7.758258	15.0603	6.32504
N	15.6286	8.081066	3.255752
N	6.941701	16.6348	11.63465
N	15.61112	9.092224	13.95124
N	6.925638	0.505555	5.290862
N	15.53179	3.202633	7.990332
N	7.023391	11.73609	16.53798
N	15.49686	14.02709	9.062481
N	7.012311	5.35755	0.462047
N	1.611137	8.048647	13.96855
N	10.13049	16.6254	5.277695
N	1.606983	9.138145	3.215323
N	10.15359	0.528299	11.61517
N	1.567666	3.239517	9.042238
N	10.20155	11.72622	0.470778
N	1.562626	13.98477	8.05841
N	10.20306	5.360522	16.55663
N	8.009475	15.555	3.066681
N	16.62067	7.005773	11.75972
N	8.052998	1.523504	13.80558

N	16.6324	10.21106	5.436672
N	8.100685	3.156484	15.34925
N	16.62967	11.83272	6.993948
N	8.104816	13.89923	1.552414
N	16.60956	5.40397	10.1891
N	9.122692	15.56998	13.83287
N	0.538171	6.992069	5.418557
N	9.047656	1.539031	3.117892
N	0.524516	10.20332	11.77145
N	9.047374	3.162148	1.558471
N	0.515811	11.78937	10.18332
N	9.105997	13.95346	15.38719
N	0.512131	5.401703	7.005275
N	3.165566	15.56492	8.03605
N	11.79904	6.944831	16.59641
N	3.130623	1.625819	9.040903
N	11.78223	10.12838	0.508842
N	3.248107	8.08949	15.5055
N	11.70706	16.63043	6.873153
N	3.239037	9.070146	1.678778
N	11.76894	0.523609	10.05327
N	13.90604	15.61194	9.004887
N	5.433415	6.95731	0.496268
N	13.93955	1.625251	7.952149
N	5.432866	10.14943	16.57063
N	14.00956	8.075432	1.696792
N	5.339721	16.65234	10.05765
N	13.96994	9.032486	15.49037
N	5.323335	0.509498	6.862783

Table B.6. Cartesian atomic coordinates and lattice vectors for ZIF-71 (RHO)

Atom Type	x	y	z
	28.5539	0	0
Lattice vectors	0	28.5539	0
	0	0	28.5539
Zn	11.28012	2.974911	7.205686
Zn	17.27378	25.57899	21.34822
Zn	17.27378	25.57899	7.205684
Zn	11.28012	2.974909	21.34822
Zn	17.27378	2.974911	21.34822
Zn	11.28012	25.57899	7.205682
Zn	11.28012	25.57899	21.34821

Zn	17.27378	2.974908	7.205686
Zn	7.205683	11.28012	2.97491
Zn	21.34822	17.27378	25.57899
Zn	7.205684	17.27378	25.57899
Zn	21.34822	11.28012	2.974909
Zn	21.34822	17.27378	2.97491
Zn	7.205683	11.28012	25.57899
Zn	21.34822	11.28012	25.57898
Zn	7.205683	17.27378	2.974915
Zn	2.974909	7.205685	11.28012
Zn	25.57899	21.34822	17.27378
Zn	25.57899	7.205681	17.27378
Zn	2.974911	21.34822	11.28012
Zn	2.974912	21.34822	17.27378
Zn	25.57899	7.205683	11.28012
Zn	25.57899	21.34822	11.28011
Zn	2.974912	7.205684	17.27378
Zn	2.974911	11.28012	21.34822
Zn	25.57899	17.27378	7.205683
Zn	25.57899	17.27378	21.34822
Zn	2.974912	11.28012	7.205684
Zn	2.97491	17.27378	7.205685
Zn	25.57899	11.28012	21.34822
Zn	25.57899	11.28012	7.205684
Zn	2.97491	17.27378	21.34822
Zn	11.28012	7.205687	25.57899
Zn	17.27378	21.34822	2.974911
Zn	17.27378	7.205682	2.974914
Zn	11.28012	21.34821	25.57898
Zn	17.27378	21.34822	25.57899
Zn	11.28012	7.205686	2.974913
Zn	11.28012	21.34822	2.974907
Zn	17.27378	7.205685	25.57899
Zn	7.205685	2.974911	17.27378
Zn	21.34822	25.57899	11.28012
Zn	7.205685	25.57899	11.28012
Zn	21.34822	2.97491	17.27378
Zn	21.34822	2.974911	11.28012
Zn	7.205684	25.57899	17.27378
Zn	21.34822	25.57899	17.27378
Zn	7.205681	2.97491	11.28012
C	13.58756	2.352359	9.099226
C	14.96633	26.20154	19.45467

C	14.96632	26.20154	9.099224
C	13.58758	2.352356	19.45467
C	14.96634	2.352357	19.45467
C	13.58756	26.20154	9.099219
C	13.58756	26.20154	19.45467
C	14.96633	2.352357	9.09923
C	9.099224	13.58757	2.352355
C	19.45467	14.96633	26.20154
C	9.099227	14.96633	26.20154
C	19.45468	13.58756	2.352356
C	19.45467	14.96632	2.352355
C	9.099229	13.58757	26.20154
C	19.45467	13.58757	26.20154
C	9.09922	14.96634	2.352356
C	2.352354	9.099225	13.58757
C	26.20155	19.45468	14.96633
C	26.20154	9.099217	14.96634
C	2.352352	19.45468	13.58757
C	2.352353	19.45468	14.96634
C	26.20154	9.099222	13.58757
C	26.20155	19.45468	13.58757
C	2.352355	9.099223	14.96634
C	2.352354	13.58757	19.45468
C	26.20154	14.96632	9.099224
C	26.20154	14.96633	19.45468
C	2.352352	13.58756	9.099218
C	2.352351	14.96633	9.099219
C	26.20154	13.58756	19.45468
C	26.20154	13.58755	9.099221
C	2.352355	14.96633	19.45468
C	13.58756	9.099233	26.20153
C	14.96633	19.45467	2.352354
C	14.96632	9.099236	2.352357
C	13.58756	19.45467	26.20154
C	14.96632	19.45467	26.20154
C	13.58756	9.099228	2.35236
C	13.58757	19.45467	2.352354
C	14.96632	9.099239	26.20154
C	9.099224	2.35236	14.96634
C	19.45468	26.20154	13.58756
C	9.099227	26.20154	13.58757
C	19.45467	2.352362	14.96633
C	19.45468	2.352362	13.58757

C	9.099226	26.20154	14.96633
C	19.45468	26.20154	14.96633
C	9.099226	2.352358	13.58757
C	9.040904	3.240042	9.040899
C	19.513	25.31385	19.513
C	19.513	25.31385	9.040898
C	9.040897	3.240044	19.513
C	19.513	3.240038	19.51299
C	9.040911	25.31386	9.040892
C	9.040903	25.31385	19.513
C	19.51301	3.240039	9.040917
C	9.040911	9.040896	3.240043
C	19.513	19.513	25.31386
C	9.04091	19.513	25.31386
C	19.513	9.040905	3.240043
C	19.513	19.513	3.240046
C	9.040914	9.040895	25.31386
C	19.513	9.040901	25.31385
C	9.040896	19.513	3.240043
C	3.240042	9.040907	9.040896
C	25.31385	19.513	19.51299
C	25.31386	9.040896	19.51299
C	3.240048	19.513	9.040898
C	3.240042	19.51301	19.51299
C	25.31386	9.040913	9.040894
C	25.31385	19.513	9.040896
C	3.240044	9.040898	19.513
C	10.21837	5.045361	9.240052
C	18.33553	23.50853	19.31384
C	18.33553	23.50854	9.240055
C	10.21837	5.045362	19.31384
C	18.33553	5.045358	19.31384
C	10.21838	23.50854	9.240044
C	10.21838	23.50853	19.31385
C	18.33554	5.045363	9.240061
C	9.240056	10.21836	5.045364
C	19.31385	18.33553	23.50854
C	9.240058	18.33553	23.50854
C	19.31385	10.21837	5.045362
C	19.31384	18.33553	5.045365
C	9.240059	10.21836	23.50854
C	19.31385	10.21837	23.50853
C	9.240052	18.33552	5.045361

C	5.045363	9.240056	10.21837
C	23.50854	19.31385	18.33552
C	23.50854	9.240048	18.33553
C	5.045362	19.31385	10.21838
C	5.045357	19.31385	18.33552
C	23.50854	9.240057	10.21836
C	23.50854	19.31385	10.21837
C	5.045364	9.24005	18.33553
C	5.045367	10.21837	19.31384
C	23.50854	18.33552	9.240055
C	23.50854	18.33553	19.31384
C	5.04536	10.21838	9.240049
C	5.045364	18.33553	9.240058
C	23.50854	10.21837	19.31384
C	23.50854	10.21838	9.240044
C	5.045362	18.33553	19.31384
C	10.21838	9.240042	23.50855
C	18.33552	19.31384	5.045365
C	18.33553	9.240055	5.045364
C	10.21838	19.31386	23.50855
C	18.33553	19.31385	23.50854
C	10.21838	9.240046	5.04536
C	10.21837	19.31384	5.045361
C	18.33553	9.240051	23.50853
C	9.240049	5.045361	18.33552
C	19.31385	23.50854	10.21837
C	9.240064	23.50853	10.21836
C	19.31385	5.045354	18.33552
C	19.31386	5.045357	10.21838
C	9.240055	23.50853	18.33553
C	19.31385	23.50853	18.33553
C	11.93251	3.293317	4.269158
C	16.62139	25.26058	24.28475
C	16.62139	25.26059	4.26916
C	11.93251	3.293326	24.28475
C	16.62139	3.293312	24.28474
C	11.93251	25.26059	4.26917
C	11.93251	25.26058	24.28475
C	16.62139	3.293312	4.269157
C	4.26915	11.93251	3.293318
C	24.28474	16.62139	25.26059
C	4.269161	16.62139	25.26059
C	24.28475	11.93251	3.293322

C	24.28474	16.62139	3.293313
C	4.269161	11.93251	25.26059
C	24.28475	11.93251	25.26058
C	4.269162	16.62139	3.293311
C	3.293314	4.269156	11.93251
C	25.26059	24.28474	16.62139
C	25.26058	4.269159	16.62139
C	3.293312	24.28474	11.93251
C	3.293309	24.28473	16.62139
C	25.26058	4.269151	11.93251
C	25.26059	24.28474	11.93251
C	3.293318	4.269155	16.62139
C	3.293316	11.93251	24.28474
C	25.26059	16.62139	4.26916
C	25.26058	16.62139	24.28475
C	3.293308	11.93251	4.269165
C	3.293314	16.62139	4.269154
C	25.26059	11.93251	24.28474
C	25.26059	11.93251	4.269169
C	3.293317	16.62139	24.28475
C	11.93251	4.269176	25.26059
C	16.62139	24.28475	3.293314
C	16.62139	4.269157	3.293313
C	11.93251	24.28473	25.26059
C	16.62139	24.28474	25.26059
C	11.93251	4.269165	3.293312
C	11.93251	24.28475	3.293319
C	16.62139	4.269156	25.26058
C	4.269162	3.293311	16.62139
C	24.28474	25.26059	11.93251
C	4.269153	25.26058	11.93251
C	24.28474	3.293314	16.62139
C	24.28473	3.293307	11.93251
C	4.269152	25.26058	16.62139
C	24.28474	25.26059	16.62139
C	4.269157	3.293312	11.93251
C	9.240055	5.045362	10.21837
C	11.21488	5.143314	5.143305
C	17.33902	23.41059	23.4106
C	17.33903	23.4106	5.143307
C	11.21489	5.143325	23.4106
C	17.33902	5.143302	23.41059
C	11.21487	23.4106	5.143316

C	11.21488	23.41058	23.4106
C	17.33901	5.143296	5.143298
C	5.143297	11.21487	5.143312
C	23.41059	17.33903	23.4106
C	5.143311	17.33903	23.4106
C	23.4106	11.21487	5.143318
C	23.4106	17.33903	5.143306
C	5.143308	11.21488	23.4106
C	23.4106	11.21487	23.41059
C	5.143305	17.33904	5.143302
C	5.1433	5.143299	11.21488
C	23.4106	23.41059	17.33903
C	23.41059	5.143308	17.33903
C	5.1433	23.41059	11.21487
C	5.143298	23.41058	17.33903
C	23.41058	5.1433	11.21487
C	23.41059	23.4106	11.21486
C	5.143308	5.143301	17.33903
C	11.16956	28.55389	7.399965
C	17.38435	1.57E-05	21.15393
C	17.38435	28.55389	7.399965
C	11.16955	28.55389	21.15393
C	7.399966	11.16955	28.5539
C	21.15393	17.38435	28.55389
C	7.399973	17.38435	0
C	21.15393	11.16955	6.89E-06
C	28.55389	7.399967	11.16955
C	5.15E-06	21.15393	17.38435
C	28.55389	7.399967	17.38435
C	4.75E-06	21.15392	11.16954
C	28.55389	11.16955	21.15393
C	4.49E-06	17.38435	7.39998
C	0	17.38435	21.15393
C	28.55389	11.16956	7.399963
C	11.16957	7.399958	28.55389
C	17.38435	21.15393	0
C	17.38434	7.39996	0
C	11.16956	21.15393	28.55388
C	7.399968	1.04E-05	17.38435
C	21.15394	1.87E-05	11.16956
C	7.399965	0	11.16955
C	21.15394	1.93E-05	17.38434
C	9.451378	0.691621	6.275727

C	19.10253	27.86228	22.27817
C	19.10252	27.86227	6.275727
C	9.451372	0.691623	22.27818
C	19.10252	0.691637	22.27817
C	9.451381	27.86226	6.275726
C	9.451377	27.86227	22.27817
C	19.10253	0.691624	6.275725
C	6.275725	9.451375	0.691625
C	22.27817	19.10253	27.86226
C	6.275729	19.10253	27.86228
C	22.27817	9.451379	0.691634
C	22.27817	19.10253	0.691622
C	6.275725	9.451377	27.86227
C	22.27817	9.451375	27.86227
C	6.275728	19.10253	0.691632
C	0.69163	6.275726	9.451378
C	27.86228	22.27817	19.10253
C	27.86226	6.275728	19.10252
C	0.691635	22.27817	9.451366
C	0.691634	22.27817	19.10252
C	27.86227	6.27573	9.451382
C	27.86227	22.27817	9.451366
C	0.691621	6.275726	19.10252
C	0.691622	9.451372	22.27818
C	27.86227	19.10254	6.275726
C	27.86227	19.10253	22.27817
C	0.69162	9.45138	6.275727
C	0.691628	19.10254	6.275729
C	27.86226	9.451377	22.27817
C	27.86226	9.451386	6.275728
C	0.691631	19.10253	22.27817
C	9.451395	6.275728	27.86227
C	19.10253	22.27817	0.691626
C	19.10252	6.275727	0.691632
C	9.451387	22.27817	27.86226
C	19.10252	22.27817	27.86227
C	9.451392	6.275728	0.691624
C	9.451378	22.27817	0.691613
C	19.10252	6.275726	27.86227
C	6.275728	0.691635	19.10252
C	22.27817	27.86228	9.451378
C	6.275724	27.86227	9.451374
C	22.27817	0.69164	19.10251

C	22.27817	0.691641	9.451384
C	6.275725	27.86228	19.10253
C	22.27817	27.86228	19.10252
C	6.275724	0.69163	9.451377
C	14.27694	3.089093	7.184875
C	14.27694	25.4648	21.36902
C	14.27694	25.4648	7.18487
C	14.27696	3.089093	21.36902
C	7.184873	14.27696	3.089095
C	21.36903	14.27696	25.4648
C	7.184876	14.27695	25.46481
C	21.36903	14.27694	3.089094
C	3.089095	7.184872	14.27696
C	25.46481	21.36902	14.27695
C	25.4648	7.184873	14.27696
C	3.089095	21.36903	14.27696
C	3.089095	14.27695	21.36903
C	25.4648	14.27693	7.184873
C	25.46481	14.27694	21.36903
C	3.089094	14.27694	7.184873
C	14.27693	7.184873	25.4648
C	14.27695	21.36902	3.089094
C	14.27693	7.184872	3.089097
C	14.27693	21.36903	25.4648
C	7.184872	3.089095	14.27696
C	21.36902	25.4648	14.27694
C	7.184873	25.4648	14.27695
C	21.36903	3.089096	14.27694
H	14.27695	3.470909	6.169969
H	14.27695	25.08299	22.38393
H	14.27695	25.08299	6.169968
H	14.27695	3.47091	22.38393
H	6.169967	14.27695	3.470913
H	22.38393	14.27695	25.08299
H	6.169969	14.27695	25.08299
H	22.38393	14.27695	3.470911
H	3.470912	6.16997	14.27695
H	25.08299	22.38393	14.27695
H	25.08299	6.169966	14.27695
H	3.470912	22.38393	14.27695
H	3.470912	14.27695	22.38393
H	25.08299	14.27695	6.169967
H	25.08299	14.27695	22.38393

H	3.470912	14.27695	6.169966
H	14.27695	6.169973	25.08299
H	14.27695	22.38393	3.470911
H	14.27695	6.169972	3.47091
H	14.27695	22.38393	25.08299
H	6.169972	3.47091	14.27695
H	22.38393	25.08299	14.27695
H	6.16997	25.08299	14.27695
H	22.38393	3.470908	14.27695
H	12.08271	0	7.985323
H	16.47119	0	20.56858
H	16.47119	0	7.98532
H	12.08271	0	20.56858
H	7.985321	12.08271	0
H	20.56858	16.47119	0
H	7.985321	16.47119	3.54E-06
H	20.56858	12.08271	0
H	0	7.985319	12.08271
H	0	20.56857	16.47119
H	0	7.985322	16.47119
H	0	20.56858	12.08271
H	0	12.08271	20.56858
H	0	16.4712	7.985321
H	0	16.47119	20.56858
H	0	12.08271	7.98532
H	12.08272	7.985322	0
H	16.47119	20.56858	0
H	16.47118	7.985321	0
H	12.08271	20.56858	28.55389
H	7.985325	0	16.47119
H	20.56858	0	12.08271
H	7.985325	0	12.08271
H	20.56858	0	16.47119
H	10.8534	5.867096	5.867097
H	17.70051	22.6868	22.6868
H	17.70051	22.6868	5.867097
H	10.8534	5.867098	22.68681
H	17.7005	5.867099	22.6868
H	10.85339	22.68681	5.867093
H	10.8534	22.6868	22.6868
H	17.7005	5.867098	5.867102
H	5.867095	10.85339	5.867097
H	22.68681	17.70051	22.68681

H	5.867097	17.70051	22.68681
H	22.68681	10.85339	5.867095
H	22.68681	17.70051	5.867095
H	5.867098	10.85339	22.6868
H	22.68681	10.85339	22.6868
H	5.867093	17.70051	5.867095
H	5.867096	5.867099	10.85339
H	22.6868	22.6868	17.70051
H	22.68681	5.867094	17.70051
H	5.867096	22.6868	10.85339
H	5.867095	22.6868	17.70051
H	22.6868	5.867093	10.85339
H	22.68681	22.68681	10.85339
H	5.867096	5.867095	17.70051
H	8.693838	2.273516	8.69384
H	19.86006	26.28038	19.86006
H	19.86006	26.28038	8.693836
H	8.693837	2.273518	19.86006
H	19.86006	2.273514	19.86006
H	8.69384	26.28038	8.693836
H	8.693839	26.28038	19.86006
H	19.86006	2.273516	8.693843
H	8.693841	8.693837	2.273517
H	19.86006	19.86006	26.28038
H	8.693841	19.86006	26.28038
H	19.86006	8.693839	2.273517
H	19.86006	19.86006	2.273518
H	8.69384	8.693836	26.28039
H	19.86006	8.693839	26.28038
H	8.693837	19.86006	2.273518
H	2.273517	8.693839	8.69384
H	26.28038	19.86006	19.86006
H	26.28038	8.693836	19.86006
H	2.273519	19.86006	8.693838
H	2.273518	19.86006	19.86006
H	26.28038	8.693841	8.693836
H	26.28038	19.86006	8.693837
H	2.27352	8.69384	19.86006
N	10.54542	1.120603	6.994224
N	18.00848	27.43329	21.55968
N	18.00848	27.43328	6.994221
N	10.54542	1.120614	21.55968
N	18.00848	1.120625	21.55968

N	10.54542	27.43328	6.994217
N	10.54542	27.43328	21.55968
N	18.00848	1.120614	6.994222
N	6.994222	10.54542	1.120616
N	21.55967	18.00848	27.43327
N	6.994229	18.00848	27.43329
N	21.55968	10.54542	1.12062
N	21.55967	18.00849	1.120611
N	6.994221	10.54542	27.43328
N	21.55968	10.54542	27.43329
N	6.994226	18.00849	1.12062
N	1.120617	6.994222	10.54542
N	27.43329	21.55967	18.00849
N	27.43328	6.994219	18.00848
N	1.120622	21.55967	10.5454
N	1.120621	21.55967	18.00849
N	27.43328	6.994219	10.54542
N	27.43329	21.55967	10.5454
N	1.120608	6.994224	18.00848
N	1.120611	10.54542	21.55967
N	27.43328	18.0085	6.994234
N	27.43328	18.00849	21.55967
N	1.120603	10.54542	6.99422
N	1.12062	18.0085	6.994234
N	27.43327	10.54541	21.55968
N	27.43328	10.54543	6.994212
N	1.120623	18.00849	21.55967
N	10.54544	6.994209	27.43329
N	18.00848	21.55967	1.120615
N	18.00847	6.994217	1.120621
N	10.54543	21.55969	27.43327
N	18.00848	21.55967	27.43328
N	10.54544	6.994213	1.120604
N	10.54543	21.55968	1.120598
N	18.00847	6.994218	27.43328
N	6.994224	1.120622	18.00849
N	21.55968	27.4333	10.54542
N	6.994224	27.43328	10.54542
N	21.55969	1.120624	18.00847
N	21.55969	1.120624	10.54543
N	6.994224	27.43329	18.00848
N	21.55968	27.43329	18.00848
N	6.994222	1.12062	10.54542

N	13.15635	2.820617	7.881455
N	15.39755	25.73328	20.67245
N	15.39754	25.73328	7.881447
N	13.15636	2.820617	20.67245
N	15.39756	2.820618	20.67245
N	13.15635	25.73328	7.881452
N	13.15634	25.73328	20.67245
N	15.39755	2.820617	7.881455
N	7.88145	13.15636	2.820617
N	20.67245	15.39755	25.73328
N	7.881449	15.39755	25.73328
N	20.67245	13.15634	2.820615
N	20.67245	15.39754	2.820617
N	7.881452	13.15635	25.73328
N	20.67245	13.15635	25.73328
N	7.881449	15.39756	2.820617
N	2.820617	7.881451	13.15635
N	25.73328	20.67245	15.39755
N	25.73328	7.881451	15.39755
N	2.820613	20.67245	13.15636
N	2.820614	20.67245	15.39755
N	25.73328	7.881451	13.15636
N	25.73328	20.67245	13.15635
N	2.820616	7.881451	15.39755
N	2.820617	13.15635	20.67245
N	25.73328	15.39753	7.88145
N	25.73328	15.39754	20.67245
N	2.820613	13.15635	7.881448
N	2.820614	15.39754	7.881445
N	25.73328	13.15635	20.67245
N	25.73328	13.15634	7.881451
N	2.820616	15.39756	20.67245
N	13.15635	7.881456	25.73328
N	15.39755	20.67245	2.820618
N	15.39755	7.881452	2.820621
N	13.15635	20.67245	25.73328
N	15.39754	20.67245	25.73328
N	13.15635	7.881452	2.820619
N	13.15635	20.67245	2.820617
N	15.39754	7.881455	25.73328
N	7.881456	2.820616	15.39755
N	20.67245	25.73328	13.15635
N	7.881453	25.73328	13.15635

N	20.67245	2.820618	15.39754
N	20.67245	2.820617	13.15636
N	7.881453	25.73328	15.39755
N	20.67245	25.73328	15.39755
N	7.881452	2.820617	13.15636
N	10.08131	3.894583	8.497079
N	18.47259	24.65931	20.05682
N	18.47259	24.65932	8.497078
N	10.08131	3.894587	20.05682
N	18.4726	3.894578	20.05681
N	10.08132	24.65932	8.497078
N	10.08131	24.65932	20.05682
N	18.4726	3.894582	8.49709
N	8.497084	10.0813	3.894586
N	20.05682	18.47259	24.65932
N	8.497089	18.4726	24.65933
N	20.05682	10.08131	3.894582
N	20.05683	18.47259	3.894586
N	8.497091	10.0813	24.65932
N	20.05682	10.08131	24.65931
N	8.497079	18.47259	3.894586
N	3.894586	8.497082	10.08131
N	24.65932	20.05682	18.47258
N	24.65932	8.497082	18.47259
N	3.894589	20.05682	10.08131
N	3.894583	20.05682	18.47258
N	24.65932	8.497092	10.0813
N	24.65931	20.05682	10.08131
N	3.894587	8.497075	18.47258
N	3.894587	10.08131	20.05682
N	24.65931	18.47259	8.497076
N	24.65931	18.47259	20.05682
N	3.894584	10.08131	8.497079
N	3.894586	18.47259	8.497079
N	24.65932	10.0813	20.05681
N	24.65932	10.08132	8.497082
N	3.894586	18.4726	20.05682
N	10.08132	8.497084	24.65932
N	18.47259	20.05682	3.894585
N	18.47259	8.497081	3.894585
N	10.08132	20.05681	24.65932
N	18.47259	20.05682	24.65931
N	10.08132	8.497078	3.894581

N	10.08131	20.05682	3.894583
N	18.47258	8.497076	24.65932
N	8.497078	3.894585	18.47258
N	20.05682	24.65931	10.08131
N	8.497087	24.65932	10.0813
N	20.05681	3.894579	18.47259
N	20.05682	3.894577	10.08132
N	8.497078	24.65931	18.47259
N	20.05682	24.65931	18.47258
N	8.49708	3.894583	10.08131
N	11.47488	3.85657	5.43889
N	17.07903	24.69733	23.11501
N	17.07903	24.69734	5.438896
N	11.47488	3.856579	23.11502
N	17.07903	3.856564	23.115
N	11.47487	24.69734	5.438892
N	11.47488	24.69732	23.11501
N	17.07902	3.856563	5.438896
N	5.438888	11.47486	3.856569
N	23.115	17.07904	24.69734
N	5.438899	17.07903	24.69734
N	23.11501	11.47487	3.856574
N	23.11501	17.07903	3.856561
N	5.438899	11.47487	24.69734
N	23.11501	11.47487	24.69733
N	5.43889	17.07904	3.856558
N	3.856561	5.438894	11.47487
N	24.69734	23.115	17.07904
N	24.69733	5.438888	17.07903
N	3.856559	23.115	11.47487
N	3.85656	23.115	17.07903
N	24.69732	5.438885	11.47487
N	24.69734	23.11501	11.47486
N	3.856567	5.438888	17.07903
N	3.856563	11.47487	23.11501
N	24.69734	17.07903	5.438894
N	24.69734	17.07904	23.11501
N	3.856557	11.47486	5.438897
N	3.856562	17.07904	5.43889
N	24.69734	11.47486	23.115
N	24.69733	11.47487	5.438896
N	3.856565	17.07903	23.11501
N	11.47488	5.438902	24.69734

N	17.07903	23.11501	3.856564
N	17.07902	5.438895	3.856564
N	11.47488	23.115	24.69733
N	17.07903	23.115	24.69734
N	11.47488	5.438895	3.856567
N	11.47487	23.11501	3.856572
N	17.07902	5.438893	24.69733
N	5.438893	3.856562	17.07903
N	23.11501	24.69734	11.47486
N	5.438895	24.69733	11.47487
N	23.11501	3.856567	17.07903
N	23.115	3.856561	11.47487
N	5.438888	24.69733	17.07903
N	23.11501	24.69734	17.07903
N	5.438894	3.856562	11.47487
Cl	12.39514	1.666547	4.129756
Cl	16.15875	26.88735	24.42414
Cl	16.15875	26.88735	4.129757
Cl	12.39514	1.666551	24.42415
Cl	16.15876	1.666545	24.42415
Cl	12.39515	26.88736	4.129756
Cl	12.39514	26.88735	24.42414
Cl	16.15875	1.666545	4.129756
Cl	4.129758	12.39515	1.666552
Cl	24.42414	16.15875	26.88735
Cl	4.129759	16.15875	26.88736
Cl	24.42414	12.39514	1.666549
Cl	24.42414	16.15875	1.666549
Cl	4.129758	12.39514	26.88735
Cl	24.42414	12.39515	26.88735
Cl	4.12976	16.15875	1.666548
Cl	1.666546	4.129756	12.39515
Cl	26.88735	24.42414	16.15875
Cl	26.88735	4.129756	16.15875
Cl	1.666546	24.42414	12.39515
Cl	1.666543	24.42414	16.15875
Cl	26.88735	4.129756	12.39514
Cl	26.88735	24.42414	12.39515
Cl	1.666549	4.129757	16.15875
Cl	1.66655	12.39515	24.42414
Cl	26.88735	16.15875	4.129758
Cl	26.88735	16.15875	24.42414
Cl	1.666544	12.39515	4.129757

Cl	1.666549	16.15875	4.12976
Cl	26.88736	12.39515	24.42414
Cl	26.88736	12.39515	4.129757
Cl	1.66655	16.15875	24.42414
Cl	12.39514	4.129754	26.88736
Cl	16.15875	24.42414	1.666549
Cl	16.15875	4.129754	1.666547
Cl	12.39515	24.42414	26.88736
Cl	16.15875	24.42414	26.88735
Cl	12.39514	4.129755	1.666545
Cl	12.39514	24.42414	1.666549
Cl	16.15876	4.129756	26.88735
Cl	4.129758	1.666545	16.15875
Cl	24.42414	26.88735	12.39515
Cl	4.129759	26.88735	12.39515
Cl	24.42414	1.666545	16.15875
Cl	24.42415	1.666542	12.39515
Cl	4.129758	26.88735	16.15875
Cl	24.42414	26.88735	16.15875
Cl	4.129757	1.666546	12.39515
Cl	11.42786	6.199465	8.925641
Cl	17.12604	22.35444	19.62827
Cl	17.12604	22.35444	8.925646
Cl	11.42786	6.199463	19.62827
Cl	17.12605	6.199462	19.62826
Cl	11.42786	22.35443	8.925636
Cl	11.42786	22.35443	19.62826
Cl	17.12605	6.199462	8.92563
Cl	8.925635	11.42785	6.199455
Cl	19.62825	17.12603	22.35444
Cl	8.925633	17.12605	22.35444
Cl	19.62826	11.42786	6.199465
Cl	19.62826	17.12604	6.199462
Cl	8.925633	11.42785	22.35444
Cl	19.62826	11.42786	22.35444
Cl	8.925646	17.12604	6.199463
Cl	6.199463	8.925636	11.42786
Cl	22.35444	19.62825	17.12604
Cl	22.35443	8.925641	17.12604
Cl	6.199463	19.62825	11.42787
Cl	6.199465	19.62825	17.12604
Cl	22.35444	8.925636	11.42785
Cl	22.35444	19.62825	11.42787

Cl	6.199459	8.925637	17.12604
Cl	6.199465	11.42786	19.62826
Cl	22.35444	17.12603	8.925649
Cl	22.35444	17.12604	19.62826
Cl	6.199468	11.42786	8.925641
Cl	6.199461	17.12603	8.925651
Cl	22.35444	11.42786	19.62826
Cl	22.35443	11.42786	8.925638
Cl	6.19946	17.12604	19.62826
Cl	11.42786	8.925636	22.35443
Cl	17.12604	19.62825	6.199461
Cl	17.12604	8.925638	6.199456
Cl	11.42786	19.62826	22.35443
Cl	17.12604	19.62826	22.35445
Cl	11.42786	8.925636	6.199469
Cl	11.42786	19.62826	6.199459
Cl	17.12604	8.925636	22.35444
Cl	8.925641	6.199466	17.12604
Cl	19.62826	22.35444	11.42786
Cl	8.925641	22.35444	11.42786
Cl	19.62826	6.199465	17.12604
Cl	19.62827	6.199472	11.42786
Cl	8.925638	22.35444	17.12604
Cl	19.62826	22.35444	17.12604
Cl	8.925636	6.199463	11.42786
Cl	12.53127	1.888013	10.33965
Cl	16.02263	26.66589	18.21426
Cl	16.02263	26.66589	10.33964
Cl	12.53127	1.888013	18.21426
Cl	16.02263	1.888013	18.21425
Cl	12.53127	26.66589	10.33964
Cl	12.53127	26.66589	18.21425
Cl	16.02263	1.888013	10.33964
Cl	10.33963	12.53127	1.888007
Cl	18.21426	16.02263	26.66589
Cl	10.33964	16.02263	26.66589
Cl	18.21426	12.53127	1.888009
Cl	18.21426	16.02263	1.88801
Cl	10.33964	12.53127	26.66589
Cl	18.21426	12.53127	26.66589
Cl	10.33964	16.02263	1.888008
Cl	1.888008	10.33964	12.53127
Cl	26.6659	18.21427	16.02263

Cl	26.66589	10.33964	16.02263
Cl	1.888004	18.21427	12.53126
Cl	1.888002	18.21427	16.02263
Cl	26.66589	10.33964	12.53127
Cl	26.66589	18.21427	12.53127
Cl	1.888009	10.33964	16.02263
Cl	1.888009	12.53127	18.21426
Cl	26.66589	16.02263	10.33964
Cl	26.66589	16.02263	18.21427
Cl	1.888003	12.53126	10.33963
Cl	1.888005	16.02263	10.33963
Cl	26.66589	12.53127	18.21426
Cl	26.66589	12.53126	10.33965
Cl	1.888009	16.02263	18.21426
Cl	12.53128	10.33966	26.66587
Cl	16.02263	18.21426	1.88801
Cl	16.02263	10.33964	1.888019
Cl	12.53127	18.21425	26.66589
Cl	16.02262	18.21426	26.66588
Cl	12.53127	10.33965	1.888014
Cl	12.53127	18.21426	1.88801
Cl	16.02262	10.33965	26.66587
Cl	10.33965	1.888012	16.02263
Cl	18.21426	26.66589	12.53127
Cl	10.33964	26.66589	12.53127
Cl	18.21425	1.888017	16.02263
Cl	18.21425	1.888015	12.53127
Cl	10.33964	26.66589	16.02263
Cl	18.21426	26.66589	16.02263
Cl	10.33964	1.888013	12.53127
Cl	8.359989	1.766579	5.537195
Cl	20.19391	26.78732	23.0167
Cl	20.19392	26.78732	5.537193
Cl	8.359986	1.766575	23.01671
Cl	20.19392	1.766579	23.01671
Cl	8.359986	26.78732	5.537192
Cl	8.359985	26.78732	23.01671
Cl	20.19391	1.766578	5.537196
Cl	5.537196	8.359988	1.766578
Cl	23.01671	20.19392	26.78732
Cl	5.537193	20.19392	26.78733
Cl	23.01671	8.359984	1.766577
Cl	23.01671	20.19392	1.766575

Cl	5.537195	8.359988	26.78732
Cl	23.01671	8.359986	26.78732
Cl	5.537191	20.19392	1.766576
Cl	1.766579	5.537194	8.359992
Cl	26.78733	23.01671	20.19392
Cl	26.78732	5.537189	20.19392
Cl	1.766572	23.01671	8.359976
Cl	1.766576	23.01671	20.19392
Cl	26.78732	5.537195	8.359989
Cl	26.78733	23.01671	8.359978
Cl	1.766577	5.537194	20.19391
Cl	1.766577	8.359986	23.01671
Cl	26.78733	20.19392	5.537187
Cl	26.78732	20.19392	23.01671
Cl	1.766578	8.359991	5.537196
Cl	1.766571	20.19392	5.537188
Cl	26.78732	8.359983	23.01671
Cl	26.78732	8.359985	5.537191
Cl	1.766577	20.19392	23.01671
Cl	8.359995	5.537196	26.78732
Cl	20.19392	23.01671	1.766576
Cl	20.19391	5.537194	1.766581
Cl	8.359984	23.01671	26.78732
Cl	20.19391	23.0167	26.78732
Cl	8.360001	5.5372	1.766583
Cl	8.359995	23.0167	1.766576
Cl	20.19391	5.537196	26.78732
Cl	5.537192	1.766579	20.19392
Cl	23.0167	26.78732	8.359993
Cl	5.537195	26.78732	8.359986
Cl	23.01671	1.766579	20.19391
Cl	23.01671	1.76658	8.359985
Cl	5.537193	26.78732	20.19392
Cl	23.0167	26.78732	20.19391
Cl	5.537194	1.766581	8.359987

Table B.7. Cartesian atomic coordinates and lattice vectors for ZIF-65 (SOD)

Atom Type	x	y	z
Lattice vectors	17.41764	0	0
	0	17.41764	0
	0	0	17.41764
C	15.22032	8.883589	2.197323

C	2.197323	8.534052	2.197323
C	2.197323	8.883589	15.22032
C	15.22032	8.534052	15.22032
C	2.197323	15.22032	8.883589
C	2.197323	2.197323	8.534052
C	15.22032	2.197323	8.883589
C	15.22032	15.22032	8.534052
C	8.883589	2.197323	15.22032
C	8.534052	2.197323	2.197323
C	8.883589	15.22032	2.197323
C	8.534052	15.22032	15.22032
C	6.511498	0.174769	10.90614
C	10.90614	17.24287	10.90614
C	10.90614	0.174769	6.511498
C	6.511498	17.24287	6.511498
C	10.90614	6.511498	0.174769
C	10.90614	10.90614	17.24287
C	6.511498	10.90614	0.174769
C	6.511498	6.511498	17.24287
C	0.174769	10.90614	6.511498
C	17.24287	10.90614	10.90614
C	0.174769	6.511498	10.90614
C	17.24287	6.511498	6.511498
C	15.24373	6.969111	3.158376
C	2.173913	10.44853	3.158376
C	2.173913	6.969111	14.25927
C	15.24373	10.44853	14.25927
C	3.158376	15.24373	6.969111
C	3.158376	2.173913	10.44853
C	14.25927	2.173913	6.969111
C	14.25927	15.24373	10.44853
C	6.969111	3.158376	15.24373
C	10.44853	3.158376	2.173913
C	6.969111	14.25927	2.173913
C	10.44853	14.25927	15.24373
C	6.969111	15.24373	3.158376
C	10.44853	2.173913	3.158376
C	6.969111	2.173913	14.25927
C	10.44853	15.24373	14.25927
C	15.24373	3.158376	6.969111
C	2.173913	3.158376	10.44853
C	2.173913	14.25927	6.969111
C	15.24373	14.25927	10.44853

C	3.158376	6.969111	15.24373
C	3.158376	10.44853	2.173913
C	14.25927	6.969111	2.173913
C	14.25927	10.44853	15.24373
C	6.534907	15.67793	11.8672
C	10.88273	1.739709	11.8672
C	10.88273	15.67793	5.550445
C	6.534907	1.739709	5.550445
C	11.8672	6.534907	15.67793
C	11.8672	10.88273	1.739709
C	5.550445	10.88273	15.67793
C	5.550445	6.534907	1.739709
C	15.67793	11.8672	6.534907
C	1.739709	11.8672	10.88273
C	15.67793	5.550445	10.88273
C	1.739709	5.550445	6.534907
C	15.67793	6.534907	11.8672
C	1.739709	10.88273	11.8672
C	15.67793	10.88273	5.550445
C	1.739709	6.534907	5.550445
C	6.534907	11.8672	15.67793
C	10.88273	11.8672	1.739709
C	10.88273	5.550445	15.67793
C	6.534907	5.550445	1.739709
C	11.8672	15.67793	6.534907
C	11.8672	1.739709	10.88273
C	5.550445	15.67793	10.88273
C	5.550445	1.739709	6.534907
H	15.55425	6.177915	3.831167
H	1.863391	11.23973	3.831167
H	1.863391	6.177915	13.58647
H	15.55425	11.23973	13.58647
H	3.831167	15.55425	6.177915
H	3.831167	1.863391	11.23973
H	13.58647	1.863391	6.177915
H	13.58647	15.55425	11.23973
H	6.177915	3.831167	15.55425
H	11.23973	3.831167	1.863391
H	6.177915	13.58647	1.863391
H	11.23973	13.58647	15.55425
H	6.177915	15.55425	3.831167
H	11.23973	1.863391	3.831167
H	6.177915	1.863391	13.58647

H	11.23973	15.55425	13.58647
H	15.55425	3.831167	6.177915
H	1.863391	3.831167	11.23973
H	1.863391	13.58647	6.177915
H	15.55425	13.58647	11.23973
H	3.831167	6.177915	15.55425
H	3.831167	11.23973	1.863391
H	13.58647	6.177915	1.863391
H	13.58647	11.23973	15.55425
H	6.845429	14.88674	12.53999
H	10.57221	2.530905	12.53999
H	10.57221	14.88674	4.877654
H	6.845429	2.530905	4.877654
H	12.53999	6.845429	14.88674
H	12.53999	10.57221	2.530905
H	4.877654	10.57221	14.88674
H	4.877654	6.845429	2.530905
H	14.88674	12.53999	6.845429
H	2.530905	12.53999	10.57221
H	14.88674	4.877654	10.57221
H	2.530905	4.877654	6.845429
H	14.88674	6.845429	12.53999
H	2.530905	10.57221	12.53999
H	14.88674	10.57221	4.877654
H	2.530905	6.845429	4.877654
H	6.845429	12.53999	14.88674
H	10.57221	12.53999	2.530905
H	10.57221	4.877654	14.88674
H	6.845429	4.877654	2.530905
H	12.53999	14.88674	6.845429
H	12.53999	2.530905	10.57221
H	4.877654	14.88674	10.57221
H	4.877654	2.530905	6.845429
N	15.84671	8.189548	3.170655
N	1.570932	9.228092	3.170655
N	1.570932	8.189548	14.24699
N	15.84671	9.228092	14.24699
N	3.170655	15.84671	8.189548
N	3.170655	1.570932	9.228092
N	14.24699	1.570932	8.189548
N	14.24699	15.84671	9.228092
N	8.189548	3.170655	15.84671
N	9.228092	3.170655	1.570932

N	8.189548	14.24699	1.570932
N	9.228092	14.24699	15.84671
N	8.189548	15.84671	3.170655
N	9.228092	1.570932	3.170655
N	8.189548	1.570932	14.24699
N	9.228092	15.84671	14.24699
N	15.84671	3.170655	8.189548
N	1.570932	3.170655	9.228092
N	1.570932	14.24699	8.189548
N	15.84671	14.24699	9.228092
N	3.170655	8.189548	15.84671
N	3.170655	9.228092	1.570932
N	14.24699	8.189548	1.570932
N	14.24699	9.228092	15.84671
N	7.137889	16.89837	11.87948
N	10.27975	0.519272	11.87948
N	10.27975	16.89837	5.538165
N	7.137889	0.519272	5.538165
N	11.87948	7.137889	16.89837
N	11.87948	10.27975	0.519272
N	5.538165	10.27975	16.89837
N	5.538165	7.137889	0.519272
N	16.89837	11.87948	7.137889
N	0.519272	11.87948	10.27975
N	16.89837	5.538165	10.27975
N	0.519272	5.538165	7.137889
N	16.89837	7.137889	11.87948
N	0.519272	10.27975	11.87948
N	16.89837	10.27975	5.538165
N	0.519272	7.137889	5.538165
N	7.137889	11.87948	16.89837
N	10.27975	11.87948	0.519272
N	10.27975	5.538165	16.89837
N	7.137889	5.538165	0.519272
N	11.87948	16.89837	7.137889
N	11.87948	0.519272	10.27975
N	5.538165	16.89837	10.27975
N	5.538165	0.519272	7.137889
N	15.56555	10.2259	1.852087
N	1.852087	7.191744	1.852087
N	1.852087	10.2259	15.56555
N	15.56555	7.191744	15.56555
N	1.852087	15.56555	10.2259

N	1.852087	1.852087	7.191744
N	15.56555	1.852087	10.2259
N	15.56555	15.56555	7.191744
N	10.2259	1.852087	15.56555
N	7.191744	1.852087	1.852087
N	10.2259	15.56555	1.852087
N	7.191744	15.56555	15.56555
N	6.856733	1.517076	10.56091
N	10.56091	15.90056	10.56091
N	10.56091	1.517076	6.856733
N	6.856733	15.90056	6.856733
N	10.56091	6.856733	1.517076
N	10.56091	10.56091	15.90056
N	6.856733	10.56091	1.517076
N	6.856733	6.856733	15.90056
N	1.517076	10.56091	6.856733
N	15.90056	10.56091	10.56091
N	1.517076	6.856733	10.56091
N	15.90056	6.856733	6.856733
Zn	0	8.70882	4.35441
Zn	0	8.70882	13.06323
Zn	4.35441	0	8.70882
Zn	13.06323	0	8.70882
Zn	8.70882	4.35441	0
Zn	8.70882	13.06323	0
Zn	8.70882	0	4.35441
Zn	8.70882	0	13.06323
Zn	0	4.35441	8.70882
Zn	0	13.06323	8.70882
Zn	4.35441	8.70882	0
Zn	13.06323	8.70882	0
O	14.92291	10.77302	0.932941
O	2.494729	6.644621	0.932941
O	2.494729	10.77302	16.4847
O	14.92291	6.644621	16.4847
O	0.932941	14.92291	10.77302
O	0.932941	2.494729	6.644621
O	16.4847	2.494729	10.77302
O	16.4847	14.92291	6.644621
O	10.77302	0.932941	14.92291
O	6.644621	0.932941	2.494729
O	10.77302	16.4847	2.494729
O	6.644621	16.4847	14.92291

O	10.77302	14.92291	0.932941
O	6.644621	2.494729	0.932941
O	10.77302	2.494729	16.4847
O	6.644621	14.92291	16.4847
O	14.92291	0.932941	10.77302
O	2.494729	0.932941	6.644621
O	2.494729	16.4847	10.77302
O	14.92291	16.4847	6.644621
O	0.932941	10.77302	14.92291
O	0.932941	6.644621	2.494729
O	16.4847	10.77302	2.494729
O	16.4847	6.644621	14.92291
O	6.214092	2.064199	9.641761
O	11.20355	15.35344	9.641761
O	11.20355	2.064199	7.775879
O	6.214092	15.35344	7.775879
O	9.641761	6.214092	2.064199
O	9.641761	11.20355	15.35344
O	7.775879	11.20355	2.064199
O	7.775879	6.214092	15.35344
O	2.064199	9.641761	6.214092
O	15.35344	9.641761	11.20355
O	2.064199	7.775879	11.20355
O	15.35344	7.775879	6.214092
O	2.064199	6.214092	9.641761
O	15.35344	11.20355	9.641761
O	2.064199	11.20355	7.775879
O	15.35344	6.214092	7.775879
O	6.214092	9.641761	2.064199
O	11.20355	9.641761	15.35344
O	11.20355	7.775879	2.064199
O	6.214092	7.775879	15.35344
O	9.641761	2.064199	6.214092
O	9.641761	15.35344	11.20355
O	7.775879	2.064199	11.20355
O	7.775879	15.35344	6.214092

Table B.8. Cartesian atomic coordinates and lattice vectors for ZIF-71 (CRB)

Atom Type	x	y	z
	9.71188	0	0
Lattice vectors	-2.9E-05	24.50292	0
	2.95E-06	8.84E-06	22.12049

C	0.088328	2.111102	9.092096
C	9.623525	22.39183	13.02839
C	4.767586	22.39181	20.15234
C	4.944267	2.111099	1.968126
C	9.623543	14.36256	1.968148
C	0.08832	10.14037	20.15236
C	4.944249	10.14037	13.02839
C	4.767604	14.36256	9.092119
C	7.791628	0.083435	5.218909
C	1.920245	24.4195	16.90154
C	6.776253	24.41949	16.27937
C	2.935737	0.08341	5.841446
C	1.920384	12.33489	5.841026
C	7.791654	12.16806	16.27904
C	2.935675	12.16806	16.9016
C	6.776061	12.33485	5.218622
C	1.193341	6.350671	9.35867
C	8.518513	18.15226	12.76182
C	3.662554	18.15226	20.41891
C	6.049279	6.350668	1.701574
C	8.518491	18.60213	1.701597
C	1.193343	5.900802	20.41891
C	6.049291	5.900798	12.76182
C	3.662572	18.60213	9.35867
C	9.314451	24.34311	3.719671
C	0.397393	0.159791	18.40084
C	5.253322	0.159814	14.77989
C	4.458511	24.34312	7.340529
C	0.397387	12.09163	7.340596
C	9.314457	12.4113	14.77994
C	4.458527	12.41128	18.40082
C	5.253336	12.09165	3.719715
C	2.572273	5.786418	10.92624
C	7.13959	18.71651	11.19427
C	2.283622	18.71652	21.98648
C	7.428212	5.786413	0.134006
C	7.13957	18.03787	0.134028
C	2.572274	6.465055	21.98648
C	7.428213	6.465051	11.19425
C	2.283651	18.0379	10.92624
C	8.0757	24.31859	3.103107
C	1.636153	0.184319	19.01738
C	6.492073	0.184341	14.16335

C	3.219761	24.31859	7.957094
C	1.636128	12.0671	7.957138
C	8.075697	12.4358	14.1634
C	3.219767	12.4358	19.01736
C	6.492106	12.06713	3.103151
C	0.360776	1.858405	12.96241
C	9.351087	22.64455	9.158082
C	4.495117	22.64447	1.902163
C	5.216717	1.858407	20.21833
C	9.351079	14.10987	20.21835
C	0.360774	10.39304	1.902163
C	5.216715	10.39306	9.158103
C	4.495138	14.10989	12.96241
C	7.130332	5.045842	12.79887
C	2.581522	19.45709	9.321619
C	7.437451	19.45706	1.738626
C	2.274383	5.045821	20.38188
C	2.581506	17.29731	20.38186
C	7.130328	7.205623	1.738626
C	2.274389	7.205627	9.321619
C	7.437475	17.2973	12.79887
C	7.94954	3.196508	8.863791
C	1.762313	21.30645	13.2567
C	6.618274	21.30642	19.92406
C	3.093609	3.196505	2.196454
C	1.762329	15.44796	2.196454
C	7.949535	9.054964	19.92403
C	3.093594	9.054961	13.2567
C	6.61826	15.44797	8.863791
C	0.827033	2.738942	14.88528
C	8.88483	21.76399	7.235214
C	4.02886	21.76399	3.825008
C	5.682964	2.738944	18.29548
C	8.88481	14.9904	18.29548
C	0.827033	9.512501	3.825008
C	5.682964	9.512527	7.235214
C	4.028889	14.9904	14.88525
C	8.25327	2.595573	7.659308
C	1.458583	21.90736	14.46118
C	6.314553	21.90738	18.71957
C	3.397339	2.595571	3.400937
C	1.45861	14.84701	3.400937
C	8.253263	9.655898	18.71955

C	3.397313	9.655896	14.46118
C	6.31454	14.84703	7.659308
C	0.916537	3.712419	13.91746
C	8.795336	20.79051	8.203029
C	3.939366	20.79051	2.857193
C	5.772458	3.712421	19.26327
C	8.795314	15.96388	19.2633
C	0.916529	8.539049	2.857215
C	5.77246	8.539051	8.203029
C	3.939393	15.96388	13.91744
H	0.99503	1.700752	9.528025
H	8.716823	22.8022	12.59246
H	3.860885	22.80218	20.58827
H	5.850969	1.700724	1.532198
H	8.716823	13.95218	1.53222
H	0.99503	10.55072	20.58829
H	5.85096	10.55074	12.59246
H	3.860894	13.95219	9.528047
H	7.300353	0.184656	6.177545
H	2.411491	24.3183	15.94297
H	7.267392	24.31832	17.23772
H	2.444383	0.184656	4.882633
H	2.411455	12.43607	4.88281
H	7.300301	12.06681	17.23786
H	2.444381	12.06684	15.94294
H	7.267531	12.43612	6.177677
H	2.997538	5.284844	11.78839
H	6.714325	19.21808	10.3321
H	1.858374	19.21806	0.72814
H	7.853469	5.284847	21.39235
H	6.714309	17.53631	21.39235
H	2.997534	6.966622	0.728118
H	7.853475	6.966625	10.3321
H	1.858388	17.53633	11.78841
H	0.050036	1.146766	12.20505
H	9.661818	23.35616	9.915443
H	4.805877	23.35616	1.144757
H	4.905987	1.14677	20.97571
H	9.661821	13.39823	20.97571
H	0.050032	11.10467	1.14478
H	4.905983	11.1047	9.915465
H	4.80588	13.39823	12.20502
N	1.37578	5.454722	10.3911

N	8.336074	19.04821	11.72939
N	3.480125	19.04819	21.45132
N	6.231718	5.454718	0.669145
N	8.336054	17.70618	0.669167
N	1.37578	6.796727	21.45132
N	6.231728	6.796747	11.72939
N	3.480126	17.70621	10.3911
N	8.014646	5.408044	11.80234
N	1.697217	19.09491	10.31817
N	6.553136	19.09488	0.742098
N	3.158708	5.408023	21.37839
N	1.697191	17.65948	21.37839
N	8.014653	6.843421	0.742098
N	3.158704	6.843424	10.31815
N	6.553158	17.6595	11.80232
N	9.125429	0.030116	5.074816
N	0.586405	24.47281	17.04569
N	5.442267	24.47284	16.13504
N	4.26943	0.030092	5.985384
N	0.586321	12.28153	5.98545
N	9.125347	12.22138	16.13508
N	4.269447	12.22138	17.04567
N	5.442523	12.28158	5.074838
N	2.253594	24.47305	6.988548
N	7.458337	0.029924	15.13179
N	2.602369	0.029876	18.04888
N	7.109504	24.47303	4.071608
N	7.458214	12.22159	4.071763
N	2.253581	12.28136	18.04884
N	7.10954	12.28136	15.13194
N	2.602411	12.22154	6.988747
N	8.961149	2.932611	9.762037
N	0.750704	21.57034	12.35845
N	5.606645	21.57032	20.82228
N	4.105208	2.932608	1.298185
N	0.75071	15.18407	1.298207
N	8.961143	9.318861	20.82228
N	4.105202	9.318857	12.35845
N	5.606651	15.18407	9.762037
N	9.410927	1.853502	7.82154
N	0.300926	22.64943	14.29895
N	5.156896	22.64943	18.88181
N	4.554996	1.8535	3.238683

N	0.300964	14.10494	3.238705
N	9.410918	10.39797	18.88181
N	4.554968	10.39797	14.29893
N	5.156876	14.10496	7.821562
N	0.616605	3.157255	12.69519
N	9.095258	21.34567	9.425297
N	4.239307	21.3457	1.634925
N	5.472537	3.157258	20.48554
N	9.095247	15.40869	20.48556
N	0.616597	9.09421	1.634925
N	5.472537	9.094213	9.425297
N	4.239326	15.40872	12.69519
N	0.475183	1.548615	14.27435
N	9.23668	22.95431	7.846137
N	4.38073	22.95431	3.214063
N	5.331124	1.548617	18.9064
N	9.236673	13.80008	18.9064
N	0.47518	10.70283	3.214085
N	5.331111	10.70285	7.846137
N	4.380742	13.80008	14.27433
Zn	9.611319	4.277577	11.17122
Zn	0.100544	20.22538	10.94927
Zn	4.956463	20.22535	0.110978
Zn	4.755381	4.277582	22.00951
Zn	0.10053	16.52902	22.00953
Zn	9.611314	7.973888	0.110978
Zn	4.755385	7.973892	10.94929
Zn	4.956478	16.52904	11.17122
Zn	0.276644	0.112226	6.913914
Zn	9.4352	24.39073	15.20658
Zn	4.57928	24.39073	17.97416
Zn	5.132583	0.112201	4.146309
Zn	9.435252	12.36366	4.146331
Zn	0.276621	12.13927	17.97418
Zn	5.132551	12.13927	15.20658
Zn	4.579283	12.36366	6.913914
Cl	9.559814	6.323031	8.316286
Cl	0.152039	18.17992	13.80422
Cl	5.00796	18.1799	19.37651
Cl	4.703884	6.323028	2.743958
Cl	0.152018	18.57446	2.74398
Cl	9.559806	5.92844	19.37653
Cl	4.703885	5.928463	13.80422

Cl	5.007968	18.57449	8.316264
Cl	1.103688	24.0862	2.960628
Cl	8.608166	0.41668	19.15986
Cl	3.752215	0.416702	14.02087
Cl	5.959628	24.08618	8.099572
Cl	8.60817	11.83472	8.099616
Cl	1.103693	12.66821	14.02089
Cl	5.959634	12.66821	19.15986
Cl	3.75221	11.83474	2.960651
Cl	7.734464	24.14452	1.442566
Cl	1.97739	0.358363	20.67792
Cl	6.833318	0.358385	12.50281
Cl	2.878535	24.14454	9.617657
Cl	1.977384	11.89306	9.617679
Cl	7.734469	12.60987	12.50283
Cl	2.87854	12.60987	20.67792
Cl	6.833313	11.89306	1.442566
Cl	7.355823	3.736554	13.854
Cl	2.356039	20.7664	8.266493
Cl	7.211959	20.76637	2.793751
Cl	2.499865	3.736507	19.32676
Cl	2.356018	15.98802	19.32674
Cl	7.355826	8.514913	2.793751
Cl	2.499868	8.51494	8.266493
Cl	7.211985	15.98801	13.854
Cl	6.510287	4.003266	9.256849
Cl	3.201576	20.49969	12.86364
Cl	8.057536	20.49967	20.31714
Cl	1.654346	4.003263	1.803395
Cl	3.20158	16.25472	1.803373
Cl	6.510274	8.248205	20.31709
Cl	1.654333	8.248202	12.86362
Cl	8.05752	16.25473	9.256872
Cl	1.033624	3.002643	16.54743
Cl	8.678239	21.50031	5.573058
Cl	3.82227	21.50028	5.487164
Cl	5.889545	3.002644	16.6333
Cl	8.678219	15.2541	16.63332
Cl	1.033615	9.248801	5.487187
Cl	5.889555	9.248826	5.573058
Cl	3.822308	15.2541	16.54743
Cl	7.474532	2.916977	6.179248
Cl	2.237321	21.58595	15.94124

Cl	7.093329	21.586	17.23954
Cl	2.618631	2.916977	4.880996
Cl	2.237376	15.16841	4.880974
Cl	7.474526	9.334492	17.23949
Cl	2.618566	9.334517	15.94122
Cl	7.093278	15.16844	6.17927
Cl	1.213427	5.365116	14.14393
Cl	8.498436	19.13784	7.97656
Cl	3.642476	19.13781	3.083685
Cl	6.069348	5.365118	19.0368
Cl	8.49842	17.61655	19.03683
Cl	1.213424	6.886351	3.083685
Cl	6.069354	6.886353	7.97656
Cl	3.642509	17.61658	14.14393

Table B.9. Cartesian atomic coordinates and lattice vectors for ZIF-71 (DFT)

Atom Type	x	y	z
	19.89611	0	0
Lattice vectors	-0.00013	19.89463	0
	0.000684	0.000842	15.41941
C	14.26876	5.626596	2.85771
C	5.6275	14.26846	12.5617
C	5.627488	14.26839	2.857664
C	14.26957	5.627464	12.56172
C	4.321417	4.321253	10.56749
C	15.57516	15.574	4.852056
C	15.57578	15.57475	10.56743
C	4.320826	4.320642	4.852026
C	12.79976	6.119171	4.374702
C	7.096903	13.77624	11.04498
C	7.09615	13.77584	4.375072
C	12.80049	6.119595	11.04465
C	3.829663	2.852276	12.0845
C	16.06764	17.04288	3.334987
C	16.06773	17.04393	12.08441
C	3.828101	2.85158	3.335079
C	17.04414	16.06575	3.334864
C	2.852538	3.828824	12.08439
C	2.851613	3.828705	3.334987
C	17.04487	16.06742	12.08427
C	6.119771	12.79973	11.04429
C	13.77683	7.095698	4.374826

C	13.77727	7.096441	11.04461
C	6.119416	12.79897	4.374471
C	12.56828	0.570889	3.882006
C	7.329095	19.32452	11.53566
C	7.326945	19.32408	3.879539
C	12.56864	0.571228	11.53737
C	9.378031	2.620855	11.59191
C	10.51951	17.27432	3.827653
C	10.51898	17.27568	11.59188
C	9.376871	2.619655	3.827807
C	17.27565	10.51766	3.827606
C	2.620928	9.376972	11.59157
C	2.619609	9.377424	3.827545
C	17.27677	10.51894	11.59177
C	0.571327	12.56867	11.53896
C	19.32549	7.327603	3.882129
C	19.32575	7.328001	11.53737
C	0.571067	12.56675	3.884843
C	13.81432	1.881652	5.07149
C	6.076691	18.01452	10.35199
C	6.088454	18.01272	5.07607
C	13.81545	1.881662	10.34831
C	8.067737	3.868294	12.78032
C	11.8303	16.02855	2.637968
C	11.82919	16.02827	12.78049
C	8.066273	3.865472	2.637999
C	16.02852	11.82802	2.638893
C	3.866526	8.066279	12.78153
C	3.86743	8.067377	2.639217
C	16.0307	11.82949	12.7813
C	1.882121	13.80975	10.34433
C	18.0153	6.080315	5.07095
C	18.01523	6.081538	10.34806
C	1.880454	13.82173	5.066294
C	13.9143	2.494208	0.691468
C	5.982005	17.40109	14.7293
C	5.981959	17.4004	0.692301
C	13.91512	2.495014	14.7285
C	7.453947	3.966871	8.3998
C	12.44262	15.9287	7.018453
C	12.44272	15.92866	8.400865
C	7.453586	3.966218	7.01742
C	15.92929	12.44169	7.019547

C	3.966792	7.453624	8.401019
C	3.96687	7.453509	7.018622
C	15.92987	12.44204	8.401975
C	2.494956	13.91451	14.72702
C	17.40167	5.980702	0.69099
C	17.40233	5.981667	14.72799
C	2.494413	13.91434	0.690019
C	12.00215	3.237294	6.17E-05
C	7.89385	16.65732	0.000324
C	6.71063	2.054402	7.709689
C	13.18593	17.84075	7.709658
C	17.84177	13.18489	7.70972
C	2.05471	6.710502	7.709766
C	3.238179	12.00273	15.4191
C	16.65911	7.893678	15.41936
C	9.360386	4.323359	2.49375
C	10.53478	15.57142	12.92532
C	10.53625	15.57055	2.493627
C	9.362122	4.325122	12.92524
C	5.621891	19.30943	10.20592
C	14.27224	0.587515	5.215831
C	14.27267	0.587369	10.20362
C	5.627041	19.30587	5.218345
C	0.585102	14.27496	5.213133
C	19.30941	5.623973	10.20359
C	19.30973	5.623462	5.215769
C	0.588586	14.26962	10.20134
C	4.324532	9.360354	12.92578
C	15.57153	10.53365	2.494043
C	15.57291	10.53535	12.9256
C	4.32399	9.361873	2.494305
H	14.7963	5.098888	2.070225
H	5.099807	14.79599	13.3492
H	5.100063	14.79613	2.070179
H	14.7972	5.099882	13.34923
H	4.849024	4.849074	9.77976
H	15.04746	15.0465	5.639695
H	15.0482	15.04694	9.779961
H	4.848602	4.848172	5.639433
H	11.80956	0.21629	3.191617
H	8.08999	19.67859	12.22388
H	8.083004	19.67921	3.186298
H	11.80978	0.216863	12.22768

H	9.732355	1.861678	10.90175
H	10.16476	18.033	4.518072
H	10.16477	18.03474	10.90165
H	9.731395	1.860952	4.518334
H	18.03466	10.16332	4.517887
H	1.862356	9.731616	10.90101
H	1.860402	9.731467	4.517717
H	18.03558	10.1644	10.90131
H	0.216615	11.81183	12.23134
H	19.67973	8.086605	3.191879
H	19.68023	8.08682	12.22768
H	0.217388	11.80483	3.197384
H	11.0011	3.653556	15.41935
H	8.896365	16.24274	15.41935
H	6.295166	1.052608	7.710353
H	13.60148	18.84257	7.709658
H	18.8436	13.60033	7.709088
H	1.052824	6.295042	7.709751
H	3.652992	11.00006	0.000108
H	16.24289	8.89467	4.63E-05
N	13.11806	5.188148	3.408707
N	6.778442	14.70689	12.01123
N	6.777763	14.70717	3.409401
N	13.11906	5.188678	12.01064
N	4.760537	3.171055	11.1185
N	15.13668	16.72462	4.301059
N	15.13675	16.72511	11.11854
N	4.75918	3.169907	4.300998
N	16.72544	15.1349	4.30089
N	3.170887	4.7598	11.11837
N	3.170405	4.759667	4.30089
N	16.7265	15.13636	11.11835
N	5.188495	13.11832	12.00995
N	14.70779	6.776973	3.408892
N	14.70827	6.778	12.01058
N	5.18883	13.11757	3.408214
N	12.74879	1.872274	4.199553
N	7.144673	18.02292	11.22097
N	7.151007	18.02301	4.200479
N	12.74985	1.872638	11.22016
N	8.076659	2.802471	11.90872
N	11.82088	17.09398	3.510074
N	11.82036	17.09406	11.90886

N	8.075511	2.800082	3.510121
N	17.09422	11.81903	3.51063
N	2.80123	8.075622	11.9093
N	2.801534	8.076079	3.510691
N	17.09622	11.82027	11.90934
N	1.872497	12.74641	11.21899
N	18.02412	7.146022	4.199183
N	18.02436	7.147142	11.21995
N	1.872664	12.75291	4.198351
N	12.69472	2.96838	1.127159
N	7.201401	16.92691	14.29301
N	7.201733	16.92637	1.127606
N	12.69565	2.969119	14.29254
N	6.97989	2.747553	8.836278
N	12.91687	17.14822	6.582654
N	12.91701	17.14816	8.836663
N	6.979272	2.746475	6.582238
N	17.14862	12.91566	6.583148
N	2.747222	6.979499	8.836787
N	2.747341	6.979336	6.582793
N	17.14964	12.9163	8.837141
N	2.969109	12.69477	14.29177
N	16.92741	7.200167	1.126881
N	16.92806	7.201204	14.29231
N	2.968664	12.69504	1.126372
N	10.19156	3.506764	3.224168
N	9.703864	16.38897	12.19558
N	9.704998	16.38708	3.223998
N	10.19306	3.507572	12.19563
N	6.442386	0.24546	10.9327
N	13.45539	19.65091	4.485583
N	13.4554	19.65098	10.93361
N	6.439613	0.243099	4.483918
N	19.65104	13.45309	4.487588
N	0.244428	6.440927	10.93372
N	0.2445	6.440913	4.485907
N	19.65322	13.45579	10.93461
N	3.508097	10.19155	12.19527
N	16.3889	9.702688	3.223844
N	16.38968	9.704212	12.1953
N	3.506207	10.19269	3.22389
Zn	12.18722	3.44715	3.050083
Zn	7.708272	16.44848	12.36979

Zn	7.70963	16.4474	3.050283
Zn	12.18848	3.447579	12.36953
Zn	6.501854	2.240822	10.75943
Zn	13.39568	17.65543	4.659669
Zn	13.39552	17.65548	10.75968
Zn	6.500032	2.238778	4.659237
Zn	17.65571	13.39368	4.660116
Zn	2.23994	6.50076	10.75974
Zn	2.240028	6.500905	4.659792
Zn	17.65755	13.39548	10.76
Zn	3.447926	12.18701	12.36897
Zn	16.44901	7.707267	3.049944
Zn	16.44937	7.708631	12.36931
Zn	3.446876	12.18837	3.04979
Cl	11.42536	5.994804	5.36597
Cl	8.471282	13.90109	10.05376
Cl	8.470417	13.90009	5.366525
Cl	11.42625	5.994801	10.05324
Cl	3.954763	1.478189	13.07608
Cl	15.94321	18.4172	2.343642
Cl	15.94275	18.41813	13.07584
Cl	3.952297	1.477145	2.343858
Cl	18.41822	15.94056	2.343272
Cl	1.478178	3.95322	13.07569
Cl	1.477404	3.953728	2.343565
Cl	18.41934	15.9432	13.07541
Cl	5.995207	11.42558	10.05275
Cl	13.90185	8.469875	5.366309
Cl	13.90192	8.470708	10.05321
Cl	5.994224	11.4247	5.365831
Cl	14.36794	3.278835	5.846439
Cl	5.512313	16.61652	9.586494
Cl	5.547742	16.61657	5.862306
Cl	14.37043	3.278879	9.574359
Cl	6.670464	4.42449	13.55326
Cl	13.22749	15.47538	1.862696
Cl	13.22642	15.47224	13.55368
Cl	6.66915	4.418759	1.862603
Cl	15.47286	13.22524	1.865486
Cl	4.419423	6.669161	13.55721
Cl	4.424157	6.670174	1.866489
Cl	15.477	13.22663	13.55634
Cl	3.278312	14.35462	9.561036

Cl	16.61815	5.52454	5.844388
Cl	16.61806	5.527271	9.573495
Cl	15.16176	2.017272	1.746541
Cl	4.734011	17.87804	13.6749
Cl	4.735014	17.87741	1.747944
Cl	15.16276	2.017982	13.67365
Cl	7.931312	5.21472	9.454257
Cl	11.96543	14.68125	5.963503
Cl	11.96572	14.6811	9.455783
Cl	7.930422	5.213355	5.96193
Cl	14.68146	11.96438	5.96506
Cl	5.214262	7.930695	9.45603
Cl	5.214525	7.930345	5.963719
Cl	14.68269	11.96537	9.457449
Cl	2.017832	15.16145	13.67142
Cl	17.87875	4.733127	1.745847
Cl	17.8794	4.734216	13.67296
Cl	2.017283	15.16241	1.744274
Cl	9.917452	5.710587	1.687901
Cl	9.977181	14.18421	13.73072
Cl	9.979233	14.18331	1.687793
Cl	9.919737	5.712319	13.73072
Cl	4.23368	19.86805	9.40288
Cl	15.65962	0.030549	6.021434
Cl	15.65987	0.029977	9.397991
Cl	4.240613	19.86122	6.026661
Cl	0.02557	15.66293	6.016022
Cl	19.86665	4.236737	9.397961
Cl	19.8674	4.236393	6.021372
Cl	0.032285	15.65578	9.393165
Cl	5.711722	9.917368	13.73176
Cl	14.18438	9.976135	1.688441
Cl	14.18561	9.978225	13.73123
Cl	5.711207	9.919635	1.68898
Cl	3.278445	14.39052	5.82846

Table B.10. Cartesian atomic coordinates and lattice vectors for ZIF-71 (CAG)

Atom Type	x	y	z
Lattice vectors	15.48359	0	0
	6.2E-05	16.63587	0
	1.26E-05	0.320113	18.87816
C	12.72853	12.33577	16.25566

C	13.4772	10.70633	17.46788
C	14.5402	11.29164	16.80534
C	10.64814	8.974921	14.78785
C	9.585983	13.72791	16.62307
C	8.749321	12.40823	15.12607
C	1.151702	14.17151	17.99149
C	0.722278	14.3503	12.49572
C	13.81986	16.42291	16.32851
C	12.89054	15.9967	14.42063
C	9.800296	9.137413	1.021969
C	1.485518	15.82683	16.64159
C	10.41781	4.405008	6.751546
C	9.647342	6.106877	7.85052
C	8.602119	5.499287	7.181515
C	12.69799	7.800349	5.106862
C	13.97879	3.317808	7.268808
C	14.48955	4.6232	5.625974
C	6.471754	2.78391	8.545953
C	6.495718	2.454888	3.229675
C	9.499296	0.437718	6.748507
C	10.04395	0.705392	4.67274
C	6.296874	0.877988	7.542295
C	13.30498	7.810761	10.17006
C	4.986942	12.93825	2.62244
C	5.735657	14.56769	1.410349
C	6.798635	13.98235	2.072935
C	2.906442	16.29901	4.090368
C	1.844171	11.54602	2.255109
C	1.007583	12.86572	3.752147
C	8.893584	11.10221	0.886783
C	8.464149	10.92382	6.382327
C	6.07787	8.851127	2.549514
C	5.148795	9.277119	4.457586
C	2.058661	16.13619	17.85611
C	9.227095	9.44669	2.236514
C	2.675944	4.232941	12.12671
C	1.905442	2.531089	11.02775
C	0.860225	3.13868	11.69679
C	4.956262	0.837748	13.77131
C	6.236817	5.320257	11.60941
C	6.747679	4.014782	13.25222
C	14.21362	5.853957	10.33232
C	14.23761	6.183077	15.64856

C	1.757472	8.200258	12.12935
C	2.3022	7.932687	14.20532
C	14.03876	7.759911	11.3359
C	5.562952	0.827136	8.70806
C	2.754921	4.62033	2.62244
C	2.006279	6.249755	1.410293
C	0.943236	5.664411	2.072859
C	4.835526	7.981081	4.090425
C	5.89762	3.227818	2.25509
C	6.73425	4.547523	3.752109
C	14.33185	2.78431	0.886745
C	14.76134	2.605799	6.382252
C	1.66404	0.533191	2.549476
C	2.593105	0.959216	4.457529
C	5.683385	7.818405	17.85626
C	13.99844	1.12872	2.236439
C	5.065882	12.55098	12.12667
C	5.836369	10.84909	11.02775
C	6.881592	11.45671	11.69674
C	2.78568	9.155599	13.77128
C	1.504908	13.63832	11.60918
C	0.994147	12.33285	13.25205
C	9.011849	14.17174	10.33226
C	8.988071	14.50086	15.64841
C	5.984182	16.51811	12.12963
C	5.439903	16.25067	14.20544
C	9.186558	16.07782	11.33563
C	2.178813	9.14547	8.708041
C	10.49686	4.017799	16.25566
C	9.74824	2.388358	17.46781
C	8.685216	2.973703	16.80532
C	12.57721	0.656917	14.78773
C	13.63948	5.41013	16.62309
C	14.47613	4.090408	15.12605
C	6.590081	5.85359	17.99151
C	7.019392	6.032249	12.49594
C	9.405794	8.10489	16.32866
C	10.33488	7.678832	14.42067
C	13.42524	0.819444	1.021931
C	6.256601	7.509112	16.64176
C	12.80763	12.72308	6.751546
C	13.57816	14.4249	7.85052
C	14.62336	13.8173	7.181459

C	10.52754	16.11828	5.106787
C	9.246739	11.63581	7.268845
C	8.73597	12.9412	5.625993
C	1.270011	11.10221	8.545896
C	1.246038	10.77311	3.229637
C	13.72613	8.755786	6.748526
C	13.18148	9.023343	4.67274
C	1.44489	9.196322	7.542295
C	9.920511	16.12856	10.16993
H	12.05823	13.04453	15.78323
H	8.478246	11.50737	14.58691
H	0.834486	13.2125	18.38468
H	14.39767	16.30653	17.23655
H	11.09904	3.665835	6.343892
H	14.54289	5.493547	4.980926
H	6.755014	3.804989	8.771773
H	9.053727	0.614406	7.717711
H	4.316594	12.22945	3.09481
H	0.736593	13.76658	4.291345
H	8.576483	12.06133	0.493739
H	6.655578	8.967617	1.641418
H	3.357194	4.972114	12.53434
H	6.801079	3.1445	13.89721
H	14.49688	4.832828	10.10653
H	1.312023	8.023608	11.16039
H	3.42525	3.911552	3.094885
H	7.005248	5.448331	4.29125
H	14.64888	3.743374	0.493683
H	1.086348	0.649631	1.641361
H	4.384654	13.2902	12.53427
H	0.940819	11.46262	13.89702
H	8.728651	13.15056	10.10653
H	6.429721	16.34131	11.16026
H	11.16718	4.726611	15.7832
H	14.74712	3.189633	14.58689
H	6.90715	4.89451	18.38464
H	8.82804	7.988417	17.23681
H	12.12641	11.98387	6.343892
H	8.682617	13.81155	4.980926
H	0.986742	12.12339	8.771698
H	14.17173	8.932491	7.717731
N	12.32126	11.36389	17.09591
N	14.05888	12.33936	16.05234

N	9.59943	10.20137	0.164127
N	10.06986	9.230472	16.01466
N	9.433372	12.40025	16.28843
N	0.900187	14.58269	16.73052
N	0.409259	13.51498	13.54982
N	13.70489	15.45795	15.39502
N	10.80738	5.422208	7.549149
N	9.091783	4.402312	6.507187
N	13.42183	6.595783	9.521934
N	13.03793	7.645994	6.436772
N	13.81566	4.597647	6.794419
N	6.865963	2.130223	7.428725
N	7.026778	3.299575	4.183286
N	9.379162	1.30148	5.72397
N	4.579665	13.91016	1.78223
N	6.317277	12.93461	2.825834
N	1.857603	15.07237	18.71405
N	2.32819	16.0435	2.863533
N	1.69174	12.87368	2.589838
N	8.641944	10.69089	2.147674
N	8.151089	11.75906	5.328209
N	5.962986	9.816017	3.483114
N	3.065475	3.215741	11.3291
N	1.349929	4.235654	12.3711
N	5.679812	2.042098	9.356241
N	5.295987	0.992052	12.44133
N	6.073724	4.040368	12.08378
N	14.60776	6.507626	11.44956
N	14.76868	5.338391	14.69495
N	1.637456	7.336615	13.15405
N	3.162251	5.592225	1.782249
N	1.424602	4.616692	2.825777
N	5.88425	6.754481	18.71409
N	5.41379	7.725528	2.863533
N	6.050092	4.555479	2.5898
N	14.58354	2.372975	2.147636
N	15.07439	3.441062	5.328133
N	1.778902	1.498064	3.483058
N	4.676342	11.53374	11.3291
N	6.391897	12.55369	12.37101
N	2.061932	10.36043	9.356222
N	2.445753	9.310021	12.44137
N	1.66807	12.35847	12.08361

N	8.617578	14.82556	11.44941
N	8.456965	13.65619	14.69481
N	6.104503	15.65447	13.15419
N	10.90419	3.045905	17.09583
N	9.166527	4.021439	16.05236
N	13.62603	1.883418	0.164108
N	13.15563	0.912567	16.01449
N	13.79196	4.082468	16.28834
N	6.841737	6.264875	16.7306
N	7.332498	5.196953	13.55004
N	9.520678	7.140001	15.39514
N	12.41813	13.74026	7.549186
N	14.13364	12.72036	6.50715
N	9.803744	14.91353	9.521897
N	10.1876	15.96384	6.436696
N	9.409894	12.91565	6.794438
N	0.875826	10.44854	7.428668
N	0.714985	11.61778	4.183268
N	13.84622	9.619498	5.723933
Zn	10.35777	10.83414	17.19998
Zn	15.03919	13.92658	15.32113
Zn	12.72882	6.07744	7.678313
Zn	8.033257	2.806365	5.855645
Zn	2.6161	14.43978	1.678193
Zn	7.297399	11.34725	3.557003
Zn	4.986894	2.560592	11.19986
Zn	0.291524	5.831651	13.02262
Zn	5.125804	6.121761	1.678268
Zn	0.444485	3.029318	3.556928
Zn	2.754919	10.87866	11.19984
Zn	7.450455	14.14955	13.02257
Zn	12.86766	2.516237	17.19991
Zn	8.186266	5.608696	15.32123
Zn	10.49674	14.39534	7.678275
Zn	15.19211	11.12446	5.85557
Cl	13.5292	9.469157	18.62294
Cl	0.69884	10.83942	16.79235
Cl	11.49353	10.16477	13.91852
Cl	10.40397	14.23466	18.02417
Cl	0.160012	15.93867	12.31909
Cl	12.35057	15.10102	13.07833
Cl	10.55364	7.677011	0.592906
Cl	9.583291	7.389329	8.954759

Cl	6.975725	5.996446	7.045895
Cl	11.8787	6.590022	4.234635
Cl	13.28381	2.792244	8.726466
Cl	6.603229	0.767607	3.295126
Cl	10.21785	1.454472	3.157957
Cl	6.51638	16.23419	6.452252
Cl	12.38558	9.135147	9.634656
Cl	5.78784	15.80493	0.255327
Cl	8.440872	14.43463	2.085999
Cl	3.751811	15.1092	4.959707
Cl	2.662228	11.03922	0.854086
Cl	7.901949	9.335441	6.558876
Cl	4.609088	10.17258	5.800106
Cl	2.812036	0.960636	18.28514
Cl	9.181339	8.502922	3.641521
Cl	1.841381	1.248605	9.923567
Cl	14.71743	2.641521	11.83241
Cl	4.137092	2.048046	14.64375
Cl	5.541868	5.845821	10.15173
Cl	14.34515	7.870326	15.58316
Cl	2.476079	7.18359	15.72007
Cl	14.2581	9.039495	12.42602
Cl	4.643533	16.1386	9.243274
Cl	1.954212	7.486976	0.255214
Cl	14.78461	6.116647	2.08598
Cl	3.990149	6.791268	4.959726
Cl	5.079511	2.721005	0.854067
Cl	15.32353	1.017389	6.5588
Cl	3.132929	1.854747	5.799974
Cl	4.930036	9.278774	18.28533
Cl	14.04415	0.18492	3.641483
Cl	5.900405	9.56659	9.923549
Cl	8.508002	10.95962	11.83241
Cl	3.604952	10.36581	14.64371
Cl	2.199828	14.16395	10.15148
Cl	8.880822	16.1881	15.58277
Cl	5.266191	15.50183	15.72031
Cl	8.966759	0.721766	12.42543
Cl	3.098317	7.821148	9.243274
Cl	9.696273	1.151137	18.62285
Cl	7.042978	2.521519	16.79231
Cl	11.73167	1.846613	13.91839
Cl	12.82133	5.916925	18.02407

Cl	7.581607	7.620625	12.31934
Cl	10.87476	6.783219	13.07832
Cl	12.67192	15.99495	0.592906
Cl	6.302543	8.452963	15.23677
Cl	13.64235	15.70733	8.954778
Cl	0.76617	14.31436	7.045819
Cl	11.34667	14.90802	4.234314
Cl	9.941719	11.11033	8.726542
Cl	1.13842	9.085872	3.294993
Cl	13.00751	9.77239	3.157976
Cl	1.225343	7.916575	6.452365
Cl	10.83998	0.816911	9.634543
Cl	1.440077	16.77039	15.23639

Table B.11. Cartesian atomic coordinates and lattice vectors for ZIF-71 (GIS)

Atom Type	x	y	z
	18.25992	0	0
Lattice vectors	-0.11403	18.14454	0
	-0.08181	0.348081	21.53754
C	5.974167	8.956951	0.031832
C	6.383825	4.473446	2.833716
C	4.350862	5.122706	2.518945
C	13.6603	1.456701	5.431746
C	0.015945	1.898119	8.290015
C	13.64931	17.58656	6.213064
C	13.31607	17.52449	4.877047
C	17.53032	18.16731	7.430668
C	3.076293	9.399137	10.76505
C	2.571938	13.8866	13.59695
C	4.605753	13.26492	13.23943
C	13.4163	16.94703	16.18891
C	8.87325	16.66502	18.99497
C	9.636747	0.549164	18.64914
C	6.15593	13.85874	18.92696
C	3.837571	9.417774	20.90656
C	3.932179	8.855295	0.732944
C	4.125308	13.13222	18.99383
C	9.135959	1.540887	2.850429
C	9.71908	17.67605	2.49562
C	2.762126	4.772029	8.166261
C	5.123546	9.274528	10.08631
C	5.122788	9.525581	11.44511

C	4.786541	5.512291	8.223594
C	17.99814	16.59391	13.56887
C	13.59722	0.811845	15.39463
C	13.37573	0.882298	16.75634
C	17.34521	0.463562	13.57485
C	12.15049	9.357968	21.52167
C	11.68736	13.92834	18.82687
C	14.19643	9.526843	20.8438
C	14.28289	8.883409	0.654806
C	13.73618	13.28655	19.04287
C	4.277522	16.9982	16.26507
C	0.453901	0.520768	13.51285
C	15.04712	9.241978	10.7499
C	15.50099	4.665282	8.066197
C	13.46439	5.338439	8.301603
C	4.613709	1.537293	5.478526
C	8.344367	17.66894	2.482288
C	11.88173	4.469306	2.721247
C	13.93263	5.130104	2.608455
C	4.382774	0.861098	17.06458
C	4.071451	0.920888	15.72098
C	8.266732	0.525071	18.64824
C	15.32469	13.73546	13.49299
C	13.0199	9.233088	11.49652
C	12.98765	9.041173	10.12794
C	13.31555	12.96686	13.3405
C	4.569922	17.73447	6.413751
C	4.906203	17.59756	5.083915
C	0.640419	18.20244	7.43687
C	14.94858	18.20702	10.78764
C	13.25254	14.33359	13.4222
C	4.456387	10.76512	16.18469
C	8.997969	11.11486	18.98022
C	4.525937	8.716402	16.86741
C	4.31391	8.718939	15.50313
C	8.317532	9.164885	18.35858
C	12.1559	0.402333	21.5229
C	14.28272	0.086496	0.680436
C	14.08844	18.39689	20.84797
C	13.91513	3.759644	2.600443
C	4.493659	7.753174	5.430045
C	-0.05967	7.509644	8.131671
C	4.340367	9.835761	5.984227

C	4.634139	9.758593	4.637055
C	0.595979	9.560837	7.984979
C	13.04141	0.174563	10.02754
C	12.87704	18.02519	11.37523
C	13.47404	3.969596	8.322881
C	-0.08815	10.95647	13.53062
C	0.670176	8.944909	13.36648
C	13.70355	14.65384	19.08045
C	9.118498	7.217328	2.680519
C	8.4431	9.246928	2.95928
C	3.044997	0.288093	10.86728
C	4.82859	4.146502	8.126201
C	13.67122	7.686056	5.387293
C	13.56027	9.708235	4.633264
C	13.77279	9.7567	5.997409
C	9.812873	9.244822	2.926693
C	5.833204	18.12656	0.060779
C	4.096828	14.50095	18.987
C	13.64456	10.72062	16.16642
C	17.56028	8.898513	13.29909
C	5.023671	0.343514	11.73337
C	5.127495	0.604415	10.3817
C	4.564252	14.63433	13.24173
C	17.48522	9.540253	7.978906
C	3.850282	18.05697	0.911189
C	3.677007	18.13689	21.09598
C	4.381474	3.753337	2.478519
C	13.59405	8.720046	16.98509
C	13.94987	8.644061	15.65497
C	9.684952	9.188004	18.2925
H	7.06047	8.959743	0.021645
H	7.448851	4.493715	3.036966
H	13.68774	2.539116	5.374651
H	-0.01276	2.873981	8.764552
H	1.989915	9.391134	10.76496
H	1.50887	13.85368	13.80918
H	13.43788	15.8629	16.24887
H	8.893717	15.60185	19.20765
H	7.238136	13.87924	18.85862
H	9.129176	2.612335	3.031926
H	1.678547	4.736907	8.131844
H	18.04409	15.50981	13.55674
H	11.06449	9.34889	21.52466

H	10.6154	13.90509	18.66523
H	4.35696	15.91687	16.19946
H	16.1313	9.289812	10.71762
H	16.5726	4.666657	7.90094
H	4.503849	2.610015	5.341461
H	10.80021	4.483393	2.800225
H	16.40555	13.78088	13.56701
H	16.03288	18.23067	10.83369
H	4.4654	11.85197	16.18639
H	8.998583	12.13348	19.35448
H	11.06993	0.422108	21.51717
H	4.499879	6.668293	5.492892
H	-0.045	6.430592	8.235181
H	18.13161	12.03656	13.61821
H	9.11184	6.146876	2.50781
H	1.966817	0.201744	10.76856
H	13.67741	6.600016	5.425587
H	6.944641	0.419212	21.50976
H	13.58118	11.80195	16.08777
N	5.245911	8.711492	1.144462
N	5.625156	5.59736	2.737443
N	13.97259	0.766352	6.552
N	17.15724	1.191413	7.972617
N	3.812663	9.676555	11.86342
N	3.338196	12.77293	13.46051
N	13.14438	17.73953	17.24974
N	9.996902	17.41812	18.86308
N	5.144719	9.553696	20.46988
N	5.435235	12.70803	18.95519
N	13.30637	0.66729	4.391268
N	10.27536	0.817064	2.727988
N	3.813061	9.121273	9.667147
N	3.472882	5.926525	8.236689
N	13.65679	17.62778	15.04578
N	16.83381	17.2896	13.60197
N	12.88278	9.673442	20.42896
N	12.45469	12.80754	18.8867
N	3.897854	17.77404	15.22467
N	0.84283	17.38196	13.52379
N	14.29141	8.967908	9.664477
N	14.75278	5.797823	8.144421
N	5.031941	0.706053	4.499408
N	8.004078	0.807314	2.715216

N	12.97635	8.710676	1.073754
N	12.63855	5.596881	2.680864
N	4.538845	17.69204	17.39542
N	7.723464	17.37941	18.87087
N	14.33277	9.4373	11.88015
N	14.63457	12.57118	13.39211
N	4.3662	0.911671	6.649608
N	1.172996	1.250831	7.984677
N	14.16904	17.88987	11.84688
N	14.5317	14.83853	13.50893
N	4.693343	10.02276	17.28959
N	7.863025	10.39182	18.78672
N	12.9759	0.257334	1.098522
N	12.60946	3.324306	2.672507
N	4.183117	8.552637	6.47509
N	1.065704	8.268905	8.080132
N	14.36678	0.35695	9.66592
N	14.76892	3.524558	8.173174
N	4.19666	10.03204	15.07949
N	1.073818	10.25529	13.50798
N	12.77517	18.29615	20.41684
N	12.40065	15.07931	18.94444
N	4.80184	8.426068	4.298592
N	7.985311	7.957739	2.803176
N	3.8525	0.637082	9.840956
N	3.538896	3.659169	8.108971
N	13.41945	8.383078	4.256723
N	10.25853	7.953402	2.753769
N	4.959947	18.10779	20.56818
N	5.38832	14.97944	18.9528
N	14.03958	9.925422	15.14602
N	17.06307	10.18041	13.41502
N	3.588082	18.2176	12.02906
N	3.269473	15.0461	13.47163
N	13.91782	8.462847	6.46542
N	17.05365	8.235025	8.068717
N	5.279509	0.19751	1.21517
N	5.675321	3.324368	2.683125
N	13.33833	10.04341	17.29557
N	10.13521	10.42541	18.69566
Zn	5.929146	7.652379	2.76583
Zn	15.10187	1.476176	8.108648
Zn	3.099939	10.70437	13.4903

Zn	12.05788	17.12961	18.87934
Zn	5.80564	10.67381	18.89088
Zn	12.28738	1.269631	2.738455
Zn	3.115137	7.965468	8.123595
Zn	14.79967	16.88848	13.51459
Zn	12.17903	10.7539	18.82825
Zn	2.886546	17.08764	13.58147
Zn	15.01393	7.86032	8.086486
Zn	5.999706	1.267073	2.797942
Zn	12.31404	7.642289	2.688251
Zn	5.672902	17.02973	18.96421
Zn	15.02787	10.52868	13.46654
Zn	3.208087	1.624892	8.16723
Cl	2.976089	6.084854	2.345912
Cl	13.65697	16.25225	7.268576
Cl	13.3209	16.10655	3.945441
Cl	16.60844	16.87033	6.873427
Cl	5.984914	12.31923	13.01757
Cl	10.6047	1.913642	18.42965
Cl	2.454901	9.249789	19.93069
Cl	2.565431	9.005845	1.734677
Cl	2.770981	12.12915	19.07102
Cl	10.67334	16.29883	2.269066
Cl	6.485658	9.431843	9.079345
Cl	6.489446	9.402702	12.45075
Cl	6.127982	6.527039	8.352496
Cl	13.39169	2.113375	14.31822
Cl	13.51193	2.301083	17.6842
Cl	16.3132	1.795503	13.64584
Cl	15.58404	9.452386	19.86196
Cl	15.66293	8.982914	1.642841
Cl	15.12247	12.33447	19.17151
Cl	1.352982	1.946816	13.425
Cl	12.0958	6.314129	8.443277
Cl	7.42171	16.27872	2.19362
Cl	15.31373	6.095799	2.524652
Cl	4.237504	2.163357	18.14848
Cl	4.061678	2.359624	14.81727
Cl	7.253585	1.854498	18.4121
Cl	11.71396	8.975982	12.55647
Cl	11.59628	9.189691	9.159378
Cl	11.99462	11.92922	13.17725
Cl	4.634422	16.50028	7.581538

Cl	5.036645	16.1215	4.261095
Cl	1.627523	16.95126	6.879586
Cl	11.83488	15.25029	13.4175
Cl	4.38757	7.346336	17.86606
Cl	4.499347	7.356611	14.50278
Cl	7.347405	7.827698	18.02251
Cl	15.50747	17.99239	1.702801
Cl	15.5663	0.433238	19.84594
Cl	15.27187	2.760673	2.496804
Cl	4.437179	11.26188	6.904247
Cl	4.53967	11.07842	3.566875
Cl	1.559622	10.94107	7.867923
Cl	11.5803	18.21213	8.992893
Cl	11.4589	18.0862	12.30965
Cl	12.11869	2.984607	8.508492
Cl	1.685985	7.597614	13.3278
Cl	15.04269	15.66267	19.26619
Cl	7.467346	10.60726	3.155508
Cl	6.249109	3.239334	8.011987
Cl	13.72312	11.04154	3.588284
Cl	13.5844	11.14888	6.955334
Cl	10.79972	10.60477	3.066601
Cl	2.699861	15.44548	19.03385
Cl	16.66768	7.477414	13.08916
Cl	6.285037	0.534775	12.85828
Cl	6.593496	0.576938	9.5236
Cl	5.886425	15.65771	13.01111
Cl	16.48078	10.89116	7.860665
Cl	2.599785	17.85974	2.047359
Cl	2.224238	18.1935	20.21212
Cl	3.048039	2.748107	2.227908
Cl	13.63221	7.40709	18.06631
Cl	14.01779	7.206756	14.75658
Cl	10.65099	7.893759	17.80782

B.2 Adsorption isotherms of water, SO_2, and CO_2

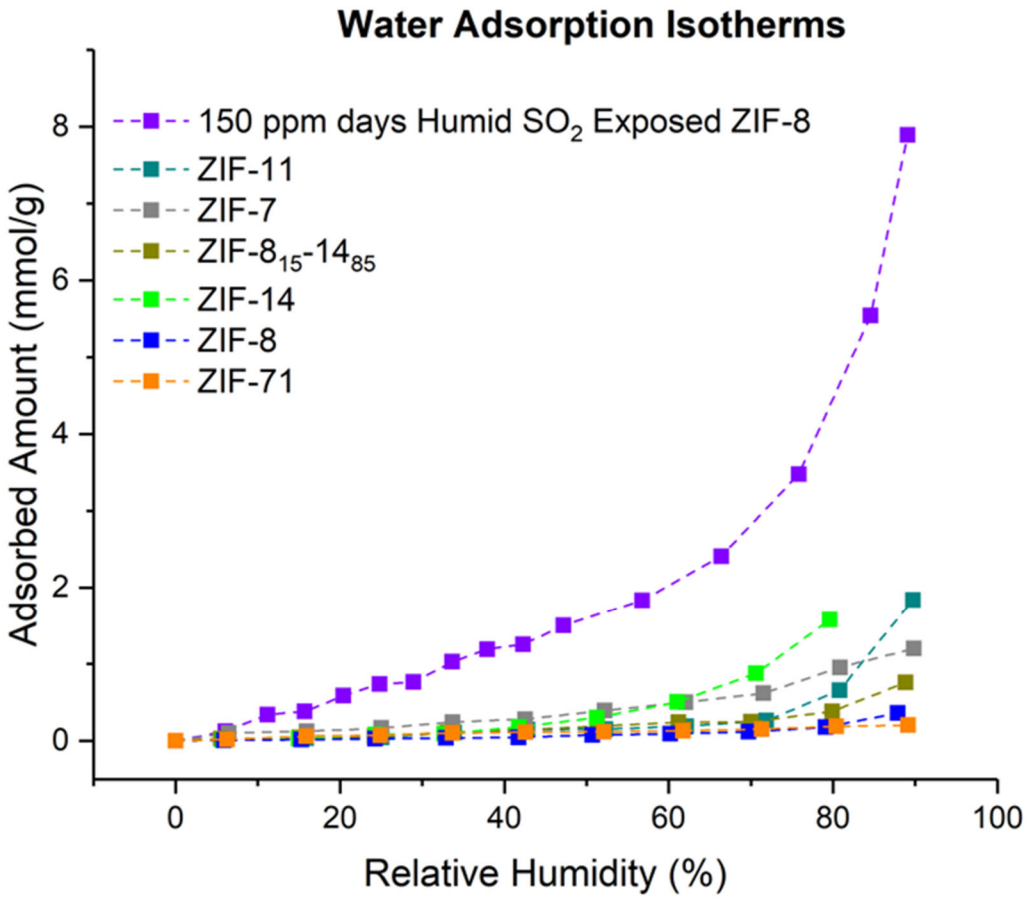

Figure B.1. Experimentally measured water adsorption isotherms of pristine ZIF-8, ZIF-14, ZIF-8_{15}-14_{85}, ZIF-11, ZIF-7, and ZIF-71 RHO, and ZIF-8 after exposure to humid SO_2.

B.3 Experimental PXRD patterns before and after NO_2 exposure

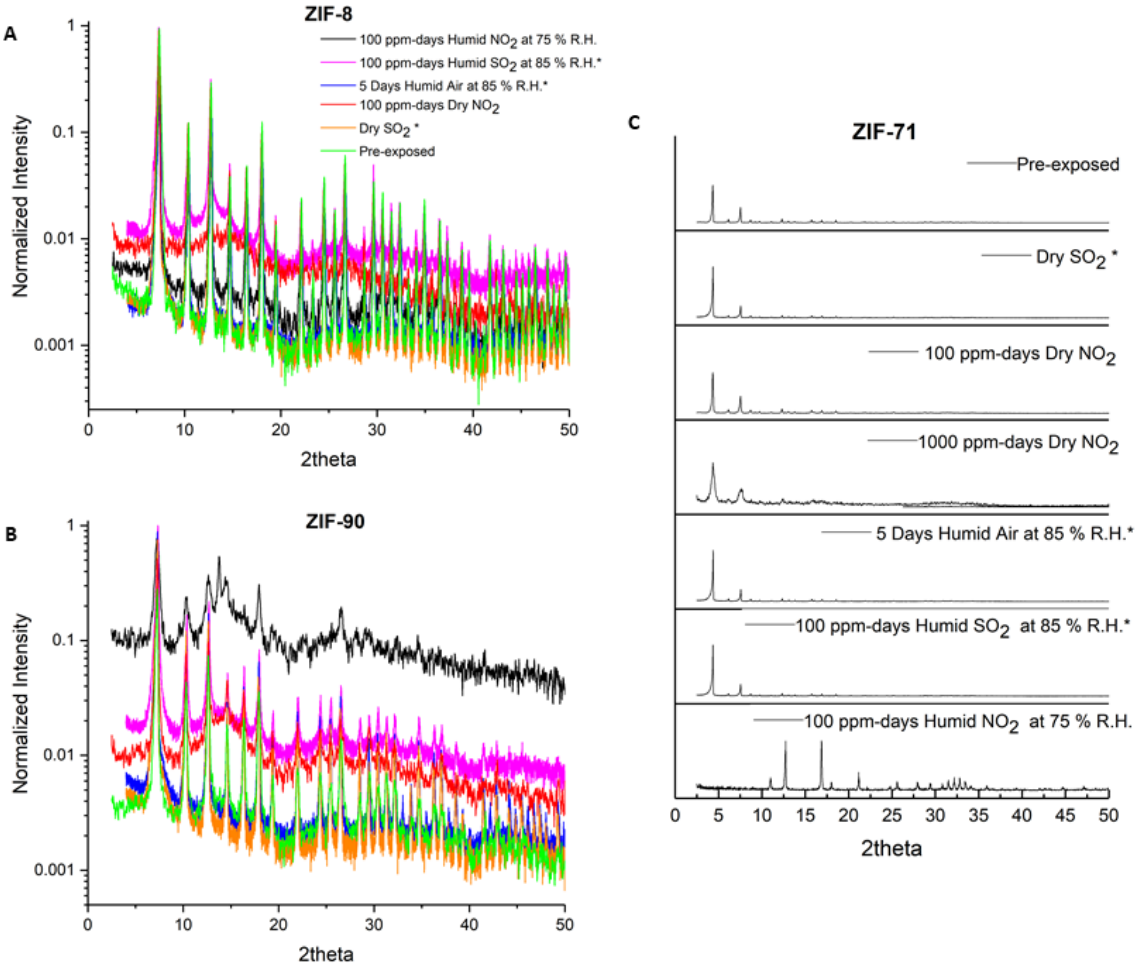

Figure B.2. PXRD patterns of A) ZIF-8, B) ZIF-90 and C) ZIF-71 after exposure to dry and humid NO_2 compared to pre-exposed samples. Figure legends in A and B are the same. *PXRD patterns of ZIFs on exposure to humid air, dry and humid SO_2 are shown for comparison. The patterns are normalized with respect to the most intense Bragg peak for each ZIF.

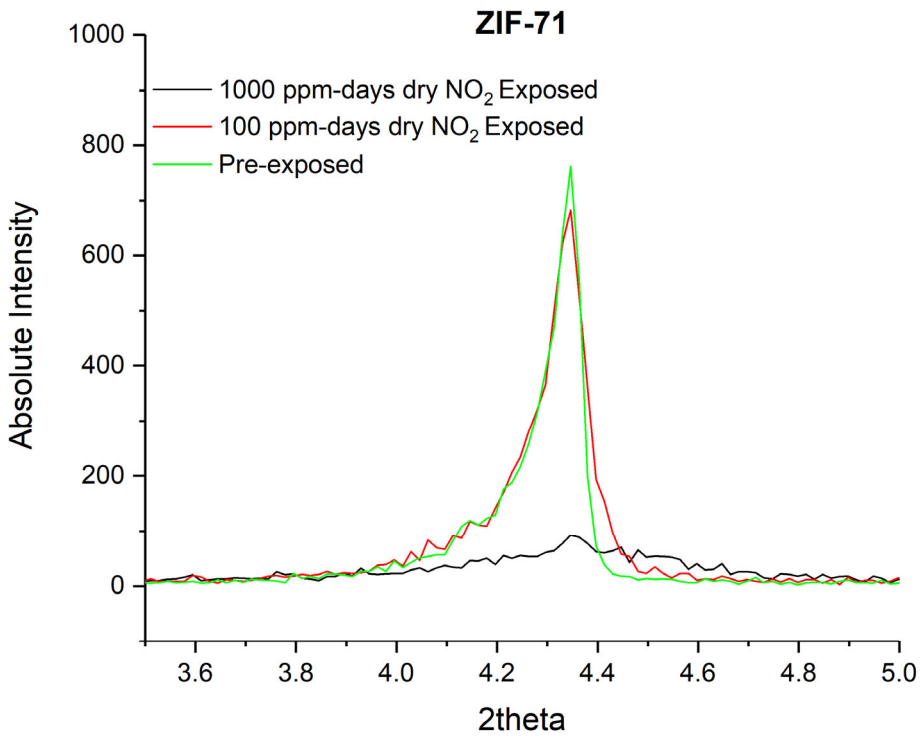

Figure B.3. The (110) PXRD peak of ZIF-71 on exposure to increasing dosage of dry NO_2 compared to the pre-exposed sample.

B.4 Experimental N_2 adsorption isotherms before and after NO_2 exposure

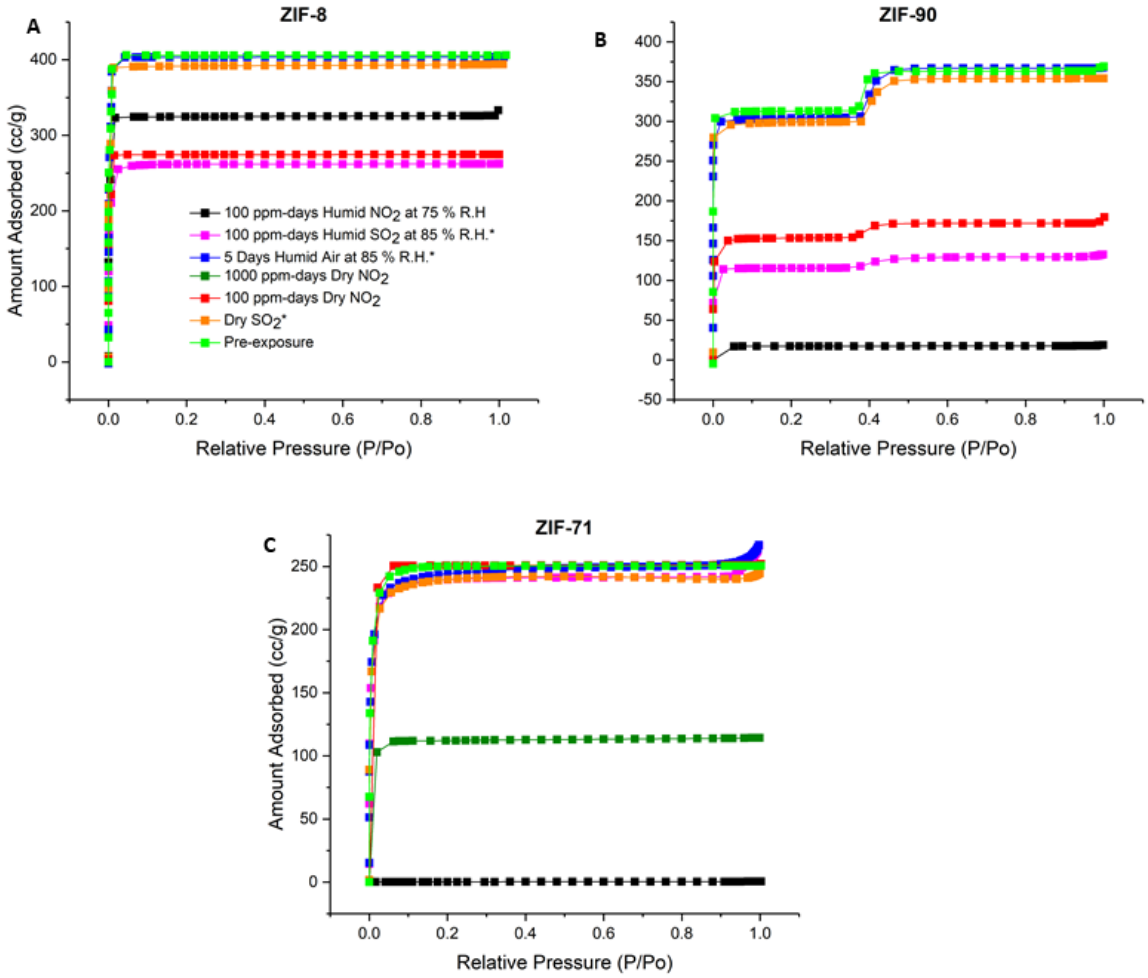

Figure B.4. N_2 physisorption at 77 K in pre-exposed and reactivated ZIFs after different exposure protocols. Figure legends are same in all. 1000 ppm-days dry NO_2 exposure was only carried out in C) ZIF-71. *Data for humid air, dry and humid SO_2 are shown for comparison.

Table B.12. Textural characteristics of pre-exposed ZIFs and ZIFs after different exposure experiments. The BET surface area is reported as a percentage relative to pre-exposed ZIF-8.
*** Material undergoes crystal phase change**
a Average SO_2 concentration during dry SO_2 isotherm measurements

Exposure Condition	Exposed Time (days)	Conc.	Overall Exposure (ppm-days)	Relative BET SA (%)			Pore Volume (cc/g)		
				ZIF-8	ZIF-90	ZIF-71	ZIF-8	ZIF-90	ZIF-71
Pre	N/A	N/A	N/A	100	100	100	0.62	0.45	0.37
Dry SO_2	0.15	99.8%	[a]1.8×10^5	98	99	98	0.6	0.44	0.34
Dry NO_2	0.1	1000 ppm	100	65	53	99	0.41	0.25	0.36
Dry NO_2	1	1000 ppm	1/000	N/A	N/A	45	N/A	N/A	0.17
Humid Air	5	0	0	99	98	99	0.61	0.44	0.33
Humid SO_2	5	20 ppm	100	61	50	97	0.38	0.22	0.34
Humid NO_2	5	20 ppm	100	81	3	0*	0.49	0.04	0*

B.5 Experimental FTIR spectra after NO_2 exposure

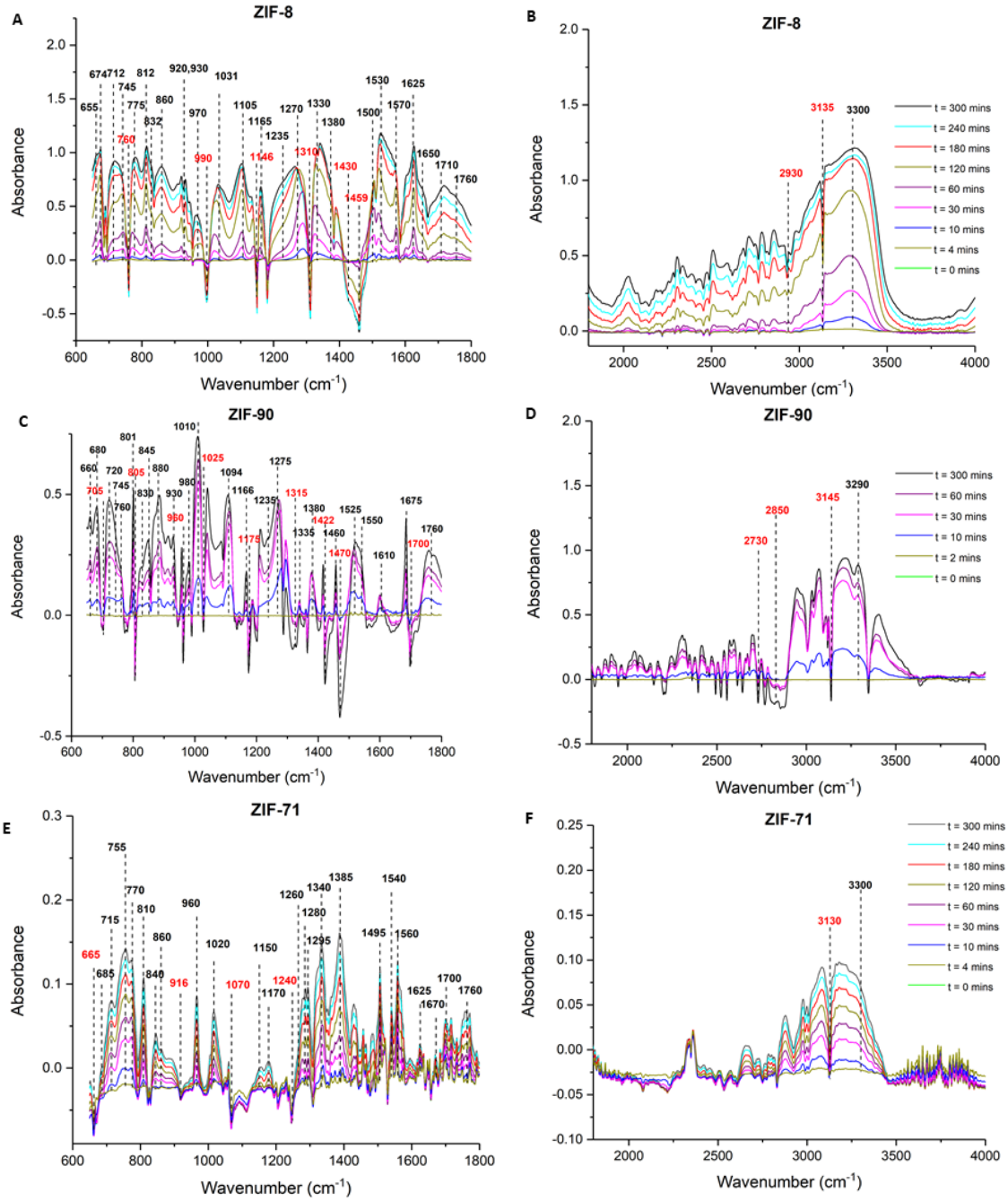

Figure B.5. In situ FTIR difference spectra of ZIFs exposed to 1000 ppm dry NO_2 over 5 hours. Decreasing peaks are marked in red. Time intervals of the FTIR spectra are identical in A and B (ZIF-8), C and D (ZIF-90) and E and F (ZIF-71).

Table B.13. Functional groups attributed to new FTIR peaks in ZIFs following 5 hours of dry NO_2 exposure at 1000 ppm. The same peaks are observed upon humid NO_2 exposure except in ZIF-71. Peaks that can be unambiguously assigned are highlighted in green.

Functional Groups	ZIF-8	ZIF-90	ZIF-71	Expected Range of Peaks (cm^{-1})
Organic Groups				
Nitro[74-77]	1530	1525	1540	1485-1570 (asym. NO_2 str.)
	1330	masked	1340	1320-1370 (sym. NO_2 str.)
	1031	1010	1020	865-1180 (aromatic C-N str.)
	920, 930	930	NA	850-1000 (aliphatic C-N str.)
	832	830	840	830-865 (NO_2 def.)
	655	660	NA	605-670 (NO_2 def. aliphatic)
Nitrite[78]	1650	1675	1670	1610-80 (N=O str.)
	812	801	810	750-850 (N-O str.)
	674	680	685	615-690 (O-N=O def.)
	1105	1094	1150	1000-1300 (C-O)
Nitrate[76-77]	1625	1610	1625	1615-1660 (asym. NO_2 str.)
	1270	1270	1280	1270-1300 (sym. NO_2 str.)
	860	845	860	840-870 (N-O str.)
	745	745	755	745-765 (NO_2 def.)
	712	720	715	680-720 (NO_2 def.)
	1105	1094	1150	1000-1300 (C-O)
Nitramine[79]	1570	1550	1560	1530-1630 (asym. NO_2 str.)
	1270	1275	1295	1260-1315 (sym. NO_2 str.)
	970	980	960	925-1030 (N-N str.)
	775	760	770	755-775 (NO_2 def.)
Nitrosamine[79]	1500	1460	1495	1450-1500 (N=O str.)
	970	980	960	925-1030 (N-N str.)
	1165	1166	1170	1160-1200 (C-N str.)
Inorganic Groups				
Nitrate[77]	1380	1380	1385	1350-1410 (asym. NO_3 str.)
	860	845	860	~800-860
	712	720	715	~710-730
Nitrite[77]	1235	1235	1260	1235-1275 (asym. NO_2 str.)
	812	801	810	800-835

B.6 REFERENCES

1. Rezaei, F.; Rownaghi, A. A.; Monjezi, S.; Lively, R. P.; Jones, C. W., SO_x/NO_x Removal from Flue Gas Streams by Solid Adsorbents: A Review of Current Challenges and Future Directions. *Energy Fuels* **2015**, *29*, 5467-5486.

2. Sanz-Pérez, E. S.; Murdock, C. R.; Didas, S. A.; Jones, C. W., Direct Capture of CO_2 from Ambient Air. *Chem Rev* **2016**, *116*, 11840-11876.

3. Sun, W.; Lin, L. C.; Peng, X.; Smit, B., Computational Screening of Porous Metal-Organic Frameworks and Zeolites for the Removal of SO_2 and NO_x from Flue Gases. *AIChE Journal* **2014**, *60*, 2314-2323.

4. EPA-452/F-03-032 Air Pollution Control Technology Fact Sheet. EPA-CICA, Ed. RTP, NC.

5. EPA-452/F-03-034 Air Pollution Control Technology Fact Sheet. EPA-CICA, Ed. RTP, NC.

6. Bobbitt, N. S.; Mendonca, M. L.; Howarth, A. J.; Islamoglu, T.; Hupp, J. T.; Farha, O. K.; Snurr, R. Q., Metal–Organic Frameworks for the Removal of Toxic Industrial Chemicals and Chemical Warfare Agents. *Chem Soc Rev* **2017**, *46*, 3357-3385.

7. DeCoste, J. B.; Peterson, G. W., Metal–Organic Frameworks for Air Purification of Toxic Chemicals. *Chem Rev* **2014**, *114*, 5695-5727.

8. Sholl, D. S.; Lively, R. P., Seven Chemical Separations to Change the World. *Nature* **2016**, *532*, 435-437.

9. Banerjee, R.; Phan, A.; Wang, B.; Knobler, C.; Furukawa, H.; O'Keeffe, M.; Yaghi, O. M., High-Throughput Synthesis of Zeolitic Imidazolate Frameworks and Application to CO_2 Capture. *Science* **2008**, *319*, 939-943.

10. Phan, A.; Doonan, C. J.; Uribe-Romo, F. J.; Knobler, C. B.; O'Keeffe, M.; Yaghi, O. M., Synthesis, Structure, and Carbon Dioxide Capture Properties of Zeolitic Imidazolate Frameworks. *Acc Chem Res* **2010**, *43*, 58-67.

11. Mottillo, C.; Friščić, T., Carbon Dioxide Sensitivity of Zeolitic Imidazolate Frameworks. *Angew Chem Int Ed Engl* **2014**, *53*, 7471-7474.

12. Zhang, H.; Liu, D.; Yao, Y.; Zhang, B.; Lin, Y. S., Stability of ZIF-8 Membranes and Crystalline Powders in Water at Room Temperature. *J Memb Sci* **2015**, *485*, 103-111.

13. Leus, K.; Bogaerts, T.; De Decker, J.; Depauw, H.; Hendrickx, K.; Vrielinck, H.; Van Speybroeck, V.; Van Der Voort, P., Systematic Study of the Chemical and

Hydrothermal Stability of Selected "Stable" Metal Organic Frameworks. *Micropor Mesopor Mater* **2016**, *226*, 110-116.

14. Bhattacharyya, S.; Pang, S. H.; Dutzer, M. R.; Lively, R. P.; Walton, K. S.; Sholl, D. S.; Nair, S., Interactions of SO_2-Containing Acid Gases with ZIF-8: Structural Changes and Mechanistic Investigations. *J Phys Chem C* **2016**, *120*, 27221-27229.

15. Zhang, C.; Han, C.; Sholl, D. S.; Schmidt, J. R., Computational Characterization of Defects in Metal-Organic Frameworks: Spontaneous and Water-Induced Point Defects in ZIF-8. *J Phys Chem Lett* **2016**, *7*, 459-64.

16. Han, R.; Sholl, D. S., Computational Model and Characterization of Stacking Faults in ZIF-8 Polymorphs. *J Phys Chem C* **2016**, *120*, 27380-27388.

17. Han, S.; Huang, Y.; Watanabe, T.; Dai, Y.; Walton, K. S.; Nair, S.; Sholl, D. S.; Meredith, J. C., High-Throughput Screening of Metal–Organic Frameworks for CO_2 Separation. *ACS Comb Sci* **2012**, *14*, 263-267.

18. Bhattacharyya, S.; Jayachandrababu, K. C.; Chiang, Y.; Sholl, D. S.; Nair, S., Butanol Separation from Humid CO_2-Containing Multicomponent Vapor Mixtures by Zeolitic Imidazolate Frameworks. *ACS Sustain Chem Eng* **2017**, *5*, 9467-9476.

19. Pang, S. H.; Han, C.; Sholl, D. S.; Jones, C. W.; Lively, R. P., Facet-Specific Stability of ZIF-8 in the Presence of Acid Gases Dissolved in Aqueous Solutions. *Chem Mater* **2016**, *28*, 6960-6967.

20. Pimentel, B. R.; Parulkar, A.; Zhou, E. K.; Brunelli, N. A.; Lively, R. P., Zeolitic Imidazolate Frameworks: Next-Generation Materials for Energy-Efficient Gas Separations. *Chem Sus Chem* **2014**, *7*, 3202-40.

21. Lu, P.; Wu, Y.; Kang, H.; Wei, H.; Liu, H.; Fang, M., What Can pKa and NBO Charges of the Ligands Tell Us About the Water and Thermal Stability of Metal Organic Frameworks? *J Mater Chem A* **2014**, *2*, 16250-16267.

22. Burtch, N. C.; Jasuja, H.; Walton, K. S., Water Stability and Adsorption in Metal-Organic Frameworks. *Chem Rev* **2014**, *114*, 10575-612.

23. Low, J. J.; Benin, A. I.; Jakubczak, P.; Abrahamian, J. F.; Faheem, S. A.; Willis, R. R., Virtual High Throughput Screening Confirmed Experimentally: Porous Coordination Polymer Hydration. *J Am Chem Soc* **2009**, *131*, 15834-15842.

24. Greathouse, J. A.; Allendorf, M. D., The Interaction of Water with MOF-5 Simulated by Molecular Dynamics. *J Am Chem Soc* **2006**, *128*, 10678-10679.

25. De Toni, M.; Jonchiere, R.; Pullumbi, P.; Coudert, F. X.; Fuchs, A. H., How Can a Hydrophobic MOF Be Water-Unstable? Insight into the Hydration Mechanism of IrMOFs. *Chem Phys Chem* **2012**, *13*, 3497-3503.

26. Tu, M.; Wiktor, C.; Rösler, C.; Fischer, R. A., Rapid Room Temperature Syntheses of Zeolitic-Imidazolate Framework (ZIF) Nanocrystals. *Chem Commun* **2014**, *50*, 13258-13260.

27. He, M.; Yao, J.; Liu, Q.; Zhong, Z.; Wang, H., Toluene-Assisted Synthesis of RHO-Type Zeolitic Imidazolate Frameworks: Synthesis and Formation Mechanism of ZIF-11 and ZIF-12. *Dalton Trans* **2013**, *42*, 16608-16613.

28. Schweinefuß, M. E.; Springer, S.; Baburin, I. A.; Hikov, T.; Huber, K.; Leoni, S.; Wiebcke, M., Zeolitic Imidazolate Framework-71 Nanocrystals and a Novel SOD-Type Polymorph: Solution Mediated Phase Transformations, Phase Selection via Coordination Modulation and a Density Functional Theory Derived Energy Landscape. *Dalton Trans* **2014**, *43*, 3528-3536.

29. Gee, J. A.; Chung, J.; Nair, S.; Sholl, D. S., Adsorption and Diffusion of Small Alcohols in Zeolitic Imidazolate Frameworks ZIF-8 and ZIF-90. *J Phys Chem C* **2013**, *117*, 3169-3176.

30. Bhattacharyya, S., et al., Acid Gas Stability of Zeolitic Imidazolate Frameworks: Generalized Kinetic and Thermodynamic Characteristics. *Chem Mater* **2018**, *30*, 4089-4101.

31. Walton, K. S.; Snurr, R. Q., Applicability of the BET Method for Determining Surface Areas of Microporous Metal−Organic Frameworks. *J Am Chem Soc* **2007**, *129*, 8552-8556.

32. Hashimoto, Y.; Tanaka, S., A New Method of Generation of Gases at Parts Per Million Levels for Preparation of Standard Gases. *Environ Sci Technol* **1980**, *14*, 413-416.

33. Zhang, N.; Zhang, J.; Zhang, Y.; Bai, J.; Wei, X., Solubility and Henry's Law Constant of Sulfur Dioxide in Aqueous Polyethylene Glycol 300 Solution at Different Temperatures and Pressures. *Fluid Ph Equilibria* **2013**, *348*, 9-16.

34. Park, K. S.; Ni, Z.; Cote, A. P.; Choi, J. Y.; Huang, R.; Uribe-Romo, F. J.; Chae, H. K.; O'Keeffe, M.; Yaghi, O. M., Exceptional Chemical and Thermal Stability of Zeolitic Imidazolate Frameworks. *Proc Natl Acad Sci USA* **2006**, *103*, 10186-91.

35. Morris, W.; Doonan, C. J.; Furukawa, H.; Banerjee, R.; Yaghi, O. M., Crystals as Molecules: Postsynthesis Covalent Functionalization of Zeolitic Imidazolate Frameworks. *J Am Chem Soc* **2008**, *130*, 12626-12627.

36. First, E. L.; Floudas, C. A., MOFomics: Computational Pore Characterization of Metal–Organic Frameworks. *Micropor Mesopor Mater* **2013**, *165*, 32-39.

37. Blöchl, P. E., Projector Augmented-Wave Method. *Phys Rev B* **1994**, *50*, 17953-17979.

38. Perdew, J. P.; Burke, K.; Ernzerhof, M., Generalized Gradient Approximation Made Simple. *Phys Rev Lett* **1996**, *77*, 3865-3868.

39. Marenich, A. V.; Cramer, C. J.; Truhlar, D. G., Universal Solvation Model Based on Solute Electron Density and on a Continuum Model of the Solvent Defined by the Bulk Dielectric Constant and Atomic Surface Tension. *J Phys Chem B* **2009**, *113*, 6378-6396.

40. Namazian, M.; Zakery, M.; Noorbala, M. R.; Coote, M. L., Accurate Calculation of the pKa of Trifluoroacetic Acid Using High-Level Ab Initio Calculations. *Chem Phys Lett* **2008**, *451*, 163-168.

41. Liptak, M. D.; Shields, G. C., Accurate pKa Calculations for Carboxylic Acids Using Complete Basis Set and Gaussian-N Models Combined with CPCM Continuum Solvation Methods. *J Am Chem Soc* **2001**, *123*, 7314-7319.

42. Manz, T. A.; Limas, N. G., DDEC6: A Method for Computing Even-Tempered Net Atomic Charges in Periodic and Nonperiodic Materials. *arXiv:1512.08270* **2015**.

43. Manz, T. A.; Sholl, D. S., Chemically Meaningful Atomic Charges That Reproduce the Electrostatic Potential in Periodic and Nonperiodic Materials. *J Chem Theor Comput* **2010**, *6*, 2455-2468.

44. Haranczyk, M.; Rycroft, C. H.; Willems, T. F.; Martin, R. L. *Zeo ++*, http://www.maciejharanczyk.info/Zeopp/download.html.

45. Martin, R. L.; Smit, B.; Haranczyk, M., Addressing Challenges of Identifying Geometrically Diverse Sets of Crystalline Porous Materials. *J Chem Inf Model* **2012**, *52*, 308-18.

46. Macrae, C. F.; Bruno, I. J.; Chisholm, J. A.; Edgington, P. R.; McCabe, P.; Pidcock, E.; Rodriguez-Monge, L.; Taylor, R.; van de Streek, J.; Wood, P. A., Mercury CSD 2.0– New Features for the Visualization and Investigation of Crystal Structures. *J Appl Crystallogr* **2008**, *41*, 466-470.

47. Liu, J.; Fang, S.; Wang, Z.; Yi, W.; Tao, F.-M.; Liu, J.-Y., Hydrolysis of Sulfur Dioxide in Small Clusters of Sulfuric Acid: Mechanistic and Kinetic Study. *Environ Sci Technol* **2015**, *49*, 13112-13120.

48. Zhao, P.; Lampronti, G. I.; Lloyd, G. O.; Wharmby, M. T.; Facq, S. B.; Cheetham, A. K.; Redfern, S. A., Phase Transitions in Zeolitic Imidazolate Framework 7: The Importance of Framework Flexibility and Guest-Induced Instability. *Chem Mater* **2014**, *26*, 1767-1769.

49. Springer, S.; Baburin, I. A.; Heinemeyer, T.; Schiffmann, J. G.; van Wüllen, L.; Leoni, S.; Wiebcke, M., A Zeolitic Imidazolate Framework with Conformational Variety: Conformational Polymorphs Versus Frameworks with Static Conformational Disorder. *Cryst Eng Comm* **2016**, *18*, 2477-2489.

50. Han, C.; Zhang, C.; Tymińska, N.; Schmidt, J. R.; Sholl, D. S., Insights into the Stability of Zeolitic Imidazolate Frameworks in Humid Acidic Environments from First-Principles Calculations. *J Phys Chem C* **2018**, *122*, 4339-4348.

51. Ebrahim, A. M.; Levasseur, B.; Bandosz, T. J., Interactions of NO_2 with Zr-Based MOF: Effects of the Size of Organic Linkers on NO_2 Adsorption at Ambient Conditions. *Langmuir* **2012**, *29*, 168-174.

52. Gray, P.; Yoffe, A., The Reactivity and Structure of Nitrogen Dioxide. *Chem Rev* **1955**, *55*, 1069-1154.

53. Kaupp, G.; Schmeyers, J., Gas/Solid Reactions with Nitrogen Dioxide. *J Org Chem* **1995**, *60*, 5494-5503.

54. Bernard, F. O.; Cazaunau, M.; Mu, Y.; Wang, X.; Daële, V. R.; Chen, J.; Mellouki, A., Reaction of NO_2 with Selected Conjugated Alkenes. *J Phys Chem A* **2013**, *117*, 14132-14140.

55. Pryor, W. A.; Lightsey, J. W.; Church, D. F., Reaction of Nitrogen Dioxide with Alkenes and Polyunsaturated Fatty Acids: Addition and Hydrogen-Abstraction Mechanisms. *J Am Chem Soc* **1982**, *104*, 6685-6692.

56. Davydov, E. Y.; Gaponova, I.; Pokholok, T.; Vorotnikov, A.; Pariiskii, G.; Zaikov, G., Features of Mechanism of Free Radical Initiation in Polymers under Exposure to Nitrogen Oxides. *Polym Adv Technol* **2008**, *19*, 475-484.

57. Giamalva, D. H.; Kenion, G. B.; Church, D. F.; Pryor, W. A., Rates and Mechanisms of Reactions of Nitrogen Dioxide with Alkenes in Solution. *J Am Chem Soc* **1987**, *109*, 7059-7063.

58. Aubin, D. G.; Abbatt, J. P., Interaction of NO_2 with Hydrocarbon Soot: Focus on Hono Yield, Surface Modification, and Mechanism. *J Phys Chem A* **2007**, *111*, 6263-6273.

59. Gao, X.; Liu, S.; Zhang, Y.; Luo, Z.; Ni, M.; Cen, K., Adsorption and Reduction of NO_2 over Activated Carbon at Low Temperature. *Fuel Process Technol* **2011**, *92*, 139-146.

60. Jeguirim, M.; Tschamber, V.; Brilhac, J.; Ehrburger, P., Interaction Mechanism of NO_2 with Carbon Black: Effect of Surface Oxygen Complexes. *J Anal Appl Pyrolysis* **2004**, *72*, 171-181.

61. Zhang, W.-J.; Bagreev, A.; Rasouli, F., Reaction of NO_2 with Activated Carbon at Ambient Temperature. *Ind Eng Chem Res* **2008**, *47*, 4358-4362.

62. Gray, P.; Yoffe, A. D., The Reactivity and Structure of Nitrogen Dioxide. *Chem Rev* **1955**, *55*, 1069-1154.

63. Pryor, W. A.; Lightsey, J. W.; Church, D. F., Reaction of Nitrogen-Dioxide with Alkenes and Poly-Unsaturated Fatty Acids - Addition and Hydrogen Abstraction Mechanisms. *J Am Chem Soc* **1982**, *104*, 6685-6692.

64. O'Neill, E.; Hinrichs, R. Z., Production of Molecular Iodine from the Heterogeneous Reaction of Nitrogen Dioxide with Solid Potassium Iodide. *J Geophys Res Atmos* **2011**, *116*.

65. Challis, B. C.; Kyrtopoulos, S. A., The Chemistry of Nitroso-Compounds. Part 11. Nitrosation of Amines by the Two-Phase Interaction of Amines in Solution with Gaseous Oxides of Nitrogen. *J Chem Soc Perkin Trans 1* **1979**, 299-304.

66. Turney, T.; Wright, G., Nitrous Acid and Nitrosation. *Chem Rev* **1959**, *59*, 497-513.

67. Zhao, Y.-L.; Garrison, S. L.; Gonzalez, C.; Thweatt, W. D.; Marquez, M., N-Nitrosation of Amines by NO_2 and NO: A Theoretical Study. *J Phys Chem A* **2007**, *111*, 2200-2205.

68. Grosjean, D., Atmospheric Chemistry of Toxic Contaminants. 6. Nitrosamines: Dialkyl Nitrosamines and Nitrosomorpholine. *J Air Waste Manage Assoc* **1991**, *41*, 306-311.

69. Li, H.; Zhu, T.; Ding, J.; Chen, Q.; Xu, B., Heterogeneous Reaction of NO_2 on the Surface of NaCl Particles. *Sci China Ser B: Chem* **2006**, *49*, 371-378.

70. Vogt, R.; Finlayson-Pitts, B. J., A Diffuse Reflectance Infrared Fourier Transform Spectroscopic Study of the Surface Reaction of NaCl with Gaseous NO_2 and HNO_3. *J Phys Chem* **1994**, *98*, 3747-3755.

71. Rodriguez, J. A.; Jirsak, T.; Dvorak, J.; Sambasivan, S.; Fischer, D., Reaction of NO_2 with Zn and ZnO: Photoemission, XANES, and Density Functional Studies on the Formation of NO_3. *J Phys Chem B* **2000**, *104*, 319-328.

72. Despres, J.; Koebel, M.; Kröcher, O.; Elsener, M.; Wokaun, A., Storage of NO_2 on BaO/TiO_2 and the Influence of NO. *Appl Catal B: Environ* **2003**, *43*, 389-395.

73. Tournas, A.; Potts, A., Surface Reactions of NO_2 with Machined Zn, Cd, Cu and Ag Surfaces Studied by He I/II Photoelectron Spectroscopy. *J Electron Spectrosc Relat Phenom* **1993**, *66*, 167-174.

74. Akhter, M.; Chughtai, A. R.; Smith, D., Reaction of Hexane Soot with Nitrogen Dioxide/Nitrogen Oxide (N_2O_4). *J Phys Chem* **1984**, *88*, 5334-5342.

75. Al-Abadleh, H. A.; Grassian, V., Heterogeneous Reaction of NO_2 on Hexane Soot: A Knudsen Cell and FT-IR Study. *J Phys Chem A* **2000**, *104*, 11926-11933.

76. Azambre, B.; Collura, S.; Trichard, J.; Weber, J., Nature and Thermal Stability of Adsorbed Intermediates Formed During the Reaction of Diesel Soot with Nitrogen Dioxide. *Appl Surf Sci* **2006**, *253*, 2296-2303.

77. Kirchner, U.; Scheer, V.; Vogt, R., Ftir Spectroscopic Investigation of the Mechanism and Kinetics of the Heterogeneous Reactions of NO_2 and HNO_3 with Soot. *J Phys Chem A* **2000**, *104*, 8908-8915.

78. Zawadzki, J.; Wiśniewski, M.; Skowrońska, K., Heterogeneous Reactions of NO_2 and NO–O_2 on the Surface of Carbons. *Carbon* **2003**, *41*, 235-246.

79. Piskorz, M.; Urbanski, T., Ultraviolet and Infrared Spectra of Some Nitramines. *Org Chem* **1963**, *6*, 615-624.

CHAPTER 4. DEFECT PROPAGATION IN ZIFS*

4.1 Introduction

Zeolitic imidazolate frameworks (ZIFs) are a subclass of crystalline porous adsorbents constructed from tetrahedrally coordinated Zn centers connected by imidazole-derived linkers, exhibiting a wide variety of accessible topologies, many of which are isomorphic to zeolites[1]. ZIFs have potential applications in chemical separations because they exhibit high thermal and chemical stability and have pore sizes comparable to small molecules[2,3]. However, like many other metal organic frameworks (MOFs)[4], ZIFs are susceptible to degradation under humid and corrosive environments[5]. Understanding and controlling the degradation of new materials in complex environments is often a prerequisite to their successful implementation in practical applications[6].

ZIF-8, one of the most well-studied ZIF structures, has 2-methylimidazole linkers and a sodalite (SOD) topology. ZIF-8 is considered to have robust hydrothermal stability[7,8,9]. Yaghi and co-workers[7] demonstrated that ZIF-8 retained crystallinity and porosity after being boiled in water and refluxing solvent for 7 days. Liu *et al*. showed that the selectivity and permeance of a ZIF-8 membrane remained constant for more than 40 days when left in atmospheric humidity[10]. However, recent experiments where ZIF-8 was contacted with pure water at room temperature revealed the release of Zn^{2+} ions from the structure, implying hydrolysis of ZIF-8 occurs in aqueous solution at a rate proportional to the ZIF-8 to water ratio[11,12]. The ratio of crystal to water appears to dictate the rate and

* Material in this chapter has been submitted for publication as Han, R.; Tyminska, N.; Schmidt, J.R.; Sholl, D. S. "Propagation of Degradation-induced Defects in Zeolitic Imidazolate Frameworks" to *J Phys Chem C* **2019**.

extent of dissolution of ZIF-8 and implies that previously observed water stability may have been a relative concentration effect; that is, exposure to sufficiently high relative concentration of pure water causes ZIF-8 to hydrolytically degrade.

It is widely hypothesized that degradation in MOFs and ZIFs begins with localized defect sites, in analogy to the highly reactive point defects in zeolites[13]. Existing modeling work on formation of ZIF-8 defects has focused on point defects induced by humid or humid acid gas (CO_2, SO_2, NO_x) environments[14-16]. Two types of defects, dangling linker (DL) and linker vacancy (LV) defects[15,17], were computationally proposed as the most likely isolated bond-breaking events in ZIFs and have been experimentally observed with IR spectroscopy[18] and solid state NMR[19]. The formation mechanisms attributed to these defects typically involve water or hydrated species attacking and breaking the Zn-N coordination bond[14]. This local description of defect formation, however, cannot fully describe the overall progression of material properties observed experimentally[17-20], where extended exposure to humid acid gases is found to progressively amorphize the crystal structure and reduce the surface area of ZIF-8 and related materials. Similar degradation is observed during aqueous exposure; aqueous SO_2 etches the (110) surface of ZIF-8 preferentially[21] and completely amorphizes the structures after extended exposures[22]. Interestingly, these processes are reversible upon appropriate post-treatment, an observation that has allowed synthesis of ZIF materials that are not easy to produce by direct synthesis[23].

In this chapter, we take an initial step towards bridging the gap between a microscopic description of individual defects in ZIF-8 and the long-term degradation observed experimentally. Specifically, we examine whether the existence of isolated

defects in ZIF-8 can promote further appearance of nearby defects. Our approach is motivated in part by previous work on UiO-66, a MOF for which inclusion of defects has been extensively examined[24]. Prior literature shows that UiO-66 can support multiple linker vacancy defects per twelve-coordinated Zr center[25]. These defects occur during crystallization, and their concentration can be tuned in synthesis by the addition of monocarboxylic acid modulators in varying proportions. Furthermore, these defect inclusions tend to cluster in controllable ways[26], analogous to the correlated Schottky vacancies that have been described[27,28] and computationally modeled[29,30] in various transition metal oxides. Computational models indicate that there is a smaller energetic penalty to form defects after removing three or four linkers per metal node, and solution-phase clustering of BDC molecules may further drive linker vacancies in the UiO-66 framework[31].

It is not clear *a priori* if clustering of defects in MOFs will generally be favorable. In the related area of radiation damage in solids, extensive studies have shown that the size of damage-induced defects follows a power law that declines steeply with increasing defect size[32,33,34]. This observation indicates that even events that locally inject enormous amounts (keV) of energy do not typically create a cascade of events leading to large defects. We acknowledge, however, that the analogy between these radiation damage events and degradation during long term exposure to reactive environments is imperfect. In the situation we envisage for MOFs the material is subjected to the possibility of many separate reactive events separated in time rather than the "short, sharp shock" of radiation damage.

In this work, we examine the hypothesis that defect propagation in ZIF-8 is promoted by the presence of existing defects. We showed previously that breaking a Zn-N

bond in ZIF-8 is exothermic, and subsequently cleaving the second Zn-N bond to create a linker vacancy is even less energetically demanding[15]. Here, we investigate a prototypical defect propagation mechanism (using water to cleave the Zn-N bond), examining the dependence of the energy of formation of a second defect on its proximity of the first defect. In this case, we show that defect clustering is energetically favorable, that is, the presence of existing defects favors further defect formation. We then examine examples where H_2SO_4 protonates the Zn-N bond and demonstrate that, in agreement with experimental observations, defect propagation is even more favorable in an acidic environment.

4.2 Simulation Methods

4.2.1 Density functional theory (DFT) calculations

Dispersion-corrected periodic density functional theory (DFT) calculations were performed using the Vienna Ab-initio Simulation Package (VASP) at the general gradient approximation (GGA) level[35], using a restricted Kohn-Sham formalism with projector-augmented wave (PAW) method pseudopotentials and the Perdew-Burke-Ernzerhof (PBE) exchange-correlation functional combined with the DFT-D3 method of Grimme[36]. The ZIF-8 unit cell was obtained from the cubic crystal structure in the Cambridge Structural Database (CSD), which contains 276 atoms with lattice constant 16.99 Å. During geometry optimization of the pristine (defect-free) ZIF-8, both lattice parameters and ionic positions were fully relaxed using a conjugate gradient algorithm with a 600 eV plane wave energy cutoff until interionic forces were smaller than 0.01 eV/Å. The optimized lattice constant was 17.18 Å. The optimized unit cell structure was then used to construct models of the

defect bulk ZIF-8. Lattice parameters were fixed in all the following energy-minimization calculations but atoms were relaxed until interionic forces were smaller than 0.01 eV/Å. A Gaussian smearing function of width 0.2 eV was used to smear the electronic occupation around the Fermi level[37]. The Brillouin zone was only sampled at the Γ-point for all calculations. VASP was used for all calculations involving fewer than 600 atoms.

To examine any possible finite size (i.e. concentration) effects, it was necessary to model defects in a 2×2×2 supercell of ZIF-8. The CP2K 4.1 code[38] with the Quickstep method[39,40] was used for these DFT supercell calculations on more than 600 atoms (Section 4.3.1.) because it is computationally more efficient than VASP. To verify the consistency between CP2K and VASP results, identical 1×1×2 ZIF-8 lattices with and without defects were relaxed using both codes, and the relative energy difference between the defect and defect free lattices were found to be in good agreement; ΔE_{CP2K} = 1.07 eV and ΔE_{VASP} = 1.08 eV, respectively. Parameters for the CP2K calculations were as follows: electronic energy was minimized until the convergence criterion for the self-consistent field procedure (1.0×10^{-7}) was reached using a standard diagonalization method (LAPACK) as implemented in CP2K; Goedecker-Teter-Hutter pseudo-potentials[41,42,43] were used to treat nuclear and core electronic densities; and valence electrons were represented by a mixed Gaussian (MOLOPT-DZVP)[44] and plane-wave (GPW)[45] (with a cutoff of 600 Ry for the finest grid) basis set scheme.

4.2.2 X-ray diffraction (XRD) simulation

Simulated XRD patterns were calculated in Mercury[46] assuming a CuKα radiation source (λ = 1.54056 Å) and symmetric pseudo-Voight peaks with 0.05° full width at half

maximum. Hydrogen atoms were assigned 0.06 $Å^2$ isotropic atomic displacements and all other atoms were assigned 0.05 $Å^2$ displacements.

4.3 Results and Discussion

To probe how bond-breaking reactions in ZIF-8 lead to structural degradation, we pose three sequential questions: (1) Does defect proximity influence the formation energy of subsequent defects? (2) How does defect proximity vary spatially and chemically? (3) Can we extrapolate from what we learn about defect proximity preference to explain degradation in complex environments on long timescales?

We start with the simplest model of a defect formation event: water-induced cleavage of the Zn-N bond in ZIF-8. The defect formation energy, ΔE, is defined as

$$\Delta E = E_{\text{defect ZIF}} - E_{\text{pristine ZIF}} - E_{H2O} \quad (4\text{-}1)$$

where $E_{\text{defect ZIF}}$, $E_{\text{pristine ZIF}}$, and E_{H2O} are the energies of a ZIF structure containing the defect, a defect-free ZIF structure, and an isolated water molecule, respectively. A negative value of ΔE denotes an exothermic reaction. Defect models were constructed in a periodic ZIF-8 unit cell and calculations were performed using the VASP software as described in Section 4.2.1.

Breaking a single Zn-N bond in ZIF-8 creates a dangling linker (DL) defect[14,15,17]. This defect can take several distinct forms, depending on the conformation of the dangling linker and termination of the open metal site. In what we denote the DL-in conformation (**Figure 4.1**, A), the linker remains in the original Zn-Imidazole-Zn plane, and the Zn-Zn distance increases from 6.0 Å to 7.9 Å. In what we denote the DL-out conformation (**Figure 4.1**, B and C), the Zn-Zn distance is closer to 7.0 Å, and the imidazole swings approximately 30° out of the plane. For each of these two conformations, we also need to

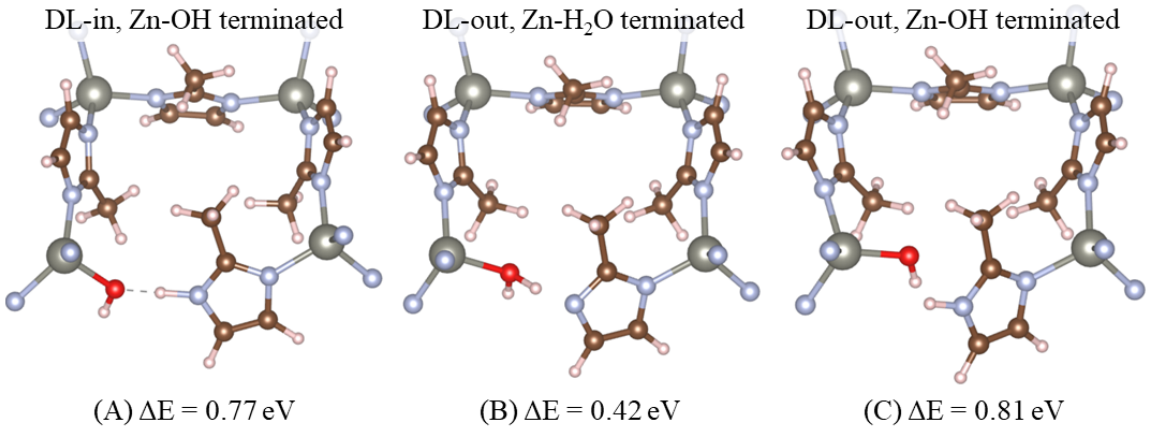

Figure 4.1. Three configurations for an isolated water-induced dangling linker (DL) defect in ZIF-8, and their associated formation energies: DL-in (A) versus DL-out (B, C) and metal terminations Zn-OH (A, C) versus Zn-H_2O (B). The two Zn terminations represent two different reactions, separated by proton transfer. This figure and all subsequent molecular structures were produced using VESTA[47].

consider whether the attacking water molecule adsorbs at the newly created open metal site (**Figure 4.1**, B), or whether it adsorbs and transfers a proton to the dangling imidazole while the remaining hydroxyl terminates the Zn (**Figure 4.1**, A and C). All of the accessible DL states and their associated formation energies are summarized in **Figure 4.1**. These energies are comparable with the single dangling linker formation energy of 0.51 eV calculated by Zhang *et al.*[14], although we point out the different lattice constant and zero damping DFT-D3 correction (as opposed to Becke-Johnson damping) used in this study. While the previous work constructed a representative dangling linker defect, we explicitly constructed distinct defect structures with dramatically different local geometries (DL-in versus DL-out) and proton transfer chemistry (Zn-OH versus Zn-H_2O) in order to fully sample conformation space. We also performed calculations probing the existence of a DL-in, Zn-H_2O terminated defect but in all cases these structures spontaneously relaxed into the more favorable DL-in, Zn-OH state. Termination has more impact than conformation on formation energy of the first defect; B is more favorable than A or C by ~0.35 eV, while

A is only 0.04 eV more favored than C. If only an isolated defect forms, we expect the most energetically stable state B to dominate. With additional DL defects, we can ask if B will always form or if the relative stability of the defects is influenced by their local defect environment. This question is addressed in Section 4.3.2.

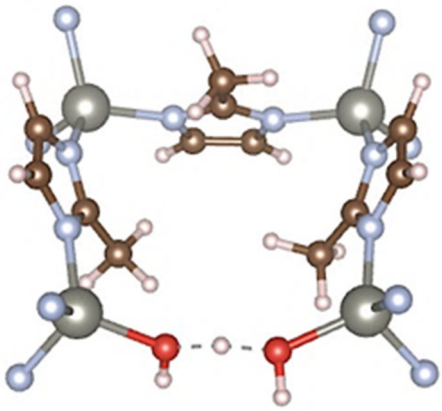

Figure 4.2. A linker vacancy (LV) defect formed by two successive bond-breaking events involving two water molecules. Once both Zn-N bonds attaching a linker to the ZIF-8 framework are hydrolyzed, the liberated imidazole is protonated by one of the water molecules, and the open Zn sites are terminated by hydrogen-bonded water and hydroxyl.

While there are many possible conformations for a dangling linker (DL) defect, there is only one defect state for a linker vacancy (LV) defect, shown in **Figure 4.2**. Two Zn-N water-induced bond-breaking events are required to form this defect. After one of the water molecules donates an H atom to protonate the liberated imidazole, the remaining OH and H_2O hydrogen bond. The linker vacancy formation energy is given as

$$\Delta E_{1LV} = E_{1LV} + E_{HL} - E_{\text{pristine ZIF8}} - 2E_{H2O} = 0.57 \text{ eV}. \quad (4\text{-}2)$$

where E_{1LV} is the energy of a ZIF structure containing a single linker vacancy defect, and E_{HL} is the energy of an isolated protonated imidazole molecule. Again, this energy is comparable to the single linker vacancy formation energy 0.62 eV calculated by Zhang *et al.*[14] However, we can also think of the LV defect as the sum of two successive Zn-N bond-

breaking events on either end of an imidazole linker. Recall that proton transfer is most important distinction for the reaction energy of breaking a single Zn-N bond to form a DL defect. It follows that one of the bond-breaking events required for LV formation involves proton transfer and the other does not; order does not matter because there is a unique product state. We can compare the energy of the linker vacancy to the energies of two isolated dangling linker defects (denoted $E_{1DL,A}$ or $E_{1DL,B}$) as follows

$$E_{1LV} + E_{HL} + E_{\text{pristine ZIF8}} - E_{1DL,A} - E_{1DL,B} = -0.62 \text{ eV}. \quad (4\text{-}3)$$

Since the energy difference between the A and B states was 0.35 eV, it is 0.27 eV more exothermic to form a LV defect than to form two infinitely separated DL defects. If we assume that the linker remains in the pore rather than being removed, as has been recently suggested[16], it is still 0.11 eV more favorable (the E_{HL} term is dropped in Equation 4-3) to form the LV defect than to form two infinitely separated DL defects. This suggests that breaking two nearby bonds is energetically favorable, an observation we examine further in the following section.

4.3.1 Clustered defects are energetically preferred in ZIF-8

The energy required to form a second defect located far in the bulk from a first defect is necessarily independent of the first defect's formation energy. Therefore, preference for or against the formation of additional defects can only be relevant within some distance from an existing defect. Here, we investigate whether proximity is favorable or unfavorable to subsequent defect formation in ZIF-8 and we establish the distance threshold at which the formation of a second defect becomes energetically independent from the first.

Since the linker vacancy is well-defined (it only has one conformation) and already represents a more clustered state than the single bond-breaking event, we can simplify the number of conformations we have to consider by considering the proximity between two linker vacancy defects. This is quantified by measuring the Zn-Zn distance between two OH-terminated metal centers. Given this definition, the closest possible defects are adjacent – two of the four imidazoles to which any one metal center is tetrahedrally coordinated are removed, creating two adjacent linker vacancies that share a Zn vertex. This situation is illustrated in **Figure 4.3**. To examine a range of defect separation distances, we constructed a 2×2×2 supercell. Within this computational volume, the farthest unique Zn-Zn separation attainable while considering periodic images is ~25 Å. We built a series of defect systems with two LVs separated by 0, ~6, ~14, ~20, and ~25 Å (see **Figure 4.3**), which is equivalent to a second LV located 0, 1, 2, 3, or 4 linkers away from a first LV. Formation energies for the 2LV systems (ΔE_{2LV}) and the infinite separation reference ($\Delta E_{2LV,\,\infty}$) are defined as follows:

$$\Delta E_{2LV} = E_{ZIF,\,2LV} + 2E_{HL} - E_{ZIF\,(2\times2\times2)} - 4E_{H2O} \tag{4-4}$$

$$\Delta E_{2LV,\,\infty} = 2 * E_{1LV\,(2\times2\times2)} \tag{4-5}$$

Structures with LVs separated by 0 and ~6 Å were constructed in 1×1×2 supercells and relaxed in CP2K and VASP to ascertain good agreement between the calculation methods (see Section 4.2.1). The optimized LV pairs were then placed into 2×2×2 supercells, and additional 2×2×2 supercells were constructed for LV pairs separated by ~14, ~20 and ~25 Å. CP2K was used to relax this set of 2×2×2 systems and calculate the LV pair formation energies. It is evident from **Figure 4.4** that forming two defects close together (within ~14 Å) is considerably more favorable than forming isolated defects.

Adjacent LVs sharing a Zn vertex (Zn-Zn = 0 Å) require 0.2 eV less energy to form than the infinite separation reference state. More than half this energy, about 0.14 eV, is associated with placing the second defect just one linker away (~6 Å). This indicates a strong preference for adjacent clustering of two linker vacancy defects.

4.3.2 Predicting the likeliest defect pair states

The results above indicate that clustering of LV defects in ZIF-8 is energetically preferred. This motivated us to systematically investigate possible ways to form a second nearby defect and predict the most favorable defect pair states. We already established that at separations beyond 14 Å forming a second LV is energetically independent of the first LV defect, so it is sufficient to consider defect pairs in a single ZIF-8 unit cell with lattice constant ~17 Å. This system size means we could calculate formation energies using VASP, as detailed in Section 4.2.1.

Formation of an initial defect by breaking the first Zn-N bond was thoroughly considered above in terms of the possible conformations and terminations (see **Figure 4.1**). Termination was the most important factor, leading to our identification of an A and B type DL defect representing Zn-OH and Zn-H_2O termination, respectively. Now we ask which bond is most favored to break *next*, after initial defect formation. To answer this question, we have several new considerations. First, the second defect can create a linker vacancy (LV), or it can create a second dangling linker (DL). In the latter case, we also need to examine which dangling linker pair states are most stable. We will further demonstrate at the end of this section that it can be more favorable to create a second dangling linker than to form the linker vacancy.

The remaining considerations in forming a second DL defect have to do with orientation and location. Since the imidazole is only cleaved on one side, there are naturally two ends of the dangling linker defect: the terminated Zn and the dangling linker.

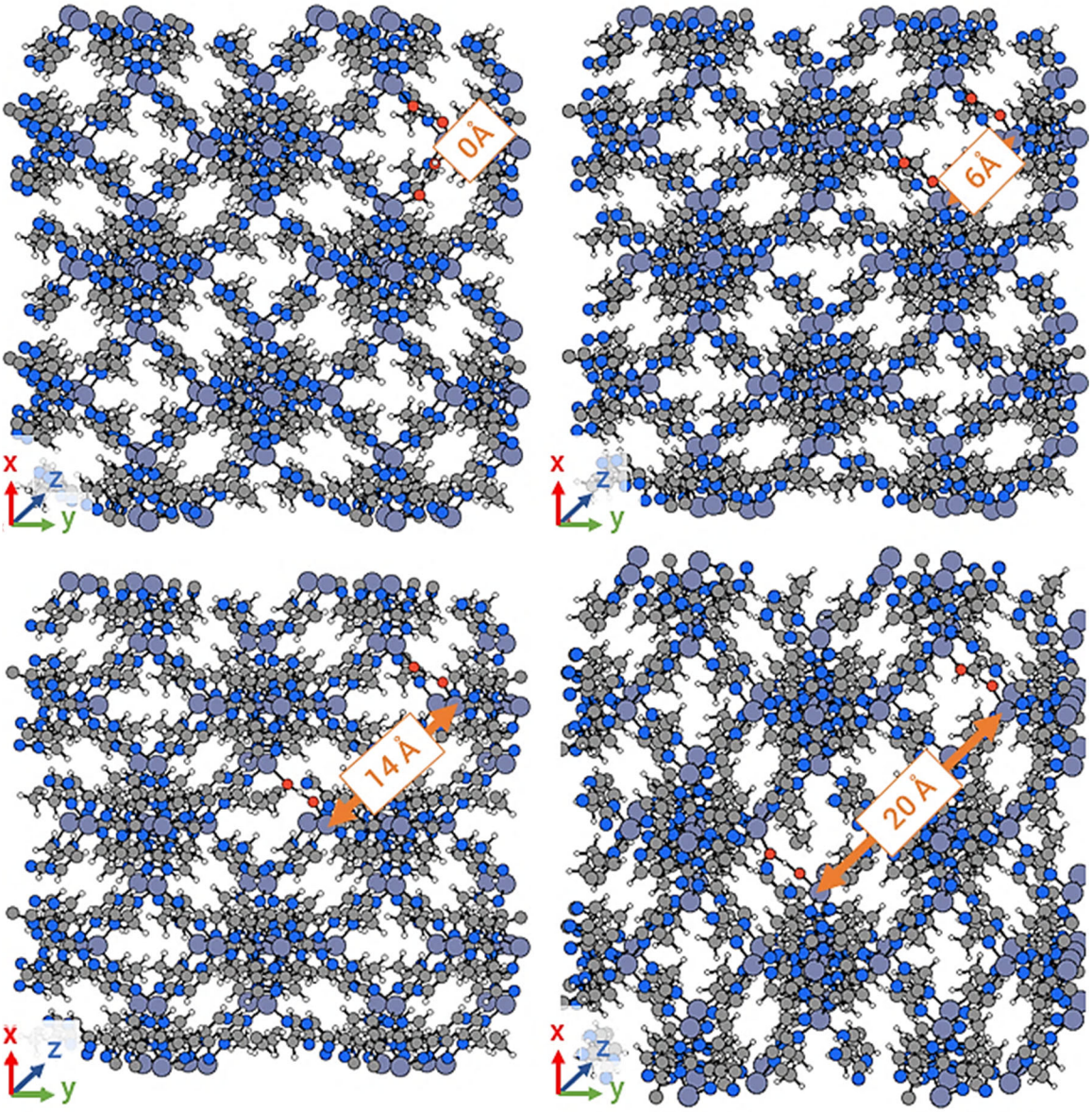

Figure 4.3. Two linker vacancy defects constructed in a 2×2×2 periodic supercell of ZIF-8 and separated by 0 Å (top left), ~6 Å (top right), ~14 Å (bottom left), ~20 Å (bottom right). These four states have the second linker vacancy located 0, 1, 2, or 3 linkers away from the first defect, respectively.

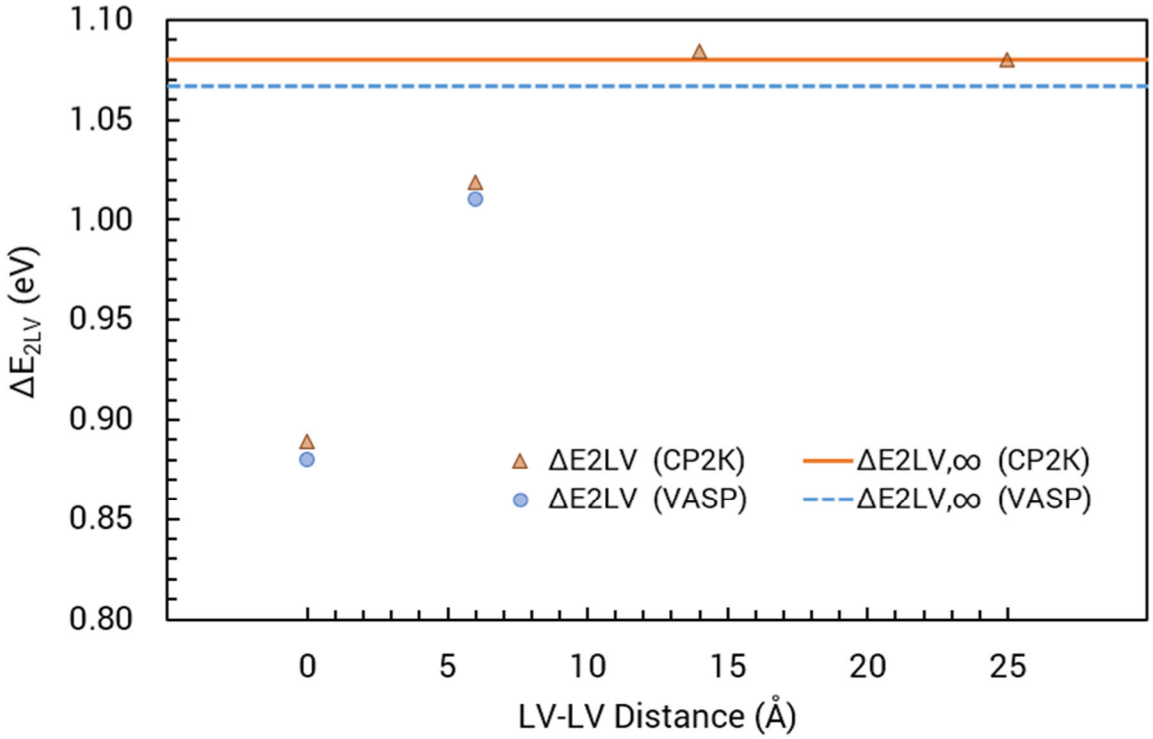

Figure 4.4. Formation energy of a second linker vacancy (LV) defect plotted as a function of its spatial separation from the first LV defect (discrete points), along with the infinite separation reference (horizontal lines). There is good agreement between formation energies calculated using CP2K and VASP.

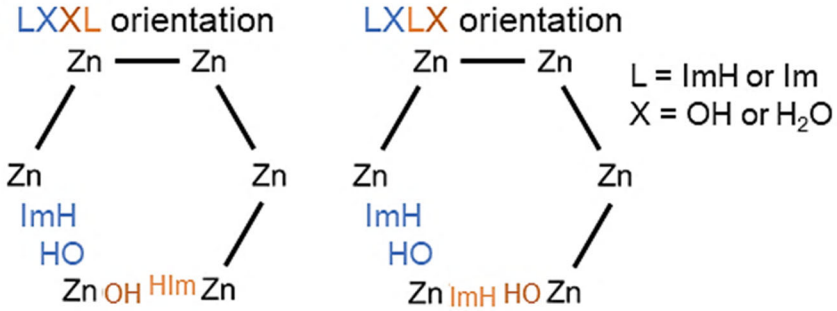

Figure 4.5. The 6-member ring ZIF-8 can be represented by a simplified schematic where the Zn nodes are connected by imidazoles represented as straight lines (black). Water-induced dangling linker (DL) defects are shown as Zn-ImH and OH-Zn. The two rings represent two ways to orient a second DL defect (orange) adjacent to a first defect (blue); the Zn-OH terminated ends can be closest (LXXL orientation) or the dangling Zn-ImH end can be closer to a Zn-OH terminated end (LXLX orientation).

Figure 4.5 illustrates two possible ways to orient a new dangling linker with respect to the first, either with the two terminated ends sharing a Zn vertex (LXXL orientation) or the

dangling linker of one defect closer to the terminated Zn of the other defect (LXLX orientation).

Two additional considerations pertain to the location of the second DL defects, namely adjacency and inclusion in the same ring. **Figure 4.6** shows four combinations of these variations represented in a simplified cartoon of the sodalite (SOD) cage. A single SOD cage is composed of 24 metal nodes and 36 linkers, but the 1×1×1 unit cell of ZIF-8 only contains 12 unique metal nodes (labelled A-L) and 24 unique linkers, shown as the grey Zn atoms and linkers in **Figure 4.6**, respectively. This implies that the SOD cage spans neighboring periodic images of the SOD unit cell, shown as blue Zn atoms and linkers. Therefore, when identifying all the unique Zn-Im-Zn pairs that can form DL defects, a closer site may be contained in a periodic image. Given a first DL defect (highlighted in cyan), the second DL defect (highlighted in orange) can be adjacent ("2DL adj") or separated ("2DL away"). There is additional variation depending on whether both defects are in the same ring, and the size of the ring. ZIF-8 only has 4-member (4M) and 6-member (6M) rings – "adj" defects can either share a 4M ring (**Figure 4.6**, bottom left) or a 6M ring (top left), and "away" defects can share a 4M ring, a 6M ring (top right), or no ring (bottom right, labelled "xN").

Accounting for all the possible combinations of forming a second DL defect given an initial A or B type DL, we built an exhaustive list of thirty-two defect pairs possible in a 1×1×1 unit cell and calculated the energy of each system. These energies are listed in **Table C.1**, where blank entries indicate that a defect state spontaneously relaxed into one of the others.

The results in **Table C.1** show that adjacent, co-terminal DL defect pairs were most favorable. This agrees with the trend we observed for a pair of linker vacancy defects in **Figure 4.4**. By comparing the optimized final geometries of defect structures, we find that conformations with bond angles closest to the ideal tetrahedral bonding angle of 109.5° are more stable. More hydrogen bonding also increases stability, which explains the preference for co-terminal defects over adjacent defects oriented with one terminated end closer to one dangling linker end.

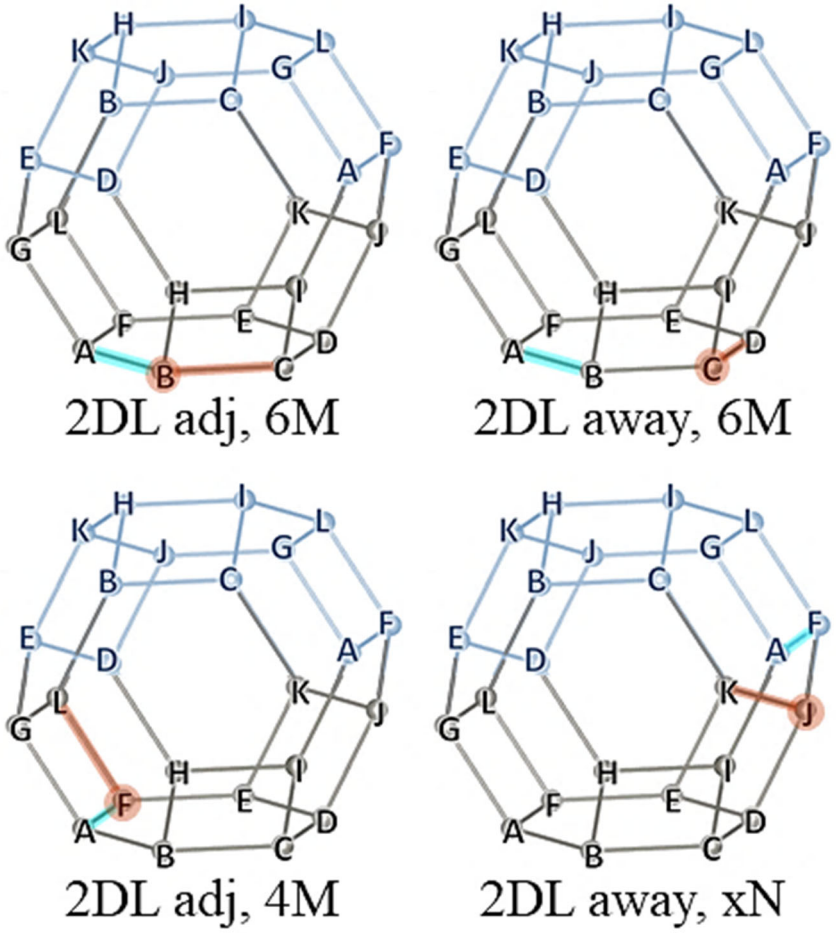

Figure 4.6. A simplified schematic of the ZIF-8 SOD cage is shown where Zn atoms (labelled with letters A-L) are connected by imidazoles (represented as straight lines). Zn atoms and imidazoles within a 1×1×1 unit cell of ZIF-8 are grey, while nodes and linkers from neighboring periodic images are blue. Given a first dangling linker (DL) defect highlighted in cyan, there are multiple choices to place a second DL defect highlighted in orange: the two defects can be adjacent ("2DL adj") or separated ("2DL away"), and they can either share a ring ("4M" or "6M") or not ("xN").

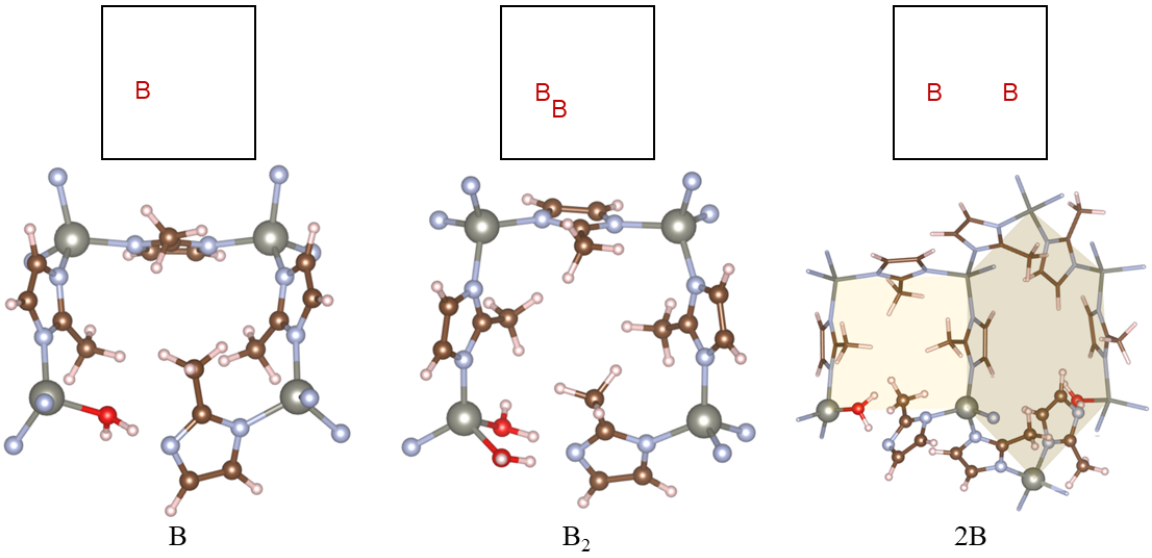

Figure 4.7. All three defects shown here are Zn-OH terminated (type B). From left to right, they are the optimized structures of the first defect B, the adjacent defect pair B_2, and a pair of defects 2B separated by one linker which do not share a ring ("away, xN" in the previously defined terminology).

Based on the above observations, we know the most energetically favorable DL pairs will have adjacent, co-terminal defects. To quantify how much more energetically favorable these systems are compared to other types of defect pairs, we can simplify our description of each defect state using a combination of A and B type dangling linkers. Since the B dangling linker was favored for the first defect, we started by considering the complex defect configurations for a pair of type B defects. **Figure 4.7** shows the single defect (left), a pair of adjacent co-terminal defects B_2 (middle), and a pair of separated defects 2B (right). We can therefore introduce the site-vacancy notation in **Figure 4.7** to indicate possible arrangements in a 1×1×1 unit cell. The energy differences for several scenarios of interest can be summarized using this notation as in **Figure 4.8**.

The results for a pair of Type B defects are shown in **Figure 4.8**. There is a 0.43 eV energetic penalty associated with forming the second defect even one linker's distance away from the first (the 2B state) instead of adjacent to the first (the B_2 state). Slightly

more energy is required to separate a defect pair by an infinite distance (the 2(B) state, which, by definition, requires twice the formation energy of the single type B defect to form). This penalty is 0.59 eV if we start from the adjacent pair, or 0.16 eV if we start with the pair separated by one linker's distance. These results indicate clear preference for a second type B defect to form in a co-terminal orientation at an adjacent location to the first. That is, the answer to the Shakespearean question "2B or not 2B" is, at least in terms of energy preference, "not 2B".

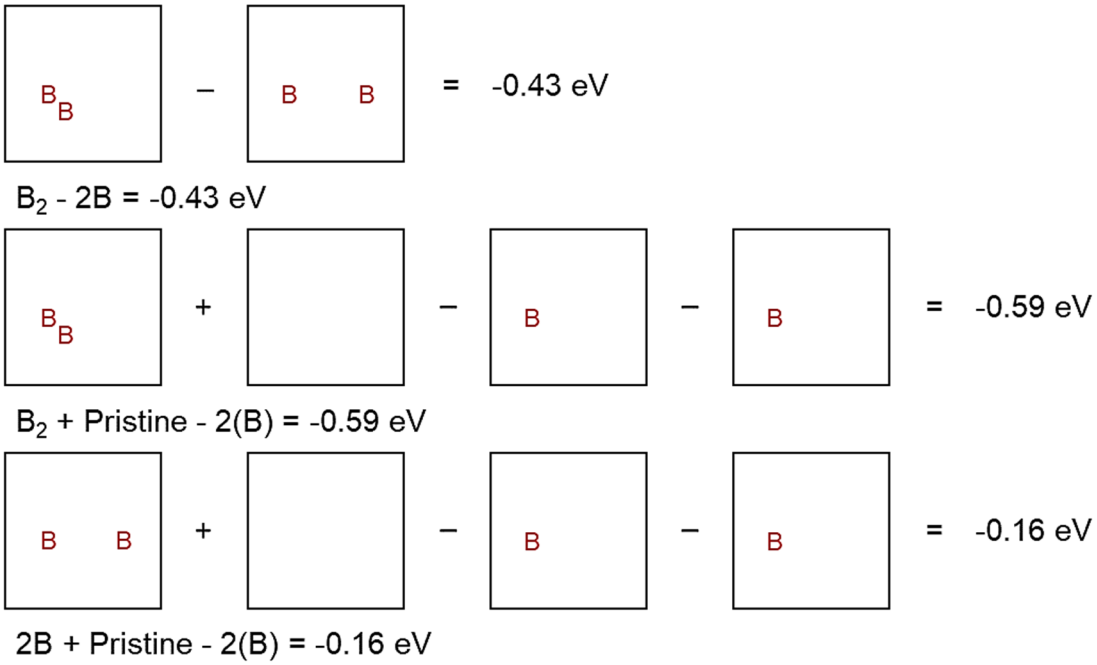

Figure 4.8. Site-vacancy notation describing the energetics of separating a pair of clustered type B defects (top), removing one of a pair of clustered defects infinitely far away (middle), or removing one of a pair of separated defects infinitely far away (bottom). Each black square represents a single ZIF-8 unit cell with periodic boundary conditions. The energies are all exothermic, indicating a preference for clustering.

We can also examine defect pairs containing type A defects. For a pair of type A defects, the A_2, 2A, and 2(A) states are defined in the same way as the B_2, 2B, and 2(B) states. For a mixed pair of type A and B defects, we define the AB state as a pair of adjacent,

co-terminally A and B defects, the A_B state as a pair of A and B defects separated by one linker's distance, and the A+B state as an infinitely separated pair of A and B defects. Site vacancy descriptions similar to **Figure 4.8** for the A only pair and mixed AB pair are included **Figure C.1** and **Figure C.2**.

Figure 4.9 compares the formation energies for all single and pair defect states discussed thus far. There are two main conclusions. First, as we already stated, B has the lowest single defect formation energy (compared to the other single defect states A and C) and therefore we expect that the first defect to form will be type B. However, when we add a defect, having two A defects adjacent and co-terminal is the most favorable pair defect state – the A_2 defect shown in **Figure 4.9** (inset) has the lowest formation energy among all single and pair defects, although the B_2 state has a comparable formation energy. It is surprising and significant that the clustered defect pair is more stable than the single defect system, indicating that the energy gain from clustering is larger in magnitude than the single defect formation energy.

To understand why the less favorable single defect A suddenly becomes more favorable when a second, adjacent A defect is introduced, we posit that the dangling linker formation energy can be split into the sum of an intrinsic energy cost to hydrolyze a Zn-N bond, ϵ, plus a "strain" cost of the surrounding framework distorting to accommodate the dangling linker, σ. Therefore, for the first defect:

$$\Delta E_{1DL} = E_{\text{defect ZIF}} - E_{\text{pristine ZIF}} - E_{H2O} = \epsilon + \sigma \tag{4-6}$$

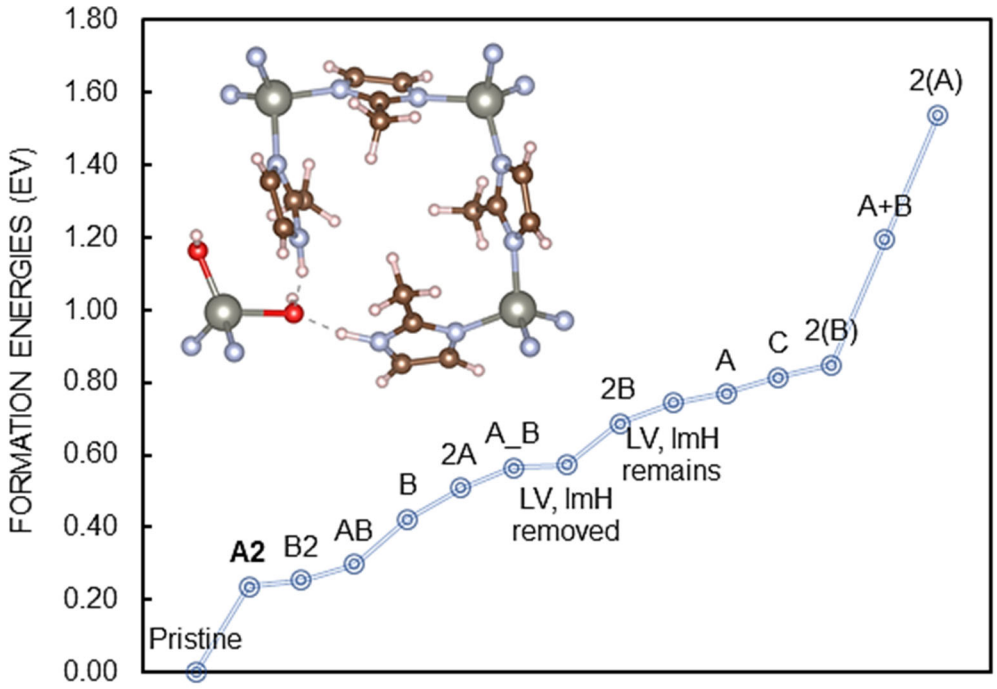

Figure 4.9. Formation energies of ZIF-8 systems with no defects, single defects, and defect pairs. The A_2 defect pair is the most stable configuration and its geometry is shown in the inset. The A_2, B_2, and AB defect pairs are oriented co-terminally and located adjacent to one another. The 2A, 2B, and A_B defect pairs are located one linker's distance apart. The 2(A), 2(B), and A+B defect pairs are located infinitely far away from one another. We also considered both linker vacancy defects where the freed linker remains near the pore window (ImH remains), and where it has diffused away (ImH removed).

If forming a second adjacent dangling linker can relieve the strain cost fully by introducing more flexibility into the larger defect site, the overall energy required to introduce two dangling linkers would be double the intrinsic energy cost:

$$\Delta E_{2DL} \approx 2\epsilon \tag{4-7}$$

In this description, the intrinsic energy cost is assumed to be approximately independent of conformation since it only depends on the nature of the Zn-N bond being broken. If this simple description is valid, the difference in energy cost to form A, B, and C type defects should be entirely explained by the strain cost, which is alleviated in the subsequent A_2,

B_2, and C_2 defects, respectively. We independently estimated ϵ and σ from the formation energies for single and pair defect states, giving the results in **Table 4.1**. These results show that the intrinsic energy cost is consistently ~0.13 eV, with significantly more variation in the strain cost for the three defect types. This approximate analysis strongly suggests that propagation of bond-breaking defects is favorable when clustering of defects creates conformations where framework strain is alleviated. This observation may be useful in considering the potential clustering of defects in a much broader range of MOFs than the single example of ZIF-8 that we have considered here.

Table 4.1. Formation energies (all in eV) of single and pair dangling linker defect states, decomposed into the sum of the intrinsic energy cost ϵ to hydrolyze a Zn-N bond and the strain cost σ of accommodating framework deformation due to the dangling linker.

Defect	$\Delta E_D = \epsilon + \sigma$	$\Delta E_{D2} = 2\epsilon$	ϵ	σ
A	0.77	0.24	0.12	0.65
B	0.42	0.25	0.13	0.30
C	0.81	0.25	0.13	0.69

4.3.3 Acid gas hydrolyzed defect pairs

Previous work has demonstrated that ZIF-8 degrades readily upon exposure to humid SO_2 and DFT calculations supported the conclusion that energetics of defect formation were significantly more favorable with H_2SO_4 (rather than H_2O) as the protonating species[17]. Here we extend that analysis by examining pairs of defects, replacing H_2O with H_2SO_4 as the acid. Based on the previous definitions of an A and B type single DL defect, depending on whether a proton is transferred from the acid to the dangling imidazole linker, we can similarly define an α and β structure for the first H_2SO_4 defect as shown in **Figure 4.10**. The formation energy of this first defect is given as

$$\Delta E_{1DL,H2SO4} = E_{\text{defect ZIF}} - E_{\text{pristine ZIF}} - E_{H2SO4} \quad (4\text{-}8)$$

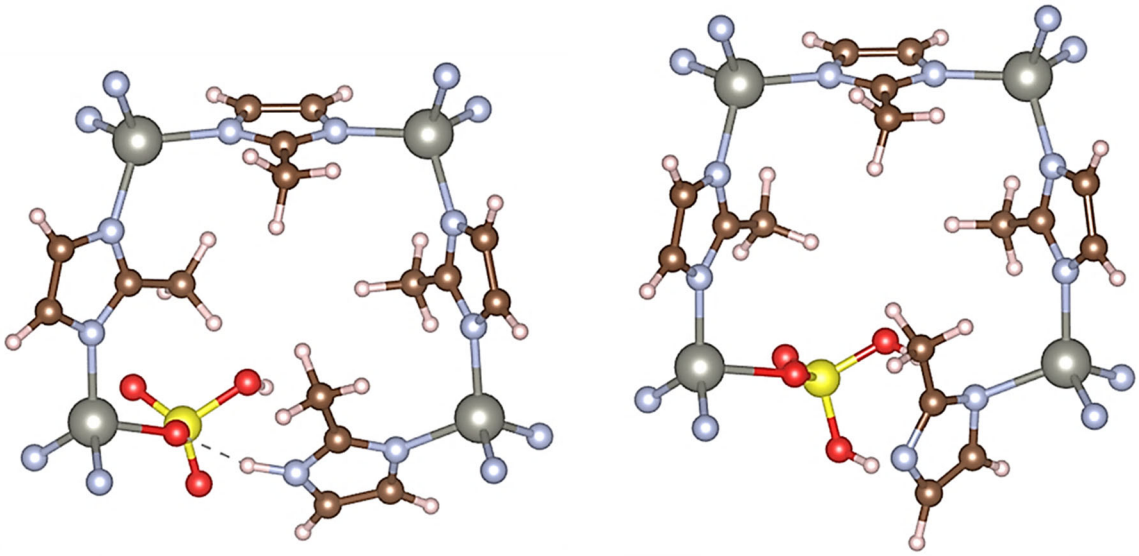

Figure 4.10. Single dangling linker defect states α and β for H_2SO_4-induced defects. The α state with proton transfer is exothermic while the β state is not.

Unlike the single water-induced defect, the α state where sulfuric acid transfers a proton to the dangling imidazole linker is preferred; the β state has a non-spontaneous formation energy (see **Figure 4.10**). This is likely due to the much higher Bronsted acidity of sulfuric acid vs. water, making proton transfer much more favorable. Based on our previous defect pair calculations involving water, we focus on the A_2 and AB states with H_2SO_4 as the degradation agent. We consider systems where one or both water molecules are replaced by sulfuric acid – the αA and αB states or the α_2 and αβ states, respectively. The reaction energy for these four defect pair states αD (D = α, β, A, or B) are calculated as shown in Equations 4-9 and 4-10, where $\Delta\Delta E_{\alpha D}$ compares the change in energy of replacing water with sulfuric acid in an otherwise identical reaction.

$$\Delta E_{\alpha D} = E_{\alpha D} + E_{\text{pristine ZIF}} - E_{\alpha} - E_{D} \tag{4-9}$$

$$\Delta\Delta E_{\alpha D} = \Delta E_{\alpha D} - \Delta E_{AD} \tag{4-10}$$

When only one water is substituted with H_2SO_4, the reaction energies are significantly more exothermic than the defect pair reaction energies with only water: $\Delta\Delta E_{\alpha A}$ = -0.55 eV and $\Delta\Delta E_{\alpha B}$ = -0.97 eV. This agrees with previous work[17] that degradation in ZIF-8 is accelerated by humid SO_2. However, when both water molecules are replaced with sulfuric acid, the reaction energies are no longer significantly more exothermic than the H_2O pair defects, $\Delta\Delta E_{\alpha_2}$ = -0.08 eV and $\Delta\Delta E_{\alpha\beta}$ = 0.52 eV. This may be due to steric reasons – H_2SO_4 is a larger molecule than H_2O – or it may indicate that the presence of water is necessary to creating a favorable αA or αB intermediate state.

4.3.4 Thermodynamics of additional defect propagation

Having exhaustively considered the relative formation energy for defect pairs, we now want to determine whether it is energetically preferable to introduce a third DL adjacent to pre-existing defects or some distance away from them. The combinations of possible triplet defect states are too extensive to be exhaustively explored, as we have done with the defect pairs. Instead, we show four sample triplet defect states in **Figure 4.11**; their corresponding defect formation energies (referenced to energy of pristine ZIF-8 and three isolated water molecules) are plotted in comparison to the defect pair formation energies in **Figure 4.12**. Two of these defect triplets (States III and IV in **Figure 4.11**) have lower formation energy than any other defect state we have examined. Some of this energetic gain from additional clustering may be due to finite size effects as we add more and more defects into a unit cell simulation model. Nevertheless, the existence of these energy downhill states suggests that adding multiple defects can reduce the overall formation energy of the system, leading to spontaneous defect propagation. It is interesting to note that the most preferred configurations for three DL defects are to share a 6M ring;

recall that for DL pairs, defects located adjacent and co-terminal in the same 4M ring were preferred. We attribute this to the increased strain cost of adding a third DL in the same 4M ring, which is less pronounced in the same 6M ring because the larger ring has more flexibility to accommodate the defects.

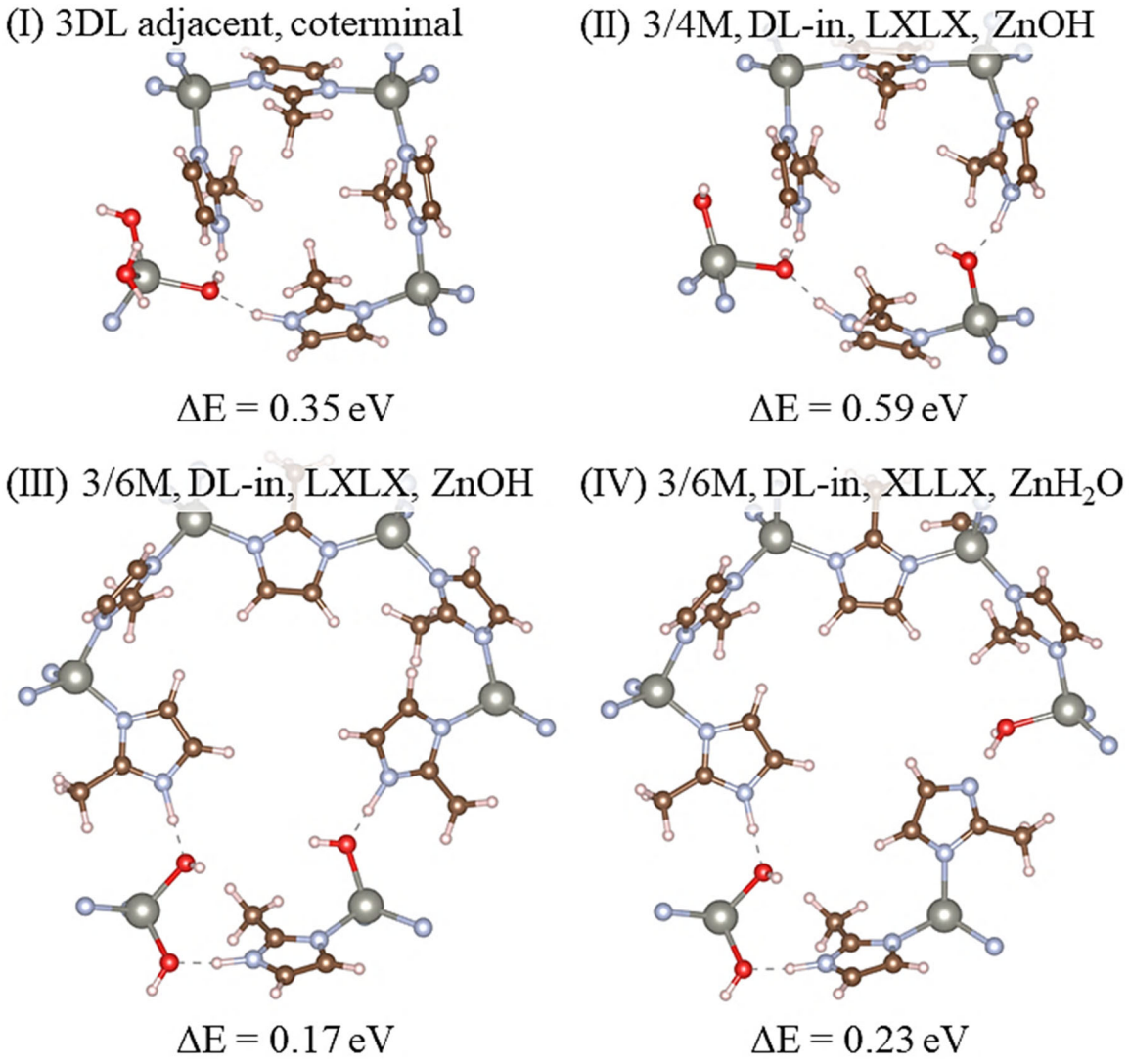

Figure 4.11. Four examples of triple defect states where water hydrolyzes three Zn-N bonds in each system to form three dangling linker defects. The three defects can be located, relative to one another, adjacent and co-terminal (I), sequentially around the same 4M ring (II), or sequentially around the same 6M ring (III and IV).

If we were to extend the above procedure, our data seems to suggest that we could identify energetically favorable states with four defects, five defects, and so on, ultimately leading to amorphization. However, it is worth noting that we have not considered entropic contributions to the defect formation process. In particular, we expect a significant increase in conformational entropy as we add more dangling linkers to the structure. At the same time, since our calculations assume that the proton-donating agent is adsorbing from the gas phase, there is a non-trivial loss of entropy associated with each adsorption event (this is less significant if the proton donor is in the solution phase). A comprehensive investigation of defect propagation must assess the entropy and free energy of the system, which is beyond the scope of the present work.

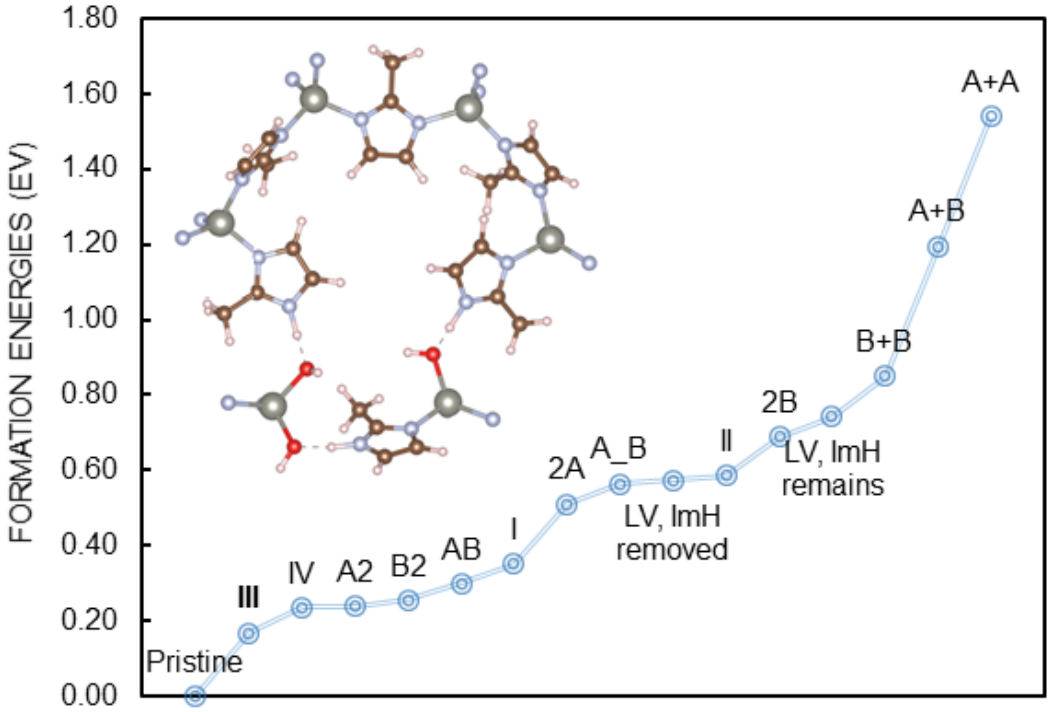

Figure 4.12. Formation energies of ZIF-8 systems with two and three defects, referenced to the pristine ZIF-8 structure. The defect triplets from **Figure 4.11** are labelled I, II, III and IV. The defect triplet labelled III (see **Figure 4.11**) is the most stable structure and its geometry is shown in the inset figure. III and IV both demonstrate examples of triple defect states with lower overall formation energy than any other defect structure.

4.3.5 Diffraction patterns of defective materials

The results above provide compelling evidence that formation of point defects in ZIF-8 can be self-propagating in the sense that the presence of initial defects favors the formation of additional nearby defects. It is useful to consider whether this description of defect formation can be connected with experimental observations of degraded materials. We have made an initial attempt to tackle this challenging task by comparing the simulated powder pattern for various models of defective materials with experimental X-ray diffraction (XRD) measurements of ZIF-8 exposed to corrosive environments. **Figure 4.13** shows experimental PXRD spectra from previous work by Bhattacharyya *et al*. for ZIF-8 exposed to 20 ppm of humid SO_2 for 5, 10, and 15 days, with each spectrum normalized to the highest intensity peak.[17] A simulated powder pattern for pristine ZIF-8 is shown for reference. Degradation of the material is associated with loss of peak intensity, an increase in broad amorphous background, changes in peak position, and the appearance of peak splitting or new peaks. The main changes in peak position are highlighted in **Figure 4.13** (labelled a-g) and they are most pronounced in the spectra taken after 10 days of exposure. After 15 days of exposure, the BET surface area of the material had decreased by 55% relative to the pre-exposed material and the crystallinity relative to the sample after 10 days of exposure was reduced.

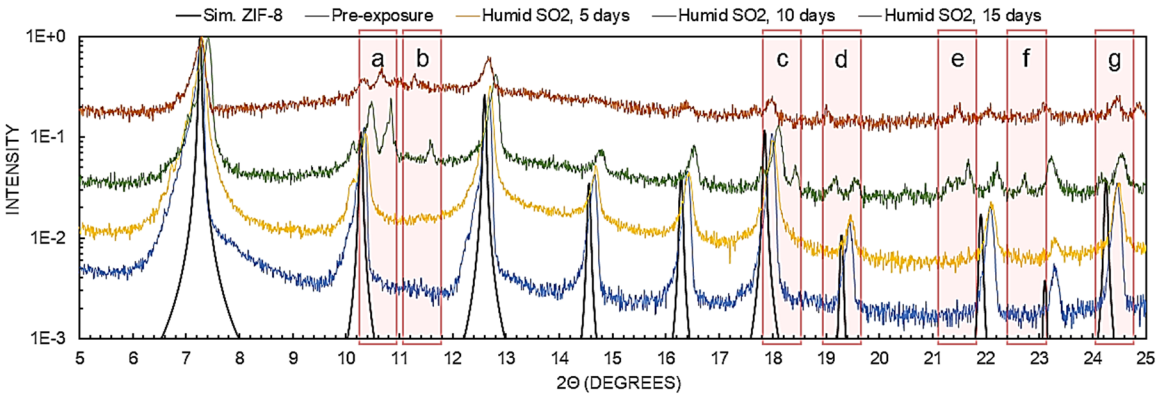

Figure 4.13. Experimental XRD spectra of ZIF-8 after exposure to humid SO_2 for 0, 5, 10, and 15 days, with the simulated powder pattern of pristine ZIF-8 shown for comparison. Each spectrum has been normalized to the highest peak intensity; no offset was used in plotting the spectra. The main instances of peak splitting and new peaks are highlighted in red and labelled a-g. Experimental data was obtained from Bhattacharyya *et al.*[11]

When considering whether models of defective structures might give insight into the experimental spectra, we can identify two extremes; one where isolated defects are spread throughout the material, and one where we have a clustered pocket of defects in an otherwise pristine material. Our earlier predictions about defect clustering behavior would suggest the latter is more likely to occur, especially in earlier stages of degradation.

To model the clustered defects, we considered two cases representing degradation restricted to a pocket of defects. We defined the simulation models by constructing 3×3×3 superlattices and introducing defects only in one 1×1×1 cell. In one case, all the linkers in the defect pocket were cleaved from the Zn framework and removed, creating a vacant defect pocket. This was approximated by a 3×3×3 simulation volume with all the atoms in one unit cell removed. In the second case, we considered a system where all the linkers in the defect pocket have been cleaved and the pocket subsequently collapses into a dense, amorphous phase. This amorphous pocket was represented by a 3×3×3 simulation model with all the atoms in one 17×17×17 $Å^3$ unit cell randomly moved to new positions within

a 14×14×14 $Å^3$ volume centered within the unit cell. In both cases, we broke all 48 Zn-N out of a total 1,296 Zn-N bonds in the 3×3×3 superlattice, giving a defect concentration of 3.7% calculated in terms of the number of Zn-N bonds. Clearly neither of these simple models accurately represents the atomic structure of a fully evolved cluster of defects, but they can provide some initial intuition. **Figure 4.14** shows simulated XRD spectra for the vacated (blue dashed line) and amorphous (blue dotted line) defect pockets. In both cases, the minor changes that appear in the spectra are not similar to what is seen experimentally. This suggests that while it seems likely that defect "pockets" can appear in the initial stages of degradation, these structures will not have a simple experimental signature accessible by powder XRD.

To model materials with spatially separated defects, we started by randomly inserted one dangling-linker defect per unit cell in a 1×1×1 superlattice. Breaking one Zn-N bond out of 48 total bonds in every unit cell gives a 4.1% defect concentration. Unlike the clustered defect model, however, the simulated spectra of the 1 defect/cell bulk structure (see **Figure C.4**) showed a sharp increase in background signal. Many of these new peaks are likely to be artefacts related to the specific periodicity of our simulation. To distinguish the new features that are caused by defects, we constructed additional 2×2×2 and 5×5×4 superlattices with 1 dangling linker defect independently inserted at random in each unit cell. The XRD simulated spectra for these models (see **Figure C.5**) showed variation in the amount of background signal. Unsurprisingly, the largest simulation volume (5×5×4 superlattice) most closely approximates a macroscopic bulk structure, showing background most similar to the background broadening we measure experimentally. Several peaks consistent across varying simulation size are indicated by

black arrows in **Figure C.5**. We also tested sensitivity to the overall concentration of defects by building models where we randomly introduced 1 dangling linker defect per 1×1×1 unit cell, 1 defect per 2 unit cells (0.5 defects/cell), or 1 defect per 3 unit cells (0.3 defects/cell) into a 3×3×3 superlattice. Reducing the defect concentration to 0.3 defects/cell significantly reduces background noise in the simulated XRD spectrum (see **Figure C.6** in Appendix C), but we find that three of the new peaks consistent across simulation size are also robust to the defect concentration, as indicated by black arrows in **Figure C.6**. These peaks occur at approximately 11.5°, 21.3° and 23.7°, corresponding to diffraction from the $(6\ 0\ \bar{3})$, $(12\ 0\ 3)$, and $(12\ 6\ 3)$ lattice planes, respectively. The reason that these particular high index lattice planes appear is not obvious to us.

Finally, we modeled a "severely degraded" limit of high defect concentration. Since experiments have shown that degraded ZIF-8 can be recovered to its pristine state through immersion in a linker-rich solution[21], we constructed two examples of this degraded state by adding to all atomic positions in a 3×3×3 superlattice a random shift drawn from a Gaussian distribution with mean $\mu = 0$ Å and standard deviation $\sigma = 0.05$ Å (**Figure 4.14**, dashed red line) or $\sigma = 0.1$ Å (**Figure 4.14**, solid red line) in three dimensions. Although these structures are not easily recognized as ZIF-8, they retain similar long-range periodicity to the pristine state, seen in the consistency of the major peaks. We can compare them to the experimentally exposed material (**Figure 4.14**, green line) as well as the main changes in peak position previously identified for the degraded structure. Significant blurring of the atomic positions ($\sigma = 0.1$ Å) is necessary to produce amorphous background comparable to that seen in experimental spectra for degraded ZIF-8; the bulk model with only slight blurring has negligible background. While there are features in this model that

resemble features attributed to defects in the experimental degraded structure, they are not sufficiently distinguishable from the overall background noise. However, it is interesting to note that the same peaks identified earlier at 11.5°, 21.3° and 23.7° are present (**Figure 4.14**, black arrows) in both bulk defect models with slight blurring and significant blurring of the atomic positions. Additionally, the peaks at 11.5° and 21.3° may match experimental features b and e.

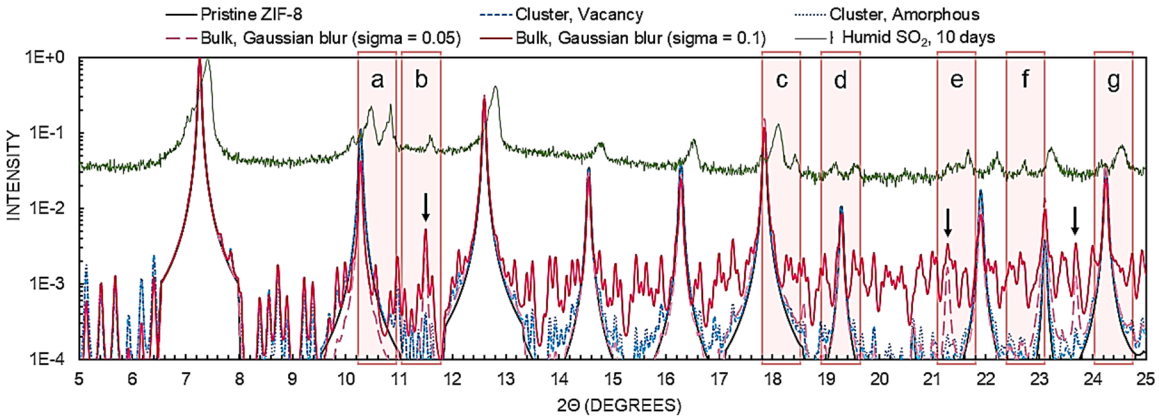

Figure 4.14. Simulated XRD patterns of ZIF-8 where defects are clustered in a single cell of a 3×3×3 superlattice (blue, short dashed and dotted), and where the bulk of the 3×3×3 superlattice is degraded (red, dashed and solid). The clustered defect structures and slightly degraded bulk structure (red, dashed) show little change from the pristine ZIF-8 spectra, but the severely degraded structure (red, solid) shows significant increase in amorphous background and new peaks (black arrows). Experimental data of ZIF-8 exposed to 20 ppm of humid SO_2 for 10 days is shown in green (from **Figure 4.13**), with the same peak splitting and new peak features highlighted as from **Figure 4.13**. All spectra are normalized to their highest peak.

We have identified defect models where the simulated power patterns are comparable to the experimental XRD spectra of degraded ZIF-8 structures in increased background noise and new peaks. The intensity and broadness of background noise are dependent on system size, but the new peaks around 11.5° and 21.3° are consistent even when we vary the system size (2×2×2, 3×3×3, or 5×5×4 systems), defect concentration (1 defect/cell, 0.5 defects/cell, and 0.3 defects/cell), and type of defect (dangling linker, or

Gaussian blurred). This suggests that even though powder XRD is a spatially averaged technique, there may be some signatures of local degradation of ZIF-8 that are detectable using XRD.

4.4 Conclusion

In this chapter, we have focused on the sequence of events that ultimately leads to degradation of ZIF-8, a prototypical MOF, in the presence of adsorbed water or humid acid gases. Using DFT calculations, we considered a wide range of scenarios for forming single or pair defect states in ZIF-8. We demonstrated that defect proximity reduces the formation energy of the second defect in a pair of defects. We also showed that the formation energy can be further reduced when a third defect is added in close proximity to an existing pair of defects. These observations strongly suggest the spontaneous formation of clusters of defects in ZIF-8 is likely in any situation where initial formation of isolated point defects will occur. In the case of defect pairs, adjacent and co-terminally located defects are favored. Among the limited set of defect triplets we considered the most energetically preferred states place the defects in 6M rings of ZIF-8 where the larger ring size can more flexibly accommodate them. A simple description that approximates the defect formation energy as the sum of an intrinsic bond-breaking cost that is independent of defect type or clustering and a strain cost associated with the local geometry and conformation around the defect site is a useful way to understand our results. This is a mechanism that is likely not restricted to ZIF-8 defects; it seems likely that a similar description will be helpful in assessing the preference for defect clustering in other MOFs.

Our DFT calculations have only examined the thermodynamics of defect clustering. The energetic preference for defect clustering suggests it is plausible that the

activation energies for creating new defects adjacent to existing defects are lower than for creating isolated defects, but we have not directly tested this hypothesis. We also cannot conclusively state that the energetic preference for defect clustering continues as the defect clusters continue to increase in size. The description given above in terms of strain relaxation hints that defect clustering is unlikely to self-terminate, but we cannot categorically rule out the possibility that configurations of more than three defects exist for which the strain cost of adding additional defects increases with cluster size.

Finally, we qualitatively considered how our calculations, which focused on water-induced defects, relate to experimentally observed degradation of ZIF-8 in the presence of humid SO_2. Our DFT calculations compared the energetics of defect propagation when we substitute water in our models with sulfuric acid and found that partial substitution results in a much more favorable degradation reaction, in agreement with the experimental observation that humid SO_2 degrades ZIF-8 much more severely than humidity alone. Second, we constructed a variety of defect models and compared the simulated powder patterns against experimental XRD spectra for degraded ZIF-8. We find new peaks around 11.5°, 21.3°, and 23.7° robust to variation of system size, defect concentration, and defect type; these peaks are likely indicative of defect presence and may match new features observed in the experimentally degraded structure.

APPENDIX C. SUPPORTING INFORMATION FOR CHAPTER 4

Table C.1. Formation Energies (in eV) of All Possible First and Second Defects

1st Defect: Dangling Linker								
(A)	DL-in, Zn-OH	0.77						
(B)	DL-out, Zn-H_2O	0.42						
(C)	DL-out, Zn-OH	0.81						
2nd Defect: Linker Vacancy								
	Linker removed	0.57						
	Linker remains	0.74						
2nd Defect: New Dangling Linker								
	DL-in				DL-out			
	LXXL orientation		LXLX orientation		LXXL orientation		LXLX orientation	
	Zn-H_2O	Zn-OH	Zn-H_2O	Zn-OH	Zn-H_2O	Zn-OH	Zn-H_2O	Zn-OH
adj, 4M	0.30	0.69	0.69		0.49	0.24	0.69	0.67
adj, 6M		0.91	0.66	0.46	0.22	0.04	0.88	0.88
away, 6M	0.45	0.42		0.25	0.53	0.97	0.66	1.00
away, xN	0.57	0.37	0.61	0.51	1.03	0.85	0.56	1.10

C.1 Site-vacancy Notation Describing A-Type Defect Pairs and Triplets

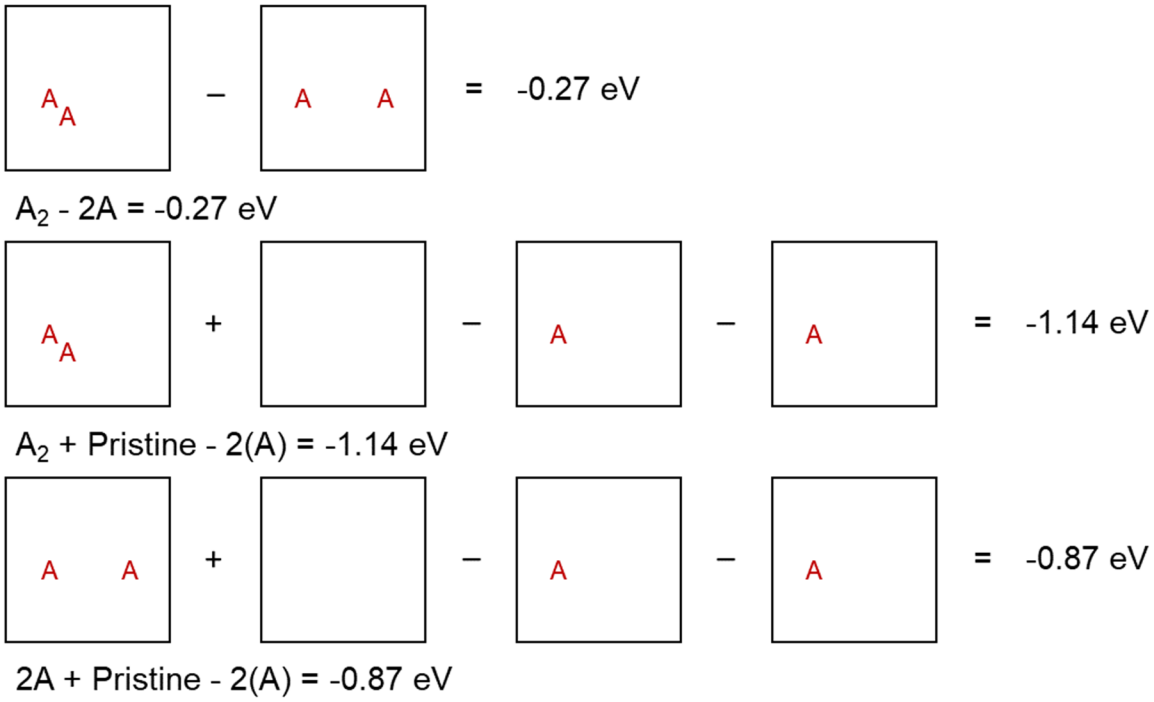

Figure C.1. Site-vacancy notation describing the energetics of separating a pair of clustered type A defects (top), removing one of a pair of clustered defects infinitely far away (middle), or removing one of a pair of separated defects infinitely far away (bottom). Each black square represents a single ZIF-8 unit cell with periodic boundary conditions. The energies are all exothermic, indicating a preference for clustering.

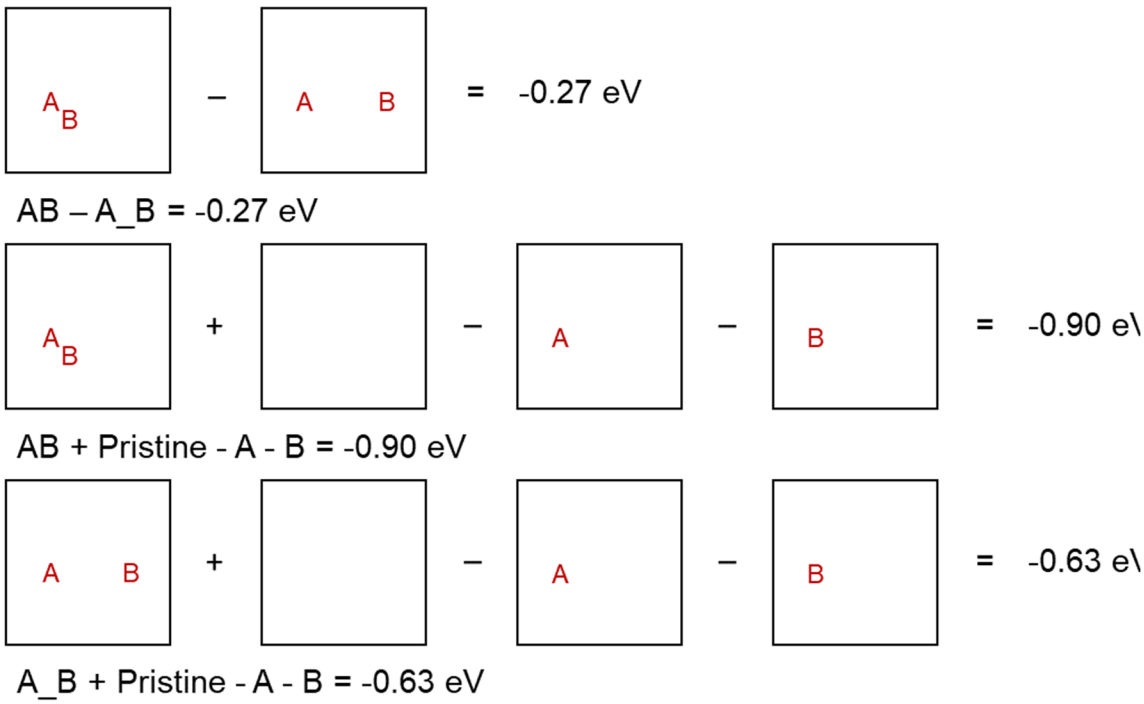

Figure C.2. Site-vacancy notation describing the same three processes as in **Figure C.1** for a mixed pair of defects. The energies are all exothermic, indicating a preference for clustering.

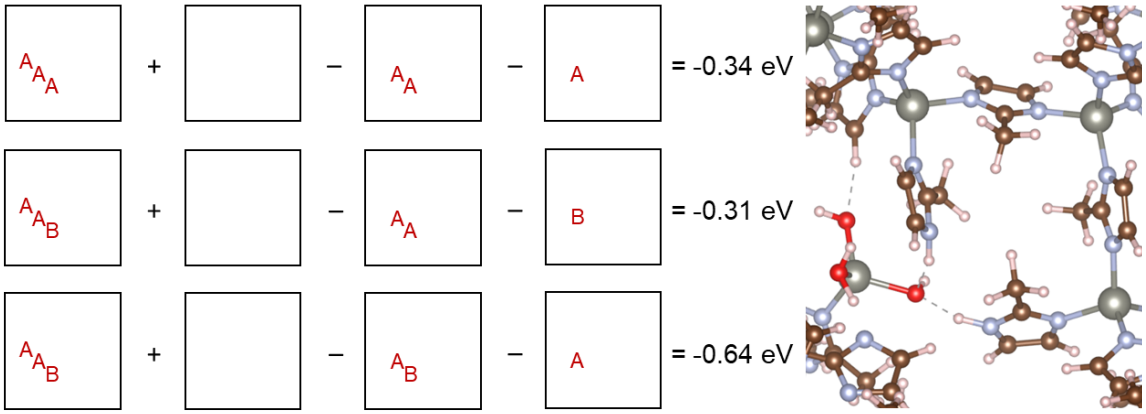

Figure C.3. Site-vacancy notation for removing one defect out of a type A triplet cluster (top), removing the type B defect out of an AAB triplet cluster (middle), and removing one type A defect out of an AAB triplet cluster (bottom). The geometry optimized AAB cluster is also shown in the right.

C.2 Additional Simulated XRD Patterns

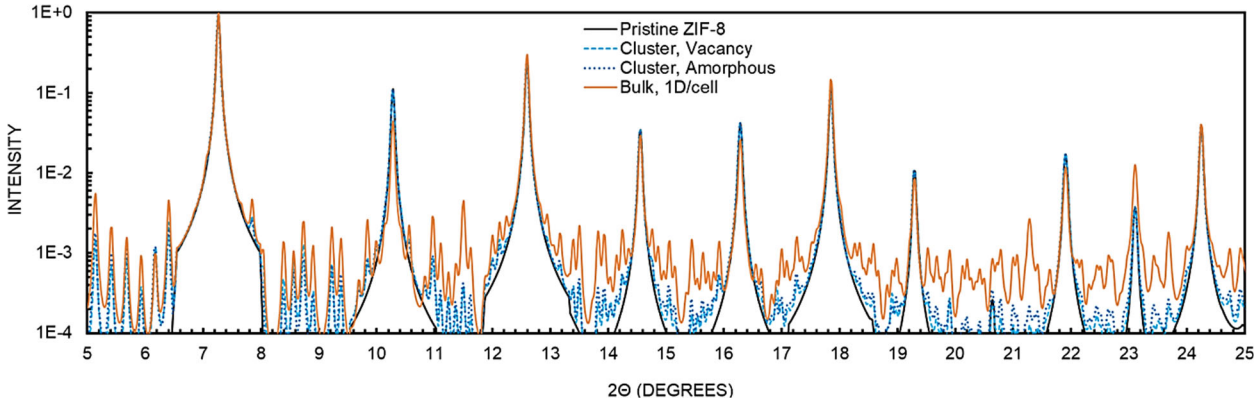

Figure C.4. Simulated XRD patterns of ZIF-8 with ~4% defect percentage distributed randomly throughout a bulk 3×3×3 superlattice (orange) or clustered in single unit cell of a 3×3×3 superlattice (blue)

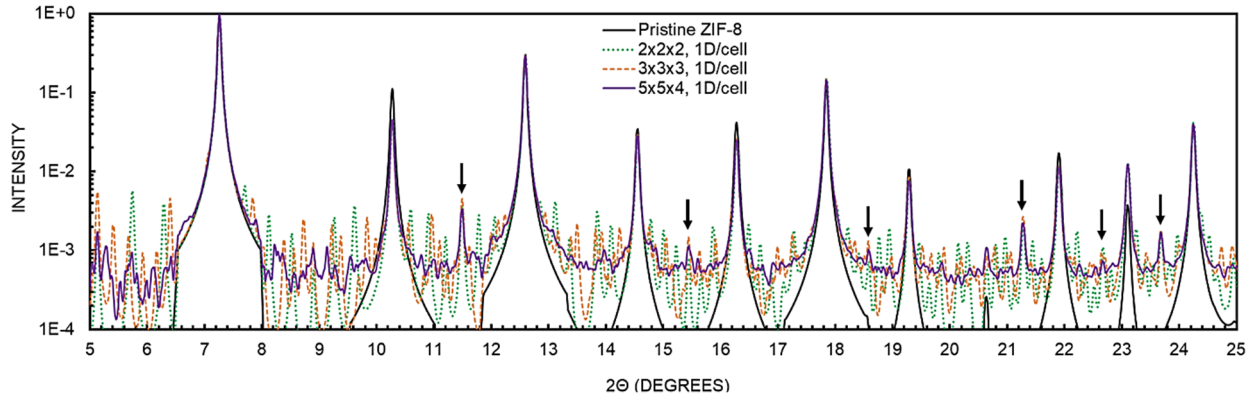

Figure C.5. Simulated XRD patterns of ZIF-8 with one randomly inserted defect per cell in a 2×2×2, 3×3×3, and 5×5×4 superlattice (~4% defect percentage). New peaks consistent across all simulation sizes are indicated by black arrows.

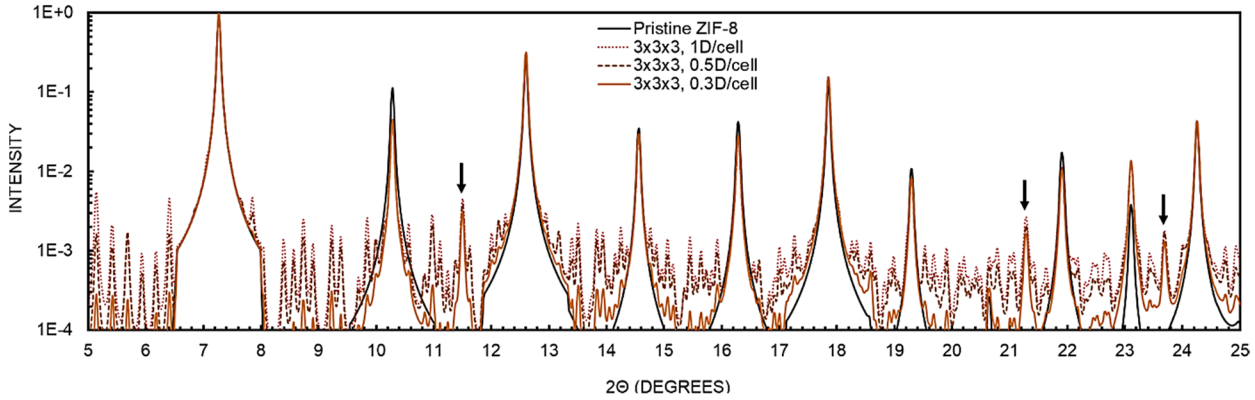

Figure C.6. Simulated XRD patterns of ZIF-8 with one randomly inserted defect per one cell, two cells, and three cells in a 3×3×3 superlattice. New peaks at 11.5°, 21.3°, and 23.7° are consistent across all defect concentrations (indicated by black arrows), and were also previously observed to be robust to simulation size (**Figure C.5**).

C.3 REFERENCES

1. Banerjee, R.; Phan, A.; Wang, B.; Knobler, C.; Furukawa, H.; O'Keeffe, M.; Yaghi, O. M., High-Throughput Synthesis of Zeolitic Imidazolate Frameworks and Application to CO_2 Capture. *Science* **2008**, *319*, 939-943.

2. Sholl, D. S.; Lively, R. P., Seven Chemical Separations to Change the World. *Nature* **2016**, *532*, 435-437.

3. Keskin, S.; van Heest, T. M.; Sholl, D. S., Can Metal-Organic Framework Materials Play a Useful Role in Large-Scale Carbon Dioxide Separations? *Chem Sus Chem* **2010**, *3*, 879-91.

4. Howarth, A. J.; Liu, Y.; Li, P.; Li, Z.; Wang, T. C.; Hupp, J. T.; Farha, O. K., Chemical, Thermal and Mechanical Stabilities of Metal–Organic Frameworks. *Nat Rev Mater* **2016**, *1*, 15018.

5. Zhou, K.; Mousavi, B.; Luo, Z.; Phatanasri, S.; Chaemchuen, S.; Verpoort, F., Characterization and Properties of Zn/Co Zeolitic Imidazolate Frameworks vs. ZIF-8 and ZIF-67. *J Mater Chem A* **2017**, *5*, 952-957.

6. Walton, K. S.; Sholl, D. S., Research Challenges in Avoiding "Showstoppers" in Developing Materials for Large-Scale Energy Applications. *Joule* **2017**, *1*, 208-211.

7. Park, K. S.; Ni, Z.; Cote, A. P.; Choi, J. Y.; Huang, R.; Uribe-Romo, F. J.; Chae, H. K.; O'Keeffe, M.; Yaghi, O. M., Exceptional Chemical and Thermal Stability of Zeolitic Imidazolate Frameworks. *Proc Natl Acad Sci USA* **2006**, *103*, 10186-91.

8. Küsgens, P.; Rose, M.; Senkovska, I.; Fröde, H.; Henschel, A.; Siegle, S.; Kaskel, S., Characterization of Metal-Organic Frameworks by Water Adsorption. *Micropor Mesopor Mater* **2009**, *120*, 325-330.

9. Burtch, N. C.; Jasuja, H.; Walton, K. S., Water Stability and Adsorption in Metal-Organic Frameworks. *Chem Rev* **2014**, *114*, 10575-612.

10. Liu, D.; Ma, X.; Xi, H.; Lin, Y. S., Gas Transport Properties and Propylene/Propane Separation Characteristics of ZIF-8 Membranes. *J Memb Sci* **2014**, *451*, 85-93.

11. Liu, X.; Li, Y.; Ban, Y.; Peng, Y.; Jin, H.; Bux, H.; Xu, L.; Caro, J.; Yang, W., Improvement of Hydrothermal Stability of Zeolitic Imidazolate Frameworks. *Chem Commun* **2013**, *49*, 9140-9142.

12. Zhang, H.; Liu, D.; Yao, Y.; Zhang, B.; Lin, Y. S., Stability of ZIF-8 Membranes and Crystalline Powders in Water at Room Temperature. *J Memb Sci* **2015**, *485*, 103-111.

13. Sholl, D. S.; Lively, R. P., Defects in Metal-Organic Frameworks: Challenge or Opportunity? *J Phys Chem Lett* **2015**, 3437-3444.

14. Zhang, C.; Han, C.; Sholl, D. S.; Schmidt, J. R., Computational Characterization of Defects in Metal-Organic Frameworks: Spontaneous and Water-Induced Point Defects in ZIF-8. *J Phys Chem Lett* **2016**, *7*, 459-64.

15. Han, C.; Zhang, C.; Tymińska, N.; Schmidt, J. R.; Sholl, D. S., Insights into the Stability of Zeolitic Imidazolate Frameworks in Humid Acidic Environments from First-Principles Calculations. *J Phys Chem C* **2018**, *122*, 4339-4348.

16. Han, C.; Verploegh, R. J.; Sholl, D. S., Assessing the Impact of Point Defects on Molecular Diffusion in ZIF-8 Using Molecular Simulations. *J Phys Chem Lett* **2018**, *9*, 4037-4044.

17. Bhattacharyya, S., Han, R.; Kim, W. G.; Chiang, Y.; Jayachandrababu, K. C.; Hungerford, J. T.; Dutzer, M. R.; Ma, C.; Walton, K. S.; Sholl, D. S.; Nair, S., Acid Gas Stability of Zeolitic Imidazolate Frameworks: Generalized Kinetic and Thermodynamic Characteristics. *Chem Mater* **2018**, *30*, 4089-4101.

18. Kwon, H. T.; Jeong, H.-K.; Lee, A. S.; An, H. S.; Lee, T.; Jang, E.; Lee, J. S.; Choi, J., Defect-Induced Ripening of Zeolitic-Imidazolate Framework ZIF-8 and Its Implication to Vapor-Phase Membrane Synthesis. *Chem Commun* **2016**, *52*, 11669-11672.

19. Lee, M. J.; Kwon, H. T.; Jeong, H.-K., Defect-Dependent Stability of Highly Propylene-Selective Zeolitic-Imidazolate Framework ZIF-8 Membranes. *J Memb Sci* **2017**, *529*, 105-113.

20. Bhattacharyya, S.; Han, R.; Joshi, J.; Zhu, G.; Lively, R. P.; Walton, K. S.; Sholl, D. S.; Nair, S., NO_2 Stability of Zeolitic Imidazolate Frameworks. *J Phys Chem C* **2018**, *123*, 2336–2346.

21. Jayachandrababu, K. C.; Bhattacharyya, S.; Chiang, Y.; Sholl, D. S.; Nair, S., Recovery of Acid-Gas-Degraded Zeolitic Imidazolate Frameworks by Solvent-Assisted Crystal Redemption (SACRed). *ACS Appl Mater Interfaces* **2017**, *9*, 34597-34602.

22. Leus, K.; Bogaerts, T.; De Decker, J.; Depauw, H.; Hendrickx, K.; Vrielinck, H.; Van Speybroeck, V.; Van Der Voort, P., Systematic Study of the Chemical and Hydrothermal Stability of Selected "Stable" Metal Organic Frameworks. *Micropor Mesopor Mater* **2016**, *226*, 110-116.

23. Pang, S. H.; Han, C.; Sholl, D. S.; Jones, C. W.; Lively, R. P., Facet-Specific Stability of ZIF-8 in the Presence of Acid Gases Dissolved in Aqueous Solutions. *Chem Mater* **2016**, *28*, 6960-6967.

24. Ling, S.; Slater, B., Dynamic Acidity in Defective UiO-66. *Chem Sci* **2016**, *7*, 4706-4712.

25. Wu, H.; Chua, Y. S.; Krungleviciute, V.; Tyagi, M.; Chen, P.; Yildirim, T.; Zhou, W., Unusual and Highly Tunable Missing-Linker Defects in Zirconium Metal-Organic Framework UiO-66 and Their Important Effects on Gas Adsorption. *J Am Chem Soc* **2013**, *135*, 10525-32.

26. Cliffe, M. J.; Wan, W.; Zou, X.; Chater, P. A.; Kleppe, A. K.; Tucker, M. G.; Wilhelm, H.; Funnell, N. P.; Coudert, F.-X.; Goodwin, A. L., Correlated Defect Nanoregions in a Metal–Organic Framework. *Nat Comm* **2014**, *5*, 4176.

27. Goodenough, J. B., Influence of Atomic Vacancies on the Properties of Transition-Metal Oxides. I. TiOx and VOx. *Phys Rev B* **1972**, *5*, 2764-2774.

28. Burdett, J. K.; Mitchell, J. F., Nonstoichiometry in Early Transition Metal Compounds with the Rocksalt Structure. *Prog Solid State Chem* **1995**, *23*, 131-170.

29. Gupta, F.; Brillant, G.; Pasturel, A., Correlation Effects and Energetics of Point Defects in Uranium Dioxide: A First Principle Investigation. *Philos Mag* **2007**, *87*, 2561-2569.

30. Alfè, D.; Gillan, M. J., Schottky Defect Formation Energy in MgO Calculated by Diffusion Monte Carlo. *Phys Rev B* **2005**, *71*, 220101.

31. Bristow, J. K.; Svane, K. L.; Tiana, D.; Skelton, J. M.; Gale, J. D.; Walsh, A., Free Energy of Ligand Removal in the Metal–Organic Framework UiO-66. *J Phys Chem C* **2016**, *120*, 9276-9281.

32. Swaminathan, N.; Morgan, D.; Szlufarska, I., Ab Initio Based Rate Theory Model of Radiation Induced Amorphization in B-SiC. *J Nucl Mater* **2011**, *414*, 431-439.

33. Tyburska-Püschel, B.; Zhai, Y.; He, L.; Liu, C.; Boulle, A.; Voyles, P. M.; Szlufarska, I.; Sridharan, K., Size Distribution of Black Spot Defects and Their Contribution to Swelling in Irradiated SiC. *J Nucl Mater* **2016**, *476*, 132-139.

34. Liu, C.; He, L.; Zhai, Y.; Tyburska-Püschel, B.; Voyles, P. M.; Sridharan, K.; Morgan, D.; Szlufarska, I., Evolution of Small Defect Clusters in Ion-Irradiated 3C-SiC: Combined Cluster Dynamics Modeling and Experimental Study. *Acta Mater* **2017**, *125*, 377-389.

35. Perdew, J. P.; Burke, K.; Ernzerhof, M., Generalized Gradient Approximation Made Simple. *Phys Rev Lett* **1996**, *77*, 3865-3868.

36. Grimme, S.; Antony, J.; Ehrlich, S.; Krieg, H., A Consistent and Accurate Ab Initio Parametrization of Density Functional Dispersion Correction (DFT-D) for the 94 Elements H-Pu. *J Chem Phys* **2010**, *132*, 154104.

37. De Vita, A.; Gillan, M. J.; Lin, J. S.; Payne, M. C.; Štich, I.; Clarke, L. J., Defect Energetics in MgO Treated by First-Principles Methods. *Phys Rev B* **1992**, *46*, 12964-12973.

38. The CP2K developers group, 2013. CP2K is freely available from http://www.cp2k.org/ (accessed May 15, 2018).

39. VandeVondele, J.; Krack, M.; Mohamed, F.; Parrinello, M.; Chassaing, T.; Hutter, J., Quickstep: Fast and Accurate Density Functional Calculations Using a Mixed Gaussian and Plane Waves Approach. *Comput Phys Commun* **2005**, *167*, 103-128.

40. Krack, M.; Parrinello, M. *Quickstep: Make the Atoms Dance*; John von Neumann Institute for Computing: Jülich, Germany, 2005; pp 29-51.

41. Goedecker, S.; Teter, M.; Hutter, J., Separable Dual-Space Gaussian Pseudopotentials. *Phys Rev B* **1996**, *54*, 1703-1710.

42. Hartwigsen, C.; Goedecker, S.; Hutter, J., Relativistic Separable Dual-Space Gaussian Pseudopotentials from H to Rn. *Phys Rev B* **1998**, *58*, 3641-3662.

43. Krack, M., Pseudopotentials for H to Kr Optimized for Gradient-Corrected Exchange-Correlation Functionals. *Theor Chem Acc* **2005**, *114*, 145-152.

44. VandeVondele, J.; Hutter, J., Gaussian Basis Sets for Accurate Calculations on Molecular Systems in Gas and Condensed Phases. *J Chem Phys* **2007**, *127*, 114105.

45. Lippert, B. G.; Parrinello, J. H.; Michele, A Hybrid Gaussian and Plane Wave Density Functional Scheme. *Mol Phys* **1997**, *92*, 477-488.

46. Macrae, C. F.; Bruno, I. J.; Chisholm, J. A.; Edgington, P. R.; McCabe, P.; Pidcock, E.; Rodriguez-Monge, L.; Taylor, R.; van de Streek, J.; Wood, P. A., Mercury CSD 2.0– New Features for the Visualization and Investigation of Crystal Structures. *J Appl Crystallogr* **2008**, *41*, 466-470.

47. Momma, K.; Izumi, F., VESTA 3 for Three-Dimensional Visualization of Crystal, Volumetric and Morphology Data. *J Appl Crystallogr* **2011**, *44*, 1272-1276.

CHAPTER 5. IMPROVING THE REPRODUCIBILITY OF MOF SYNTHESIS*

5.1 Introduction

There have been increasing concerns that many, if not most, published findings in modern research are false[1-3]. Systematic efforts to examine this issue have been undertaken in biomedicine and psychology, but less is known about reproducibility in the materials-oriented research that underpins much of modern chemical engineering. Previous studies have examined the robustness of CO_2 uptake in porous adsorbents[4-5]. Eleven independent experimental groups measured CO_2 adsorption in a well-defined zeolite that is readily available to researchers through NIST and demonstrated good agreement between 13 experiments[5]. Park *et al*. also investigated the consistency among CO_2 adsorption in a few well-studied MOFs and produced a set of criteria to determine consensus standards for these measurements[4]. However, this focus on specific applications may underestimate what is known about reproducibility of the underlying materials. This suggests a more foundational question that can be asked about reproducibility of materials-oriented research: once the synthesis of a new material is reported, how often is the synthesis independently replicated? If new materials in the literature are not made again, (or more precisely, their synthesis is not reported again in the open literature) then it inevitably follows that nothing can be known about the reproducibility of these materials or their properties.

* Some material in this chapter has been submitted for publication as Han, R.; Walton, K.S.; Sholl, D. S. "Does Chemical Engineering Research Have a Reproducibility Problem?" to *Annu Rev Chem Biomol Eng* **2019**.

In this chapter, we examine the above questions with respect to the synthesis of metal-organic framework (MOF) materials. The vast majority of MOF experiments are associated with only a few materials, yet more than 22,000 MOFs are catalogued in the Cambridge Structural Database (CSD)[6], and a disorder-free subset of at least 5,000 structures have been prepared and curated in the Computation Ready Experimental (CoRE) MOF database[7]. Here we selected a representative sample of 130 materials from the CoRE MOF database and examined their history in the open literature. We present statistical observations that may generalize to the larger database, before concluding with an anecdotal case study of several highly repeated syntheses.

5.2 Methods[†]

We selected 130 MOFs (~2.6% of the total) from the CoRE MOF database[7] listed in **Table D.1**, all initially published between 2007 and 2013. Where possible, we chose examples in which the original report described a single CoRE MOF structure; this greatly simplified analysis of later papers that cited the original results. In some cases where the original paper identified an isoreticular family of structures but only a single material was entered into the CoRE MOF database, we looked for citations that re-synthesized any variant reported by the original paper. We compared the number of citations on original papers found by Google Scholar and Web of Science; results from the two search engines typically differed by five or fewer citations. We randomly selected 114 papers with between 14 and 57 citations as determined by Google Scholar. The "real" number of citations could be lower since Google Scholar occasionally double-

[†] Data were collected with help from Mayank Agrawal in Dr. David Sholl's research group, as well as undergraduate researchers Akshay Chiddarwar and Dinushka Herath at the Georgia Institute of Technology, Atlanta, GA.

counts citations if they exist in different formats (e.g. journal link versus pdf document). We removed citing papers in non-English language journals from the total number of citations since we were unable to determine if re-synthesis occurred in these works. The 114 publications were combined with 16 papers (ranging from 8 to 168 citations) that had been selected more arbitrarily for an earlier pilot study[8]. That each original paper in the complete set of 130 MOFs had, on average, 34 citations (as of current writing) suggests these materials had properties of interest or values to the community, and therefore we should expect some of them to be re-synthesized.

The number of average citations per paper did not depend strongly on time since publication, as seen in **Table 5.1**. Although papers published in 2013 had about 27 citations per year each (one and a half standard deviations below the average of 34 citations per paper across all years) the trend in previous years suggests a small increase in the number of citations per paper per year. We did not normalize the annualized citation count against elapsed time in subsequent analyses.

Table 5.1. Breakdown from 2007 to 2013 of the number of original papers, total number of citations, and average citations per paper for the 130 MOFs investigated.

Original Publication Year	Number of Original Papers	Total Number of Citations	Avg Citations per Paper per Year
2007	15	473	32
2008	15	458	31
2009	13	454	35
2010	22	825	38
2011	25	933	37
2012	24	938	39
2013	16	427	27

We examined each of the 4,508 papers that cited one of the original 130 synthesis reports to determine which materials had been synthesized again. We did not make judgments about the quality or outcome of repeat syntheses; if authors stated that they had made the same material as in an earlier paper, then we considered this an "exact" repeat synthesis. Only replicates with identical chemical formula and topology to the original material were considered exact reproduced syntheses. However, as previously discussed in Section 5.2, instances where the original paper reported a series of isoreticular structures but only a single material was entered into the CoRE MOF database, we considered citations that reproduced any variant synthesized in the original paper as exact re-syntheses. Variations in guest solvent inclusion or crystal lattice parameters (provided the topology and space group were still identical) were permissible for exact re-syntheses. Chemical variants of a MOFs sharing the same name, such as MIL-96 (Ga)[9] and MIL-96 (Cr)[10], were not counted as exact repeats but instead as "modified" syntheses. A citation was also considered to have performed a modified re-synthesis if an organic linker was functionalized, if a metal center was substituted, if the crystal structure was a polymorph of the original structure, or if guest inclusions significantly changed the primary property of interest (such as the use of different cations). Our discussion below does not include double counting; if a citing paper repeated an exact synthesis and then further modified it, we counted this is an example of an exact repeat synthesis but did not include the modified synthesis. We also examined the citing papers to see if they shared one or more authors with the original report. If there was any overlap of authors between two papers, they were classified as having the same authors.

5.3 Results and Discussion

5.3.1 Summary of repeated syntheses

Figure 5.1 shows counts of repeated syntheses grouped by replicate classification (**1a**, exact or **1b**, modified) and author set (same authors or new authors). Of the 130 materials we surveyed, approximately a third (43/130) had not been synthesized again by any authors and nearly two thirds (80/130) had not been synthesized by a new group of authors separate from the original authors. Strikingly, instances of modified replicates outnumber exactly repeated materials by a significant margin; there are 252 modified syntheses and only 25 exact syntheses. Among the 15 materials for which an exact re-synthesis was reported, the average number of re-syntheses was 1.6 per material. Among the 84 materials for which modified synthesis was reported, the average number of re-syntheses was 3.0 per material. Recall that in our notation, a material was only recorded as having a modified synthesis reported if that report did not include data on synthesis of the original material. It seems likely that in many of the studies that developed modified syntheses, the original material was also produced during the course of the new work. This suggests that authors are consciously choosing to not include information about replicate syntheses when they report their work. If this is correct, the research community is missing the opportunity to strengthen the reliability of published literature by reporting the replicate experiments.

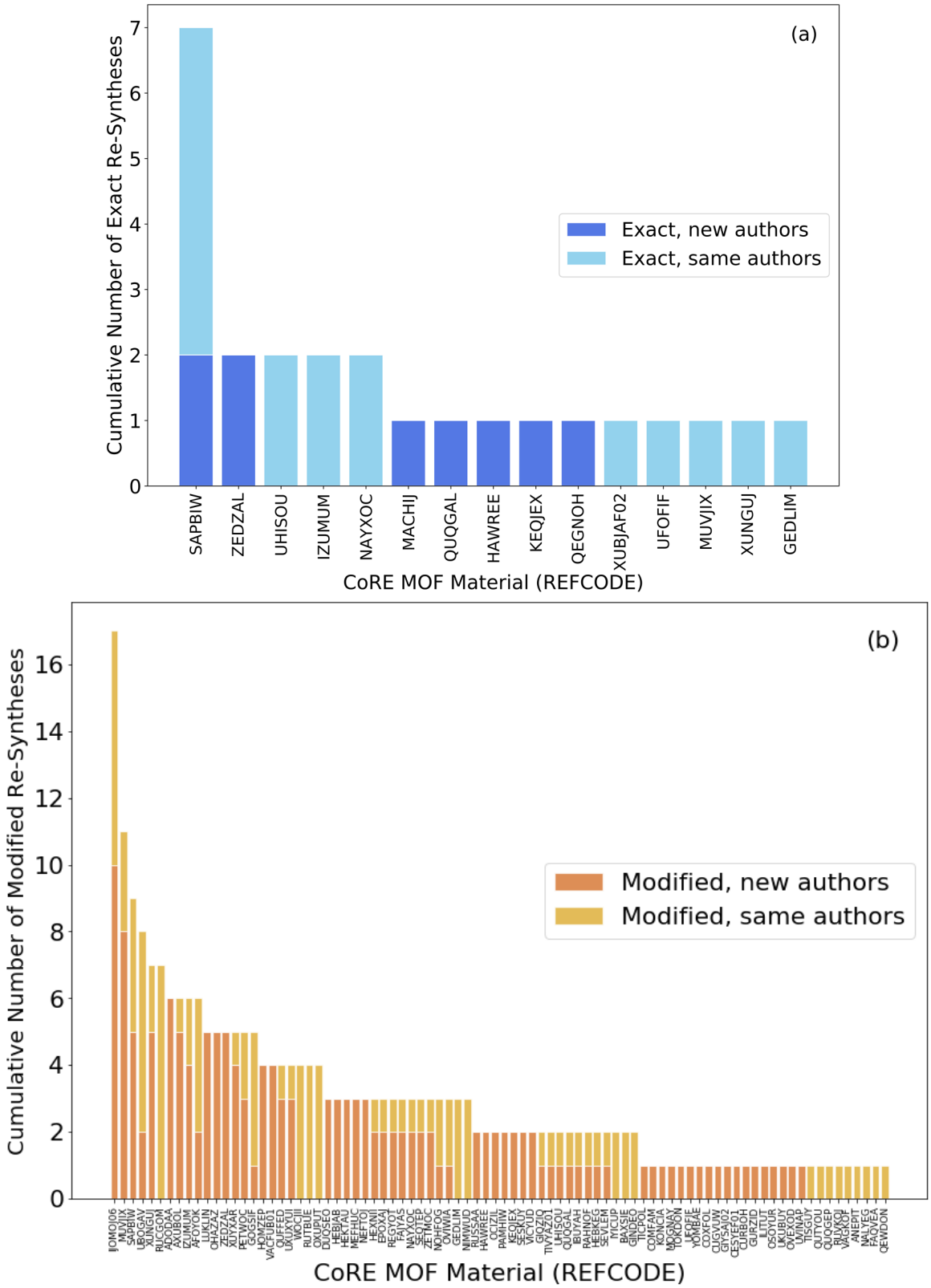

Figure 5.1. Exact repeated syntheses of 130 MOFs (**1a**) and modified repeated syntheses of 130 MOFs (**1b**) separated by the same authors or new set of authors. Larger images are provided in **Figure D.1.**

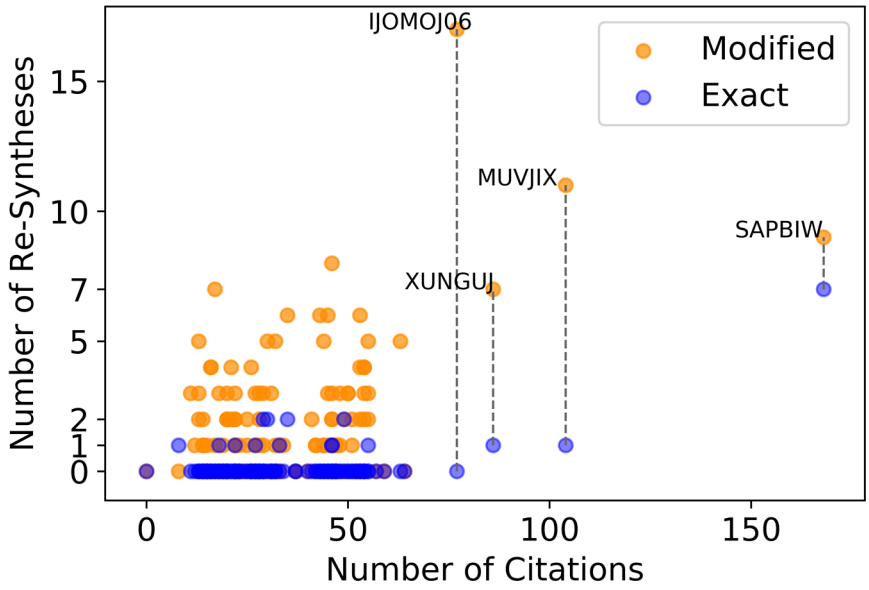

Figure 5.2. Number of exact (blue) and modified (orange) repeated syntheses plotted against total number of citations. Most papers had fewer than 75 citations each and were re-synthesized fewer than 8 times. The four materials labelled on the figure had the highest counts of total repeated synthesis as well as the most citations.

Figure 5.2 shows there is not a strong correlation between the number of replicates and the number of citations of the initial paper. The four materials with the most citations, however, also had the highest counts of total repeated syntheses. With the highest number of repeat syntheses, SAPBIW (16 total repeats) is the material more commonly known as bio-MOF-100. This material has exceptionally high surface area (4,300 m^2/g) and pore volume (4.3 cm^3/g), as well as interesting bio-compatibility and anionic chemistry through its zinc-adeninate building clusters[11]. This MOF was exactly re-synthesized (at least) 7 times, twice by an independent set of authors and five times by researchers who were also on the original paper, and re-synthesized with modifications 9 times. Some of the exact replicates were application-driven, such as Wei *et al*. who explored the dye encapsulation capabilities of bio-MOF-100[12], but other authors

synthesized the original material as a foundation for subsequent linker exchange and functionalization[13]. Therefore, as suggested previously, it is likely that researchers who explored modified replicates also reproduced the original bio-MOF-100 at some point without explicitly reporting the synthesis.

On the other hand, there were no exact replicates reported for the chiral $Mn_3(HCOO)_6$ MOF with reference code IJOMO06[14]; all 17 re-syntheses were modified, typically examining other chiral and antiferromagnetic materials that substituted Mn with Fe or Ni, used functionalized linkers, or explored different topologies. The remaining two of the four most highly cited and re-synthesized materials were MUVJIX (12 total repeats), demonstrating encapsulation of photoactive metal-diimine clusters in a framework to access new excitation states[15]; and XUNGUJ (8 total repeats), introducing a microporous lithium salt with hydrogen sorption capabilities despite a lack of exposed Li^+ ions[16]. Each material was exactly replicated once; the remaining re-syntheses were all modifications of the original MOFs to explore different properties.

Table 5.2. Hierarchy of replication in materials research and classification of MOFs investigated in this work.

	Exact Synthesis by Independent Researchers	**Exact Synthesis by Original Researchers**
3+ replicates		SAPBIW[11] (5 replicates)
2 replicates	SAPBIW[11] ZEDZAL[17]	UHISOU[18] IZUMUM[19] NAYXOC[20]
1 replicate	MACHIJ[21] QUQGAL[22] HAWREE[23] KEQJEX[24] QEGNOH[25]	XUBJAF02[26] UFOFIF[27] MUVJIX[15] XUNGUJ[16] GEDLIM[28]
0 replicates	123 materials from set in **Table D.1** not listed here	121 materials from set in **Table D.1** not listed here

A modified re-synthesis was more likely to be published by different authors (145 out of 228), but most of the exactly repeated syntheses were carried out by the same group as the original report (16 out of 25). **Table 5.2** groups all instances of exact re-syntheses by number of replicates and author set. Only one material (SAPBIW) was exactly re-synthesized more than twice, and only five materials had their syntheses repeated exactly twice. Out of the latter category, two materials (ZEDZAL and SAPBIW) were replicated by a new set of researchers completely independent of the original authors. Ten materials were re-synthesized exactly once, five of which were replicated by independent researchers.

The discussion above suggests a natural hierarchy of replicate experiments in analogy to Olympic medals, which has also been recommended as a way to increase reproducibility in the research community[8]. The bronze medal designation is given for repeating synthesis and characterization in one's own lab. Although it could be argued idealistically that this is a part of scientific norms and should not be dignified with a medal, more than 80% of the original papers investigated failed to explicitly meet this standard. A silver medal designation is given for materials that have been characterized by two independent groups, even though synthesis of the material might have only taken place in one laboratory. None of the 130 original materials were observed to meet this standard. A gold medal designation is given for materials that have been produced independently (and characterized) by more than one group. In the language we used above, a gold medal is associated with exact re-synthesis by a separate group of researchers. **Figure 5.3** shows the "medal stand" for the 130 MOFs we examined.

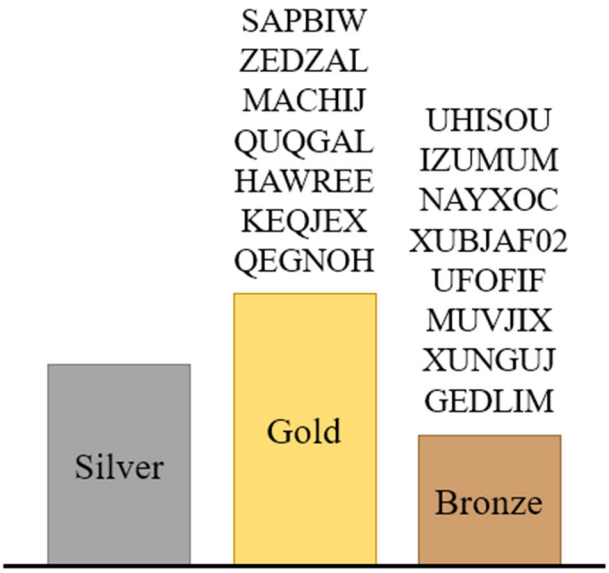

Figure 5.3. "Olympic medal stand" of reproducibility for the 130 MOFs examined.

Re-synthesizing a material alone is not enough to verify whether the synthesis was successful in reproducing the same MOF. In Section 5.3.2 we examine the characterization techniques that are most frequently performed and present a case study on the gold medal experiments in Section 5.3.3 where we compare the synthesis methods and subsequent product characterization reported by the replicate experiment against the original.

5.3.2 Material characterization of original syntheses

The analysis above provides a systematic set of experiments where the issue of reproducibility can be considered. For the 115 materials (88% of the total) where exact synthesis has not been replicated in the open literature, no direct conclusions about reproducibility for any aspect of the materials' properties can be made. Before we can determine whether repeated syntheses of the other 15 materials gave consistent results, we first consider the experimental techniques used to characterize the 130 MOFs in their

original papers. As with our methods for counting repeated syntheses, we looked for the authors to state that they had measured a property, regardless of whether data or results were explicitly reported. Single crystal X-ray diffraction (SC XRD) was used to solve the structure of the newly identified MOF in all but three of the 130 original reports; for those materials (GUKZAO[29], IYICUP[30], and PEMRIK[31]), the powder diffraction pattern was sufficient for the authors to determine the crystal structure. Thermoanalytics were the second most commonly used technique (103/130), typically thermogravimetric analysis (TGA), sometimes combined with differential thermal analysis (DTA) or differential scanning calorimetry (DSC). Powder XRD was often performed as well (99/130), occasionally at variable temperature and in conjunction with TGA. Most reports (83/130) also included some form of infrared spectroscopy (IR). These four experiments are useful for determining the chemistry, stoichiometry, and crystal structure of an unknown species. Only 59 of the original 130 papers used all four characterization methods.

Table 5.3 Ten Most Frequently Measured Properties Across 130 Original Papers

Measurement Type	Number of Papers
Single Crystal X-Ray Diffraction (SC XRD)	127
Thermogravimetric Analysis (TGA)	103
Powder X-Ray Diffraction (PXRD)	99
Infrared Spectroscopy (FTIR)	83
Gas Sorption	53
Fluorescence	38
Surface Area	34
Magnetic Susceptibility	28
Nuclear Magnetic Resonance (NMR)	25
Ultraviolet-Visible (UV-vis) Spectroscopy	19

In addition to characterizing the material, most of the original reports also measured properties of interest ranging from sorption performance[32,33], to magnetic behavior[26,34], to photoactivity[35,36]. While the specific experiments and conditions varied, we were interested in quantitative correlations among the most frequently performed types of measurements in order to explore motivations behind MOF discovery and identify possible connections between application and reproducibility. **Table 5.3** aggregates counts of the 10 most performed measurements across all 130 original papers, and **Figure 5.4** shows the correlation matrix between number of citations of the original paper, number of total repeated syntheses (including exact and modified replicates) of the original paper, and measurements performed by the original paper. The elements $\rho_{X,Y}$ of the correlation matrix are calculated using the Pearson correlation coefficient[37] defined as

$$\rho_{X,Y} = \mathrm{E}[(X - \mu_X)(Y - \mu_Y)]/\sigma_X\sigma_Y \quad (5\text{-}1)$$

where X and Y are the two variables whose correlation is being calculated, E is the expectation value, μ_X is the mean of X, σ_X is the standard deviation of X, μ_Y is the mean of Y, and σ_Y is the standard deviation of Y. The correlation coefficient has value between +1 (dark orange) and -1 (dark blue), inclusive, corresponding respectively to total positive linear correlation or total negative linear correlation; a value of 0 indicates no linear correlation. Although interpretation of the correlation coefficient is context dependent, it has been suggested that a value of |0.8| indicates strong correlation[38]. Here we use a scale where coefficients between |0.25|-|0.50| are designated low correlation, coefficients between |0.50|-|0.75| are designated medium correlation, and coefficients above |0.75| are designated high correlation. Therefore, based on the correlations in **Figure 5.4**, none of the characterization methods are strongly correlated with citations on

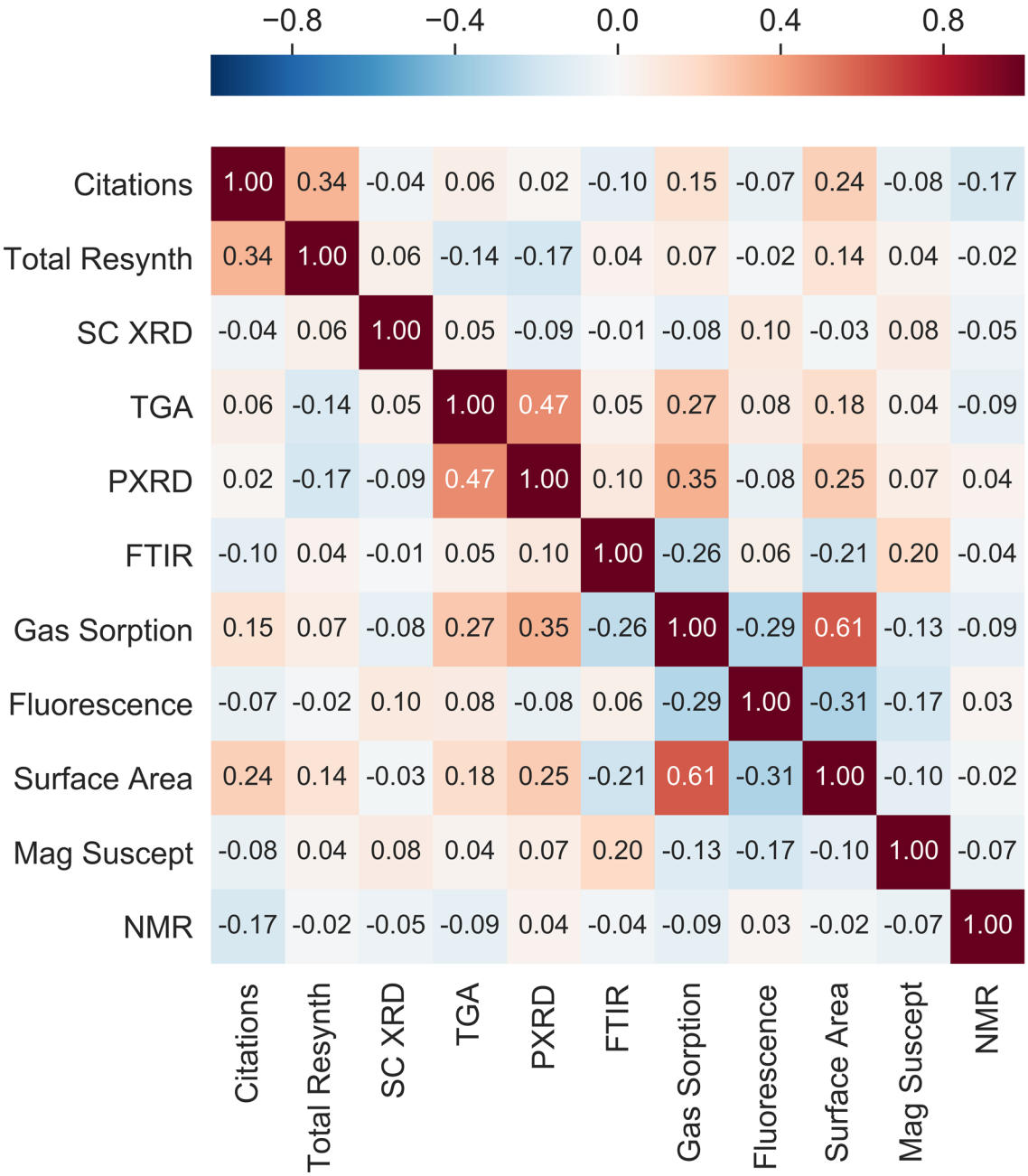

Figure 5.4. Correlation matrix between number of citations of the original paper, number of total repeated syntheses (including exact and modified replicates) of the original paper, and the characterization methods used by the original paper.

total replicates. As observed previously, the covariance between number of citations and re-synthesis frequency is fairly low. TGA and PXRD are also weakly covariant with each other, and with both surface area and gas sorption measurements. Unsurprisingly, surface

area and gas sorption are correlated; surface area is typically estimated by measuring N_2 uptake and fitting to the Brunauer-Emmett-Teller (BET) or Langmuir adsorption equations. It is interesting to note that 53 of the 130 papers report adsorption isotherms but only 34 papers measured the surface area of the material. Weak covariance is also seen between fluorescence and UV-vis spectroscopy, two properties that can both measure emission or excitation of photonic states. Fluorescence and FTIR are also weakly anti-correlated with surface area and gas sorption. These correlations are not surprising, and are likely driven by the application and primary interest in each paper.

5.3.3 Case study

Only two MOFs, SAPBIW and ZEDZAL, were exactly synthesized more than once by sets of researchers distinct from the original authors. These provide an anecdotal sample on which to comment on the quality and consistency of reproduced syntheses. For each material, we compare the reported synthesis and characterization results of the replicates.

SAPBIW, also known as the anionic bio-MOF-100, was first reported in 2012 by An *et al.*[11] and has a chemical formula of $Zn_8(adeninate)_4(BPDC)_6O_2 \bullet 4(methyl)_2NH_2$ where BPDC denotes biphenyldicarboxylate. The original authors reported SC XRD, TGA, PXRD, FTIR, and N_2 adsorption isotherms. Liu *et al*. reported exact replication of bio-MOF-100 in 2015[39] synthesized via stepwise ligand exchange starting from a separate isoreticular structure (bio-MOF-101). The reproduced synthesis was characterized with TGA and PXRD, the latter of which was “in good agreement with simulated spectra, indicating the successful synthesis of [bio-MOF-100]”. Liu *et al*. also investigated the extraction efficiencies of bio-MOF-100 coated fibers towards organic

pollutants. Wei *et al*. also replicated synthesis in 2016[12] for use as a host matrix to encapsulate photoactive dyes. The pristine bio-MOF-100 structure was analyzed using PXRD, and FTIR; dye-encapsulated MOFs were subject to photoirradiation and lasing experiments.

Figure 5.5 shows PXRD curves collected using all using a CuKα radiation source from the original and citing papers. This was the only characterization performed by all three sets of authors. The positions of the four most intense peaks in the original paper are indicated by the red lines; while the peaks from Wei *et al*. are closely aligned with the original report, three of the peaks reported by Liu *et al*. show a systematic offset. If we compare the TGA curves (**Figure 5.6**) from the original paper and the replicate synthesized by Liu *et al*., the two measurements superficially appear quite different. In the original report, An *et al*. (black solid line) performed TGA of the as-synthesized crystal under a N_2 atmosphere from 25-600 °C at a rate of 1 °C/min using a TGA Q500 thermal analysis system. The resultant curve shows an initial 60% weight loss step after heating to ~200 °C which was assigned to loss of guest molecules, specifically 49 DMF and 31 H_2O molecules per formula unit. The second step between 350-450 °C was attributed to structural decomposition. Liu *et al*. (blue dashed line) used a Netzsch-209 Analyzer to gather TGA data under a N_2 atmosphere from 25-800 °C at a 10 °C/min ramp rate. The difference in ramp rate from An *et al*. means that comparisons between the two experiments must be made cautiously. In An *et al*.'s data, there is only one weight loss step that occurs around 400-500 °C, which is likely associated with structural

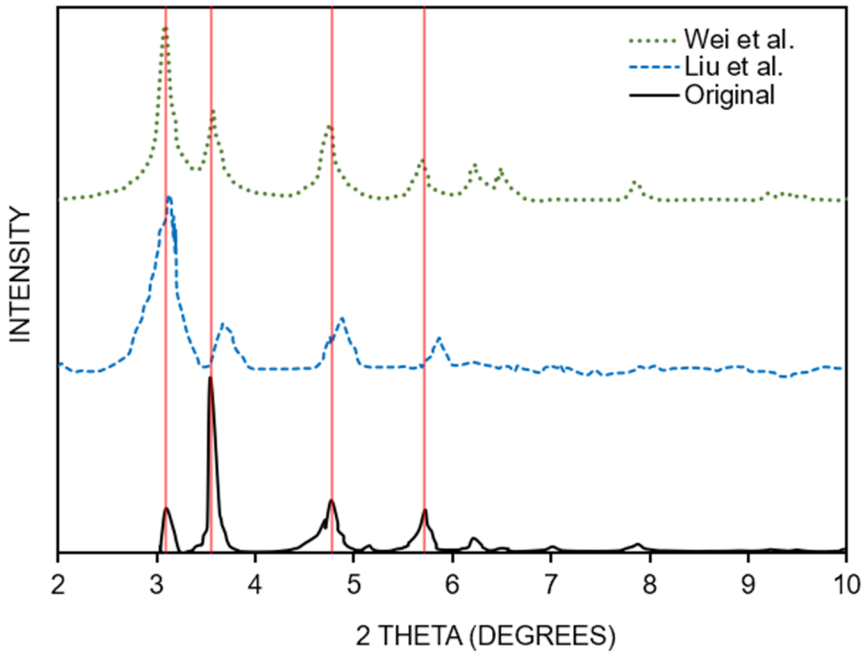

Figure 5.5. PXRD spectra for original and repeated syntheses of bio-MOF-100. Vertical red lines indicate positions of the five most intense peaks for the original material. Data were digitized and reproduced from An *et al.*[11] (original), Liu *et al.*[39], and Wei *et al.*[12]

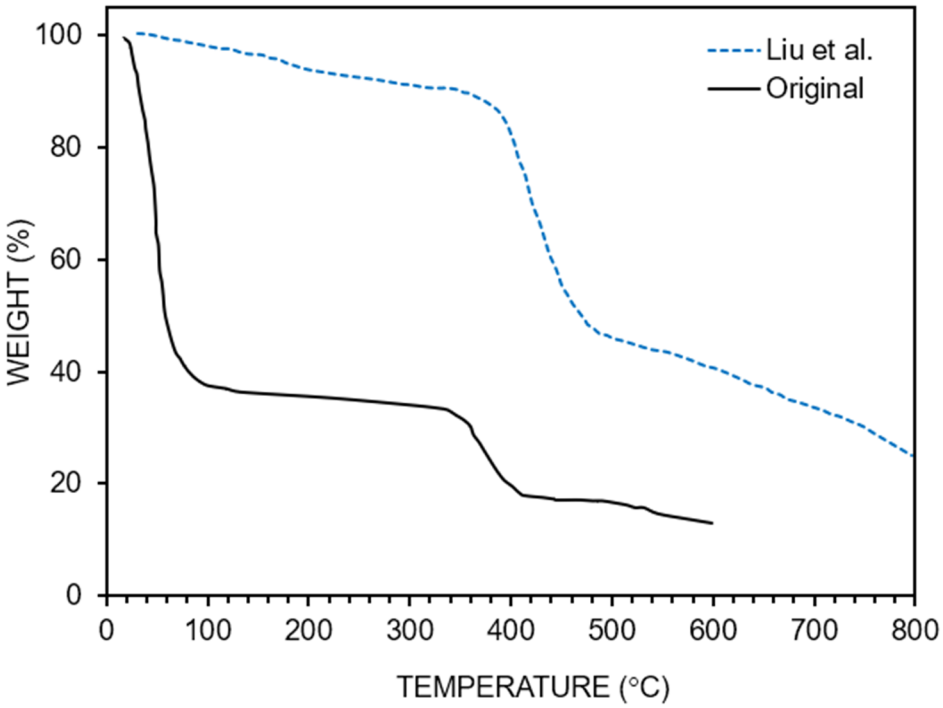

Figure 5.6. TGA curves for original and repeated syntheses of bio-MOF-100. Data were digitized and reproduced from An *et al.*[11] (original) and Liu *et al.*[39].

decomposition. The re-synthesis used a ligand exchange procedure carried out in DMF with no mention of water, so we would not expect the initial guest solvent composition in the pores of the two experiments to be similar. Both curves approach 80% weight loss after structural decomposition, but the considerable difference between the weight loss that can be ascribed to solvent make it difficult to conclude that the two experiments are fully consistent.

ZEDZAL refers to Ln-LOF, a family of isostructural lanthanide-organic frameworks (LOFs) formulated as Ln(BTB)(H_2O) where Ln = {Y, La, Ce, Pr, Nd, Sm, Eu, Gd, Tb, Dy, Ho, Er, Yb}, and BTB = 1,3,5-benzenetrisbenzoic acid[17]. Lin *et al*. measured and reported SC XRD, TGA, PXRD, FTIR, and sorption of N_2, CO_2, CH_4, and benzene vapor for all the Ln-LOFs they synthesized. Although only a single representative structure was included in the CoRE MOF database, following our definition in Section 5.2, we looked for citing papers that re-synthesized any variant of the Ln-LOFs presented in the original paper. Shi *et al*. synthesized hollow nanospheres of TbBTB (as opposed to the needle-like crystals of the original material) to study the π-system based fluorescence of the benezenetrisbenzoic acid ligands[40]. This material was characterize using PXRD, TGA, FTIR, and N_2 adsorption, in addition to time-resolved fluorescence spectrometry. Zhao *et al*. made a series of mixed Nd-Yb LOFs in 2016 with needle morphology[41], including the pure materials NdBTB and YbBTB which could be compared against the identical Nd-LOF and Yb-LOF reported by Lin *et al*. PXRD, TGA, and FTIR were reported for the mixed-metal LOFs, with additional emission and excitation data also calculated.

Figure 5.7 shows PXRD spectra of original and replicate syntheses of TbBTB (**Figure 5.7a**, top) and NdBTB (**Figure 5.7b**, bottom) measured using CuKα radiation. Positions of the five most intense peaks of each original synthesis are indicated by the vertical red lines. For the TbBTB material, it is evident that the powder pattern measured by Shi *et al*. does not match the simulated spectra they were anticipating; the authors suspected this discrepancy arose because the "spheres [they synthesized] were impure and may have multiphase crystal structures". However, neither the simulated nor measured PXRD match the pattern reported by the original authors. The original spectra has twinned peaks at 6.3° and 10.8°, while the simulated and measured patterns of Shi *et al*. show single peaks. Although the shapes of the PXRD spectra for the NdBTB materials (**Figure 5.7b**) are more similar between the original material and the re-synthesis by Zhao *et al*., there are multiple peaks visible in the original spectra that do not appear in the powder pattern of the replicate material.

Figure 5.8 shows the TGA curves for the original and replicated materials. Lin *et al*. initially performed TGA on a Q600 SDT TGA-DTA-DSC analyzer from 25-650 °C at a 5 °C/min heating rate under N_2. The TGA curves of the original TbBTB and NdBTB materials have a similar shape, with a first weight loss step from 100-200 °C associated with removal of DMF solvent, while the second step between 500-600 °C was attributed to structural decomposition. Zhao *et al*. carried out TGA until nitrogen using a Netzsch TG209F3 instrument at a ramp rate of 5 °C/min. Since this curve was measured using the same heating rate in the same N_2 atmosphere, the results should be directly comparable to that measured by the original authors. While the shape of the curve is similar to the TGA

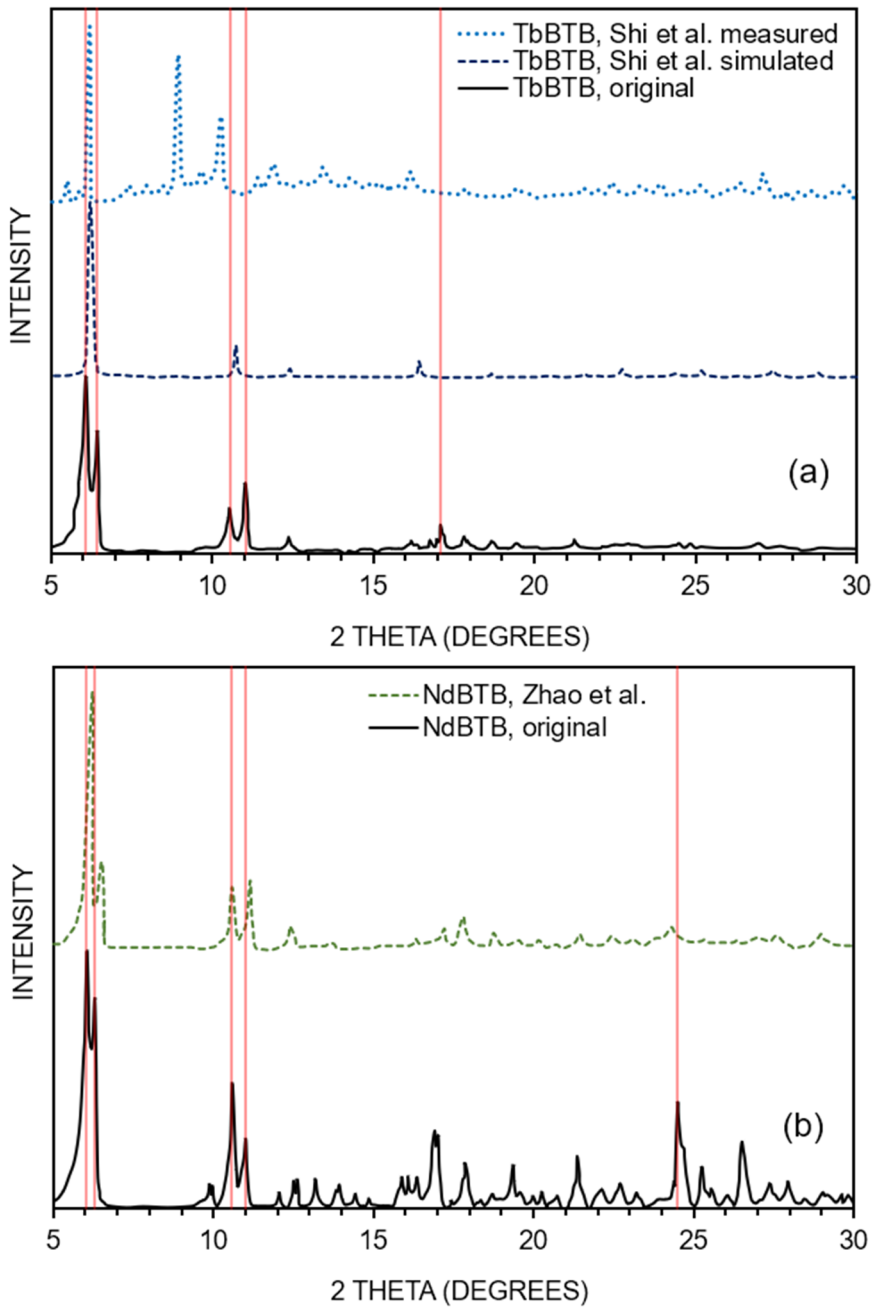

Figure 5.7. PXRD spectra for original and repeated syntheses of TbBTB (**7a**, top) and NdBTB (**7b**, bottom). Vertical red lines indicate positions of the five most intense peaks for the original material. Data were digitized and reproduced from Lin *et al*.[17] (original), Shi *et al*.[40], and Zhao *et al*.[41]

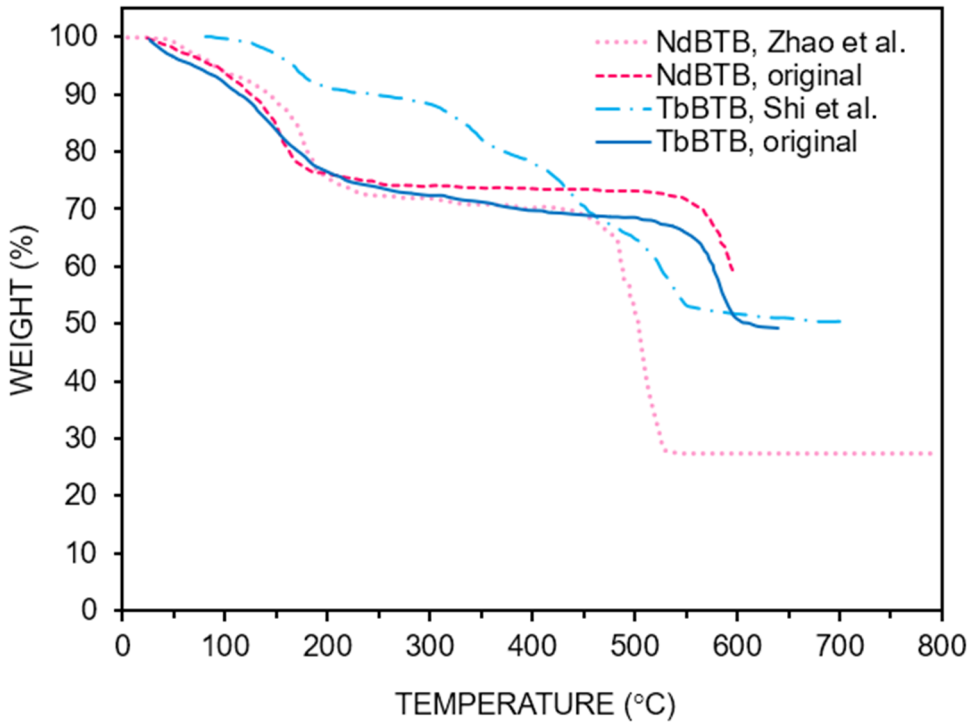

Figure 5.8. TGA curves for original and repeated syntheses of TbBTB and NdBTB. Data were digitized and reproduced from Lin *et al*.[17], Shi *et al*.[40], and Zhao *et al*.[41]

measurement by Lin *et al*., the second weight loss step associated with structural decomposition occurs significantly earlier, around 400-500 °C, and appears to result in a much higher percent of weight loss overall. Shi *et al*. performed TGA in a N_2 atmosphere at an unknown heating rate and reported grams of material loss. We converted this to percentage weight loss by assuming the starting weight of 2.04 g correspond to 100% mass. The replicate TbBTB curve was noted to exhibit several complex weight loss steps at approximately 150 °C, 300 °C, 400 °C, and 600 °C. Shi *et al*. attributed the steps between 150-300°C to removal of physical trapped and chemically coordinated solvent in the nanospheres, respectively, while decomposition occurs around 400-550 °C. This behavior may differ from that seen in the needle-like materials because the hollow

spheres trap a large amount of solvent molecules that vacate more gradually with increasing temperature.

These two case studies of SAPBIW and ZEDZAL suggest that detailed comparison of characterization for original and exact replicate materials reveals inconsistencies. Some of these may be due to difference in measurement procedure, but a certain amount of variability must be attributed to discrepancy in the underlying syntheses. When authors re-synthesize a material using alternative synthesis procedures, it is not surprising that the resulting material may have different characterization, but it then becomes necessary to develop a measurement standard by which we can determine whether the re-synthesized material is truly the same as the original material. As demonstrated by the discussion on characterization techniques reported in the original papers (Section 5.3.2), it is likely that multiple types of measurements are necessary to accurately compare a replicate material against the original. Though it is beyond the scope of this work, we can imagine extending the adsorption isotherm consistency analysis performed by Park *et al*.[4] to other forms of experimental measurement in order to identify a suite of standard material characterizations that should be performed and compared for every synthesis.

5.4 Conclusion

We have identified a lack of reproduced syntheses reported in the literature on MOF research. Having selected a sample of 130 materials from the CoRE MOF database, we followed the citations on each original paper to determine whether the original material had been re-synthesized. Replicate experiments were classified as either “exact” if an identical material to one reported by the original paper was stated to have been

produced, or otherwise “modified” if the original material had been re-synthesized with metal substitution, linker functionalization, alternate topology, or significantly different guest inclusions. We also noted whether each re-synthesis had been performed by a new set of authors entirely independent of the original researchers, or whether there was overlap between the author groups. Out of 130 papers surveyed, only 15 of the materials introduced by those papers were ever reproduced exactly, and only 2 out of the 15 exact replicates were reproduced more than once by a completely new set of authors. Comparing characterization of exact replicates against the original reported characterization suggested that exact reproduced syntheses may not be truly consistent with an original material.

To strengthen the quality of reported research, we suggest increased performance and publication of replication experiments. A hierarchy for standard of replication has been proposed in analogy to the “Olympic medal” scoring system; fewer than 20% of the papers in this study met even the bronze standard, which is simply for researchers to re-synthesize a material in their own lab and publish the results of doing so. We suspect that the number of replicate experiments is underreported, and we encourage researchers to explicitly report repeated syntheses and characterization. Finally, it would be useful to define material standards for experimental measurements. Pioneering efforts have already established robust standards of CO_2 adsorption in various MOFs, however, we demonstrated in this study that gas sorption is a less frequently measured property. Establishing consensus results for PXRD, TGA, and FTIR measurements would allow greater accuracy and consistency of MOF experiments.

APPENDIX D. SUPPORTING INFORMATION FOR CHAPTER 5

Table D.1. Year of publication, reference code, number of citations, number of exact syntheses by same and new authors, and number of modified syntheses by same and new authors, of all 130 materials selected from the CoRE MOF database.

Year	CSD Code	Citations	Exact, new authors	Exact, same authors	Modified, new authors	Modified, same authors
2007	CETGOY[42]	49	0	0	0	0
2007	DIXHIC[35]	15	0	0	0	0
2007	GIQZIQ[32]	21	0	0	1	1
2007	HEXNII[43]	20	0	0	2	1
2007	HOMZEP[9]	54	0	0	4	0
2007	IJOMOJ06[14]	77	0	0	10	7
2007	KIFJIT[44]	32	0	0	0	0
2007	PIKBUH[45]	27	0	0	0	0
2007	RIPTAM[36]	26	0	0	0	0
2007	SINXET[46]	19	0	0	0	0
2007	TICPOL[47]	19	0	0	1	0
2007	TIRLIQ[48]	17	0	0	0	0
2007	TISGUY[33]	48	0	0	0	1
2007	TIVYAZ01[49]	41	0	0	1	1
2007	XUBJAF02[26]	8	0	1	0	0
2008	AFOYOK[50]	53	0	0	2	4
2008	COMFAM[51]	32	0	0	1	0
2008	GOGSIF[34]	13	0	0	1	4
2008	KOLWEO[52]	52	0	0	0	0
2008	KONCIA[53]	44	0	0	1	0
2008	LOPZAS[54]	24	0	0	0	0
2008	MOGNAY[55]	14	0	0	1	0
2008	NOHFOG[56]	31	0	0	1	2
2008	RIWSUM[57]	27	0	0	0	0
2008	SODZIV[58]	19	0	0	0	0
2008	TOKDON[59]	44	0	0	1	0
2008	UFOFIF[27]	22	0	1	1	0
2008	WOCJII[60]	21	0	0	0	4
2008	XOJWEZ[61]	47	0	0	0	0
2008	YOMBAE[62]	15	0	0	1	0
2009	COXFOL[63]	29	0	0	1	0
2009	CUGVUW[64]	22	0	0	1	0
2009	GIYSAJ02[65]	47	0	0	1	0

2009	GUKZAO[29]	37	0	0	0	0
2009	LUKLIN[66]	55	0	0	5	0
2009	MUNPAN[67]	28	0	0	0	0
2009	OHAZAZ[68]	44	0	0	5	0
2009	OHOLIH[69]	15	0	0	0	0
2009	QUFFED[70]	53	0	0	3	1
2009	QUTYOU[71]	42	0	0	0	1
2009	RUCGOM[72]	17	0	0	0	7
2009	UHISOU[18]	49	0	2	1	1
2009	VACFUB01[73]	16	0	0	4	0
2010	CESYEF01[74]	17	0	0	1	0
2010	CURBOH[75]	25	0	0	1	0
2010	DUQSEO[76]	54	0	0	3	0
2010	EKARUE[77]	15	0	0	0	0
2010	GURZID[78]	12	0	0	1	0
2010	ILITUT[79]	46	0	0	1	0
2010	LUPYAX[80]	52	0	0	0	0
2010	MACHIJ[21]	27	1	0	0	0
2010	MUTVUT[81]	40	0	0	0	0
2010	MUVJIX[15]	104	0	1	8	3
2010	NUZCER[82]	43	0	0	0	0
2010	OSOYUR[83]	46	0	0	1	0
2010	OWIZAW[84]	30	0	0	0	0
2010	QUQGAL[22]	46	1	0	1	1
2010	QUQGEP[85]	27	0	0	0	1
2010	RUSSAA[86]	13	0	0	2	0
2010	RUTBUE[87]	16	0	0	0	4
2010	RUVKOJ[88]	14	0	0	0	1
2010	UKUBUY[89]	33	0	0	1	0
2010	VAGKOF[90]	47	0	0	0	1
2010	XUNGUJ[16]	86	0	1	5	2
2010	XUYXAR[91]	32	0	0	4	1
2011	ANEPIT[92]	51	0	0	0	1
2011	AXUBOL[93]	43	0	0	5	1
2011	EBUREA[94]	26	0	0	0	0
2011	EMITUQ[95]	26	0	0	0	0
2011	EPOXAJ[96]	46	0	0	2	1
2011	EZOXEX[97]	23	0	0	0	0
2011	HAWREE[23]	55	1	0	2	0
2011	IBUYAH[98]	22	0	0	1	1
2011	IJEXUR[99]	31	0	0	0	0
2011	IYICUP[30]	20	0	0	0	2
2011	IZUMUM[19]	35	0	2	4	2

2011	NALYEG[100]	28	0	0	0	1
2011	OCIZIL[101]	53	0	0	2	0
2011	OVEXOD[102]	42	0	0	1	0
2011	OVIWIA[103]	48	0	0	1	2
2011	OXUPUT[104]	26	0	0	0	4
2011	OYUJUO[105]	22	0	0	0	0
2011	PAMHIW[39]	14	0	0	2	0
2011	RAHNOF[106]	54	0	0	1	1
2011	REGYOT[107]	50	0	0	2	1
2011	UBOGAV[108]	46	0	0	2	6
2011	UVEVUN[109]	59	0	0	0	0
2011	UVINAP[110]	45	0	0	1	0
2011	UXUXYUI[111]	54	0	0	3	1
2011	UZIJUJ[112]	14	0	0	0	0
2012	ADODAA[113]	45	0	0	6	0
2012	BAXSIE[114]	51	0	0	0	2
2012	FAJYAS[115]	13	0	0	2	1
2012	FAQVEA[116]	34	0	0	0	1
2012	FATLUJ[117]	57	0	0	0	0
2012	GEDLIM[28]	18	0	1	0	3
2012	HARNAR[118]	18	0	0	0	0
2012	HEBJAB[119]	55	0	0	3	0
2012	HEBKEG[120]	28	0	0	1	1
2012	HEKTAU[121]	45	0	0	3	0
2012	KEQJEX[24]	46	1	0	2	0
2012	LASMAV[122]	22	0	0	0	0
2012	LECGIL[123]	29	0	0	0	0
2012	MEFHUC[124]	27	0	0	3	0
2012	NAYXOC[20]	29	0	2	2	1
2012	NEFTOJ[125]	11	0	0	3	0
2012	PEMRIK[31]	64	0	0	0	0
2012	QEGNOH[25]	33	1	0	0	0
2012	SAKNOJ[126]	31	0	0	0	0
2012	SAPBIW[11]	168	2	5	5	4
2012	SESKUY[127]	22	0	0	2	0
2012	VEPDEB[128]	15	0	0	0	0
2012	WIFGOJ[129]	47	0	0	0	0
2012	ZEDZAL[17]	30	2	0	5	0
2013	BETZOR[130]	18	0	0	0	0
2013	DEYLUQ[131]	29	0	0	0	0
2013	DEYNIG[132]	23	0	0	0	0
2013	FEZREJ[133]	15	0	0	0	0
2013	GINDEO[134]	20	0	0	0	2

2013	LELMEW[135]	16	0	0	0	0
2013	NIMWUD[136]	22	0	0	0	3
2013	PETWOC[137]	63	0	0	3	2
2013	QEWDON[138]	23	0	0	0	1
2013	RIDGIW[139]	37	0	0	0	0
2013	SEQTEP[140]	28	0	0	2	1
2013	SETDUS[141]	18	0	0	0	0
2013	SEVLEM[142]	25	0	0	1	1
2013	VICYUD[143]	20	0	0	2	0
2013	VIDPIJ[144]	20	0	0	0	0
2013	ZETMOC[145]	50	0	0	2	1

(a)
Exact, new authors
Exact, same authors
Cumulative Number of Exact Re-Syntheses
0
1
2
3
4
5
6
7
CoRE MOF Material (REFCODE)
SAPBIW
ZEDZAL
UHISOU
IZUMUM
NAYXOC
MACHIJ
QUQGAL
HAWREE
KEQJEX
QEGNOH
XUBJAF02
UFOFIF
MUVJIX
XUNGUJ
GEDLIM

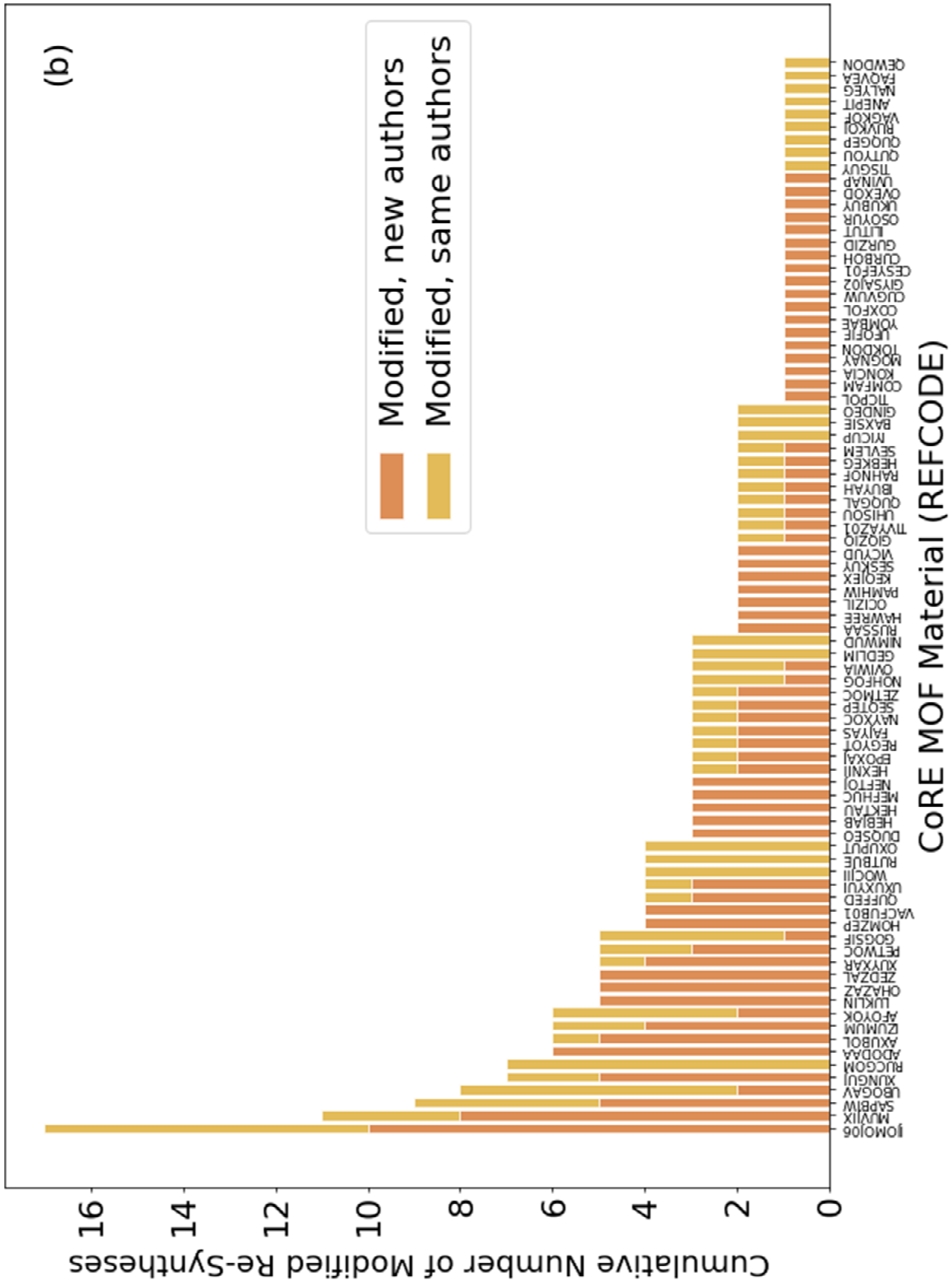

Figure D.1. Exact (**1a**, top) and modified (**1b**, bottom) repeated synthesis of 130 MOFs, larger version of **Figure 5.1**.

D.1 REFERENCES

1. Colhoun, H. M.; McKeigue, P. M.; Smith, G. D., Problems of Reporting Genetic Associations with Complex Outcomes. *Lancet* **2003**, *361*, 865-872.

2. Ioannidis, J. P. A., Microarrays and Molecular Research: Noise Discovery? *Lancet* **2005**, *365*, 454-455.

3. Ioannidis, J. P., Why Most Published Research Findings Are False. *PLOS Med* **2005**, *2*, e124.

4. Park, J.; Howe, J. D.; Sholl, D. S., How Reproducible Are Isotherm Measurements in Metal–Organic Frameworks? *Chem Mater* **2017**, *29*, 10487-10495.

5. Nguyen, H. G. T., et al., A Reference High-Pressure CO_2 Adsorption Isotherm for Ammonium ZSM-5 Zeolite: Results of an Interlaboratory Study. *Adsorption* **2018**, *24*, 531-539.

6. Allen, F., The Cambridge Structural Database: A Quarter of a Million Crystal Structures and Rising. *Acta Cryst B* **2002**, *58*, 380-388.

7. Chung, Y. G.; Camp, J.; Haranczyk, M.; Sikora, B. J.; Bury, W.; Krungleviciute, V.; Yildirim, T.; Farha, O. K.; Sholl, D. S.; Snurr, R. Q., Computation-Ready, Experimental Metal–Organic Frameworks: A Tool to Enable High-Throughput Screening of Nanoporous Crystals. *Chem Mater* **2014**, *26*, 6185-6192.

8. Han, R.; Walton, K. S.; Sholl, D. S., Does Chemical Engineering Research Have a Reproducibility Problem? submitted to *Annu Rev Chem Biomol Eng* **2019**.

9. Volkringer, C.; Loiseau, T.; Férey, G.; Morais, C. M.; Taulelle, F.; Montouillout, V.; Massiot, D., Synthesis, Crystal Structure and ^{71}Ga Solid State NMR of a MOF-Type Gallium Trimesate (MIL-96) with μ_3-oxo Bridged Trinuclear Units and a Hexagonal 18-Ring Network. *Micropor Mesopor Mater* **2007**, *105*, 111-117.

10. Long, P.; Wu, H.; Zhao, Q.; Wang, Y.; Dong, J.; Li, J., Solvent Effect on the Synthesis of MIL-96 (Cr) and MIL-100 (Cr). *Micropor Mesopor Mater* **2011**, *142*, 489-493.

11. An, J.; Farha, O. K.; Hupp, J. T.; Pohl, E.; Yeh, J. I.; Rosi, N. L., Metal-Adeninate Vertices for the Construction of an Exceptionally Porous Metal-Organic Framework. *Nat Commun* **2012**, *3*, 604.

12. Wei, Y.; Dong, H.; Wei, C.; Zhang, W.; Yan, Y.; Zhao, Y. S., Wavelength-Tunable Microlasers Based on the Encapsulation of Organic Dye in Metal–Organic Frameworks. *Adv Mater* **2016**, *28*, 7424-7429.

13. Liu, S.; Zhou, Y.; Zheng, J.; Xu, J.; Jiang, R.; Shen, Y.; Jiang, J.; Zhu, F.; Su, C.; Ouyang, G., Isoreticular Bio-MOF 100–102 Coated Solid-Phase Microextraction Fibers for Fast and Sensitive Determination of Organic Pollutants by the Pore Structure Dominated Mechanism. *Analyst* **2015**, *140*, 4384-4387.

14. Zhang, B.; Wang, Z. M.; Kurmoo, M.; Gao, S.; Inoue, K.; Kobayashi, H., Guest-Induced Chirality in the Ferrimagnetic Nanoporous Diamond Framework $Mn_3(HCOO)_6$. *Adv Funct Mater* **2007**, *17*, 577-584.

15. Blake, A. J.; Champness, N. R.; Easun, T. L.; Allan, D. R.; Nowell, H.; George, M. W.; Jia, J.; Sun, X.-Z., Photoreactivity Examined through Incorporation in Metal−Organic Frameworks. *Nat Chem* **2010**, *2*, 688.

16. Abrahams, B. F.; Grannas, M. J.; Hudson, T. A.; Robson, R., A Simple Lithium (I) Salt with a Microporous Structure and Its Gas Sorption Properties. *Angew Chem Int Ed Engl* **2010**, *49*, 1087-1089.

17. Lin, Z.; Zou, R.; Xia, W.; Chen, L.; Wang, X.; Liao, F.; Wang, Y.; Lin, J.; Burrell, A. K., Ultrasensitive Sorption Behavior of Isostructural Lanthanide–Organic Frameworks Induced by Lanthanide Contraction. *J Mater Chem* **2012**, *22*, 21076-21084.

18. Liu, H.-K.; Tsao, T.-H.; Zhang, Y.-T.; Lin, C.-H., Microwave Synthesis and Single-Crystal-to-Single-Crystal Transformation of Magnesium Coordination Polymers Exhibiting Selective Gas Adsorption and Luminescence Properties. *Cryst Eng Comm* **2009**, *11*, 1462-1468.

19. Pérez-Yánez, S.; Beobide, G.; Castillo, O.; Cepeda, J.; Luque, A.; Aguayo, A. T.; Román, P., Open-Framework Copper Adeninate Compounds with Three-Dimensional Microchannels Tailored by Aliphatic Monocarboxylic Acids. *Inorg Chem* **2011**, *50*, 5330-5332.

20. Ibarra, I. A.; Hesterberg, T. W.; Holliday, B. J.; Lynch, V. M.; Humphrey, S. M., Gas Sorption and Luminescence Properties of a Terbium(III)-Phosphine Oxide Coordination Material with Two-Dimensional Pore Topology. *Dalton Trans* **2012**, *41*, 8003-8009.

21. Yue, Q.; Yan, L.; Zhang, J.-Y.; Gao, E.-Q., Novel Functionalized Metal−Organic Framework Based on Unique Hexagonal Prismatic Clusters. *Inorg Chem* **2010**, *49*, 8647-8649.

22. Banerjee, D.; Kim, S. J.; Li, W.; Wu, H.; Li, J.; Borkowski, L. A.; Philips, B. L.; Parise, J. B., Synthesis and Structural Characterization of a 3-D Lithium Based Metal−Organic Framework Showing Dynamic Structural Behavior. *Cryst Growth Des* **2010**, *10*, 2801-2805.

23. Han, Z.-B.; Lu, R.-Y.; Liang, Y.-F.; Zhou, Y.-L.; Chen, Q.; Zeng, M.-H., Mn(II)-Based Porous Metal–Organic Framework Showing Metamagnetic Properties and High Hydrogen Adsorption at Low Pressure. *Inorg Chem* **2011**, *51*, 674-679.

24. Stylianou, K. C.; Rabone, J.; Chong, S. Y.; Heck, R.; Armstrong, J.; Wiper, P. V.; Jelfs, K. E.; Zlatogorsky, S.; Bacsa, J.; McLennan, A. G., Dimensionality Transformation through Paddlewheel Reconfiguration in a Flexible and Porous Zn-Based Metal–Organic Framework. *J Am Chem Soc* **2012**, *134*, 20466-20478.

25. Yang, F.; Li, B.; Xu, W.; Li, G.; Zhou, Q.; Hua, J.; Shi, Z.; Feng, S., Two Metal–Organic Frameworks Constructed from One-Dimensional Cobalt (II) Ferrimagnetic Chains with Alternating Antiferromagnetic/Ferromagnetic and AF/AF/FM Interaction: Synthesis, Structures, and Magnetic Properties. *Inorg Chem* **2012**, *51*, 6813-6820.

26. Zhang, C.-Z.; Mao, H.-Y.; Wang, Y.-L.; Zhang, H.-Y.; Tao, J.-C., Syntheses of Two New Hybrid Metal-Organic Polymers Using Flexible Aliphatic Dicarboxylates and Pyrazine: Crystal Structures and Magnetic Studies. *J Phys Chem Solids* **2007**, *68*, 236-242.

27. Kosaka, W.; Hashimoto, K.; Ohkoshi, S.-I., Three-Dimensional Manganese Octacyanoniobate-Based Pyroelectric Ferrimagnet. *Bull Chem Soc Jpn* **2008**, *81*, 992-994.

28. Lässig, D.; Lincke, J. R.; Gerhardt, R.; Krautscheid, H., Solid-State Syntheses of Coordination Polymers by Thermal Conversion of Molecular Building Blocks and Polymeric Precursors. *Inorg Chem* **2012**, *51*, 6180-6189.

29. He, J.; Yang, C.; Xu, Z.; Zeller, M.; Hunter, A. D.; Lin, J., Building Thiol and Metal-Thiolate Functions into Coordination Nets: Clues from a Simple Molecule. *J Solid State Chem* **2009**, *182*, 1821-1826.

30. Kobayashi, A.; Suzuki, Y.; Ohba, T.; Noro, S.-I.; Chang, H.-C.; Kato, M., Ln−Co-Based Rock-Salt-Type Porous Coordination Polymers: Vapor Response Controlled by Changing the Lanthanide Ion. *Inorg Chem* **2011**, *50*, 2061-2063.

31. Gao, W.-Y.; Yan, W.; Cai, R.; Williams, K.; Salas, A.; Wojtas, L.; Shi, X.; Ma, S., A Pillared Metal–Organic Framework Incorporated with 1,2,3-Triazole Moieties Exhibiting Remarkable Enhancement of CO_2 Uptake. *Chem Commun* **2012**, *48*, 8898-8900.

32. Senkovska, I.; Fritsch, J.; Kaskel, S., New Polymorphs of Magnesium-Based Metal–Organic Frameworks $Mg_3(ndc)_3$ (ndc = 2,6-Naphthalenedicarboxylate). *Eur J Inorg Chem* **2007**, *2007*, 5475-5479.

33. Hu, S.; Zhang, J.-P.; Li, H.-X.; Tong, M.-L.; Chen, X.-M.; Kitagawa, S., A Dynamic Microporous Metal–Organic Framework with BCT Zeolite Topology: Construction, Structure, and Adsorption Behavior. *Cryst Growth Des* **2007**, *7*, 2286-2289.

34. Kiskin, M. A.; Aleksandrov, G. G.; Bogomyakov, A. S.; Novotortsev, V. M.; Eremenko, I. L., Coordination Polymers of Cobalt (II) with Pyrimidine and Pyrazine:

Syntheses, Structures and Magnetic Properties. *Inorg Chem Commun* **2008**, *11*, 1015-1018.

35. Chang, W.-M.; Cheng, M.-Y.; Liao, Y.-C.; Chang, M.-C.; Wang, S.-L., Template Effect of Chain-Type Polyamines on Pore Augmentation: Five Open-Framework Zinc Phosphates with 16-Ring Channels. *Chem Mater* **2007**, *19*, 6114-6119.

36. Li, M.; Yuan, L.; Li, H.; Sun, J., A 3D Heterometallic Metal–Organic Framework Constructed from Luminescent Building Blocks, Exhibiting Reversible Dehydration and Rehydration Procedure. *Inorg Chem Commun* **2007**, *10*, 1281-1284.

37. Pearson, K., Note on Regression and Inheritance in the Case of Two Parents. *Proc R Soc Lond A* **1895**, *58*, 240-242.

38. Asuero, A.; Sayago, A.; Gonzalez, A., The Correlation Coefficient: An Overview. *Crit Rev Anal Chem* **2006**, *36*, 41-59.

39. Liu, X.; Oh, M.; Lah, M. S., Adsorbate Selectivity of Isoreticular Microporous Metal–Organic Frameworks with Similar Static Pore Dimensions. *Cryst Growth Des* **2011**, *11*, 5064-5071.

40. Shi, N.; Zhang, Y.; Xu, D.; Song, C.; Jin, X.; Liu, D.; Xie, L.; Huang, W., Π-System Based Coordination Polymer Hollow Nanospheres for the Selective Sensing of Aromatic Nitro Explosive Compounds. *New J Chem* **2015**, *39*, 9275-9280.

41. Zhao, D.; Zhang, J.; Yue, D.; Lian, X.; Cui, Y.; Yang, Y.; Qian, G., A Highly Sensitive Near-Infrared Luminescent Metal–Organic Framework Thermometer in the Physiological Range. *Chem Commun* **2016**, *52*, 8259-8262.

42. Chen, Z.-F.; Zhang, S.-F.; Luo, H.-S.; Abrahams, B. F.; Liang, H., $Ni_2(R^*COO)_4(H_2O)(4,4'\text{-bipy})_2$—a Robust Homochiral Quartz-Like Network with Large Chiral Channels. *Cryst Eng Comm* **2007**, *9*, 27-29.

43. Cordes, D. B.; Hanton, L. R.; Spicer, M. D., Six-Coordinated Cd(II) Centers as Four- or Six-Connected Nodes in Coordination Polymer Networks Containing Bis(4-Pyridyl)Amine. *Cryst Growth Des* **2007**, *7*, 328-336.

44. Burrows, A. D.; Cassar, K.; Mahon, M. F.; Warren, J. E., The Stepwise Formation of Mixed-Metal Coordination Networks Using Complexes of 3-Cyanoacetylacetonate. *Dalton Trans* **2007**, 2499-2509.

45. Smith, G.; Wermuth, U. D.; Young, D. J.; White, J. M., Polymeric Structures in the Metal Complexes of 5-Sulfosalicylic Acid: The Rubidium(I), Caesium(I) and Lead(II) Analogues. *Polyhedron* **2007**, *26*, 3645-3652.

46. Zhang, H.-Y.; Yu, H.-J.; Xu, H.-X.; Ren, J.-S.; Qu, X.-G., Structural Diversity of Lanthanide–Amino Acid Complexes Under Near Physiological pH Conditions and Their Recognition of Single-Stranded DNA. *Polyhedron* **2007**, *26*, 5250-5256.

47. Schull, T. L.; Henley, L.; Deschamps, J. R.; Butcher, R. J.; Maher, D. P.; Klug, C. A.; Swider-Lyons, K.; Dressick, W. J.; Bujoli, B.; Greenwood, A. E., Organometallic Supramolecular Mixed-Valence Cobalt (I)/Cobalt (II) Aquo Complexes Stabilized with the Water-Soluble Phosphine Ligand p-TPPTP (p-Triphenylphosphine Triphosphonic Acid). *Organometallics* **2007**, *26*, 2272-2276.

48. Luisi, B. S.; Ma, Z.; Moulton, B., Tri-Metal Secondary Building Units: Toward the Design of Thermally Robust Crystalline Coordination Polymers. *J Chem Crystallogr* **2007**, *37*, 743-747.

49. Luo, F.; Che, Y.-X.; Zheng, J.-M., A Ternary Metal−Organic Framework Built on Triangular Organic Spacers, Square and Tetrahedral CO_2 Secondary Building Units. *Cryst Growth Des* **2008**, *8*, 176-178.

50. Bondar, O. A.; Lukashuk, L. V.; Lysenko, A. B.; Krautscheid, H.; Rusanov, E. B.; Chernega, A. N.; Domasevitch, K. V., New Microporous Copper(II) Coordination Polymers Based Upon Bifunctional 1,2,4-Triazole/Tetrazolate Bridges. *Cryst Eng Comm* **2008**, *10*, 1216-1226.

51. Han, L.; Zhao, W.; Zhou, Y.; Li, X.; Pan, J., One-Pot Synthesis of Supramolecular Isomers with Two-Dimensional 4^4 Grid and Three-Dimensional $6^4 \cdot 8^2$ NbO Frameworks: Solvothermal in Situ Ligand Formation and Conformational Isomers Separation. *Cryst Growth Des* **2008**, *8*, 3504-3507.

52. Heck, R.; Bacsa, J.; Warren, J. E.; Rosseinsky, M. J.; Bradshaw, D., Triply Interpenetrated (3,4)- and (3,5)-Connected Binodal Metal–Organic Networks Prepared from 1,3,5-Benzenetrisbenzoate and 4,4′-Bipyridyl. *Cryst Eng Comm* **2008**, *10*, 1687-1692.

53. Zhang, X.-J.; Xing, Y.-H.; Han, J.; Zeng, X.-Q.; Ge, M.-F.; Niu, S.-Y., A Series of Novel Ln−Succinate−Oxalate Coordination Polymers: Synthesis, Structure, Thermal Stability, and Fluorescent Properties. *Cryst Growth Des* **2008**, *8*, 3680-3688.

54. Liu, Y.-J.; Huang, J.-S.; Chui, S. S.-Y.; Li, C.-H.; Zuo, J.-L.; Zhu, N.; Che, C.-M., A Noncentrosymmetric 3D Coordination Polymer of Metallocalix[4]arene. *Inorg Chem* **2008**, *47*, 11514-11518.

55. Zhou, Y.-X.; Shen, X.-Q.; Du, C.-X.; Wu, B.-L.; Zhang, H.-Y., 1D, 2D and 3D Coordination Polymers of Aromatic Carboxylate Tb^{III}: Structure, Thermolysis Kinetics and Fluorescence. *Eur J Inorg Chem* **2008**, *2008*, 4280-4289.

56. Kerbellec, N.; Daiguebonne, C.; Bernot, K.; Guillou, O.; Le Guillou, X., New Lanthanide Based Coordination Polymers with High Potential Porosity. *J Alloys Compd* **2008**, *451*, 377-383.

57. Lee, H. Y.; Park, J.; Lah, M. S.; Hong, J.-I., One-Dimensional Double Helical Structure and 4-Fold Type [2 + 2] Interpenetration of Diamondoid Networks with Helical Fashion. *Cryst Growth Des* **2008**, *8*, 587-591.

58. Hernández-Ahuactzi, I. F.; Höpfl, H.; Barba, V.; Román-Bravo, P.; Zamudio-Rivera, L. S.; Beltrán, H. I., Pore-Size Tuning in Double-Pillared Metal-Organic Frameworks Containing Cadmium Clusters. *Eur J Inorg Chem* **2008**, *2008*, 2746-2755.

59. Zhu, S.; Zhang, H.; Zhao, Y.; Shao, M.; Wang, Z.; Li, M., Synthesis, Structures and Luminescence of Three Coordination Polymers Constructed from Rigid 1,3,5-Benzenetricarboxylic Acid and Flexible Bis(Imidazol-1-ylmethyl)-Benzene. *J Mol Struct* **2008**, *892*, 420-426.

60. Thétiot, F.; Duhayon, C.; Venkatakrishnan, T. S.; Sutter, J.-P., Modular Assembling of $[Zr(C_2O_4)_4]^{4-}$ and $[DabcoH_2]^{2+}$ Units in Supramolecular Hybrid Architectures Including an Open Framework with Reversible Sorption Properties (Dabco = 1, 4-Diazabicyclo[2.2.2]octane). *Cryst Growth Des* **2008**, *8*, 1870-1877.

61. Xie, Y.-M.; Liu, J.-H.; Wu, X.-Y.; Zhao, Z.-G.; Zhang, Q.-S.; Wang, F.; Chen, S.-C.; Lu, C.-Z., New Ferroelectric and Nonlinear Optical Porous Coordination Polymer Constructed from a Rare $(CuBr)_\infty$ Castellated Chain. *Cryst Growth Des* **2008**, *8*, 3914-3916.

62. Li, G.; Salim, C.; Hinode, H., Hydrothermal Syntheses and Crystal Structures of Two Hybrid Materials Constructed from Polyoxometalate Clusters and Metal–Dipyridine Complexes. *Solid State Sci* **2008**, *10*, 121-128.

63. Luo, F.; Zheng, J.-m.; Long, G. J., Unique Anionic Eight-Connected Net with $3^6 4^{18} 5^3 6$ Topology Derived from a Rare $Co_6(\mu_3\text{-}OH)_2(\mu\text{-}H_2O)(CO_2)_{12}$ Building Block. *Cryst Growth Des* **2009**, *9*, 1271-1274.

64. Liu, D.; Li, M.; Li, D., Reversible Solid–Gas Chemical Equilibrium between a 0-Periodic Deformable Molecular Tecton and a 3-Periodic Coordination Architecture. *Chem Commun* **2009**, 6943-6945.

65. Gándara, F.; de la Peña-O'Shea, V. C. A.; Illas, F.; Snejko, N.; Proserpio, D. M.; Gutiérrez-Puebla, E.; Monge, M. A., Three Lanthanum MOF Polymorphs: Insights into Kinetically and Thermodynamically Controlled Phases. *Inorg Chem* **2009**, *48*, 4707-4713.

66. Wang, X.-S.; Ma, S.; Yuan, D.; Yoon, J. W.; Hwang, Y. K.; Chang, J.-S.; Wang, X.; Jørgensen, M. R.; Chen, Y.-S.; Zhou, H.-C., A Large-Surface-Area Boracite-Network-Topology Porous MOF Constructed from a Conjugated Ligand Exhibiting a High Hydrogen Uptake Capacity. *Inorg Chem* **2009**, *48*, 7519-7521.

67. Nelson, A. P.; Parrish, D. A.; Cambrea, L. R.; Baldwin, L. C.; Trivedi, N. J.; Mulfort, K. L.; Farha, O. K.; Hupp, J. T., Crystal to Crystal Guest Exchange in a Mixed Ligand Metal−Organic Framework. *Cryst Growth Des* **2009**, *9*, 4588-4591.

68. Han, Z.-B.; Zhang, G.-X.; Zeng, M.-H.; Ge, C.-H.; Zou, X.-H.; Han, G.-X., Synthesis, Crystal Structure and Magnetic Properties of Two 3-D Gadolinium Complexes. *Cryst Eng Comm* **2009**, *11*, 2629-2633.

69. Seo, J.; Chun, H., Hysteretic Gas Sorption in a Microporous Metal–Organic Framework with Nonintersecting 3D Channels. *Eur J Inorg Chem* **2009**, *2009*, 4946-4949.

70. Hunger, J.; Krautscheid, H.; Sieler, J., Hydrothermal Synthesis and Structure of Coordination Polymers by Combination of Bipyrazole and Aromatic Dicarboxylate Ligands. *Cryst Growth Des* **2009**, *9*, 4613-4625.

71. Yue, Q.; Sun, Q.; Cheng, A.-L.; Gao, E.-Q., Metal−Organic Framework Based on $[Zn_4O(COO)_6]$ Clusters: Rare 3D Kagomé Topology and Luminescence. *Cryst Growth Des* **2009**, *10*, 44-47.

72. Konno, T.; Yoshinari, N.; Taguchi, M.; Igashira-Kamiyama, A., Drastic Change in Dimensional Structures of D-Penicillaminato $(Au^{I}_2Pt^{II}_2Zn^{II})_n$ Coordination Polymers by Moderate Change in Solution pH. *Chem Lett* **2009**, *38*, 526-527.

73. Wu, Y.; Li, D.; Fu, F.; Tang, L.; Wang, J.; Yang, X. G., Microporous 3-D Chiral Metal-Organic Framework with a Quartzlike Topology Based on an Achiral Building Unit. *J Coord Chem* **2009**, *62*, 2665-2674.

74. Kalf, I.; Mathieu, P.; Englert, U., From Crystal to Crystal: A New Polymorph of (4-Carboxylatopyridine) Silver (I) by Topotactic Dehydration of Its Monohydrate. *New J Chem* **2010**, *34*, 2491-2495.

75. Ohara, K.; Inokuma, Y.; Fujita, M., The Catalytic Z to E Isomerization of Stilbenes in a Photosensitizing Porous Coordination Network. *Angew Chem Int Ed Engl* **2010**, *49*, 5507-5509.

76. Rodríguez-Diéguez, A.; Salinas-Castillo, A.; Sironi, A.; Seco, J.; Colacio, E., A Chiral Diamondoid 3D Lanthanum Metal–Organic Framework Displaying Blue-Greenish Long Lifetime Photoluminescence Emission. *Cryst Eng Comm* **2010**, *12*, 1876-1879.

77. Zhang, N.; Li, M.-X.; Wang, Z.-X.; Shao, M.; Zhu, S.-R., Synthesis, Structures and Thermal Stabilities of Five Copper (II) Coordination Polymers Based on 2,4,6-Tris (Pyridyl)-1,3,5-Triazine and 1,2,4,5-Benzenetetracarboxylate Ligands. *Inorganica Chim Acta* **2010**, *363*, 8-14.

78. Dey, B.; Das, A.; Choudhury, S. R.; Jana, A. D.; Lu, L.-P.; Zhu, M.-L.; Mukhopadhyay, S., Three Dimensional Metal–Malonate Frameworks with Pillared Layered Architecture: Unusual Role of Metal–Chelate as Pillar. *Inorganica Chim Acta* **2010**, *363*, 981-987.

79. Barron, P. M.; Wray, C. A.; Hu, C.; Guo, Z.; Choe, W., A Bioinspired Synthetic Approach for Building Metal−Organic Frameworks with Accessible Metal Centers. *Inorg Chem* **2010**, *49*, 10217-10219.

80. Xue, M.; Zhang, Z.; Xiang, S.; Jin, Z.; Liang, C.; Zhu, G.-S.; Qiu, S.-L.; Chen, B., Selective Gas Adsorption within a Five-Connected Porous Metal–Organic Framework. *J Mater Chem* **2010**, *20*, 3984-3988.

81. Huang, X.-Y.; Yue, K.-F.; Jin, J.-C.; Liu, J.-Q.; Wang, C.-J.; Wang, Y.-Y.; Shi, Q.-Z., Three-Dimensional Fivefold Interpenetrating Microporous Metal–Organic Framework Based on Mixed Flexible Ligands. *Inorg Chem Commun* **2010**, *13*, 338-341.

82. Yu, Q.; Zeng, Y.-F.; Zhao, J.-P.; Yang, Q.; Hu, B.-W.; Chang, Z.; Bu, X.-H., Three-Dimensional Porous Metal−Organic Frameworks Exhibiting Metamagnetic Behaviors: Synthesis, Structure, Adsorption, and Magnetic Properties. *Inorg Chem* **2010**, *49*, 4301-4306.

83. Zou, R.; Zhong, R.; Han, S.; Xu, H.; Burrell, A. K.; Henson, N.; Cape, J. L.; Hickmott, D. D.; Timofeeva, T. V.; Larson, T. E., A Porous Metal−Organic Replica of α-PbO_2 for Capture of Nerve Agent Surrogate. *J Am Chem Soc* **2010**, *132*, 17996-17999.

84. Liu, D.; Xie, Z.; Ma, L.; Lin, W., Three-Dimensional Metal−Organic Frameworks Based on Tetrahedral and Square-Planar Building Blocks: Hydrogen Sorption and Dye Uptake Studies. *Inorg Chem* **2010**, *49*, 9107-9109.

85. Hu, B.-W.; Zhao, J.-P.; Tao, J.; Sun, X.-J.; Yang, Q.; Zhang, X.-F.; Bu, X.-H., A New Azido-Nickel Compound with Three-Dimensional Kagomé Topology. *Cryst Growth Des* **2010**, *10*, 2829-2831.

86. Chen, F.; Zheng, F.-K.; Liu, G.-N.; Wu, A.-Q.; Wang, M.-S.; Guo, S.-P.; Wu, M.-F.; Liu, Z.-F.; Guo, G.-C.; Huang, J.-S., Crystal Structure and Magnetic Property of a 3D Heterometallic Coordination Polymer Constructed by 3-Cyanobenzoate and 3-(5H-Tetrazol) Benzoate Ligands. *Inorg Chem Commun* **2010**, *13*, 278-281.

87. Hassanzadeh Fard, Z.; Hołyńska, M.; Dehnen, S., Organotin Chalcogenide Salts: Synthesis, Characterization, and Extended Crystal Structures. *Inorg Chem* **2010**, *49*, 5748-5752.

88. Thuéry, P.; Masci, B., Two-and Three-Dimensional Europium−Organic Assemblies with the All-Cis and All-Trans Isomers of 1,2,3,4,5,6-Cyclohexanehexacarboxylic Acid. *Cryst Growth Des* **2010**, *10*, 3626-3631.

89. Zhang, J.; Xue, Y.-S.; Liang, L.-L.; Ren, S.-B.; Li, Y.-Z.; Du, H.-B.; You, X.-Z., Porous Coordination Polymers of Transition Metal Sulfides with PtS Topology Built on a Semirigid Tetrahedral Linker. *Inorg Chem* **2010**, *49*, 7685-7691.

90. Platero-Prats, A. E.; de la Peña-O'Shea, V. A.; Snejko, N.; Monge, Á.; Gutiérrez-Puebla, E., Dynamic Calcium Metal–Organic Framework Acts as a Selective Organic Solvent Sponge. *Chem Eur J* **2010**, *16*, 11632-11640.

91. Jia, J.; Shao, M.; Jia, T.; Zhu, S.; Zhao, Y.; Xing, F.; Li, M., Coordination Polymers of Biphenyl-2,4,2′,4′-Tetracarboxylic Acid—Synthesis, Structures and Adsorption Properties. *Cryst Eng Comm* **2010**, *12*, 1548-1561.

92. Li, B.; Li, G.; Liu, D.; Peng, Y.; Zhou, X.; Hua, J.; Shi, Z.; Feng, S., Coordination Polymers Constructed by 1,3-Bi(4-Pyridyl)propane with Four Different Conformations and 2,2′-Dinitro-4,4′-Biphenyldicarboxylate Ligands: The Effects of Metal Ions. *Cryst Eng Comm* **2011**, *13*, 1291-1298.

93. Jiang, G.; Wu, T.; Zheng, S.-T.; Zhao, X.; Lin, Q.; Bu, X.; Feng, P., A Nine-Connected Mixed-Ligand Nickel-Organic Framework and Its Gas Sorption Properties. *Cryst Growth Des* **2011**, *11*, 3713-3716.

94. Meng, M.; Zhong, D.-C.; Lu, T.-B., Three Porous Metal–Organic Frameworks Based on an Azobenzenetricarboxylate Ligand: Synthesis, Structures, and Magnetic Properties. *Cryst Eng Comm* **2011**, *13*, 6794-6800.

95. Yamada, T.; Iwakiri, S.; Hara, T.; Kanaizuka, K.; Kurmoo, M.; Kitagawa, H., Porous Interpenetrating Metal−Organic Frameworks with Hierarchical Nodes. *Cryst Growth Des* **2011**, *11*, 1798-1806.

96. Lhoste, J.; Henry, N.; Roussel, P.; Loiseau, T.; Abraham, F., An Uranyl Citrate Coordination Polymer with a 3D Open-Framework Involving Uranyl Cation-Cation Interactions. *Dalton Trans* **2011**, *40*, 2422-2424.

97. Kanoo, P.; Ghosh, A. C.; Maji, T. K., A Vanadium (VO^{2+}) Metal–Organic Framework: Selective Vapor Adsorption, Magnetic Properties, and Use as a Precursor for a Polyoxovanadate. *Inorg Chem* **2011**, *50*, 5145-5152.

98. Wu, H.; Ma, J.-F.; Liu, Y.-Y.; Yang, J.; Liu, H.-Y., Diverse Topologies of Six Coordination Polymers Constructed from a Tris (4-Imidazolylphenyl) Amine Ligand and Different Carboxylates. *Cryst Eng Comm* **2011**, *13*, 7121-7128.

99. Zhao, L.-M.; Zhang, Z.-J.; Zhang, S.-Y.; Cui, P.; Shi, W.; Zhao, B.; Cheng, P.; Liao, D.-Z.; Yan, S.-P., Metal–Organic Frameworks Based on Transition-Metal Carboxylate Clusters as Secondary Building Units: Synthesis, Structures and Properties. *Cryst Eng Comm* **2011**, *13*, 907-913.

100. Volkringer, C.; Mihalcea, I.; Vigier, J.-F. o.; Beaurain, A.; Visseaux, M.; Loiseau, T., Metal–Organic-Framework-Type 1D-Channel Open Network of a Tetravalent Uranium Trimesate. *Inorg Chem* **2011**, *50*, 11865-11867.

101. Wang, F.; Ke, X.; Zhao, J.; Deng, K.; Leng, X.; Tian, Z.; Wen, L.; Li, D., Six New Metal–Organic Frameworks with Multi-Carboxylic Acids and Imidazole-Based Spacers: Syntheses, Structures and Properties. *Dalton Trans* **2011**, *40*, 11856-11865.

102. Li, B.; Yang, F.; Li, G.; Liu, D.; Zhou, Q.; Shi, Z.; Feng, S., Construction of Coordination Polymers Based on Bent 4-Amino-3,5-Bis(3-Carboxyphenyl)-1,2,4-

Triazole Ligand: Diverse Structural Topology and Photoluminescent and Magnetic Properties. *Cryst Growth Des* **2011**, *11*, 1475-1485.

103. Alsobrook, A. N.; Hauser, B. G.; Hupp, J. T.; Alekseev, E. V.; Depmeier, W.; Albrecht-Schmitt, T. E., From Layered Structures to Cubic Frameworks: Expanding the Structural Diversity of Uranyl Carboxyphosphonates Via the Incorporation of Cobalt. *Cryst Growth Des* **2011**, *11*, 1385-1393.

104. Adelani, P. O.; Albrecht-Schmitt, T. E., Pillared and Open-Framework Uranyl Diphosphonates. *J Solid State Chem* **2011**, *184*, 2368-2373.

105. Ren, G.; Liu, S.; Ma, F.; Wei, F.; Tang, Q.; Yang, Y.; Liang, D.; Li, S.; Chen, Y., A 9-Connected Metal–Organic Framework with Gas Adsorption Properties. *J Mater Chem* **2011**, *21*, 15909-15913.

106. Yan, Y.; Blake, A. J.; Lewis, W.; Barnett, S. A.; Dailly, A.; Champness, N. R.; Schröder, M., Modifying Cage Structures in Metal–Organic Polyhedral Frameworks for H_2 Storage. *Chem Eur J* **2011**, *17*, 11162-11170.

107. Gong, Y.-N.; Meng, M.; Zhong, D.-C.; Huang, Y.-L.; Jiang, L.; Lu, T.-B., Counter-Cation Modulation of Hydrogen and Methane Storage in a Sodalite-Type Porous Metal–Organic Framework. *Chem Commun* **2012**, *48*, 12002-12004.

108. Adelani, P. O.; Albrecht-Schmitt, T. E., Heterobimetallic Copper (II) Uranyl Carboxyphenylphosphonates. *Cryst Growth Des* **2011**, *11*, 4676-4683.

109. Zhang, P.; Li, B.; Zhao, Y.; Meng, X.; Zhang, T., A Novel (3,36)-Connected and Self-Interpenetrated Metal–Organic Framework with High Thermal Stability and Gas-Sorption Capabilities. *Chem Commun* **2011**, *47*, 7722-7724.

110. Chen, S.-S.; Lv, G.-C.; Fan, J.; Okamura, T.-a.; Chen, M.; Sun, W.-Y., Entangled Coordination Frameworks with 1,4-Di(1H-Imidazol-4-yl)Benzene. *Cryst Growth Des* **2011**, *11*, 1082-1090.

111. Zhao, X.; Wu, T.; Zheng, S.-T.; Wang, L.; Bu, X.; Feng, P., A Zeolitic Porous Lithium–Organic Framework Constructed from Cubane Clusters. *Chem Commun* **2011**, *47*, 5536-5538.

112. Ma, R.; Chen, C.; Sun, B.; Zhao, X.; Zhang, N., A New 3D Metal–Organic Framework with (4,8)-Connected AlB_2 Topology Constructed from Coordinated Evolution of a C_3 Symmetry Ligand. *Inorg Chem Commun* **2011**, *14*, 1532-1536.

113. Su, S.; Zhang, Y.; Zhu, M.; Song, X.; Wang, S.; Zhao, S.; Song, S.; Yang, X.; Zhang, H., An Active-Site-Accessible Porous Metal–Organic Framework Composed of Triangular Building Units: Preparation, Catalytic Activity and Magnetic Property. *Chem Commun* **2012**, *48*, 11118-11120.

114. Sen, R.; Saha, D.; Koner, S., Controlled Construction of Metal–Organic Frameworks: Hydrothermal Synthesis, X-Ray Structure, and Heterogeneous Catalytic Study. *Chem Eur J* **2012**, *18*, 5979-5986.

115. Zhang, Y.; Wang, Q.; Xiao, Y.-J.; Han, J.; Zhao, X.-L., Structure Diversity of a Series of New Coordination Polymers Based on a C_3-Symmetric Tridentate Ligand with Rosette Architecture. *Polyhedron* **2012**, *33*, 127-136.

116. Sun, L.; Ma, L.; Cai, J.-B.; Liang, L.; Deng, H., Novel Tetrazole-Based Metal–Organic Frameworks Constructed from in Situ Synthesize Bifunctional Ligands: Syntheses, Structure and Luminescent Properties. *Cryst Eng Comm* **2012**, *14*, 890-898.

117. Lu, Z.; Xing, H.; Sun, R.; Bai, J.; Zheng, B.; Li, Y., Water Stable Metal–Organic Framework Evolutionally Formed from a Flexible Multidentate Ligand with Acylamide Groups for Selective CO_2 Adsorption. *Cryst Growth Des* **2012**, *12*, 1081-1084.

118. Song, X.-Z.; Qin, C.; Guan, W.; Song, S.-Y.; Zhang, H.-J., An Unusual Three-Dimensional Self-Penetrating Network Derived from Cross-Linking of Two-Fold Interpenetrating Nets Via Ligand-Unsupported Ag–Ag Bonds: Synthesis, Structure, Luminescence, and Theoretical Study. *New J Chem* **2012**, *36*, 877-882.

119. Ahmad, M.; Das, R.; Lama, P.; Poddar, P.; Bharadwaj, P. K., Synthesis, Characterization, and Magnetic Studies of Coordination Polymers with Co (II) and Mn (II) Ions. *Cryst Growth Des* **2012**, *12*, 4624-4632.

120. Kundu, T.; Sahoo, S. C.; Banerjee, R., Variable Water Adsorption in Amino Acid Derivative Based Homochiral Metal Organic Frameworks. *Cryst Growth Des* **2012**, *12*, 4633-4640.

121. Wen, L.; Ke, X.; Qiu, L.; Zou, Y.; Zhou, L.; Zhao, J.; Li, D., Assembly of Two Porous Cadmium (II) Frameworks: Selective Adsorption and Luminescent Property. *Cryst Growth Des* **2012**, *12*, 4083-4089.

122. Chen, Q.; Xue, W.; Wang, B.-Y.; Zeng, M.-H.; Chen, X.-M., Unprecedented Binodal (7,9)-Connected Network Based on Distinct Tricobalt (II) Clusters: Structure, Topology and Cooperative Magnetism. *Cryst Eng Comm* **2012**, *14*, 2009-2014.

123. Ruan, C.-Z.; Wen, R.; Liang, M.-X.; Kong, X.-J.; Ren, Y.-P.; Long, L.-S.; Huang, R.-B.; Zheng, L.-S., Two Triazole-Based Metal–Organic Frameworks Constructed from Nanosized Cu_{20} and Cu_{30} Wheels. *Inorg Chem* **2012**, *51*, 7587-7591.

124. Dau, P. V.; Tanabe, K. K.; Cohen, S. M., Functional Group Effects on Metal–Organic Framework Topology. *Chem Commun* **2012**, *48*, 9370-9372.

125. Wen, L.; Shi, W.; Chen, X.; Li, H.; Cheng, P., A Porous Metal-Organic Framework Based on Triazoledicarboxylate Ligands–Synthesis, Structure, and Gas-Sorption Studies. *Eur J Inorg Chem* **2012**, *2012*, 3562-3568.

126. Fang, Q.-R.; Yuan, D.-Q.; Sculley, J.; Lu, W.-G.; Zhou, H.-C., A Novel MOF with Mesoporous Cages for Kinetic Trapping of Hydrogen. *Chem Commun* **2012**, *48*, 254-256.

127. Majumder, M.; Sheath, P.; Mardel, J. I.; Harvey, T. G.; Thornton, A. W.; Gonzago, A.; Kennedy, D. F.; Madsen, I.; Taylor, J. W.; Turner, D. R., Aqueous Molecular Sieving and Strong Gas Adsorption in Highly Porous MOFs with a Facile Synthesis. *Chem Mater* **2012**, *24*, 4647-4652.

128. Muñoz-Lara, F. J.; Gaspar, A. B.; Muñoz, M. C.; Lysenko, A. B.; Domasevitch, K. V.; Real, J. A., Fast Detection of Water and Organic Molecules by a Change of Color in an Iron (II) Microporous Spin-Crossover Coordination Polymer. *Inorg Chem* **2012**, *51*, 13078-13080.

129. Tseng, T.-W.; Luo, T.-T.; Chen, S.-Y.; Su, C.-C.; Chi, K.-M.; Lu, K.-L., Porous Metal–Organic Frameworks with Multiple Cages Based on Tetrazolate Ligands: Synthesis, Structures, Photoluminescence, and Gas Adsorption Properties. *Cryst Growth Des* **2012**, *13*, 510-517.

130. Jeong, E.; Lee, W. R.; Ryu, D. W.; Kim, Y.; Phang, W. J.; Koh, E. K.; Hong, C. S., Reversible Structural Transformation and Selective Gas Adsorption in a Unique Aqua-Bridged Mn (II) Metal–Organic Framework. *Chem Commun* **2013**, *49*, 2329-2331.

131. Wang, L.; Yan, Z.-H.; Xiao, Z.; Guo, D.; Wang, W.; Yang, Y., Reactant Ratio-Modulated Entangled Cd (II) Coordination Polymers Based on Rigid Tripodal Imidazole Ligand and Tetrabromoterephthalic Acid: Interpenetration, Interdigitation and Self-Penetration. *Cryst Eng Comm* **2013**, *15*, 5552-5560.

132. Wen, Z.-Z.; Wen, X.-L.; Cai, S.-L.; Zheng, S.-R.; Fan, J.; Zhang, W.-G., The Construction of Cu(I)/Cu(II) Coordination Polymers Based on Pyrazine–Carboxylate: Structural Diversity Tuned by in Situ Hydrolysis Reaction. *Cryst Eng Comm* **2013**, *15*, 5359-5367.

133. Huang, Y.-Y.; Zhang, X.; Yao, Y.-G., Employing Heterometallic Trinuclear Cluster as Building Subunit to Construct a New Coordination Polymer with Rare 3D Inorganic–Cd–O–Ba–Connectivity. *Inorganica Chim Acta* **2013**, *397*, 38-41.

134. Chen, L.; Zhang, L.; Li, S.-L.; Qiu, Y.-Q.; Shao, K.-Z.; Wang, X.-L.; Su, Z.-M., Self-Assembly of Metal–Organic Frameworks Based on N-Donor Ligand and Flexible Tricarboxylic Acids with Different Angular Characters. *Cryst Eng Comm* **2013**, *15*, 8214-8221.

135. Lian, T.-T.; Chen, S.-M.; Wang, F.; Zhang, J., Metal–Organic Framework Architecture with Polyhedron-in-Polyhedron and Further Polyhedral Assembly. *Cryst Eng Comm* **2013**, *15*, 1036-1038.

136. Li, C.-P.; Chen, J.; Liu, P.-W.; Du, M., Structural Diversity and Fluorescent Properties of Cd^{II} Coordination Polymers with 5-Halonicotinates Regulated by Solvent and Ligand Halogen-Substituting Effect. *Cryst Eng Comm* **2013**, *15*, 9713-9721.

137. Falaise, C.; Volkringer, C.; Vigier, J. F.; Henry, N.; Beaurain, A.; Loiseau, T., Three-Dimensional MOF-Type Architectures with Tetravalent Uranium Hexanuclear Motifs (U_6O_8). *Chem Eur J* **2013**, *19*, 5324-5331.

138. Song, X.-Z.; Song, S.-Y.; Zhao, S.-N.; Hao, Z.-M.; Zhu, M.; Meng, X.; Zhang, H.-J., Two High-Connected Metal–Organic Frameworks Based on d^{10}-Metal Clusters: Syntheses, Structural Topologies and Luminescent Properties. *Dalton Trans* **2013**, *42*, 8183-8187.

139. Zhang, H. X.; Fu, H. R.; Li, H. Y.; Zhang, J.; Bu, X., Porous ctn-Type Boron Imidazolate Framework for Gas Storage and Separation. *Chem Eur J* **2013**, *19*, 11527-11530.

140. Zhan, C.; Zou, C.; Kong, G.-Q.; Wu, C.-D., Four Honeycomb Metal–Organic Frameworks with a Flexible Tripodal Polyaromatic Acid. *Cryst Growth Des* **2013**, *13*, 1429-1437.

141. Murdock, C. R.; Lu, Z.; Jenkins, D. M., Effects of Solvation on the Framework of a Breathing Copper MOF Employing a Semirigid Linker. *Inorg Chem* **2013**, *52*, 2182-2187.

142. Wu, Y.; Zhou, X.-P.; Yang, J.-R.; Li, D., Gyroidal Metal–Organic Frameworks by Solvothermal Subcomponent Self-Assembly. *Chem Commun* **2013**, *49*, 3413-3415.

143. Xing, F.; Jia, J.; Liu, L.; Zhong, L.; Shao, M.; Bai, Y.-L.; Zhao, Y.; Zhu, S.; He, X.; Li, M., Synthesis, Structure and Adsorption of Coordination Polymers Constructed from 3,3′,5,5′-Azobenzenetetracarboxylic Acid and Zn Ions. *Cryst Eng Comm* **2013**, *15*, 4970-4980.

144. Zhao, J.-P.; Zhao, R.; Song, W.-C.; Yang, Q.; Liu, F.-C.; Bu, X.-H., Azido-Directed Formation of an Unprecedented Mn (II)-Organic Framework with Nanoscale Cubic Cage Units. *Cryst Growth Des* **2013**, *13*, 437-439.

145. Ablet, A.; Li, S. M.; Cao, W.; Zheng, X. J.; Wong, W. T.; Jin, L. P., Luminescence Tuning and White-Light Emission of Co-Doped Ln–Cd–Organic Frameworks. *Chem Asia J* **2013**, *8*, 95-100.

CHAPTER 6. CONCLUSIONS

6.1 Dissertation Impact

The work presented in this dissertation comprises a broad study of metal-organic frameworks (MOFs) disorder, beginning with computational description of defects and bridging to experimental measurements. While the models here were based on zeolitic imidazolate frameworks (ZIFs), the overarching insights about defect prevalence, distribution, and degradation pattern will be applicable to many crystalline nanoporous materials.

Extended defects, particularly those in the bulk of a MOF material, are notoriously difficult to characterize through experimental measurements alone. Drawing on the well-known stacking faults in aluminosilicates, we proposed hypothetical ZIF-8 polymorphs containing the analogous stacking faults in Chapter 2. After constructing extended periodic lattices with and without a fault and energy minimizing the structures using force field methods, we were able to determine a favorable defect formation energy between 0.1-1.0 kJ/mol/Zn atom. This energy scale was comparable with the energy difference between different polymorphs, indicating that not only do stacking faults require negligible energy to form in synthesis, they may have an enthalpically favorable stabilizing effect. Based on this finding, we predict that extended defects are likely ubiquitous in real ZIFs. To seek evidence of these defects in an experimental structure, we simulated X-ray diffraction (XRD) patterns to estimate density of defects from the diffraction spectra. We determined two sets of correlations for XRD peak intensity and area with stacking fault ratio (SFR), a measure of defect density in a structure. Significant changes were identified in the

experimentally measured powder pattern of a topologically isomorphic hybrid-linker ZIF, consistent with our conclusions about the prevalence of MOF extended defects.

We extended the scope of our investigation into ZIF defects in Chapter 3 by considering stability of 10 ZIF materials in various humid and acid gas environments. Previous literature reports about water stability of carboxylate MOFs indicated that various parameters – ligand p*K*a, atomic charge, formation enthalpy – were correlated strongly with experimentally observed stability. Our aim was to identify a similar set of stability predictors for ZIFs. Detailed computational models were constructed for the adsorbent, adsorbate, and defect state in each degradation reaction. Careful comparison against experimental characterization was necessary to ensure we were accurately describing the physical phenomenon. Surprisingly, none of the calculated stability predictors correlated well with experimental degradation results. We conclude that ligand p*K*a and atomic charge cannot predict ZIF stability. Of the 10 ZIF materials studied, only one was stable to humid CO_2 and SO_2 exposure. Computational efforts to explain the exceptional stability of ZIF-71 RHO were unable to determine a precise difference in the degradation mechanism; rather, the stability of this material is likely a synergistic combination of transport, kinetics, and sterics. Another surprising but important conclusion was the low stability of all 10 ZIFs in dry and humid NO_2 environments. Computational methods were valuable in predicting complex hydrogen abstraction and free radical degradation pathways, as well as in predicting the likely defect product. Fourier transform infrared spectroscopy (FTIR) experiments were able to confirm the presence of intermediate and product species.

At this point, having studied ZIF defects at the local bond-breaking level and at the extended stacking fault scale, we sought a degradation mechanism that could bridge the

two extremes and explain how single point defects accumulate until the bulk structure degrades. In Chapter 4, we began by considering how a first point defect forms and determined the relative energetic favorability of all possible single defect states. Having done so, we then systematically examined where and how a second and third defect forms, finding an overwhelming preference for additional defects to cluster in adjacent sites. Additionally, we are able to decompose defect formation energy into an intrinsic energy of reaction and a strain energy due to geometry. Favorable defect propagation can then be explained as a means to reduce or eliminate the strain energy; this is a powerful understanding with implications for defects in any ordered nanoporous material. Finally, we simulated XRD patterns for varying concentrations of defects, distributed with different spatial densities throughout the lattice.

In Chapter 5, we carried out meta-analysis on the reproducibility of MOF synthesis research. Following on previous studies regarding the reproducibility of CO_2 adsorption isotherms, we ask a more fundamental question: how often is MOF synthesis repeated, and if repeated, how consistent are the results? We selected a set of 130 papers that reported new materials from the CoRE MOF database and tracked the citations of each of the 130 papers to determine whether those original materials have ever been re-synthesized. Replicate syntheses were classified as exact if they made the identical material or modified if the new synthesis contained a single substitution, and we also categorized syntheses performed by researchers who had been involved in the publication of the original paper, or an entirely independent group of researchers form the original authors. The results reveal a dearth of repeat syntheses: there were 25 examples of exact re-synthesis from the original 130 MOFs (associated with only 15 materials), only 7 of which were associated with

completely separate authors. Only 2 materials had been repeated more than once by distinct author groups. These metrics are likely pessimistic; it is probable that of the 252 modified re-syntheses, many also repeated the exact material initially without reporting the results. We propose a replication hierarchy that awards "Olympic medal" standards to different levels of reproducibility. The gold medal standard would be awarded to the two materials that were repeated twice each by distinct author groups. However, when we compare original and replicate material characterization reported for these two materials, non-trivial differences among measurements suggests that a consensus standard is lacking.

6.2 Suggested Directions for Future Work

There are several interesting research projects that are natural extensions of the previously summarized work:

1) Determining ZIF-71 RHO stability mechanism and application

The exceptional stability of ZIF-71 RHO to humid CO_2 and SO_2 environments makes it a promising candidate for industrial application. Adsorption loading simulations to determine and predict the distribution of adsorbents in the pores will likely illuminate how transport, sterics, and hydrophobicity differ in ZIF-71 RHO compared to other RHO topology ZIFs and ZIF-71 SOD. Identifying the transition state and performing nudged elastic band (NEB) DFT calculations may elucidate unusually low kinetics of the degradation reaction in ZIF-71 RHO. Understanding the mechanism for stability is key to designing other humid acid gas stable materials and even designing membrane or impregnated devices.

2) Modelling MOF interaction with more complex acid gases

We have presented detailed mechanistic models for H_2O, CO_2, SO_2, and NO_x interaction with a variety of ZIFs, but these are all fairly simple acid gases. To truly predict stability in industrially relevant conditions, it will be useful to a) identify more complex attacking species and b) examine multicomponent degradation. As illustrated with NO_x, more complex attacking species often require a different degradation pathway, and the same is likely true for H_2S, aromatic pollutants, and other reactive species. There is also a lack of understanding regarding interaction with multiple acid gases, but the detailed defect models presented here for single component acid gases provide a good foundational platform for computational description of multicomponent acid gas degradation.

3) Establishing a consensus standard for experimental measurements

Analysis of characterization reported in MOF synthesis suggests that PXRD, TGA, and FTIR are standard measurements which should be performed for all syntheses. These methods have the advantage of being relatively routine; they should be reproducible even if performed with different available commercial instruments, so long as adequate care is taken with sample preparation. Using characterization of well-studied MOFs to determine criteria for outliers, the same metrics can then be applied to determine if repeat characterization of less synthesized MOFs are truly consistent.